

Non-Linear Analysis of Jack-Up Structures Subjected to Random Waves

by

Mark Jason Cassidy



A thesis submitted for the degree of
Doctor of Philosophy
at the University of Oxford

New College
Trinity Term 1999

ABSTRACT

Non-Linear Analysis of Jack-Up Structures Subjected to Random Waves

A thesis submitted for the degree of Doctor of Philosophy

Mark Jason Cassidy
New College, Oxford
Trinity Term 1999

There is a steadily increasing demand for the use of jack-up units in deeper water and harsher environments. Confidence in their use in these environments requires jack-up analysis techniques to reflect accurately the physical processes occurring. This thesis is concerned with the models appropriate for the dynamic assessment of jack-ups, an important issue in long-term reliability considerations. The motivation is to achieve a balanced approach in considering the non-linearities in the structure, foundations and wave loading.

A work hardening plasticity model is outlined for the combined vertical, moment and horizontal loading of spudcan footings on dense sand. Empirical expressions for the yield surface in combined load space and a flow rule for prediction of footing displacements during yield are given. Theoretical lower bound bearing capacity factors for conical footings in sand have been derived and are used in a strain-hardening law to define the variation in size of the yield surface with the plastic component of vertical penetration. The complete incremental numerical model has been implemented into a plane frame analysis program named JAKUP.

The spectral content of wave loading is considered using NewWave theory, and the importance of random wave histories shown by constraining the deterministic NewWave into a completely random surface elevation. Using this technique, a method for determining short-term extreme response statistics for a sea-state is demonstrated. A numerical experiment on an example jack-up and central North Sea location is shown to emphasise the difference in long-term extreme response according to various footing assumptions. The role of sea-state severity in the variation of short-term extreme response statistics is also highlighted.

Finally, probabilistic methods are used to develop further understanding of the response behaviour of jack-ups. A sensitivity study of influential variables (with probabilistic formulations as opposed to deterministic values) has been conducted using the response surface methodology.

ACKNOWLEDGEMENTS

My supervisors Prof. Guy Houlsby and Prof. Rodney Eatock Taylor were always accessible with friendly support; for their invaluable guidance I would like to express my gratitude and appreciation. Thanks also to Dr Paul Taylor for the many useful discussions and encouragement.

Financial support from the Rhodes Trust is gratefully acknowledged. Furthermore, I would like to thank all of the staff at Rhodes House for their support (thanks Sally for the loan of the laptop. I managed not to tell anyone. Well, until now!).

Thanks to Byron Byrne, Elle Leane and Lori Ormrod for their comments. To Byron, you made life in the department more rewarding and sharing turnip pudding more challenging, and Elle, thanks for the continual encouragement and for highlighting the risks of giant squid loading. The “feminine critique” of this thesis to be published by Leane, E. and Ormrod, L. soon. Thanks also to David Williams and Dr Brendon Ruck for their time spent listening and commenting on my work at various stages in its development and to Nicola Houliston for all her help.

Thanks to all my friends whose enjoyable company helped keep me out of the lab, especially the Australians: Elle, Attila, Kate, Peter R., Robbo, Peter B., Byron, Andrew, Cam and Dale, the "honorarys": Roger, Lori, Annette, Emma, Claus and Dykema and those whose company I dearly missed after you left: Zukes, Eleanor, Maria, Tracy and Sarah. Thanks also to my friends in Brisbane who endured poor correspondence and Julie and Zac for their encouragement from London.

With admiration, appreciation and apologies, I thank my parents; and Brenda, your warm encouragement always means so much. For all of your love I cannot thank you enough.

Notation

Nomenclature used in thesis (excluding those which only appear once). Symbols have been placed under chapter headings.

Chapter 1:

H	horizontal load
M	moment load
u	horizontal footing displacement
V	vertical load
w	vertical footing displacement
q	rotational footing displacement

Chapter 2:

A_h, A_{Eh}	hydrodynamic area and equivalent hydrodynamic area respectively
C	system damping matrix
C_d	drag coefficient
C_m	inertia coefficient
D_h, D_{Eh}	hydrodynamic diameter and equivalent hydrodynamic diameter respectively
F	force per unit length on a member (defined by the Morison equation)
K	system stiffness matrix
M	system mass matrix
N	number of degrees of freedom in the system
P	vector of nodal loads
\dot{s}, \ddot{s}	structural velocity and acceleration of a point on a member respectively
t	time
u_t	horizontal water particle velocity normal to member
\ddot{u}	horizontal wave acceleration
x	vector of nodal displacements
\dot{x}	vector of nodal velocities
\ddot{x}	vector of nodal accelerations
z	vertical displacement
b	stability parameter in Newmark method
d	dissipation parameter in Newmark method
r	density of water
y	shape function

Chapters 3 and 4:

a	eccentricity of the yield surface
A	plan area of footing
B	width of strip footing
B'	effective width of footing
C_1	elastic flexibility factor (vertical)
C_2	elastic flexibility factor (moment)
C_3	elastic flexibility factor (horizontal)

Notation

C_4	elastic flexibility factor (coupled)
d	(as prefix) increment in value
e	eccentricity of applied load on footing [= M/V]
f	dimensionless initial plastic stiffness factor
f	yield function
f_p	factor determining limiting magnitude of vertical load as $w_p \rightarrow \infty$
g	plastic potential function
g	non-dimensional shear modulus factor
G	elastic shear modulus
h_0	dimension of yield surface (horizontal)
H	horizontal load
H_{Inter}	intercept of the ellipse on the H co-ordinate axis
i_g	inclination factor in bearing capacity formulation
k	initial plastic stiffness
k'	rate of change of association factors
k'_h, k'_m	rate of change of association factors \mathbf{a}_h and \mathbf{a}_m respectively
k_1	elastic stiffness factor (vertical)
k_2	elastic stiffness factor (moment)
k_3	elastic stiffness factor (horizontal)
k_4	elastic stiffness factor (coupled)
K_v	vertical experimental stiffness
m_0	dimension of yield surface (moment)
M	moment load
M_{Inter}	intercept of the ellipse on the M co-ordinate axis
N_g	vertical bearing capacity factor
p_a	atmospheric pressure
$P_{damping}$	vector of damping force component of the dynamic equation of motion
P_{ext}	vector of externally applied loads
$P_{inertial}$	vector of inertial force component of the dynamic equation of motion
P_{int}	vector of internal structural loads
q_p	plastic deviator displacement
Q	general deviator force
r	radius at the surface of a partially penetrated conical footing
R	radius of circular footing
s_{fp}	experimental vertical load normalised by the theoretical maximum V_0
s_g	shape factor in bearing capacity formulation
t	time
u	horizontal footing displacement
u_p	plastic horizontal footing displacement
V	vertical load
V_0	maximum vertical load capacity when $H=0$ and $M=0$
V_{0m}	peak value of V_0 in strain hardening law
V'_0	maximum vertical load for the current plastic potential shape
V_{peak}	maximum vertical bearing capacity
w	vertical footing displacement

Notation

w_p	plastic vertical footing displacement
w_{pm}	value of plastic vertical displacement at the peak value of V_0 (i.e. at V_{0m})
x	vector of nodal displacements
a	roughness factor
a_0	value of the association factor without any displacements
a_∞	value of the association factor as displacements tend to infinity
a_h, a_m	horizontal and moment association factor respectively
a_{h0}, a_{m0}	value of association without any horizontal displacement or rotation respectively
$a_{h\infty}, a_{m\infty}$	association factor as horizontal displacement or rotation tend to infinity respectively
a_v	general association factor
b	cone apex angle
b	exponent in equation for modified parabola
b_1, b_2	exponents in equation for doubly modified parabola
b_1, b_2	curvature factor exponents in equation for yield surface
b_3, b_4	curvature factor exponents in equation for plastic potential
d_p	dimensionless vertical plastic displacement at V_{0m} [= $w_{pm}/2R$]
f	friction angle of sand
g, g'	unit weight and submerged unit weight of soil
l	multiplication factor determining the magnitude of plastic displacement increments
m, m'	coefficient in equation for modified parabola (horizontal and moment respectively)
q	rotational footing displacement
q_p	plastic rotational footing displacement
n	Poisson's ratio
z_a	association parameter for determining vertical plastic displacements

Subscripts:

e	elastic
ep	elasto-plastic
exp	represents experimental values from the swipe tests (Chapter 3)
Exp	represents experimental evidence of flat circular plates (Chapter 4)
p	plastic
$pre - load$	condition of variable immediately following vertical pre-loading of the spudcans
$start$	value at the commencement of the swipe test
$theory$	represents theoretical values from the swipe tests (Chapter 3)
$Theory$	represents theoretical bearing capacity approach (Chapter 4)

Chapters 5 and 6:

a_n, b_n	independent random variable Fourier components
c_n	amplitude of wavelet
d	water depth (measured vertically from mean water-level to sea bed)
d	(as prefix) increment in value
$E[]$	the mean or expected value
$F_n(z)$	horizontal attenuation factor at depth z for the n^{th} wavelet
H_s	significant wave height

Notation

j	integer representing sea-state occurrence (<i>i.e.</i> 1 in 10^j year sea-state)
k	wave number
k_p	wave number corresponding to the peak in the wave energy spectrum
n	wavelet number (between 1 and N)
N	number of increments (Fourier components or wavelets)
N_{crest}	number of crests in short-term time period
Q, R	random coefficients used in NewWave constraining procedure
$Q(x)$	cumulative probability (probability of non-exceedence of x)
$r(\mathbf{t})$	autocorrelation function for ocean surface elevation
$\dot{r}(\mathbf{t})$	differentiation of autocorrelation function with respect to time
rn	random number
$R_{50\%}$	50% exceedence value of response
$sf_{0.2}, sf_{0.8}$	factors used to scale 100-year short-term statistics to other return period statistics
S_{hh}	wave energy spectrum
t	time
T	time period
T_p	period representing the peak frequency in the sea-state spectrum
T_z	mean zero crossing period
u, \dot{u}	horizontal wave velocity and acceleration respectively
$V_{0_{pre-load}}$	initial vertical load value per spudcan immediately following pre-load
x	response value
x	spatial distance relative to the numerical analysis reference point
X	spatial distance relative to the initial position of the crest respectively
z	vertical displacement
\mathbf{a}	crest elevation (measured vertically from mean water-level to wave maximum)
$\dot{\mathbf{a}}$	gradient of surface elevation at crest
\mathbf{d}_{deck}	horizontal displacement of the deck
∇	delta stretching parameter
e	spectral bandwidth
f	random phase angle
g	peak enhancement factor (in JONSWAP spectrum)
h	ocean surface elevation
\dot{h}	gradient of ocean surface elevation
l	factor in second spectral moment
m	mean value of random variables
s	standard deviation of random variables
t	time lag
w	angular frequency
w_{max}	maximum defined angular frequency

Subscripts:

c	constrained process
r	random process

Chapter 7:

a, b_i, c_i, d_{ij}	components of second-order response surface with mixed terms
-----------------------	--

Notation

C_d	drag coefficient
C_m	inertia coefficient
d	(as prefix) increment in value
f	dimensionless initial plastic stiffness factor
$f - \mathbf{d}_p$	combination of hardening law parameters f and \mathbf{d}_p
f_X	density function of set [X]
F_X	distribution function of set [X]
g	non-dimensional shear modulus factor
$G(X)$	failure function for set of basic variables [X]
H_s	significant wave height
k	number of basic random variables in set
m_0	dimension of yield surface (moment)
m_{0h}	zeroth spectral moment
N_{crest}	number of crests in short-term time period
N_g	vertical bearing capacity factor
P_f	probability of failure
$Q(x)$	cumulative probability (probability of non-exceedence of x)
R, S	component's resistance and service response respectively
\hat{S}	service response predicted by the response surface
$S_{m_{x_i}}$	sensitivity measure of the i^{th} basic random variable
T_z	mean zero crossing period
u	horizontal current velocity
$wind$	total wind force on jack-up hull
X	set of basic variables
Z	basic variable in standardised Gaussian space
\mathbf{a}	unit vector defining direction of the design point in standardised Gaussian space
\mathbf{a}	crest elevation (measured vertically from mean water-level to wave maximum)
$\bar{\mathbf{a}}_{mod}, \bar{\mathbf{a}}_{mean}$	modal and mean most probable wave crest elevation respectively in short-term sea-state
\mathbf{b}	reliability index
\mathbf{d}_{deck}	horizontal displacement of the deck
$\hat{\mathbf{d}}_{deck}$	response surface prediction of horizontal deck displacement
\mathbf{d}_p	dimensionless vertical plastic displacement at V_{0m}
\mathbf{e}_{rel}	measure of relative error (used to compare the response surface and JAKUP \mathbf{d}_{deck} predictions)
\mathbf{m}	mean value of random variables
\mathbf{s}	standard deviation of random variables
Φ	standard normal distribution function
\mathbf{z}_i	omission sensitivity factor

CONTENTS

ABSTRACT

ACKNOWLEDGEMENTS

NOTATION

CHAPTER 1 – INTRODUCTION

1.1	Jack-Up Units	1-1
1.1.1	General	1-1
1.1.2	History	1-1
1.1.3	Considerations in Jack-Up Analysis Modelling	1-3
1.1.3.1	Structural Modelling	1-3
1.1.3.2	Modelling of Foundation Behaviour	1-4
1.2	The Need for Further Research	1-5
1.3	Research Aims	1-6
1.3.1	Foundation Modelling	1-6
1.3.2	Random Wave Modelling	1-7
1.3.3	Probabilistic Approach	1-8
1.4	Thesis Outline	1-8

CHAPTER 2 - ANALYSIS OF JACK-UP UNITS

2.1	Introduction	2-1
2.2	Literature Review of Jack-Up Analysis Techniques	2-1
2.2.1	Dynamic Effects	2-2
2.2.2	Geometric Non-Linearities in Structural Modelling	2-3
2.2.3	Environmental Wave Loading	2-4
2.2.3.1	NewWave Theory	2-4
2.2.3.2	Constrained NewWave	2-5
2.2.3.3	Alternative Methods for Full Random Time Domain Simulation	2-6
2.2.4	Spudcan Footings – Models for Foundation Response	2-6
2.2.5	Overall Jack-Up Analysis – A Summary of Models Used	2-8
2.3	Overview of JAKUP – The Analysis Program used in Thesis	2-10
2.3.1	Dynamic Analysis	2-10
2.3.2	The Structural Model	2-11
2.3.3	The Foundation Model	2-11
2.3.4	Environmental Loading Models	2-11
2.3.4.1	Wave Loading	2-11
2.3.4.2	Wind Loading	2-13
2.4	Example Structure used in Analyses	2-13

CHAPTER 3 - STRAIN HARDENING PLASTICITY MODEL FOR SPUDCANS ON DENSE SAND

3.1	Introduction	3-1
3.2	Literature Review	3-1

Contents

3.2.1	Introduction - Combined Loading on Foundations	3-1
3.2.2	Traditional Bearing Capacity Theories	3-2
3.2.3	Alternative Yield Surface Loci	3-6
3.2.4	Concluding Remarks - Combined Loading on Foundations	3-6
3.2.5	Use of Plasticity Theory for Combined Loading of Offshore Foundations	3-7
3.3	Development of Model C	3-9
3.3.1	Introduction to Experimental Tests and Data	3-9
3.3.2	Elastic Response: Choice of an Elastic Stiffness Matrix	3-11
3.3.3	Development of a Strain Hardening Law	3-14
3.3.4	Development of a Three-Dimensional Normalised Yield Surface	3-15
3.3.5	Comparisons with Other Yield Surfaces	3-21
3.3.5.1	The Deviatoric/Normal Plane ($H/V_0:V/V_0$, $M/2RV_0:V/V_0$ or $Q/V_0:V/V_0$)	3-21
3.3.5.2	The π Plane ($M/2RV_0:H/V_0$)	3-21
3.3.6	Development of the Plastic Potential	3-22
3.3.6.1	Incremental Plastic Displacements at Yield: π Plane	3-22
3.3.6.2	Incremental Plastic Displacements at Yield: Deviatoric/Normal Plane	3-24
3.3.6.3	Numerical Evaluation of Plastic Potential Size	3-33
3.3.6.4	Comments on Model C's Plastic Potential	3-34

CHAPTER 4 – NUMERICAL FORMULATION OF MODEL C FOR THE ANALYSIS OF JACK-UP UNITS

4.1	Introduction	4-1
4.2	Features of Model C	4-1
4.2.1	General Structure of Model C	4-1
4.2.2	Numerical Formulation of Model C	4-2
4.2.3	Implementation of Model C in the FORTRAN Program OXC	4-5
4.3	Retrospective Prediction of Experimental Tests	4-6
4.3.1	Vertical Penetration Test	4-7
4.3.2	Moment and Horizontal Swipe Tests from $V \approx 1600$ N	4-7
4.3.3	Moment and Horizontal Swipe Tests from $V \approx 200$ N	4-8
4.3.4	Constant Vertical Load Tests	4-9
4.3.5	Radial Displacement Tests	4-10
4.4	Considering the Conical Shape of Spudcans	4-11
4.4.1	Vertical Bearing Capacity of Conical Footings	4-11
4.4.2	Adaptation of Model C for Conical Shape of Spudcans	4-12
4.4.2.1	Flat Plates	4-12
4.4.2.2	Conical Spudcans	4-13
4.5	Implementation of Model C into JAKUP	4-14
4.6	Concluding Remarks	4-17

CHAPTER 5 - APPLICATION OF NEWWAVE THEORY IN THE ANALYSIS OF JACK-UP UNITS

5.1	Introduction	5-1
5.2	Theoretical Background	5-1
5.2.1	Linear Random Wave Theory	5-1
5.2.2	NewWave Theory	5-2
5.2.3	Wave Energy Spectrum	5-5
5.3	Implementation of NewWave into JAKUP	5-7

Contents

5.3.1	Wave Dispersion Relationship	5-8
5.3.1.1	Implementation of NewWave in JAKUP - Dispersion Relationship	5-10
5.4	NewWave Kinematics	5-10
5.4.1	Theory	5-10
5.4.2	Example of NewWave Kinematics in JAKUP	5-12
5.4.3	Example Response of a Jack-Up Subjected to NewWave Loading	5-13
5.5	Discussion of NewWave	5-14
5.5.1	Calculation of Kinematics – Linear Stretching/Extrapolation Procedures	5-14
5.5.2	Second-Order NewWave Theory	5-15
5.5.2.1	The Second-Order Correction Suggested by Taylor (1992)	5-15
5.5.2.2	Second-Order NewWaves Suggested by Jensen (1996)	5-16
5.5.2.3	Comparisons of the Second-Order Formulations with Linear Kinematics	5-17

CHAPTER 6 - EVALUATION OF EXTREME RESPONSE STATISTICS USING CONSTRAINED NEWWAVE

6.1	Introduction	6-1
6.2	Theoretical Background	6-2
6.2.1	Numerical Random Wave Simulation	6-2
6.2.1.1	Implementation in JAKUP	6-3
6.2.2	Constraining a NewWave into a Random Background	6-3
6.2.2.1	Example Response of a Jack-Up Subjected to a Constrained NewWave	6-5
6.3	Using Constrained NewWave in the Evaluation of Response Statistics of Jack-Ups	6-6
6.3.1	Overview	6-6
6.3.2	Methodology Adopted for the Evaluation of Short-Term Statistics	6-7
6.3.3	Example Numerical Results for One Sea-State ($H_s = 12$ s and $T_z = 10.805$ s)	6-9
6.3.4	Verification of Short-Term Extreme Response Results	6-10
6.4	Evaluation of Long-Term Statistics: A Numerical Experiment on an Example Jack-Up	6-11
6.4.1	Overview	6-11
6.4.1.1	Review of Extrapolation Methods	6-11
6.4.1.2	Response Based Design Conditions	6-13
6.4.2	Example Calculations for a Central North Sea Jack-Up	6-13
6.4.3	First Long-Term Numerical Experiment - Wave Loading Only	6-15
6.4.3.1	Methodology Adopted to Numerically Scale Short-Term Extreme Response Distributions	6-17
6.4.3.2	Monte Carlo Sampling of Long-Term Extreme Exceedence Probabilities	6-19
6.4.3.3	Long-Term Loads on the Jack-Up Legs	6-20
6.4.4	Second Long-term Numerical Experiment - All Environmental Forces	6-21
6.4.5	Measuring the Relative Importance of the Random Background	6-22
6.4.6	Further Discussion of Long-Term Results	6-24

CHAPTER 7 - APPLICATION OF PROBABILISTIC MODELS IN THE RESPONSE ANALYSIS OF JACK-UPS

7.1	Introduction	7-1
7.2	Literature Review	7-2
7.2.1	General Reliability Theory	7-2
7.2.2	Reliability Calculation Techniques	7-3
7.2.3	Use of Reliability Theory for the Analysis of Jack-Up Units	7-4
7.3	Aims of Numerical Experiments	7-6

7.4	Use of the Response Surface Method (RSM)	7-7
7.5	Choice of Random Variables and their “Predicted” Variability	7-10
7.5.1	Random Variables Influencing the Dynamic Response of Jack-Ups	7-11
7.5.2	Distributions of Random Variables used in Numerical Experiments	7-13
7.6	Short-Term Analysis (100-year return period)	7-15
7.6.1	NewWave with Most Probable Highest Amplitude (<i>i.e.</i> $\alpha = 0.93H_s$)	7-15
7.6.1.1	Calculating Probability of Exceedence Results from a Monte Carlo Simulation of the RS	7-16
7.6.1.2	The Mean Most Probable Highest Amplitude	7-16
7.6.1.3	How Precise is the Response Surface Fit?	7-17
7.6.1.4	Sensitivities of the Basic Random Variables	7-18
7.6.1.5	Calculations Using First Order Reliability Methods (FORM)	7-20
7.6.1.6	Using Only 7 Basic Random Variables – Repeat Calculation	7-22
7.6.2	Short-Term Sea-States with Variable Wave Amplitudes	7-23
7.6.2.1	Methodology Adopted	7-23
7.6.2.2	Numerical Experiment for 100-Year Return Period	7-24
7.7	Long-Term Numerical Experiment with Probabilistic Random Variables	7-25
7.7.1	Short-Term Results	7-25
7.7.2	Long-Term Results	7-27

CHAPTER 8 – CONCLUDING REMARKS

8.1	Introduction	8-1
8.2	Conclusions – Main Findings	8-1
8.2.1	Foundation Modelling	8-1
8.2.2	Numerical Modelling of Random Wave Loading	8-2
8.2.3	Probabilistic Approach to Developing Extreme Response Statistics	8-3
8.3	Directions for Future Work	8-5
8.3.1	Extension to Three Dimensions	8-5
8.3.2	Foundation Theories for Spudcan Footings	8-6
8.3.3	Physical Validation of Model C	8-6
8.3.4	Wave Models	8-7
8.4	Conclusion	8-8

REFERENCES

APPENDIX A

TABLES

FIGURES

Chapter 1 – Introduction

1.1 Jack-Up Units

1.1.1 General

Most of the world's offshore drilling in water depths up to 120m is performed from self-elevating mobile units, commonly known as jack-ups. Typical units consist of a buoyant triangular platform resting on three independent truss-work legs, with the weight of the deck and equipment more or less equally distributed. A rack and pinion system is used to jack the legs up and down through the deck. An example of such a unit is shown in Fig.1.1.

Jack-ups are towed to site floating on the hull with the legs elevated out of the water. On location, the legs are lowered to the sea-bed, where they continue to be jacked until adequate bearing capacity exists for the hull to climb out of the water. The foundations are then pre-loaded by pumping sea-water into ballast tanks in the hull. This 'proof tests' the foundations by exposing them to a larger vertical load than would be expected during service. The ballast tanks are emptied before operations on the jack-up begin. It is usual for the total combined pre-load (*i.e.* jack-up mass and sea-water) to be about double the mass of the jack-up.

1.1.2 History

The earliest reference to a jack-up platform is in the description of a United States patent application filed by Samuel Lewis in 1869 (Veldman and Lagers, 1997). It wasn't until 85 years later in 1954 that Delong McDermott No. 1 became the first unit to utilise the jack-up principle for offshore drilling. Delong McDermott No. 1 was a conversion of one of the successful 'Delong Docks': a pontoon with a number of tubular legs which could be moved up and down through cut-outs in the pontoon. The Delong Docks, which were mostly used as

mobile wharves for industrial purposes during the 1940s, could be towed into location with their legs drawn up. Once in position their legs could be lowered and the pontoon elevated off the water using the same principle as the modern jack-up. Interestingly, Delong Docks were used in World War II as mobile docks by the United States Army after the invasion of Normandy and before the major harbours of Western Europe were liberated (Veldman and Lagers, 1997).

Like many of the early jack-ups to follow, Delong McDermott No. 1 resembled a standard drilling barge with attached legs and jacks, which were often many in number. In 1956 R.G. LeTourneau, a former entrepreneur in earthmoving equipment (Ackland, 1949), revolutionised the design of jack-ups by reducing the number of legs to three (Stiff *et al.*, 1997). Another innovative design change was the electrically driven rack and pinion jacking system which allowed for continuous motion in any jacking operation. This replaced ‘gripper’ jacks where slippage often occurred on the smooth leg surface (Veldman and Lagers, 1997). Both revolutionary features are common on today’s rigs. Zepata’s “Scorpien”, used in water depths up to 25 m in the Gulf of Mexico, was the first of many operated by the company Marathon LeTourneau. They dominated early jack-up design during the 1960s and 1970s with rigs of increasing size.

Since their first employment, jack-ups have continued to be used in deeper waters (Carlsen *et al.*, 1986). Other companies, including Bethlehem, Friede and Goldman, Marine Structures Consultants and Mitsui have contributed to the rise in water depth capacity (Veldman and Lagers, 1997). This development is continuing with some of the largest units being used in about 120m of water in the relatively harsh North Sea environment (Hambly and Nicholson, 1991; Veldman and Lagers, 1997). Furthermore, jack-ups are now operating for extended periods at one location, often in the role of a production unit (Bennett and Sharples, 1987). An example of the long-term use of jack-ups is in the Siri marginal field

development in the Danish sector of the North Sea. A purpose built jack-up is being used in 60 m water depths as a production platform with an expected life of ten years (Baerheim *et al.*, 1997). A further example is the Shearwater development, where jack-up drilling is planned to continue for two and a half years at a 90 m water depth in the Northern North Sea (Offshore Technology, 1999).

1.1.3 Considerations in Jack-Up Analysis Modelling

Before a jack-up can operate at a given site, an assessment of its capacity to withstand a design storm, usually for a 50-year return period, must be performed. In the past, with jack-ups used in relatively shallow and calm waters, it has been possible to use overly simplistic and conservative jack-up analysis techniques for this assessment. However, as jack-ups have moved into deeper and harsher environments, there has been an increased need to understand jack-up behaviour and develop analysis techniques. The publication of the ‘Guidelines for the Site Specific Assessment of Mobile Jack-Up Units’ (SNAME, 1994) was an attempt by the offshore industry to standardise jack-up assessment procedures. The guidelines also detail categories of jack-up modelling sophistication based on the latest research. A brief introduction to some aspects of jack-up modelling is given below, while expanded explanations, including state-of-the-art practices, are detailed in Chapter 2.

1.1.3.1 Structural Modelling

As illustrated by the example unit in Fig. 1.1, a jack-up consists of a large number of members with intricate structural detail. It is conventional, however, to analyse jack-ups using a mathematical model which simplifies this structural detail considerably. (Hoyle, 1992). One representative example is Brekke *et al.* (1990), who calibrated a simplified model with only six structural nodes per leg against structural measurements of a North Sea jack-up in firm sandy conditions. Other examples include Daghigh *et al.* (1997), who used a three-dimensional finite element model with legs discretised to fourteen nodes each, and

Manuel and Cornell (1996), who used a plane frame model with loading in the jack-up's axis of symmetry. For the latter two-dimensional model, two legs were assumed to act as the same upwave leg with relevant properties doubled. In both cases the detailed lattice legs were assumed as equivalent beam elements.

The use of jack-up units in deeper water has several detrimental effects on their structural response, including:

- increased flexibility caused by longer effective leg length. This increases the natural period of the jack-up and in most situations moves the structure's principal natural period closer to the dominant wave periods of the sea-state. Consequently, inclusion of dynamic effects in the modelling of jack-up response is critical.
- the assumption of small displacement behaviour is no longer valid, with structural nonlinearities occurring due to large axial loads in the legs caused by the deck's weight.

Even with knowledge of these considerations, linear structural behaviour and quasi-static analyses are still inappropriately applied in jack-up assessments; they will be discussed further in Chapter 2.

1.1.3.2 Modelling of Foundation Behaviour

The foundations of independent-leg jack-up platforms approximate large inverted cones known as 'spudcans'. Roughly circular in plan, they typically have a shallow conical underside with a sharp protruding spigot, as shown in Fig. 1.2. For the larger units operating in the North Sea spudcan diameters in excess of 20 m have become common.

In a perfectly calm sea vertical self-weight is the only loading on the spudcans. During a storm, however, environmental wind and wave forces impose additional horizontal and moment loads onto the foundations of the jack-up, as well as alter the vertical load. An

understanding of spudcan performance under these combined load conditions is essential to the analysis of jack-up response.

In a conventional jack-up site assessment, the maximum vertical footing reaction produced from the structural analysis (factored for safety and usually made with the foundations modelled as pinned footings) is used to determine the amount of pre-load required during the installation of the unit (Reardon, 1986). In a calculation of foundation capacity, the semi-empirical methods developed by Meyerhof (1951, 1953), Brinch Hansen (1961, 1970) and Vesic (1975) may be used to consider the detrimental effect of concurrent vertical, moment and horizontal load on vertical bearing capacity. These methods are not amenable to implementation into dynamic structural analysis programs, thus limiting their application to single checks on design capacity.

1.2 The Need for Further Research

From their introduction, the accident rate involving jack-ups has exceeded that of other offshore installations. (Young *et al.*, 1984; Sharples *et al.*, 1989; Leijten and Efthymiou, 1989; Boon *et al.*, 1997). Young *et al.* attribute about one third of accidents to foundation failure whilst Leijten and Efthymiou attribute over half of the accidents resulting in total rig loss to structural or foundation failure. Furthermore, the failure rate for jack-ups can be interpreted as increasing with the harshness of conditions. Structural and foundation behaviour are areas where the understanding of jack-up behaviour needs to be improved in an attempt to reduce the number of accidents.

Due to the demand for longer commitment of jack-ups to a single location, as well as their use in deeper water and harsher conditions, long-term reliability calculations are becoming increasingly important. As the results of any reliability analysis can only be judged on the

accuracy of the individual components used in the analysis, the understanding of jack-up behaviour and the ability to model it confidently is paramount. With analysis techniques that reflect accurately the physical processes occurring, a reduction of failure rates is possible.

1.3 Research Aims

This thesis is concerned with extreme response modelling of jack-up units on sand when subjected to random ocean waves. Whilst maintaining a balanced approach to jack-up modelling, it aims to extend knowledge of analysis techniques in three key areas:

- foundation modelling,
- random wave loading,
- and the probabilistic approach to developing extreme response statistics.

The purpose of this approach is to achieve understanding and confidence in all the components affecting jack-up response.

1.3.1 Foundation Modelling

The use of strain hardening plasticity theory is seen as the best approach to modelling soil behaviour with a terminology amenable to numerical analysis. A major objective of this project was to develop an elasto-plastic model for spudcan behaviour on sand and fully integrate it into a dynamic structural analysis program.

1.3.2 Random Wave Modelling

Hydrodynamic loading on jack-up platforms can be calculated by integrating wave forces on the leg from the seabed to the instantaneous free-water level. This can be achieved by using the Morison equation, which is discussed further in Chapter 2. Variation of the free-water surface, as well as other non-linearities such as drag dominated loading and relative motion effects, can be accounted for in the time domain. In the jack-up industry regular

wave theories such as the linear Airy wave and the higher-order Stokes' fifth theory are widely accepted methods of determining the kinematics required in the Morison equation (SNAME, 1994). Based on one frequency component, these theories do not account for the random nature of the ocean environment and give an unrepresentative response.

For dynamically responding structures such as jack-ups, it is important to simulate all of the random, spectral and non-linear properties of wave loading. The investigation of these properties as applied to jack-up response analysis is an aim of this thesis. NewWave theory, a “deterministic random”¹ wave theory developed by Tromans *et al.* (1991), is used in this investigation.

In this project, both foundation and random wave modelling are constrained to behaviour within a single vertical plane. This confines the foundation model to a three degrees of freedom problem, *i.e.* the model needs to define the load:displacement relationship for a spudcan for three loads (V, M, H) and their corresponding displacements (w, \mathbf{q}, u) , as shown in Fig. 1.3. Though a foundation model with six degrees of freedom could be developed and implemented into a three-dimensional structural jack-up model, this was considered outside the scope of this investigation. The wave model is bound to uniaxial loading conditions along the jack-up's axis of symmetry. With a three-dimensional model, however, the multidirectional nature of the sea could be considered.

¹ By itself NewWave is deterministic and accounts for the spectral content of the sea. However, by constraining a NewWave within a completely random background, the random properties of wave loading can be investigated (Taylor *et al.*, 1995).

1.3.3 Probabilistic Approach

One of the primary project aims was to investigate the dynamic response of jack-ups within a consistent theoretical framework. The probabilistic modelling of variables achieves this not only for singular loading examples but also for long-term conditions—a necessity if the reliability of jack-ups is to be evaluated. Using this consistent framework, a quantitative comparison of modelling assumptions (especially for foundations) and among input variables was a research objective.

1.4 Thesis Outline

The outline of this thesis broadly follows four topics described in section 1.1.3 and 1.3: jack-up analysis techniques (and structural modelling), foundation models, account of random wave loading and probabilistic modelling. As these topics are distinctively varied, a review of literature on the separate topics is included at the beginning of each chapter rather than having one chapter devoted solely to literature reviews.

Jack-Up Analysis Techniques (and Structural Modelling): **Chapter 2** contains a literature review of analysis techniques relevant to the overall analysis of the structural response of jack-up units. Whilst the state-of-the-art procedures in each modelling area are highlighted, emphasis is also placed on determining, for an individual study of jack-up response, the level of complexity in each model component used. The dynamic analysis program JAKUP and the example structure used in this thesis are also introduced.

Foundation Model: **Chapters 3 and 4** concentrate on foundation models of jack-up spudcan footings in sand. Following an introduction to existing knowledge of combined loading on flat circular footings, **Chapter 3** describes the development of Model C, a work hardening plasticity model for circular footings on dense sand. The numerical formulation of Model C

is detailed in **Chapter 4** and retrospective prediction of experimental data shows this formulation in practice. Model C is extended by a description of a numerical model accounting for the conical features of spudcan footings and the incorporation of Model C into the dynamic structural analysis program JAKUP is also presented.

Wave Model: **Chapter 5** focuses on wave loading models suitable for the analysis of jack-up units. NewWave theory is described as a deterministic alternative to regular wave theories and its theoretical background and implementation into JAKUP are detailed. Example JAKUP analyses are shown, to emphasise differences in predicted response due to linear wave theory stretching procedures, second-order effects in NewWave and various footing assumptions. In **Chapter 6** the importance of random wave histories is shown by constraining a deterministic NewWave into a completely random surface elevation. Extreme response statistics for an example jack-up in the Central North Sea are evaluated utilising this ‘Constrained NewWave’ in a simplified method of full random time domain simulation. The quantitative differences between footing assumptions are outlined for example long-term conditions.

Probabilistic Modelling: **Chapter 7** concentrates on probabilistic modelling of jack-up extreme response calculations. Variables which influence the dynamic response of jack-ups are investigated by attributing their inherent statistical variability to a probabilistic distribution. Comparisons between using deterministic mean values and probabilistic distributions for these variables are drawn.

Chapter 8 summarises the main findings of the thesis, indicating achievement of the research aims and outlining areas and topics where further research would be beneficial.

Chapter 2 – Analysis of Jack-Up Units

2.1 Introduction

This chapter reviews literature relevant to the analysis of jack-up units, with particular reference to areas of analysis where techniques have improved to reflect more accurately aspects of non-linear behaviours. Interaction between these areas is investigated for individual studies found in the literature. This chapter also presents the dynamic analysis program named JAKUP and the example structure used in this thesis.

2.2 Literature Review of Jack-Up Analysis Techniques

Jack-ups were originally designed for use in the relatively shallow waters of parts of the Gulf of Mexico. Due to their economic importance within the offshore industry, there has been a steady increase in demand for their use in deeper water and harsher environments (Carlsen *et al.*, 1986). There is also a desire for a longer-lasting commitment of a jack-up at a single location, especially in the role of a production unit (Bennett and Sharples, 1987). To be confident of their use in these environments, there has been a need for changes in analysis techniques to make them more accurate, avoiding unnecessary conservatism which were once commonplace.

More realistic modelling of jack-ups based upon the relevant physical processes has been developed in a number of areas, the most significant being:

- dynamic effects,
- geometric non-linearities in structural modelling,
- environmental wave loading,
- models for foundation response.

Many individual studies have been published on jack-up response. Rather than detailing the strengths and weaknesses of each assessment, a review of the development of each area, highlighting the current state-of-the-art procedures will be given. In section 2.2.5, a table summarising the application of these developments in a representative set of jack-up studies is presented. It is shown that while many studies utilise state-of-the-art procedures for one or two aspects, there are few which bring all components to the same level of complexity.

2.2.1 Dynamic Effects

Conventionally, jack-up assessments have used the same quasi-static analysis methods employed for fixed structures (Hambly and Nicholson, 1991); however, the need to consider dynamic effects has long been acknowledged (Hattori *et al.*, 1982; Grenda, 1986; Bradshaw, 1987). With use in deeper water, the contribution of dynamic effects to the total response has become more important as the natural period of the jack-up approaches the peak wave periods in the sea-state.

Debate exists as to the appropriate method of accounting for the dynamic effects in a representative and practical manner. The main techniques that have been employed are (i) time domain, (ii) frequency spectral domain, and (iii) simplified empirical methods in conjunction with a quasi-static analysis. Time domain techniques provide the most complete analysis option with the ability to reflect the actual physical processes and non-linearities within the system; however, they are computationally time-consuming. The frequency spectral domain method offers a more numerically efficient solution, but as the behaviour of the jack-up must be linearised, some physical processes become inaccurately modelled. These include the non-linearities in loading from the Morison drag term and free surface inundation effects. In addition, only a linear structure and foundations can be

implemented. Indirect solution techniques do exist to factor in the non-linearities in the frequency domain—see Naess and Pisano (1997) amongst others; however, the ability to reflect non-linearities directly is still forfeited. The third method accounts for dynamic effects by using empirical factors to scale the quasi-static wave load amplitude. These global response Dynamic Amplification Factors (DAFs) are usually calculated based on a single degree of freedom oscillator, subjected to harmonic loading. This simplified method makes no attempt to model accurately the physical response process and provides no clear picture of the factors controlling the response. Therefore, although DAFs are supposedly calibrated to give conservative results, there can be no confidence in this under all conditions.

In summary: due to their ability to model all non-linearities, the time domain techniques are the most versatile methods in the analysis of the extreme response of jack-ups and will therefore be the focus of this thesis.

2.2.2 Geometric Non-Linearities in Structural Modelling

For non-conservative modelling of jack-up response, structural non-linearities must be taken into account. Additional moments are developed due to load eccentricities and are commonly referred to as $P - \Delta$ effects. Also, the axial loads reduce flexural stiffness in the leg elements, simultaneously increasing the natural period and dynamic amplifications in the sway mode. Methods with varying degrees of sophistication exist to account for both of these features, from simple linear analysis (Brekke *et al.*, 1990) to full large displacement non-linear formulations which trace the load-deflection path (Karunakaran *et al.*, 1992; Martin, 1994). For efficiency, dynamic analysis of jack-ups typically make use of equivalent beam models rather than attempt to model the complex lattice structure.

2.2.3 Environmental Wave Loading

For dynamically responding structures such as jack-ups it is important to simulate all of the random, spectral and non-linear properties of wave loading. The extreme dynamic response depends not only on the load being currently applied, but also on the load history. Therefore, the most accurate methods of estimating extreme response are based on random time domain simulation of the ocean surface and corresponding kinematics. For severe storm conditions, response statistics are typically evaluated over a three-hour period. Acquiring confidence in random time domain simulation results is, however, computationally time-consuming; and for the sake of convenience, deterministic wave theories, which include Airy and Stokes V, are still widely used for calculating wave loading on jack-ups (SNAME, 1994). However, comparisons of deterministic regular wave and validated random wave theories show that the regular wave theories tend to overestimate wave kinematics and thereby the fluid load (Tromans *et al.*, 1991). Moreover, regular wave theories assume all the wave energy is concentrated in one frequency component rather than the broad spectrum of the ocean environment and hence give an unrepresentative dynamic response.

2.2.3.1 NewWave Theory

NewWave theory, a deterministic method described by Tromans *et al.* (1991), accounts for the spectral composition of the sea, and can be used as an alternative to both regular wave and full random time domain simulations of lengthy time periods. By assuming that the surface elevation can be modelled as a Gaussian random process, the expected elevation at an extreme event (for example a crest) can be theoretically derived. The surface elevation around this extreme event is modelled by the statistically most probable shape associated with its occurrence, and is given by the autocorrelation function of the Gaussian process

defining the sea-state. Further theoretical details of NewWave theory are presented in Chapter 5.

For structures which respond quasi-statically, NewWave theory has been used successfully in the prediction of global response (Tromans and van de Graaf, 1992; Winterstein *et al.*, 1998). It has also been validated against both measured global loading and conventional random wave modelling on a real platform by Elzinga and Tromans (1992) and on standard column examples (Tromans *et al.*, 1991).

2.2.3.2 Constrained NewWave

NewWave theory can be used within a random time series of surface elevation by mathematically incorporating the NewWave (of pre-determined height) into the random background (Taylor *et al.*, 1995). This is performed in a rigorous manner such that the constrained sequence is statistically indistinguishable from the original random sequence. Constrained NewWave allows for easy and efficient evaluation of extreme response statistics. This is achievable without the need to simulate many hours of real time random seas, most of which is of no interest. This is provided the required extreme response correlates, on average, with the occurrence of a large wave within a random sea-state. Use of Constrained NewWave for the calculation of extreme response is shown for a simplified jack-up in a study by Harland (1994). The application of Constrained NewWave to the study of jack-up response is discussed further in Chapter 6.

2.2.3.3 Alternative Methods for Full Random Time Domain Simulation

Other methods to reduce computation time whilst maintaining accuracy in obtaining extreme response statistics have been suggested. Reducing the simulation time period in a time domain analysis and then extrapolating the extreme response to the duration required is one common method; see, for example, Kjeøy *et al.* (1989) or Karunakaran *et al.* (1992).

However, by fitting a general probabilistic model to the extremes, bias can be introduced to the results, and furthermore, there is much uncertainty as to the amount of bias present.

Other researchers have attempted to find “design wave” segments. It is believed that a segment of random sea can be chosen such that the response to it is directly correlated to the response of the entire period. Within the jack-up industry, for example, Hoyle and Snell (1997) identified 200-second segments from their base case three-hour simulation. They concluded that for further variations in the analyses only the segments needed to be used and could be linearly scaled according to the load required. Unfortunately, there is little guarantee that when the analysis conditions change from the base case the chosen segments will be representative of the extreme response, especially in a highly non-linear jack-up analysis.

2.2.4 Spudcan Footings – Models for Foundation Response

There has been much interest in recent years in the level of foundation fixity developed by spudcan footings. If some foundation fixity is taken into account, critical member stresses (usually at the leg/hull connection) and other response values are reduced (Chiba *et al.*, 1986; Norris and Aldridge, 1992). With higher levels of moment restraint, the natural period of the jack-up is also reduced, usually improving the dynamic characteristics of the rig. It is still widely accepted practice, however, to assume pinned footings (infinite horizontal and vertical and no moment restraint) in the analysis of jack-ups (Reardon, 1986; Frieze *et al.*, 1995). This creates overly conservative results. Another approach used, and an improvement on pinned footings, is the use of linear springs. Brekke *et al.* (1990) for example, calibrated linear springs with offshore measurements and reported a 40% reduction in critical member stresses in comparison to pinned cases. Unfortunately, while linear springs are easy to implement into structural analysis programs, they do not account

for the complexities and non-linearities of spudcan behaviour, and this simplistic approach can produce unrealistic results which may also be unconservative.

Various authors have attempted to implement non-linear springs in their structural analysis. For example, Hambly *et al.* (1990) and Hambly and Nicholson (1991) calibrated their springs against measurements in the North Sea with spring stiffnesses calculated at each instantaneous time step. To achieve this, however, the structural analysis was minimised to a single degree of freedom problem, which did not allow for consideration of other non-linearities (such as variation in the application of wave loading).

Another approach widely used is the non-linear stiffness model recommended in the SNAME (1994) procedures and based on the findings described by Osborne *et al.* (1991). Using the yield surface principle, a locus of vertical, moment and horizontal forces define a boundary at which loads can be applied without significant penetration of the footing. The size of this surface is fixed and relates to the vertical pre-load value. Within this surface a pseudo-elastic stiffness is assumed, with the rotational stiffness non-linearly reduced from its original elastic stiffness according to how close the load combination is to the yield surface. For spudcans on sand the horizontal elastic stiffness is also reduced. Hoyle and Snell (1997), for example, implemented this model; however, it does not account for any work-hardening of the soil with stiffness reducing to zero at the yield surface boundary. Furthermore, cross coupling effects are not implemented.

Manuel and Cornell (1996) compared the sensitivity of the dynamic response statistics at two sea-states to different support modelling conditions: pinned, fixed, linear springs, and a non-linear rotational spring model based on two parameters fitting a non-linear curve (the horizontal and vertical springs were still linear). They noted that not only were there large differences in the response extremes, but also that the model employed at the soil/structural

interface significantly affected the root-mean-squared (rms) response statistics (six samples were taken for a duration of 0.57 hours each). Manuel and Cornell concluded that the stiffer foundation models, whilst predicting smaller rms response, exhibited more non-Gaussian behaviour due to smaller dynamic forcing components (*i.e.* with more foundation fixity the natural period of the structure moved away from the peak period of the two sea-states investigated).

The use of strain-hardening plasticity theory has emerged as the best approach to model soil behaviour with a methodology amenable to numerical analysis. This is because the response of the foundation is expressed purely in terms of force resultants. Though first used as a geotechnical solution to another problem by Roscoe and Schofield (1956), it has recently been used in the examination of jack-up performance (for instance by Schotman (1989), Martin (1994) and Thompson (1996)).

2.2.5 Overall Jack-Up Analysis – A Summary of Models Used

Table 2.1 details the level of complexity used in the analysis of jack-up response in a representative set of studies published in the last fifteen years, with the four areas previously highlighted as conventionally conservative broken into components of increasing degrees of sophistication (and accuracy). This table demonstrates the considerable diversity in the level of complexity used in jack-up analyses with no standard approach dominating. All of the components in Table 2.1 have been assessed for appropriate modelling of the physical processes and graded with a three category system: **a** represents state-of-the-art practice, **b** a compromise solution (adequate under some circumstances) and **g** an inadequate method (which usually produces overly conservative response).

Some general comments on each of the four areas are:

Structural: Most of the studies performed in recent years have implemented structural non-linearities. This is an area where the application of advances in structural theory have been successfully applied to jack-up modelling and techniques have reached a sophisticated level. Other advances, for example plasticity of space frame structures (Al-Bermani and Kitipornchai, 1990) or the use of super finite elements (Lewis *et al.*, 1992) could give more accurate results in a more detailed manner, but without the same high level of accuracy being shown in the other areas, the advantages are ineffectual.

Foundations: Single studies are often complex in one or two of the areas but have the simplest of assumptions in the others. This is especially true for foundation modelling, with many studies using detailed structural models or advanced wave mechanics whilst still using the simplest of foundation assumptions (*i.e.* pinned footings).

Dynamics: Within the published works used in Table 2.1, time domain simulation occurs more often than frequency domain dynamic analysis and can be assumed as the only generally accepted method which captures the non-linear characteristics of a jack-up analysis accurately.

Wave loading: The use of point loads or regular wave theories does not adequately represent wave loading on jack-ups. However, when used, the level of sophistication in random wave loading is highly variable. For example, the number and length of simulations used to estimate response levels differ widely. Most studies use simplifying assumptions due to the extensive computational time needed to perform random time domain simulation properly.

2.3 Overview of JAKUP – The Analysis Program used in Thesis

An overview of the components of the dynamic structural analysis program used in this thesis are described here. Named JAKUP, it is capable of considering the major non-linearities in jack-up response. The initial development of JAKUP was by Martin (1994) and Thompson (1996).¹ Further developments of the foundation and wave models of JAKUP resulting from this thesis are outlined in sections 2.3.3 and 2.3.4.

2.3.1 Dynamic Analysis

To analyse the results of jack-up unit response against time, the dynamic equation of motion must be solved. In this instance this equation can be expressed for a N degree of freedom system as

$$M(t)\ddot{x}(t) + C(t)\dot{x}(t) + K(t)x(t) = P(t) \quad (2.1)$$

where $M(t)$, $C(t)$ and $K(t)$ are the mass, damping and stiffness matrices at time t respectively. $P(t)$ represents the externally applied forces at the nodal positions, and $\ddot{x}(t)$, $\dot{x}(t)$ and $x(t)$ the nodal accelerations, velocities and displacements at time t . As discussed in section 2.2.1, because of the need to model non-linearities, analysis in the time domain using numerical step-by-step direct integration techniques provides the most versatile method to solve Eqn 2.1 (and analyse jack-ups). Within this thesis, the Newmark $\mathbf{b} = 0.25$, $\mathbf{d} = 0.5$ method is used, since it is an unconditionally stable and highly accurate solution algorithm. For further details see Thompson (1996), who reviewed methods for solving the equations of motion in a discretized system.

¹ Martin (1994) initially developed a structural model including his elasto-plastic model for spudcan behaviour on clay (entitled Model B and further detailed in Chapter 3). Thompson (1996) extended JAKUP to consider dynamic behaviour and regular wave loading.

2.3.2 The Structural Model

For the modelling of jack-up response, structural non-linearities must be considered if reasonable accuracy is to be achieved. Euler and $P-\Delta$ effects are both accounted for in JAKUP by using Oran's (1973[a]) formulation of beam column theory to specify the stiffness matrix. The load-deflection path is traced according to Kassimali (1983), except the consideration of plastic hinge formation has not been implemented. Further modifications to produce the additional end rotations on the beam due to the presence of shear are also implemented (Martin, 1994). Both the mass and damping matrix of Eqn 2.1 are time invariant with the former derived as a consistent mass matrix using cubic Hermitian polynomial shape functions and the latter by use of Rayleigh damping. Structural damping coefficients are defined for the lowest two modes, *i.e.* surge and sway in a jack-up. This creates artificially high damping in the higher modes. Implementation of the structural model of JAKUP was performed by Martin (1994) and Thompson (1996), where further details of the formulations can be found.

2.3.3 The Foundation Model

JAKUP has the capabilities of modelling pinned, fixed or linear springs as the foundations of the jack-up. Furthermore, a strain hardening plasticity model for spudcan footings on dense sand has been developed and its numerical formulation implemented into JAKUP. This is discussed in Chapters 3 and 4.

2.3.4 Environmental Loading Models

2.3.4.1 Wave Loading

Linear NewWave theory, second-order NewWave formulations, Constrained NewWave and a method for full random wave analysis have been implemented in JAKUP to evaluate surface elevations and wave kinematics, as is described in Chapters 5 and 6. JAKUP then

uses the extended Morison equation to calculate the hydrodynamic loads on the jack-up legs. As used here to calculate the horizontal loads on the vertical member, the equation consists of a drag and an inertia component and incorporates current and relative motion between the structure and the fluid. The horizontal force per unit length on the member can be expressed as

$$F(x, z, t) = \frac{1}{2} C_d \rho D_h (u_t - \dot{s}) |u_t - \dot{s}| + C_m \rho A_h \dot{u} - (C_m - 1) \rho A_h \ddot{s} \quad (2.2)$$

where D_h and A_h are the hydrodynamic cross sectional diameter and area respectively, u_t the velocity vector sum of current and wave resolved normal to the members axis, \dot{u} the acceleration of the wave and \dot{s} and \ddot{s} the structural velocity and acceleration respectively at the point with horizontal position x and vertical elevation z . C_d and C_m are the drag and inertia coefficients respectively. The drag term is entirely empirical and is due to vortices created as flow passes the member, while the inertia term is due to the pressure gradient in an accelerating fluid.

In a number of jack-up studies, the relative motion between the structure and the water is considered, either explicitly in the relative Morison formulation (Kjeø *et al.*, 1989; Chen *et al.*, 1990; Karunakaran *et al.*, 1992; Manuel and Cornell, 1996) or as additional hydrodynamic damping combined with the structural damping in the dynamic analysis (Carlsen *et al.*, 1986). Chen *et al.* (1990) and Manuel and Cornell (1996) have shown that significantly larger response is predicted if relative velocity effects are ignored (*i.e.* there is an absence of hydrodynamic damping). This difference may be as much as 40% in the root-mean-squared (rms) levels of response under random loading (Manuel and Cornell, 1996). However, because the relative Morison formulation predicts stronger non-Gaussian behaviour, this difference is not as large for extreme response estimates.

Details of the formulation of the relative motion Morison equation in JAKUP can be found in Thompson (1996). Horizontal particle kinematics are calculated at the undeflected beam position, with the equivalent nodal load, P_{ij} , found by integrating the distributed load with the corresponding shape function:

$$P_{ij} = \int_{length} \mathbf{y}_{ij}(z) F(x, z, t) dz. \quad (2.3)$$

$\mathbf{y}_{ij}(z)$ is the shape function evaluated at elevation z . In Thompson (1996), seven point Gauss integration was used. However, the number of Gauss points is now user-defined for each member, allowing more accurate measurement of kinematics, especially close to the free surface.

2.3.4.2 Wind Loading

Wind loads on the hull make up a small but nevertheless significant proportion of the loading on a jack-up (Vugts, 1990; Patel, 1989). Wind forces acting on the jack-up hull are applied as constant point loads at the relevant nodes within a JAKUP numerical analysis. However, wind loading on the exposed surface of the jack-up legs was not deemed necessary. More details of wind force values are given when used in Chapter 6 and 7.

2.4 Example Structure used in Analyses

Fig. 2.1 shows a schematic diagram of the idealised plane frame jack-up used in all analyses in this thesis. The mean water depth was assumed to be 90 m with the rig size typical of a three-legged jack-up used in harsh North Sea conditions. Fig. 2.1 represents an equivalent beam model, with the corresponding stiffnesses and masses of the beams shown. The hull is also represented as a beam element with a rigid leg/hull connection. Though non-linearities in the leg/hull jack houses are recognised as significant (Grundlehner, 1989;

Spidsøe and Karunakaran, 1993), they were not included in the analyses. Example structural node locations on the legs are shown in Fig. 2.1.

The hydrodynamic modelling of the leg is performed by idealising the detailed lattice leg to comprise one “equivalent” vertical tubular section located at the geometric centroid of the actual leg according to the SNAME procedures (1994). The detailed leg section used is one described by Nielsen *et al.* (1994) and is shown in Fig. 2.2. Table 2.2 represents the calculation procedure used to determine the equivalent hydrodynamic diameter D_{Eh} and the equivalent area A_{Eh} , with values calculated as 8.50 m and 3.66 m² respectively. A marine growth of 10 mm on all members has been assumed, similar to growths used in other jack-up studies. Recently, Hoyle and Snell (1997) used 25 mm and Karunakaran (1993) between 10 and 40 mm depending on depth. Hydrodynamic coefficient values for tubular sections of $C_d = 1.1$ and $C_m = 2.0$ are utilised.² Use of the equivalent leg members assumes that no shielding or blockage occurs.

² There is considerable uncertainty in the C_d and C_m values appropriate for the calculation of leg forces offshore, with many values in publication. As the coefficients need to be empirically derived, they are based on the analysis of both the measurement of force and of the kinematics. Uncertainty in the kinematics is one reason for many different results found in different investigations of force coefficients (Vugts, 1990). When choosing coefficients, the parameters to be considered are the Keulegan-Carpenter and Reynolds numbers and the relative roughness. Consideration must also be given to the wave model being used. For extreme response analysis of jack-ups, post-critical Reynold numbers ($1.0 \times 10^6 - 4.5 \times 10^6$) and high Keulegan-Carpenter numbers are expected (SNAME, 1994); however, the amount of roughness is uncertain. The values chosen here reflect recommended values in SNAME for tubular sections (for rough sections $C_d = 1.0$ and $C_m = 1.8$ and for smooth $C_d = 0.7$ and $C_m = 2.0$). In a joint industry project led by Shell Offshore Inc., forcing coefficients were obtained using a one meter diameter instrumented cylinder (Rodenburg and Kallstrom, 1986). Reynolds numbers greater than 10^6 , as well as forced oscillations and random waves, were studied. For high Keulegan-Carpenter numbers, C_d values approached 1.2 and 0.7 for rough and smooth cylinders respectively. Tromans *et al.* use coefficients detailed by Rodenburg (1986) with the NewWave model with values of $C_d = 0.63$ and 1.17 for smooth and rough cylinders respectively and a C_m of 1.8. Other values used in published studies of jack-ups include Løseth and Hague (1992) $C_d = 1.0$ and $C_m = 1.75$ and Karunakaran (1993) $C_d = 1.0$ and $C_m = 2.0$.

Chapter 3 - Strain Hardening Plasticity Model for Spudcans on Dense Sand

3.1 Introduction

In this chapter an incremental work hardening plasticity model (Model C) is described. It has been developed for flat circular footings on dense sand subjected to a combination of vertical, moment and horizontal loading (V , M , H). Model C is based on a series of experimental tests performed at the University of Oxford by Gottardi and Houlsby (1995). Circular footings are representative of spudcans, typical pad footings found on jack-up drilling platforms. A description of the incorporation of the conical features of spudcan footings into Model C is presented in Chapter 4. The model follows “Model B” described by Martin (1994) for spudcans on clay.

3.2 Literature Review

3.2.1 Introduction - Combined Loading on Foundations

Bearing capacity methods have been commonly used to calculate the ultimate capacity of spudcan footings under combined loading, with failure evaluated from inclined and eccentric load conditions. Recently a number of experimentally based studies have led to the development of an alternative to bearing capacity methods for foundations subjected to combined loads. These studies have led to the development of complete plasticity models to replace bearing capacity factors.

3.2.2 Traditional Bearing Capacity Theories

In the offshore industry, the calculation of the bearing capacity of foundations on frictional material generally uses procedures described by Meyerhof (1951, 1953), Brinch Hansen (1961, 1970) and Vesic (1975). For a surface strip footing, the maximum vertical bearing capacity is calculated as

$$V_{peak} = 0.5\mathbf{g}'BN_{\mathbf{g}}A \quad (3.1)$$

where \mathbf{g}' is the submerged unit weight of the soil, B and A the width and plan area of the footing respectively, and $N_{\mathbf{g}}$ the bearing capacity factor.

In the application of these procedures to jack-ups, the vertical capacity is reduced by the assumption that a spudcan behaves as a flat circular footing. A shape factor is applied and usually takes the value of $s_{\mathbf{g}} = 0.6$. Furthermore, it is well known that the bearing capacity of a foundation subjected to pure vertical load is reduced when concurrent horizontal and/or moment loads are applied. In a calm sea vertical self-weight is the sole load on the foundations of a jack-up. During a storm, however, environmental forces impose horizontal and moment loads onto the foundations.

Meyerhof (1953) proposed that inclination factors be used to scale the reduction of vertical bearing capacity caused by simultaneous horizontal loading, as shown in Fig. 3.1(a). Applying the same shape factors as for the pure vertical loading, for a circular footing of radius R , the bearing capacity becomes

$$V_{peak} = 0.5s_{\mathbf{g}}i_{\mathbf{g}}\mathbf{g}'(2R)N_{\mathbf{g}}A \quad (3.2)$$

where $i_{\mathbf{g}}$ is the inclination factor defined, for a soil of friction angle \mathbf{f} , as

$$i_g = \left(1 - \frac{\Omega}{F}\right)^2 \quad \text{and} \quad \Omega = \tan^{-1}\left(\frac{H}{V}\right). \quad (3.3a)$$

Brinch Hansen (1963, 1970) retained Meyerhof's basic approach, but defined the inclination factor in terms of a ratio of horizontal to vertical load, unconditional on soil properties:

$$i_g = \left(1 - 0.7 \frac{H}{V}\right)^5. \quad (3.3b)$$

For eccentric loading as shown in Fig. 3.1(b), Meyerhof (1953) suggested that for calculating bearing capacities an "effective area" concept should be used. The load carrying contact area, and thus the bearing capacity, is reduced such that the centroid of the effective area coincides with the applied vertical load. For a strip footing Meyerhof defined the effective width as $B_e = B - 2e$, where e is the eccentricity of the applied load as depicted in Fig. 3.2(a). For circular footings he did not specify a B_e value explicitly, only drawing the effective area graphically (Fig. 3.2(b)). Brinch Hansen (1970) retains this effective area approach, as does Vesic (1975), although modifying the area capable of carrying load for circular footings to be as shown in Fig. 3.3. The American Petroleum Institute (API, 1993) recommends procedures for determining the effective foundation dimensions as

$$A' = B'L' = \pi R^2 - 2e\sqrt{R^2 - e^2} - 2R^2 \sin^{-1}\left(\frac{e}{R}\right) \quad \text{and}$$

$$\frac{L'}{B'} = \sqrt{\frac{R+e}{R-e}}. \quad (3.4)$$

A locus of limiting behaviour can be established in $V:M:H$ space by combining these three empirical formulations, *i.e.* vertical, eccentric and inclined loading. "Failure" is predicted

for any foundation design load state exceeding this capacity criterion. If the maximum vertical load is defined as the pure vertical bearing capacity, $V_{peak} = 0.5s_g g' 2RN_g A$, and assuming the moment load $M = Ve$, the failure interaction surfaces can be derived as

$$\frac{V}{V_{peak}} = \frac{1}{0.6} \frac{A'B'}{A2R} \left(1 - 0.4 \left(1 - 0.7 \frac{H}{V} \right)^5 \frac{B'}{L'} \right) \left(1 - 0.7 \frac{H}{V} \right)^5 \quad (\text{Brinch Hansen, 1970}) \quad (3.5a)$$

$$\frac{V}{V_{peak}} = \frac{A'B'}{A2R} \left(\frac{1 + 0.1 \tan^2(45^\circ + \mathbf{f}/2)(B'/L')}{1 + 0.1 \tan^2(45^\circ + \mathbf{f}/2)} \right) \left(1 - \frac{\tan^{-1}(H/V)}{\mathbf{f}} \right)^2.$$

(Meyerhof, 1953) (3.5b)

In the derivation of these failure surfaces, the shape factors defined by Brinch Hansen and Meyerhof have been used:

$$s_g = 1 - 0.4i_g(B'/L') \quad (\text{Brinch Hansen, 1970}) \quad (3.6a)$$

$$s_g = 1 + 0.1 \tan^2(45^\circ + \mathbf{f}/2)(B'/L'). \quad (\text{Meyerhof, 1953}) \quad (3.6b)$$

Fig. 3.4 shows both Brinch Hansen and Meyerhof curves for a typical sand (for this example $\mathbf{f} = 43^\circ$), with all loads normalised by the maximum vertical load V_{peak} . Figs 3.4(a) and (b), represent planar cuts through the three dimensional surfaces along the V/V_{peak} axes under the conditions $M = 0$ and $H = 0$ respectively, whereas Fig. 3.4(c) shows the shape in the $M/2RV_{peak} : H/V_{peak}$ plane at three V/V_{peak} load levels.

In the $H/V_{peak} : V/V_{peak}$ plane, both Brinch Hansen's and Meyerhof's curves are parabolic in shape, starting with no horizontal and vertical load, *i.e.* $H/V_{peak} = 0$ and $V/V_{peak} = 0$,

and finishing at $H/V_{peak} = 0$ and $V/V_{peak} = 1$. Both are skewed with peak horizontal load values occurring at $V/V_{peak} < 0.5$. Fig. 3.4(b) shows that both curves are skewed parabolic in shape in the $M/(2RV_{peak}) : V/V_{peak}$ plane, with a maximum moment occurring at $V/V_{peak} < 0.5$. This is a similar result to Fig. 3.4(a). The yield loci defined from Meyerhof's and Brinch Hansen's theories are considered conservative compared with existing experimental evidence for strip and circular footings (Dean *et al.*, 1993). Comparisons with the experimental results of Gottardi and Houlsby (1995) will be described in section 3.3.5.

Moment can be developed on a footing with either positive or negative eccentricity, as depicted in Fig. 3.5. In Fig. 3.4(c) quadrant (A) represents positive eccentricity and (B) negative. For the analysis of jack-up platforms, the expectation is that the largest loading on the foundations would be with positive eccentricity. Nonetheless, it is important in the development of a model to consider all (V, M, H) load cases. Meyerhof commented on the differences between the two cases, but only developed a solution for the positive case, with no indication of a procedure to solve for negative eccentricity. Zaharescu (1961) made a detailed investigation of the difference between negative and positive eccentricity, using a flat strip footing on sand. He found that there is a larger moment capacity in the negative eccentricity case for the same H and V loading. Despite this finding, Brinch Hansen and Vesic retained Meyerhof's approach, and their results are based only on positive eccentricity. This is illustrated in Fig. 3.4(c) where the capacity is assumed symmetric for both negative moment and horizontal load, contrary to Zaharescu's findings.

3.2.3 Alternative Yield Surface Loci

As an alternative failure envelope in the $V:M:H$ plane, Butterfield and Ticof (1979) suggested for strip footings on sand a yield surface parabolic along the V axis, but elliptical

perpendicular to it. Fig. 3.6 shows their surface, which they described as “cigar-shaped”. The surface was based solely on the interpretation of a large number of load controlled tests, not relying on any empirical bearing capacity formula. Butterfield and Ticoft recommended that the size of their yield surface be determined by fixed dimensionless peak loads, with values $M / BV_0 \approx 0.1$ and $H/V_0 \approx 0.12$, where V_0 is the maximum vertical load experienced. The surface is symmetric about all axes and peaks at $V/V_0 = 0.5$. Nova and Montrasio (1991) gave additional verification of this surface as a good description of combined load bearing capacity for surface strip footings on sand.

Research performed at Cambridge University has also shown the cigar-shaped surface suitable for modelling the combined load bearing capacity of conical and spudcan footings on sand. This work was co-ordinated by Noble Denton and Associates (1987) and is also summarised by Dean *et al.* (1993). For this surface the peak loads were retained at $V/V_0 = 0.5$, but values of $M/2RV_0 = 0.0875$ and $H/V_0 = 0.14$ were suggested. (Note: for conical footings, compared with strip footings, $2R$ replaces B .)

3.2.4 Concluding Remarks - Combined Loading on Foundations

The bearing capacity formulations and yield surface loci described in sections 3.2.2 and 3.2.3 have been developed empirically and verified experimentally in sand mainly for strip and square footings, with only a small number of experiments on circular footings or actual spudcans. The original intended use was for onshore conventional shallow foundation designs, where horizontal loads and moment are relatively small when compared with vertical load. These formulae have been adequate, though usually overly conservative for predicting failure under combined loads, but because of their empirical nature they cannot be applied within numerical analysis.

3.2.5 Use of Plasticity Theory for Combined Loading of Offshore Foundations

Recent research has not used the procedures of conventional bearing capacity factors but has relied on the interpretation of experimental data in terms of the concepts of plasticity theory. The exploration of the shape of the yield surface within three dimensional space ($V:M:H$) allows for consistent procedures amenable to numerical analysis. This approach was pioneered by Roscoe and Schofield (1956) when they discussed the design of short pier foundations in sand in terms of the plastic moment resistance of the footing in $M:V$ space.

Schotman (1989) was first in describing a complete non-linear spudcan foundation load:displacement model which he implemented into a relatively simple structural analysis of a jack-up. The model was framed within plasticity theory in ($V:M:H$) load space, though it still relied heavily on numerous empirical assumptions. For instance, the yield surface shape was not defined experimentally, but was a limiting condition of empirical vertical bearing capacity formula. The elasticity constants and plastic potential were calibrated using limited finite element analysis. By factoring the environmental load, Schotman investigated the load distribution between the footings when yield occurs, as well as its effect on structural stability. Loading was applied as a point load at a set location on each leg.

Tan (1990) made a detailed investigation of the $H:V$ yield loci for various conical and spudcan footings on saturated sand. His physical model tests were performed in a geotechnical centrifuge at Cambridge University. Tan found that for spudcan footings on sand, the $H:V$ yield locus was not symmetric about $V/V_0 = 0.5$, and suggested that the peak horizontal load occurred at about $V/V_0 \approx 0.4$. Although Tan did not develop a full

plasticity model, he did combine his yield locus and plastic potential with theoretical elasticity behaviour and a semi-empirical hardening law based on bearing capacity theory. The resulting model was verified with retrospective simulation of both load and displacement controlled tests. Though Tan modelled experimental data with an incremental plasticity method, it was in two dimensional $H:V$ space with no moment component.

Martin (1994) investigated spudcan footing behaviour on cohesive soil with a programme of physical model tests involving combined loading on reconstituted speswhite kaolin. The test results were interpreted and theoretically modelled in terms of a work hardening plasticity theory in three dimensions, which was named Model B. Martin used theoretical stiffness factors to define elastic behaviour, and theoretical lower bound bearing capacity solutions to define vertical bearing capacity with vertical penetration. He found from his physical experiments on clay that the general shape of the $V:M/2R:H$ yield surface remained constant while expanding with increased penetration. This allowed the definition of the yield surface to be normalised in one expression by V_0 , the pure vertical load capacity at any depth. A modified cigar-shaped yield surface similar to Butterfield and Ticof (1979) was used.

Martin (1994) found that the shape of the yield surface could be modelled as roughly parabolic in the $H/V_0 = 0$ and $M/2RV_0 = 0$ planes, with adjustments made to the curvature at relatively high and low stresses. The surface was found to be elliptical in the plane of constant V/V_0 , with a rotation such that the major and minor axes of the ellipse do not coincide with the H/V_0 and $M/2RV_0$ co-ordinate axes. Gottardi and Butterfield (1993) also found this to be the case for their tests on surface strip footings on dense sand. Their study concentrated on a load level of $V/V_0 = 0.5$. However, in contradiction to Gottardi and Butterfield, Martin found that for a spudcan footing (rather than a flat footing)

the yield surface had a positive eccentricity. This implies that the maximum horizontal and moment capacity occurs in the positive quadrants in $M/2RV_0 : H/V_0$ space. Gottardi and Butterfield's study confirmed Zaharescu's (1961) observation that maximum moment capacity occurs with negative eccentricity. Martin attributed the difference in Model B to the use of spudcans with an angular underside profile rather than a flat footing.

3.3 Development of Model C

3.3.1 Introduction to Experimental Tests and Data

The combined loading of a footing results in a complex state of stresses in the underlying soil. By expressing the response of the footing purely in terms of force resultants (V, M, H) the model defined can be coupled directly to a numerical analysis of a structure. Fig. 3.7 outlines the positive directions of force resultants, (V, M, H) and the corresponding displacements (w, \mathbf{q}, u), with directions and notations for the combined loading problem as recommended by Butterfield *et al.* (1997). For dimensional consistency, the model will be formulated with moment and rotation described as $M/2R$ and $2R\mathbf{q}$ respectively.

The numerical model described in this chapter is based on a series of 29 loading tests performed by Gottardi and Houlsby (1995) on a rough, rigid, flat circular footing resting on dry, dense Yellow Leighton-Buzzard sand. The tests were carried out using the displacement controlled load cell device designed and constructed by Martin (1994) and located in the University of Oxford laboratory. The footings were subjected to a variety of vertical translations, horizontal translations and rotation combinations with the corresponding loads being measured. By varying the applied displacement path, the load:displacement behaviour of a strain hardening plasticity model could be investigated

and theoretically modelled. The major components of a strain hardening plasticity model are:

- An empirical expression for the yield surface in $(V, M/2R, H)$ space. This failure envelope represents a yield locus defining permissible load states.
- A strain hardening expression to define the variation of vertical load with vertical displacement. The yield surface expands and contracts with vertical plastic penetration and plastic heave respectively, with its size determined by V_0 , the vertical load capacity.
- A suitable flow rule to allow predictions of the footing displacements during yield.
- A model for elastic load:displacement behaviour within the yield surface.

To develop these components, the experimental displacement paths required were as follows, with the expected load path directions depicted in Fig. 3.8:

- *Swipe Tests.* The footing is subjected to a horizontal displacement or rotation after being penetrated vertically to a prescribed level, in this case $V = 1600$ N. The load path followed can be assumed to be a track of the yield surface appropriate to that penetration. Tan (1990) first argued this assumption when he made his detailed investigation of the $(H:V)$ yield loci for various conical and spudcan footings on saturated sand. Investigation of the yield surface at low stress is achieved by vertically loading to the same vertical penetration then unloading to a low stress, in this case $V = 200$ N before making a swipe. The swipe tests could be thought of as constant vertical penetration tests.
- *Constant V Tests.* Similar to a swipe test except rather than holding the vertical penetration constant, the vertical load is fixed while the footing is driven horizontally and/or rotated. According to plasticity theory, the yield surface should expand or

contract according to the strain hardening relationship, with the tests providing information on the load:displacement relationship (flow rule) at yield.

- *Radial Displacement Tests.* Straight paths of different combinations of vertical, horizontal and rotational displacements are applied to the footing to provide information about the hardening law and flow rule. Vertical loading tests, where the footing is purely penetrated in the vertical direction, are one specific example; these can be used to deduce a vertical strain hardening law.
- *Elastic Stiffness Tests.* Though the elastic stiffness matrix may be derived using numerical methods (for example, finite element analysis of a footing), experimental footing tests with small excursions in all three directions, after unloading from a prescribed vertical load, can be used to establish approximate elastic stiffness coefficients. With these the validity of any numerical selections can be determined.

3.3.2 Elastic Response: Choice of an Elastic Stiffness Matrix

Elastic response of the soil needs to be defined for any increments within the yield surface, with existing theoretical and numerical elastic solutions considered for use in Model C.

The American Petroleum Institute (API) (1993) has recommended elastic solutions for rigid circular footings on the surface of a homogeneous elastic half space subjected to vertical, horizontal or moment loads. These closed form solutions are referenced in Poulos and Davis (1974) and can be written in uncoupled matrix form as

$$\begin{pmatrix} V \\ M/R \\ H \end{pmatrix} = \begin{bmatrix} \frac{4GR}{1-\mathbf{n}} & 0 & 0 \\ 0 & \frac{8GR}{3(1-\mathbf{n})} & 0 \\ 0 & 0 & \frac{32GR(1-\mathbf{n})}{7-8\mathbf{n}} \end{bmatrix} \begin{pmatrix} w \\ R\mathbf{q} \\ u \end{pmatrix} \quad (3.7)$$

where G and \boldsymbol{n} are the shear modulus and Poisson ratio of the soil respectively. The terms were derived with contradictory assumptions, with the vertical and moment solutions developed for smooth footings while the horizontal term assumed a rough footing with no vertical deflections. Bell (1991) showed that these solutions are exact only for incompressible soils ($\boldsymbol{n} = 0.5$). For these soils the smooth and rough cases equate and cross coupling does not exist. However, as most sands have $\boldsymbol{n} < 0.5$, the API recommendations are imprecise for use in the analysis of jack-up foundations.

In response to limited consistent information on the elastic response of flat circular footings, Bell (1991) conducted extensive research using finite element methods. He investigated the effects of footing embedment for a full range of Poisson ratios concluding that vertical, rotational and horizontal stiffness increase with depth of penetration. His work also showed that cross coupling between the horizontal and rotational footing displacements is important. Bell expressed this mathematically as

$$\begin{pmatrix} V \\ M/2R \\ H \end{pmatrix} = 2GR \begin{bmatrix} k_1 & 0 & 0 \\ 0 & k_2 & k_4 \\ 0 & k_4 & k_3 \end{bmatrix} \begin{pmatrix} w \\ 2R\boldsymbol{q} \\ u \end{pmatrix} \quad (3.8)$$

and set out tabulated values of $k_1 \dots k_4$ for flat footings. As footings on dense sand are usually considered as shallow footings, the results for the surface condition can be assumed, allowing for constant k values. For elastic behaviour within the yield surface in Model C, Bell's results for $\boldsymbol{n} = 0.2$ were used,¹ with the values as follows:

$$k_1 = 2.65; \quad k_2 = 0.46; \quad k_3 = 2.30; \quad k_4 = -0.14.$$

¹ Lade (1977) found that a Poisson's ratio of 0.2 is appropriate for a wide range of sands.

These stiffness coefficients have been adjusted for rotations normalised by $2R$ rather than R as in Bell's thesis. Ngo-Tran (1996) furthered Bell's finite element investigation deriving factors for Eqn 3.8, considering the effects of the cone angle of conical footings, footing penetration, and Poisson's ratio.

The elastic stiffness tests and the vertical unload-reload loops provide information on the stiffness coefficients observed during Gottardi and Houlsby's (1995) experiments. Vertical unload and reload loops were performed nine times on the vertical load tests, as shown in Fig. 3.9, and seventeen times in the pre-peak region of the swipe and vertical load tests. Though non-linear behaviour was observed, by averaging the unload section of the loops, the vertical stiffness can be estimated as $K_v = 14.93$ kN/mm. A large scatter in elastic stiffness was observed, with a normal standard deviation for the 26 tests of 3.5 kN/mm. Horizontal and moment elastic stiffness were estimated from the elastic stiffness tests. The values were calculated as $K_h = 1.85$ and $K_m = 0.54$ kN/mm respectively. However, as only two pilot elasticity tests and one fully successful test were performed, and given the scatter seen in the vertical case, some doubt should be cast over these results. In the horizontal and moment excursions cross coupling was evident, with rotation about the axis normal to the direction of the horizontal load observed, and similarly, horizontal displacements during moment loading. It is of interest to note that small amounts of positive vertical displacements were recorded throughout the duration of these excursions, suggesting the existence of plastic behaviour within a region that will be theoretically modelled as fully elastic.

3.3.3 Development of a Strain Hardening Law

The following empirical formula defines the vertical bearing capacity with plastic embedment (w_p):

$$V_0 = \frac{k w_p}{1 + \left(\frac{k w_{pm}}{V_{0m}} - 2 \left(\frac{w_p}{w_{pm}} \right) + \left(\frac{w_p}{w_{pm}} \right)^2 \right)} \quad (3.9)$$

where k is the initial plastic stiffness, V_{0m} is the peak value of V_0 , and w_{pm} the value of plastic vertical penetration at this peak. This formula was developed as a closed form solution to fit the data from two vertical load tests by Gottardi *et al.* (1997). However, by extending the fit to all the vertical load tests, and minimising the error squared between the experimental and theoretical values, the parameters have been defined as

$$k = 2175 \text{ N/mm}; \quad V_{0m} = 2050 \text{ N}; \quad w_{pm} = 3.16 \text{ mm}$$

with the best fit shown in Fig. 3.9.

A formula that models post-peak work softening as well as pre-peak performance was essential, however, Eqn 3.9 unrealistically implies $V_0 \rightarrow 0$ as $w_p \rightarrow \infty$. Therefore, it can only be used for a limited range of penetrations. For jack-ups in dense sand, loading post-peak would not be expected; however, for a complete foundation model, Eqn 3.9 can be altered to

$$V_0 = \frac{k w_p + \left(\frac{f_p}{1 - f_p} \right) \left(\frac{w_p}{w_{pm}} \right)^2 V_{0m}}{1 + \left(\frac{k w_{pm}}{V_{0m}} - 2 \left(\frac{w_p}{w_{pm}} \right) + \left(\frac{1}{1 - f_p} \right) \left(\frac{w_p}{w_{pm}} \right)^2 \right)} \quad (3.10)$$

where f_p is a dimensionless constant that describes the limiting magnitude of vertical load as a proportion of V_{0m} (i.e. $V_0 \rightarrow f_p V_{0m}$ as $w_p \rightarrow \infty$ (see Fig. 3.10)). It is possible to use the same parametric values of k , V_{0m} and w_{pm} in Eqn 3.10.

3.3.4 Development of a Three-Dimensional Normalised Yield Surface

The swipe test load paths are used to determine a three-dimensional yield surface with loads normalised by V_0 , the ultimate bearing capacity. All swipe tests outlined in Gottardi and Houlsby (1995) are used, with Fig. 3.11 showing the basic shape mapped out in the deviatoric/normal planes ($H/V_0 : V/V_0$ and $M/2RV_0 : V/V_0$). Initially V_0 has been assumed as the vertical load at the start of the swipe, therefore all tests begin at $V/V_0 = 1$. However, the load paths of the swipe tests do not follow a yield surface of constant V_0 ; with a steady increase in vertical plastic penetration, slight expansion of the yield surface occurs. This penetration is partly the result of elasticity in the soil, but more importantly, due to a testing rig of finite stiffness. Therefore, as the vertical load reduces during the course of the swipe, by calculating the additional plastic penetration due to the rig stiffness, a correction to V_0 can be computed using the theoretical hardening law. This can be explained in more detail using Fig. 3.12, noting that plastic vertical displacements have been already evaluated by subtracting the theoretical elastic component from the experimental results according to Eqn 3.8. At the commencement of the swipe, V_{0start} is known and w_{pstart} can be calculated by solving the quadratic equation

$$\left(\frac{w_{pstart}}{w_{pm}} \right)^2 \left(\frac{1 - f_p (V_{0m}/V_{0start})}{1 - f_p} \right) + \left(\frac{k}{V_{0m}} - \frac{k}{V_{0start}} - \frac{2}{w_{pm}} \right) w_{pstart} + 1 = 0 \quad (3.11)$$

which has been formulated by rearranging the hardening law of Eqn 3.10. As all swipes started on the rising section of the hardening curve, the lower root of Eqn 3.11 is the solution for w_{pstart} . For each experimental data point, the vertical load V_{exp} and the experimental penetration w_{pexp} are known, with the theoretical yield surface size $V_{0theory}$ and its corresponding theoretical plastic penetration $w_{ptheory}$ requiring evaluation. As depicted in Fig. 3.12, $w_{ptheory}$ may be written as

$$w_{ptheory} = w_{pstart} + dw_p + \frac{V_{0theory} - V_{exp}}{K_v} \quad (3.12)$$

where $K_v = 14.93$ kN/mm as evaluated by using the vertical unload-reload loops. By substituting $w_{ptheory}$ into Eqn 3.11, a solution for $V_{0theory}$ can be evaluated, thus determining the theoretical size of the yield surface at that experimental point.

The shape of the yield surface in the $M/2RV_0 : H/V_0$ plane is difficult to visualise from Fig. 3.11. However, by taking the yield points at varying V/V_0 positions and plotting them in the π plane ($M/2RV_0 : H/V_0$), as in Fig. 3.13, a clearer picture can be seen. The yield points map out a parabolic section in the deviatoric/normal planes (Fig. 3.11) and a rotated elliptical section in the π plane, as shown in Fig. 3.13 by the highlighted $V/V_0 = 0.2, 0.5$ and 0.8 values. The cigar-shaped yield surface as used by Houlsby and Martin (1992) and Gottardi *et al.* (1997) is a good first estimate of the basic shapes presented in Figs 3.11 and 3.13, and can be written as

$$f = \left(\frac{H}{h_0 V_0} \right)^2 + \left(\frac{M/2R}{m_0 V_0} \right)^2 - \frac{2aH M/2R}{h_0 m_0 V_0^2} - 16 \left(\frac{V}{V_0} \right)^2 \left(1 - \frac{V}{V_0} \right)^2 = 0. \quad (3.13)$$

The first three terms (the H and $M/2R$ terms), for constant V/V_0 values, map out a rotated ellipse in the π plane whilst the fourth term (the V term) represents the parabolic section in the deviatoric/normal planes. The parameters h_0 and m_0 are the intercepts of the ellipse with the respective co-ordinate axes, whilst a determines the eccentricity of the ellipse.

Eqn 3.13 incorrectly predicts a peak at $V/V_0 = 0.5$, which can be seen in Fig. 3.14 to be an overestimate. In Fig. 3.14 the force relationships in the $H/V_0 : V/V_0$ and the $M/2RV_0 : V/V_0$ planes have been collapsed onto a single plane by defining a general deviator force as

$$Q^2 = \left(\frac{H}{h_0}\right)^2 + \left(\frac{M/2R}{m_0}\right)^2 - \frac{2aH M/2R}{h_0 m_0}. \quad (3.14)$$

Additionally, the theoretical curve underestimates the yield surface location at both low and high stress levels ($V/V_0 < 0.3$ and $V/V_0 > 0.8$). A correction needs to be introduced to yield surface Eqn 3.13 to account for both of these features.

While investigating the interaction diagram for strip footings on sand, Nova and Montrasio (1991) used a modified parabola of the form

$$\frac{H_{Inter}}{V_0} = \mathbf{m} \frac{V}{V_0} \left(1 - \frac{V}{V_0}\right)^{\mathbf{b}} \quad (3.15)$$

where H_{Inter} is the intercept of the ellipse on the H co-ordinate axis and \mathbf{m} scales the magnitude of the peak load. Nova and Montrasio noted that with $\mathbf{b} = 0.95$ an improved fit of their data occurred. The choice of \mathbf{b} controls the vertical load level at which the peak

horizontal load occurs, and in this form, with $\mathbf{b} < 1$, the peak horizontal load shifts to a vertical load value of $V/V_0 > 0.5$. In addition, with $\mathbf{b} < 1$, the tip of the parabola is rounded off, implying the slope at $V/V_0 = 1$ is vertical. This allows differentiation of the yield surface at that point—a numerically desirable condition if associated flow is assumed. The analogous expression in terms of moment is

$$\frac{M_{Inter}}{BV_0} = \mathbf{m}' \frac{V}{V_0} \left(1 - \frac{V}{V_0}\right)^{\mathbf{b}} \quad (3.16)$$

where B is the width of the strip footing. Nova and Montrasio (1991) and Gottardi and Butterfield (1993) both described Eqn 3.16 as a good fit for experimental strip footing data on sand.

As seen in Fig. 3.14, experimental data shows that the peak horizontal and moment loads occur at vertical loads of $V/V_0 < 0.5$. Unfortunately, Eqns 3.15 and 3.16 are only capable of shifting the peak from $V/V_0 = 0.5$ towards $V/V_0 = 1$ if a rounded parabola at $V/V_0 = 1$ is to be maintained. Therefore with only one \mathbf{b} defined, the experimental data cannot be successfully modelled. For the same reason, Martin (1994) in his analysis of combined loading on clay, proposed the introduction of a second \mathbf{b} factor and adjusted \mathbf{m} to preserve the magnitude of the desired peak load. Martin's modifications can be written as

$$\frac{H_{Inter}}{V_0} = h_0 \left[\frac{(\mathbf{b}_1 + \mathbf{b}_2)^{(\mathbf{b}_1 + \mathbf{b}_2)}}{\mathbf{b}_1^{\mathbf{b}_1} \mathbf{b}_2^{\mathbf{b}_2}} \right] \left(\frac{V}{V_0} \right)^{\mathbf{b}_1} \left(1 - \frac{V}{V_0} \right)^{\mathbf{b}_2} \quad (3.17)$$

or

$$\frac{M_{Inter}}{2RV_0} = m_0 \left[\frac{(\mathbf{b}_1 + \mathbf{b}_2)^{(\mathbf{b}_1 + \mathbf{b}_2)}}{\mathbf{b}_1^{\mathbf{b}_1} \mathbf{b}_2^{\mathbf{b}_2}} \right] \left(\frac{V}{V_0} \right)^{\mathbf{b}_1} \left(1 - \frac{V}{V_0} \right)^{\mathbf{b}_2} . \quad (3.18)$$

These expressions allow the peak to be shifted along the V/V_0 by varying the \mathbf{b}_1 and \mathbf{b}_2 values, whilst maintaining the peak horizontal and moment load at h_0V_0 and m_02RV_0 respectively. For the conditions $\mathbf{b}_1 < \mathbf{b}_2 < 1$, the peak horizontal load will occur at $V/V_0 < 0.5$, with the parabola rounded off and differentiable at both $V/V_0 = 0$ and $V/V_0 = 1$.

An expression for the fully normalised $V/V_0 : M/2RV_0 : H/V_0$ yield surface can be obtained by substituting Eqns 3.17 and 3.18, the expressions relating the $V/V_0 : H/V_0$ and $V/V_0 : M/2RV_0$ interaction, into the general elliptical equation relating the $M/2RV_0 : H/V_0$ interaction:

$$f(V, M/2R, H) = \left(\frac{H}{h_0V_0} \right)^2 + \left(\frac{M/2R}{m_0V_0} \right)^2 - \frac{2aHM/2R}{h_0m_0V_0^2} - \left[\frac{(\mathbf{b}_1 + \mathbf{b}_2)^{(\mathbf{b}_1 + \mathbf{b}_2)}}{\mathbf{b}_1^{\mathbf{b}_1} \mathbf{b}_2^{\mathbf{b}_2}} \right]^2 \left(\frac{V}{V_0} \right)^{2\mathbf{b}_1} \left(1 - \frac{V}{V_0} \right)^{2\mathbf{b}_2} = 0. \quad (3.19)$$

This equation defines the yield surface of Model C.

With the yield surface equation defined as $f = 0$, the parametric values of h_0 , m_0 , a , \mathbf{b}_1 and \mathbf{b}_2 were derived to minimise the deviation of experimental $(V, M/2R, H)$ load states from this theoretical surface. A FORTRAN program was written to quantify this deviation for different permutations of the yield surface parameters. A total error value was evaluated as the sum of the theoretical values of f^2 for all the data points equally weighted, for all the swipe tests. As previously outlined, adjustments were made to the experimental values when calculating V_0 to take soil elasticity and rig stiffness into consideration. The minimal

total error was found, establishing the following combination of yield surface parameters as the best fit:

$$h_0 = 0.116; \quad m_0 = 0.086; \quad a = -0.2; \quad \mathbf{b}_1 = 0.9; \quad \mathbf{b}_2 = 0.99 \text{ or } 1.0.$$

The Model C yield surface shape is shown in three-dimensions in Fig. 3.15. The parameter \mathbf{b}_2 could either be defined as 0.99 or 1.0 depending on whether it is essential to have a rounded off yield surface at $V/V_0 = 1$, with little difference in the overall yield surface shape. However, if the differential is not needed to be defined at $V/V_0 = 1$, as is the case when a separate plastic potential is defined, then $\mathbf{b}_2 = 1.0$ allows for a mathematically less complex yield surface expression. The value of $a = -0.2$ implies an anti-clockwise rotation of the axes and agrees with both Zaherescu's (1961) and Gottardi and Butterfield's (1993) observation on sands that the failure locus in the $M/2RV_0 : H/V_0$ plane is not symmetric with respect to the co-ordinate axes but is rotated with a negative sense of eccentricity.

3.3.5 Comparisons with Other Yield Surfaces

In this section comparisons are made between various planar sections of the Model C yield surface (Eqn 3.19) and the predictions of some other yield surfaces described in the literature review. The experimental value of $\mathbf{f} = 43^\circ$ is used in all theoretical formulations.

3.3.5.1 The Deviatoric/Normal Plane ($H/V_0 : V/V_0$, $M/2RV_0 : V/V_0$ or $Q/V_0 : V/V_0$)

Figs 3.16(a) and (b) shows Eqn 3.19 for comparison with the experimental values and also Brinch Hansen's (1970) and Meyerhof's (1953) bearing capacity predictions. The assumption that the peak bearing capacity V_{peak} is equivalent to V_0 is made to determine the

adequacy of the bearing capacity interaction curves as yield surface models. Both in the horizontal and moment directions Eqn 3.19 fits the experimental values consistently well. The maximum size of the yield surface occurs when $V/V_0 = 0.474$, agreeing with Tan's (1990) assessment that the maximum size of the yield surface in the $H:V$ plane occurs at $V/V_0 < 0.5$. For most conditions, Fig. 3.16 confirms that both Meyerhof's and Brinch Hansen's results would be conservative if used as a yield surface in this context. The deviatoric/normal plane of $M/2R = 0$ is an exception, with Fig. 3.16(a) showing that Brinch Hansen's results are not conservative when compared with the Model C surface. Fig. 3.14 compares Eqn 3.19 with the experimental data in the $Q/V_0 : V/V_0$ plane, and shows that the use of the two **b** factors does provide a justifiably better fit, especially at the peak and low load levels.

3.3.5.2 The π Plane ($M/2RV_0 : H/V_0$)

Fig. 3.16(c) shows interaction in the π plane for three representative load levels $V/V_0 = 0.2, 0.5$ and 0.8 , for both Eqn 3.20 and for Brinch Hansen and Meyerhof's solutions. The experimental data points derived from the six sideswipe tests and their reflections have also been plotted and can be seen to fit Eqn 3.19 well, especially for the $V/V_0 = 0.5$ case. Again, it is evident that Brinch Hansen's and Meyerhof's solutions are conservative for all load levels compared to Model C and the experimental data. They are, however, more accurate in the positive quadrants of $M/2RV_0 : H/V_0$ space, an understandable result given that the Brinch Hansen solution is based on positive eccentricities and ignores negative eccentricity loading.

3.3.6 Development of the Plastic Potential

To model load-deflection behaviour, incremental plastic displacements at yield are used to define a suitable flow rule. To achieve this, the displacements were investigated on two planes: the π plane ($M/2RV_0 : H/V_0$) and the deviatoric/normal planes ($H/V_0 : V/V_0$ and $M/2RV_0 : V/V_0$). Swipe and constant V tests provide information about the flow rule in the π plane, with the tests designed to explore all loading directions. Constant V tests also provide data in the deviatoric plane as they contain substantial plastic displacements in the vertical as well as the radial direction. In addition, the plastic displacements of the radial displacement tests present information on flow in the deviatoric/normal plane at one ratio of incremental displacements per test.

3.3.6.1 Incremental Plastic Displacements at Yield: π Plane

Within plasticity theory, if associated flow is assumed in the π plane, the theoretical change in horizontal displacement and rotation can be derived for the yield surface of Eqn 3.19 as

$$du_p = \mathbf{I} \frac{\mathfrak{f}}{\mathfrak{f}H} = \mathbf{I} \left(\frac{2H}{h_0^2 V_0^2} - \frac{2a M/2R}{h_0 m_0 V_0^2} \right) \quad (3.20)$$

$$2Rd\mathbf{q}_p = \mathbf{I} \frac{\mathfrak{f}}{\mathfrak{f}(M/2R)} = \mathbf{I} \left(\frac{2M/2R}{m_0^2 V_0^2} - \frac{2aH}{h_0 m_0 V_0^2} \right) \quad (3.21)$$

where \mathbf{I} is a multiplier which can be derived from the condition of continuity with the strain hardening law. The ratio of plastic strain rate can be written in terms of the current load state as

$$\frac{du_p}{2Rd\mathbf{q}_p} = \frac{H2R \frac{m_0}{h_0} - aM}{M \frac{h_0}{m_0} - aH2R}. \quad (3.22)$$

The incremental experimental plastic displacement ratios for the six swipe tests and four constant V tests have been plotted against their load state in Fig. 3.17. The plastic displacements were evaluated by subtracting the theoretical elastic displacement component from the total experimental displacements using the matrix of Eqn 3.8. This introduces uncertainty due to doubt in the magnitude of the estimated elastic components and especially their dependence on choice of shear modulus. However, with the value of $G = 59.8 \text{ MN/m}^2$ (based upon Eqn 4.1 with the dimensionless shear modulus factor $g = 4000$, a typical value recommended for use in Model C) used in this computation there is only a relative difference of up to 16% between the evaluated plastic displacements and the total experimental displacements. The theoretical associated flow curve has been presented in Fig. 3.17. With the experimental data falling both sides of the curve, the assumption of associated flow in the π plane is reasonable. As the experimental displacements are for a large range of vertical load levels, associated flow can be justified in the π plane along the entire yield surface.

3.3.6.2 Incremental Plastic Displacements at Yield: Deviatoric/Normal Plane

By using the general deviator force, Q as defined in Eqn 3.14, the plastic displacements in this radial direction are defined according to plasticity theory as

$$dq_p = \mathbf{I} \frac{\mathcal{I}f}{\mathcal{I}Q} = \mathbf{I}2Q. \quad (3.23)$$

Combining Eqns 3.14, 3.20, 3.21 and 3.23, dq_p can be written in terms of horizontal displacements and moment rotations as

$$dq_p^2 = \frac{1}{1-a^2} \left[(h_0 du_p)^2 + (m_0 2Rd\mathbf{q}_p)^2 + 2a(h_0 du_p)(m_0 2Rd\mathbf{q}_p) \right]. \quad (3.24)$$

For the constant V tests, the arrows in Fig. 3.18 show the incremental plastic displacement directions in the $Q:V$ plane for a number of yield points at various V_0 values. The theoretical yield surfaces are calculated using Eqn 3.19, and as in the π plane, plastic displacements are evaluated by subtracting the estimated elastic component from the raw experimental data. In constant V tests, the yield surface expands and then contracts according to the hardening law. In Fig. 3.18, crosses indicate the flow directions on the expanding yield surface, while circles represent contraction. Fig. 3.18 indicates non-association in the deviatoric/normal plane, with the displacement directions containing a larger vertical displacement component than if associated flow was assumed, in which case displacements would be perpendicular to the yield surface. As the yield surface expands with increasing load Q , the incremental plastic displacement directions remain almost constant, implying that on this load path the displacement ratios are insensitive to the force ratio. This was an observation also made for constant V type tests by Gottardi and Butterfield (1995) in their series of model tests on a surface strip footing on dense sand, and mentioned in Gottardi *et al.* (1997). After reaching a peak radial load, and with the yield surface contracting, Fig. 3.18 shows the displacement directions contain a slightly larger component of vertical displacement when compared with the expanding surface; an explanation for this will be explored later.

The direction of plastic flow in the deviatoric/normal plane for the radial displacement tests is shown by the arrows in Fig. 3.19, with yield points selected at $V_0 = 400\text{ N}$ intervals. Strong non-association in the deviatoric/normal plane is also clear from these tests. With each test providing information at one ratio of Q to V , it is evident that for increasing Q/V , the ratio of radial to vertical displacements dq_p/dw_p also increases. Test gg22 shows that

there is still a prediction of vertical penetration rather than heave at $Q/V \approx 3$, even though this is in the region of the theoretical yield surface to the left of the peak in Q . Interestingly, though the displacement vectors of test gg22 are pointing into the yield surface, this phenomenon is a function of mapping the angle $\tan^{-1}(dq_p/dw_p)$ onto the $Q:V$ plane. A displacement vector directed inwards from a yield surface is unusual, but can occur on certain mappings of non-associated flow (irrespective of the mapping, an associated flow vector will, however, always point in the direction of the outward normal to the yield surface). It should not be confused with an inward directed force vector, which would indicate elasticity. If the displacement directions were plotted against the yield surface in the three dimensional $(V/V_0 : M/2RV_0 : H/V_0)$ plane, the vector would not be inward directed.

With non-association so clearly visible, a plastic potential g , differing from the yield surface, must be defined to model the force-displacement relationship. The simplest plastic potential would be one based upon the shape of the yield surface.

Martin (1994) developed a work-hardening elasto-plastic model for clay assuming associated flow in the π plane. He used an “association parameter” z_a to adjust vertical displacements to match those observed experimentally, with

$$\mathbb{W}_p = z_a \mathbb{W}_{p \text{ associated}} \quad (3.25)$$

This association parameter took on two different values, both less than one, depending on the direction of the vertical displacement. This simplified model, which requires no separate plastic potential to be defined, works adequately for Martin’s experiments on clay, but would not model the sand tests well. For example, for load states at V values less than that at the peak in Q on the yield surface, the prediction of heave is not appropriate for

dense sand. This can be seen in test gg22 in Fig. 3.19, where vertical penetration is still being observed.

In investigating the $H:V$ yield loci for spudcan footings on saturated sand, Tan (1990) suggested a plastic potential that used the same yield surface equations, but with a “plastic potential parameter” to distort the peak of the surface in the deviatoric/normal plane. In the three dimensional case for Model C, based on the yield surface described by Eqn 3.19 this concept could be formulated as

$$g(V, M/2R, H) = \left(\frac{H}{h_0 V'_0} \right)^2 + \left(\frac{M/2R}{m_0 V'_0} \right)^2 - 2a \frac{H M/2R}{h_0 m_0 V_0'^2} - \mathbf{a}_v^2 \left(\frac{(\mathbf{b}_1 + \mathbf{b}_2)^{(\mathbf{b}_1 + \mathbf{b}_2)}}{(\mathbf{b}_1)^{\mathbf{b}_1} (\mathbf{b}_2)^{\mathbf{b}_2}} \right)^2 \left(\frac{V}{V'_0} \right)^{2\mathbf{b}_1} \left(1 - \frac{V}{V'_0} \right)^{2\mathbf{b}_2} = 0 \quad (3.26)$$

where V'_0 defines the value of maximum vertical load for the current plastic potential shape (that is, $H = 0$ and $M/2R = 0$). The association parameter \mathbf{a}_v allows for variation of the vertical displacement magnitude and location of the “parallel point”² at a desired vertical load level. However, these two requirements are linked and with only one parameter it is difficult to model both adequately.

Increasing h_0 or m_0 with two association factors, rather than scaling the vertical component, enables the plastic potential’s shape to change in the radial plane. This consequently reduces radial plastic displacements. This method has the advantage of more

² At the peak of the plastic potential a parallel point exists where continuous radial distortion occurs with no change in vertical plastic displacements and consequently no change in the yield surface size. Accurate prediction of this point is important as it describes the transition between settlement and heave of the footing and where sliding failures will occur.

flexibility in modelling subtle differences between horizontal and moment loading results.

Using two association factors the plastic potential may be defined as

$$g(V, M/2R, H) = \left(\frac{H}{\mathbf{a}_h h_0 V'_0} \right)^2 + \left(\frac{M/2R}{\mathbf{a}_m m_0 V'_0} \right)^2 - 2a \frac{H M/2R}{\mathbf{a}_h \mathbf{a}_m h_0 m_0 V_0'^2} - \left(\frac{(\mathbf{b}_1 + \mathbf{b}_2)^{(\mathbf{b}_1 + \mathbf{b}_2)}}{(\mathbf{b}_1)^{\mathbf{b}_1} (\mathbf{b}_2)^{\mathbf{b}_2}} \right)^2 \left(\frac{V}{V'_0} \right)^{2\mathbf{b}_1} \left(1 - \frac{V}{V'_0} \right)^{2\mathbf{b}_2} = 0. \quad (3.27)$$

If \mathbf{a}_h and \mathbf{a}_m are constant and equal, Eqn 3.27 is equivalent to Eqn 3.26 for the same value of \mathbf{a}_v . Fig. 3.20 indicates how factoring h_0 and m_0 by scalars \mathbf{a}_h and \mathbf{a}_m affects the theoretical predictions of force to displacement ratios. If $\mathbf{a}_h, \mathbf{a}_m = 1$, the plastic potential and yield surface coincide and associated flow is implied. If $\mathbf{a}_h, \mathbf{a}_m < 1$, the intersection of the plastic potential and the yield surface creates a flattened plastic potential with $V'_0 > V_0$ (plastic potential ₍₁₎ in Fig. 3.20). This increases the ratio of radial to vertical displacement when compared with associated flow at that force level. Conversely, if $\mathbf{a}_h, \mathbf{a}_m > 1$, the surface expands in the Q plane with $V'_0 < V_0$ and the amount of radial to vertical displacement is reduced (plastic potential ₍₂₎ in Fig. 3.20).

Fig. 3.21 shows for all constant V and radial displacement tests the ratio of radial to vertical plastic displacements, dq_p/dw_p , for their current force ratio, Q/V . The figure is formulated in terms of the angle of the force ratio $\tan^{-1}(Q/V)$ and the angle of the displacement ratio $\tan^{-1}(dq_p/dw_p)$ as depicted in Fig. 3.22. A value of $\tan^{-1}(dq_p/dw_p) = 90^\circ$ indicates the transition from vertical penetration to heave and is marked on Fig. 3.21(a). Unfortunately, all of the constant V and radial displacement test data is concentrated in the region of $\tan^{-1}(dq_p/dw_p) < 30^\circ$; this area is highlighted in Fig. 3.21(b). The difference in

horizontal and moment loading has been indicated in Fig. 3.21(b), with moment loading consistently showing higher ratios of dq_p/dw_p for the same load level. Eqn 3.27 with $\mathbf{a}_h \neq \mathbf{a}_m$ allows for this difference to be theoretically modelled. Additionally, Fig. 3.11 indicates that the parallel point of sideswipe tests is not located at the same V/V_0 level, but varies for different loading positions in the π plane. This too can be modelled by Eqn 3.27.

In Fig. 3.23, a theoretical plot of associated flow corresponding to

$$\frac{dq_p}{dw_p} = \frac{2Q}{\mathcal{H}/\mathcal{H}'} \quad (3.28)$$

has been added for comparison with the experimental results, and as expected substantially overestimates dq_p/dw_p for all force ratios. By systematically increasing \mathbf{a}_h and \mathbf{a}_m in Eqn 3.27 the increasing degree of non-association can be compared with the experimental results. Values between 1.75 and 3.0 correspond to sections of the results, but no single value fits all. By simply replacing the yield surface parameters \mathbf{b}_1 and \mathbf{b}_2 in Eqn 3.27 with two new values, \mathbf{b}_3 and \mathbf{b}_4 , to allow for different variations in curvature at the minimum and maximum vertical stress levels respectively, a better fit can be achieved. The new plastic potential may be written as

$$g(V, M/2R, H) = \left(\frac{H}{\mathbf{a}_h h_0 V_0'} \right)^2 + \left(\frac{M/2R}{\mathbf{a}_m m_0 V_0'} \right)^2 - 2a \frac{H M/2R}{\mathbf{a}_h \mathbf{a}_m h_0 m_0 V_0'^2} - \left(\frac{(\mathbf{b}_3 + \mathbf{b}_4)^{(\mathbf{b}_3 + \mathbf{b}_4)}}{(\mathbf{b}_3)^{\mathbf{b}_3} (\mathbf{b}_4)^{\mathbf{b}_4}} \right)^2 \left(\frac{V}{V_0'} \right)^{2\mathbf{b}_3} \left(1 - \frac{V}{V_0'} \right)^{2\mathbf{b}_4} = 0. \quad (3.29)$$

Fig. 3.24 compares the experimental displacement directions with theoretical predictions with $\mathbf{b}_3 = 0.55$ and $\mathbf{b}_4 = 0.65$. By reducing \mathbf{b}_3 and \mathbf{b}_4 from their equivalent yield surface

values, the plastic potential is steepened with respect to the V axis at both low and high stress levels, allowing for a substantial decrease in the ratio of radial to vertical displacements at small and large Q/V values. Two separate theoretical curves are needed to fit adequately the constant V and radial displacement tests and are shown in Fig. 3.24 ($\mathbf{a}_h = \mathbf{a}_m = 1.75$ and $\mathbf{a}_h = \mathbf{a}_m = 2.4$ respectively). Due to the differences in the experimental displacement directions, one solution encompassing both constant V and radial displacement tests could not be found with uniform \mathbf{a}_h and \mathbf{a}_m values, though a compromise solution has been shown in Fig. 3.24 ($\mathbf{a}_h = \mathbf{a}_m = 2.05$).

Given the variance in the two types of experimental tests, the question of which loading directions are important for the foundation modelling of jack-up rigs needs to be addressed. Jack-ups are preloaded vertically to approximately twice their service vertical load before being subjected to any radial loading. For Model C this expands the yield surface to the size of the pre-load as shown along A→B→C in Fig. 3.25. When subjected to environmental loads on the legs, radial load on the footings will naturally increase with vertical load being shed from the upwave leg to the downwave leg. This creates load paths as shown by C→D and C→E in Fig. 3.25. The downwave leg's path contains elements of both the constant V and radial displacement tests and could be seen as a combination of the two. However, no experiments directly explored the surface subjected to a loading path similar to the upwave leg at low vertical load levels. It is imperative for the modelling of jack-ups that the flow rule is consistent for both constant V and radial displacement tests and justifiable at low vertical load levels.

Fig. 3.21(b) shows that for an expanding yield surface in the constant V tests (pre-peak of the strain hardening law), the displacement ratio remains relatively constant with increasing force ratio. For a contracting surface (post-peak of the strain hardening law), dq_p/dw_p

reduces, indicating that proportionately less radial displacement was measured than for the same radial loads when the surface was previously expanding. Both expanding and contracting behaviour in the constant V tests indicate “stiffening” occurring in the radial force-displacement relationships. This implies that in the horizontal plane, to continue the same rate of horizontal displacements increasing levels of horizontal load must be applied. The same is true for moment rotation. To model this behaviour, the association factors \mathbf{a}_h and \mathbf{a}_m could increase with horizontal and moment displacements, indicating a greater degree of non-association, rather than remaining constant. An appropriate form of variation could be similar to the pre-peak region of the vertical hardening law, a hyperbolic function, but with limiting \mathbf{a}_h and \mathbf{a}_m values, written as

$$\mathbf{a}_h = \frac{k'_h \mathbf{a}_{h0} + \mathbf{a}_{h\infty} (u_p)}{k'_h + (u_p)} \quad (3.30)$$

$$\mathbf{a}_m = \frac{k'_m \mathbf{a}_{m0} + \mathbf{a}_{m\infty} (2Rq_p)}{k'_m + (2Rq_p)} \quad (3.31)$$

where \mathbf{a}_{h0} and \mathbf{a}_{m0} represent the association factors with no previous plastic radial displacements. As indicated in Fig. 3.26, k'_h and k'_m relate the rate at which \mathbf{a}_h and \mathbf{a}_m approach their limiting values of $\mathbf{a}_{h\infty}$ and $\mathbf{a}_{m\infty}$ respectively.

Fig. 3.27(a) indicates how Eqns 3.30 and 3.31 will map onto the $\tan^{-1}(Q/V)$: $\tan^{-1}(dq_p/dw_p)$ plane for a typical constant V test. Commencing at the origin A, under the application of radial load, the test will start by tracking close to the \mathbf{a}_0 curve. With increasing plastic radial displacements the test will move across the lines of increasing constant \mathbf{a} to B, the position of a fully expanding yield surface at the peak of the strain hardening law. As it would be unusual for a jack-up in dense sand to load past point B, it is

important to fit this load:displacement gradient between A→B reasonably well. The rate at which the plastic potential expands controls this gradient and is determined by the parameter k'_h or k'_m . For a contracting yield surface, B→C on Fig. 3.27(a), radial load is decreasing and the test path will asymptotically approach the \mathbf{a}_∞ curve.

Each of the six radial displacement tests provides an accurate picture of the force ratio at one rate of displacement and, as shown in Fig. 3.21, the displacement ratios dq_p/dw_p are consistently lower than those of the constant V tests. The reduction of the displacement ratio with radial displacement, as seen in the behaviour of the constant V tests, is also not consistent with the radial displacement results. This implies that the force-displacement flow is sensitive to the direction of loading and any plastic potential must take this difference into account if it is to model all loading combinations adequately. One explanation for the disparity is that the constant V tests were loaded primarily in the vertical direction (to $V = 1600$ N) before any radial displacements were applied to the footing. This contrasts with the radial displacement tests, where radial displacements were applied immediately at $V = 0$. If radial stiffness were to vary with horizontal and moment displacement, as postulated about the constant V tests, an assumption that this rate is proportional to the vertical displacement history of the footing would be physically sound. If the footing has been loaded vertically to a higher level, compacting the underlying soil under vertical stress, the radial displacements needed to expand the plastic potential fully would be proportionally greater. To account for this, radial displacements can be normalised by the plastic vertical displacements, allowing Eqns 3.30 and 3.31 to be written as

$$\mathbf{a}_h = \frac{k'_h \mathbf{a}_{h0} + \mathbf{a}_{h\infty} (u_p/w_p)}{k'_h + (u_p/w_p)} \quad (3.32)$$

$$\mathbf{a}_m = \frac{k'_m \mathbf{a}_{m0} + \mathbf{a}_{m\infty} (2R\mathbf{q}_p/w_p)}{k'_m + (2R\mathbf{q}_p/w_p)}. \quad (3.33)$$

The effect on the path of the constant V test described in Fig. 3.27(a) is minimal, although different k' values need to be selected. Fig. 3.27(b) shows the expected theoretical position of radial displacement tests of different force ratios. As w_p starts at zero, the theoretical displacement ratios can be assumed to be close to the \mathbf{a}_∞ curve. Therefore, for the two load paths, Eqns 3.32 and 3.33 allow different theoretical flow paths to be followed.

The parametric values of the plastic potential relationships have been derived by minimising the least squared error of the difference between the experimental angular direction in the deviatoric/normal plane and the theoretical direction, as depicted in Fig. 3.28. Eqns 3.32 and 3.33 contain six new parameters; however, this can be rationalised to three. If the initial \mathbf{a}_{h0} and \mathbf{a}_{m0} curves are assumed as the associated conditions, \mathbf{a}_{h0} and \mathbf{a}_{m0} can be replaced in Eqns 3.32 and 3.33 with the numerical value one. This assumption is supported by the constant V experimental data shown in Fig. 3.24. Furthermore, the rate of variation of \mathbf{a}_h and \mathbf{a}_m can be assumed the same, reducing k'_h and k'_m to the one term, k' . With the plastic potential defined as in Eqn 3.29, the following values were evaluated:

$$\mathbf{b}_3 = 0.55; \quad \mathbf{b}_4 = 0.65; \quad \mathbf{a}_{h\infty} = 2.5; \quad \mathbf{a}_{m\infty} = 2.15; \quad k' = 0.125.$$

Fig. 3.29 shows that the theoretical displacement ratios calculated using the expanding plastic potential are close to the experimental ratios for both the constant V and radial displacement tests. The theoretical \mathbf{a}_h and \mathbf{a}_m values were calculated assuming the experimental plastic displacements.

3.3.6.3 Numerical Evaluation of Plastic Potential Size

To evaluate the size of the plastic potential (*i.e.* the magnitude of V'_0 in Eqn 3.29), a factor $x = V'_0/V_0$ can be defined to relate the primed (plastic potential) and non-primed (yield surface) values. The value of x for a certain load V/V_0 can be obtained from the numerical solution of

$$\sqrt{\frac{A}{B}} x^{(1-b_3)} = \frac{\left(\frac{(\mathbf{b}_1 + \mathbf{b}_2)^{(\mathbf{b}_1 + \mathbf{b}_2)}}{(\mathbf{b}_1)^{\mathbf{b}_1} (\mathbf{b}_2)^{\mathbf{b}_2}} \right) \left(\frac{V}{V_0} \right)^{(\mathbf{b}_1 - \mathbf{b}_3)} \left(1 - \frac{V}{V_0} \right)^{\mathbf{b}_2}}{\left(\frac{(\mathbf{b}_3 + \mathbf{b}_4)^{(\mathbf{b}_3 + \mathbf{b}_4)}}{(\mathbf{b}_3)^{\mathbf{b}_3} (\mathbf{b}_4)^{\mathbf{b}_4}} \right) \left(1 - \frac{V/V_0}{x} \right)^{\mathbf{b}_4}} \quad (3.34)$$

where

$$A = \left(\frac{H}{h_0} \right)^2 + \left(\frac{M/2R}{m_0} \right)^2 - \frac{2aH M/2R}{h_0 m_0} \quad (3.35)$$

$$B = \left(\frac{H}{\mathbf{a}_h h_0} \right)^2 + \left(\frac{M/2R}{\mathbf{a}_m m_0} \right)^2 - \frac{2aH M/2R}{\mathbf{a}_h \mathbf{a}_m h_0 m_0} \quad (3.36)$$

3.3.6.4 Comments on Model C's Plastic Potential

The experimental evidence did not support the application of associated flow in Model C and a plastic potential function g was defined. Plastic displacements occur when the force point is located on the yield surface and in the direction normal to the plastic potential shape, as defined by Eqn 3.29. The non-dimensional association factors \mathbf{a}_h and \mathbf{a}_m relate the size of the yield surface to the shape of the plastic potential and are formulated as hyperbolic functions in terms of plastic displacements. The rates which \mathbf{a}_h and \mathbf{a}_m vary in Model C are depicted in Fig. 3.30.

Model C's plastic potential is defined by five parameters, arguably an overly complex arrangement to explain the flow rule of shallow circular footings. However, systematic variation of the association factors makes modelling the differences caused by the loading direction possible, resulting in greater confidence in the ability to model a real jack-up load path. Furthermore, with uncoupled horizontal and moment association factors, greater flexibility in the modelling of the location of the parallel point is possible. For different radial load paths, the point may occur at unique V/V_0 levels, the importance of which will be highlighted in the retrospective predictions of the experimental swipe tests in Chapter 4.

As a less complicated alternative, with only three parameters, the compromise solution shown in Fig. 3.24 could be used (*i.e.* $\mathbf{b}_3 = 0.55$, $\mathbf{b}_4 = 0.65$ and $\mathbf{a}_h = \mathbf{a}_m = 2.05$). Further physical experimentation, especially at low Q/V load levels could lead to a more accurately defined, and perhaps a less complex, flow rule.

Chapter 4 – Numerical Formulation of Model C for the Analysis of Jack-Up Units

4.1 Introduction

The numerical formulation of Model C is described in this chapter. Retrospective prediction of the Gottardi and Houlsby (1995) experiments has been performed, with examples showing the capabilities of Model C detailed. A description of a numerical model accounting for the conical features of spudcan footings is also presented. Finally, the formulation used to incorporate Model C into the dynamic structural analysis program JAKUP is detailed.

4.2 Features of Model C

4.2.1 General Structure of Model C

Model C is defined by twenty parameters, most of which are dimensionless. There are three quantities, however, which define the dimensions of the model. These factors are the footing radius R , the effective unit weight of the soil \mathbf{g} and the shear modulus G ; R and \mathbf{g} are user-defined, whereas G is estimated using the expression

$$\frac{G}{p_a} = g \sqrt{\frac{2R\mathbf{g}}{p_a}} \quad (4.1)$$

where p_a is atmospheric pressure and g is a non-dimensional shear modulus factor. This equation is derived from the empirical observation that the shear modulus depends approximately on the square root of the stress level, with $2R\mathbf{g}$ a representative estimate (Wroth and Houlsby, 1985). Table 4.1 outlines the twenty Model C parameters and gives typical values.

The vertical strain hardening law for Model C, as formulated in Eqn 3.10, describes the isotropic variation of the yield surface size. Numerical values of k , V_{0m} and w_{pm} were derived for the experimental conditions based on one radius and one sand. Assuming the same shape of the vertical strain hardening law, k and w_{pm} can be defined for different sized footings by introducing the dimensionless parameters f and \mathbf{d}_p , where

$$k = f2RGk_1 \quad (4.2)$$

and

$$w_{pm} = 2R\mathbf{d}_p. \quad (4.3)$$

The values of f and \mathbf{d}_p were determined from the experimental results as 0.144 and 0.0316 respectively. V_{0m} can be calculated for different sands from bearing capacity theory as

$$V_{0m} = \mathbf{g}N_g\mathbf{p}R^3 \quad (4.4)$$

where N_g is the dimensionless bearing capacity for a circular footing (for example values see Bolton and Lau (1993) or section 4.4.1).

4.2.2 Numerical Formulation of Model C

If the loading increment is entirely within the yield surface, then elastic displacements are described by Eqn 3.8. However, when the footing is yielding, plastic displacements are in the direction normal to the plastic potential with a multiplication factor \mathbf{l} determining the magnitude of the plastic displacement increment according to

$$\begin{pmatrix} dw_p \\ 2Rd\mathbf{q}_p \\ du_p \end{pmatrix} = \mathbf{I} \begin{pmatrix} \frac{\mathcal{I}g}{\mathcal{I}V} \\ \frac{\mathcal{I}g}{\mathcal{I}M/2R} \\ \frac{\mathcal{I}g}{\mathcal{I}H} \end{pmatrix}. \quad (4.5)$$

Since the flow rule is defined in terms of plastic displacements, Model C has been formulated in terms of flexibility rather than stiffness. Therefore, for an elasto-plastic increment during yielding, the elastic and plastic components are summed to give

$$\begin{pmatrix} dw_{ep} \\ 2Rd\mathbf{q}_{ep} \\ du_{ep} \end{pmatrix} = \begin{pmatrix} dw_e \\ 2Rd\mathbf{q}_e \\ du_e \end{pmatrix} + \begin{pmatrix} dw_p \\ 2Rd\mathbf{q}_p \\ du_p \end{pmatrix} = \begin{bmatrix} C_1 & 0 & 0 \\ 0 & C_2 & C_4 \\ 0 & C_4 & C_3 \end{bmatrix} \begin{pmatrix} dV \\ dM/2R \\ dH \end{pmatrix} + \mathbf{I} \begin{pmatrix} \frac{\mathcal{I}g}{\mathcal{I}V} \\ \frac{\mathcal{I}g}{\mathcal{I}M/2R} \\ \frac{\mathcal{I}g}{\mathcal{I}H} \end{pmatrix} \quad (4.6)$$

where $C_1 \dots C_4$ are the elastic flexibility factors given by

$$\begin{aligned} C_1 &= \frac{1}{2GR} \frac{1}{k_1} & C_2 &= \frac{1}{2GR} \frac{k_3}{k_2k_3 - k_4^2} \\ C_3 &= \frac{1}{2GR} \frac{k_2}{k_2k_3 - k_4^2} & C_4 &= \frac{1}{2GR} \frac{k_4}{k_4^2 - k_2k_3} \end{aligned}. \quad (4.7)$$

For any incremental load or displacement through yield, any change in the value of f must be zero ($df = 0$) so that the force point ($V, M/2R, H$) remains on the yield surface. For compatibility with the strain hardening law a solution for \mathbf{I} , the magnitude of plastic displacements, exists and may be determined from the condition $df = 0$, where

$$df = \left(\frac{\mathcal{I}f}{\mathcal{I}V} dV + \frac{\mathcal{I}f}{\mathcal{I}M/2R} dM/2R + \frac{\mathcal{I}f}{\mathcal{I}H} dH \right) + \frac{\mathcal{I}f}{\mathcal{I}V_0} dV_0 = 0. \quad (4.8)$$

As V_0 and dV_0 are dependent on the vertical penetration w_p , using the chain law and the plastic potential relationship $dw_p = \mathbf{l} \partial g / \partial V$, Eqn 4.8 can be rewritten and solved for \mathbf{l} :

$$df = \left(\frac{\mathcal{f}}{\mathcal{V}} dV + \frac{\mathcal{f}}{\mathcal{M}/2R} dM/2R + \frac{\mathcal{f}}{\mathcal{H}} dH \right) + \frac{\mathcal{f}}{\mathcal{V}_0} \frac{\mathcal{V}_0}{\mathcal{w}_p} \mathbf{l} \frac{\mathcal{g}}{\mathcal{V}} = 0. \quad (4.9)$$

The overall increment form of Model C can therefore be represented as

$$\begin{bmatrix} 1 & 0 & 0 & 0 & 0 & 0 & 0 \\ 0 & 1 & 0 & 0 & 0 & 0 & 0 \\ 0 & 0 & 1 & 0 & 0 & 0 & 0 \\ \hline C_1 & 0 & 0 & -1 & 0 & 0 & \frac{\mathcal{g}}{\mathcal{V}} \\ 0 & C_2 & C_4 & 0 & -1 & 0 & \frac{\mathcal{g}}{\mathcal{M}/2R} \\ 0 & C_4 & C_3 & 0 & 0 & -1 & \frac{\mathcal{g}}{\mathcal{H}} \\ \hline \frac{\mathcal{f}}{\mathcal{V}} & \frac{\mathcal{f}}{\mathcal{M}/2R} & \frac{\mathcal{f}}{\mathcal{H}} & 0 & 0 & 0 & B_{7,7} \end{bmatrix} \begin{pmatrix} dV \\ dM/2R \\ dH \\ dw \\ 2Rd\mathbf{q} \\ du \\ \mathbf{l} \end{pmatrix} = \begin{pmatrix} dV_0 \\ dM/2R_0 \\ 2Rd\mathbf{q} \\ dH_0 \\ du \\ 0 \end{pmatrix} \quad (4.10)$$

where $B_{7,7}$ is derived from Eqn 4.9 and equates to

$$B_{7,7} = \frac{\mathcal{g}}{\mathcal{V}} \frac{\mathcal{V}_0}{\mathcal{w}_p} \frac{\mathcal{f}}{\mathcal{V}_0}. \quad (4.11)$$

Expressions for $\partial f / \partial V$, $\partial f / \partial (M/2R)$, $\partial f / \partial H$ and $\partial f / \partial V_0$ can be evaluated in closed form by differentiating the yield surface Eqn 3.19, and $\partial g / \partial V$, $\partial g / \partial (M/2R)$ and $\partial g / \partial H$ by differentiating the plastic potential Eqn 3.29 and $\partial V_0 / \partial w_p$ from the strain hardening law of Eqn 3.10. These processes are uncomplicated; however, the somewhat lengthy results will not be presented here.

With the incremental plasticity solution described by Eqn 4.10, any combination of control commands can be used. An increment may have full displacement, full load or a mixture of

displacement/load control, with the matrix adjusted so that the numerical value 1 aligns with that row's control type. For calculations inside the yield surface the elastic matrix consists of the first six rows and columns of Eqn 4.10.

4.2.3 Implementation of Model C in the FORTRAN Program OXC

The strain hardening plasticity theory of Model C has been implemented in a FORTRAN program named OXC, which, for any load, displacement or combinational path can evaluate the resulting loads/displacements. In OXC the input path is broken up into a number of stages, in which the numerical increments and type of control are described.

For each stage in sequence, a trial solution of Eqn 4.10 is evaluated. Whether an elastic or an elasto-plastic formulation is used depends on where the previous step's load state finished. If it finished on the yield surface ($f = 0$), an elasto-plastic increment is used, whereas if it finished within the yield surface ($f < 0$), an elastic increment is used. An elasto-plastic increment is used for the first step.

An UPDATE routine is then applied to control this trial load/displacement solution according to the numerical formulation of Model C. The UPDATE subroutine is displacement controlled, using the change in displacement calculated for one entire stage. Initially UPDATE assumes that the increment is elastic and makes a trial solution of the load state based on this assumption. The location of this trial load state with respect to the existing yield surface is then checked with three possible cases arising:

Case 1: If $f_{trial} < 0$, the trial load space is located within the yield surface, implying an elastic increment. The trial load space values are accepted as the final load state.

Case 2: If $f_{trial} = 0$, the trial load space is located on the yield surface. This also implies an elastic increment and the trial load state is accepted as the final load state.

Case 3: If $f_{trial} > 0$, the trial load space is located outside the existing yield surface and the increment is elasto-plastic.

For *Case 3* the trial load state is incorrect, with the correct solution being defined by an elasto-plastic step. To account for non-linearities in this calculation, the displacement increment is divided into a number of equal substeps. For each substep, the change in load is calculated and the total load updated for that increment. Using that updated load state, a new V_0 is evaluated so that the requirement $f = 0$ is satisfied. Therefore, the yield surface expands over that substep increment and the new yield surface size is calculated before the next substep.

It would not be pertinent to describe all subroutines found within OXC here. Further details of the key subroutines, solver techniques and tolerance values can be found in Cassidy (1996).

4.3 Retrospective Prediction of Experimental Tests

To investigate the capabilities of Model C to model footing behaviour, numerical simulations were carried out for a number of representative experiments using OXC. In each of these simulations the values of three of the experimentally measured quantities (e.g. the displacements) were taken as input, and the other three quantities (e.g. the loads) were calculated for comparison with the experiments. No idealisation of the experimental input data was carried out, so that the input values contain all the minor fluctuations associated with experimental measurements, with OXC able to handle such perturbations. As the simulations were carried out on the same tests as were used for the development of Model C, the quality of the fit is of course expected to be good. The purpose of this exercise is, however, twofold: (a) to demonstrate that Model C can be implemented numerically and

used to simulate footing behaviour and (b) to assess the overall capability of the model to capture the salient features of the original data.

4.3.1 Vertical Penetration Test

Fig. 4.1(a) shows the experimental results for a vertical penetration test. Fig. 4.1(b) is a simulation of this same test in which the measured displacement is taken as input and the vertical load calculated. Model C gives loads that accurately represent the original test and this is principally a test of the chosen strain hardening law. The three vertical unload/reload loops pre-peak are modelled well, although Model C does not reflect the hysteresis which occur in the experimental results. This does make a slight, but not too significant, reduction in the displacements compared to their corresponding loads. It can be seen that OXC has the ability to predict the location of the existing yield surface when being reloaded in an unload-reload loop. It does not overshoot the yield surface because a bisection algorithm is used to determine the proportion of the increment that is elastic, with the remaining proportion allocated as elasto-plastic.

In Figs 4.2 to 4.6, (a) and (b) represent the measured experimental data, whilst (c) and (d) are Model C simulations.

4.3.2 Moment and Horizontal Swipe Tests from $V \gg 1600$ N

In a swipe test the footing is load controlled in the vertical direction until it reaches a prescribed load, in this case $V \approx 1600$ N. Rotation or horizontal displacement is then applied to the footing with the trace corresponding to a track along the yield surface, appropriate for that embedment.

Fig. 4.2 represents a moment swipe starting at $V \approx 1600$ N. Prior to the swipe the footing is loaded in the purely vertical direction with only small amounts of horizontal and moment

load being developed. However, for clarity, only the swipe has been plotted. Model C simulates the magnitude of peak moment adequately, reaching a value just over $M/2R = 150$ N. The numerical peak moment in Fig. 4.2(d) and the experimental peak moment in Fig. 4.2(b) occurred at the same vertical load. Additionally, Figs 4.2(a) and (c) show that the amount of rotation before the peak was modelled accurately. However, in this test Model C locates the parallel point slightly lower than the experiment (point A in Fig. 4.2(d)). In the Model C simulation in Fig. 4.2(d), movement back along the yield surface can be seen to occur, for instance at $V \approx 800$ N and again at $V \approx 600$ N.

Fig. 4.3 represents an equivalent swipe, but in the horizontal direction, with Model C load controlled to $V \approx 1600$ N and then displacement controlled for the swipe. OXC models the track along the yield surface very well, with the peak horizontal load almost exactly matching that of the experiment at just over 200 N. Fig. 4.3(c) shows Model C predicting a very similar displacement path to the experiments (Fig. 4.3(a)), verifying the flow rule for this case. The simulation stops tracking at around the same horizontal and vertical load levels, indicating accurate prediction of the parallel point in the horizontal plane. Further justification of the use of two independent association factors (\mathbf{a}_h and \mathbf{a}_m) in the flow rule is given by the more accurate prediction of the parallel point for both the moment and horizontal swipes than would be possible if there were only one.

4.3.3 Moment and Horizontal Swipe Tests from $V \gg 200$ N

Fig. 4.4 represents moment and horizontal swipes starting at $V \approx 200$ N, highlighting the yield surface at low vertical loads. In order to depict the experiments, Model C is load controlled to $V \approx 1600$ N, then unloaded to $V \approx 200$ N, before displacement controlled throughout the swipe. Figs 4.4(a) and (c) show that at low vertical loads both the experimental results and Model C depict work hardening, with Model C simulating the

experiment well. This was not the case horizontally. Fig. 4.4(b) shows that the experiment elastically loads in the horizontal direction before yielding occurs at $H \approx 80$ N (A→B), then tracks along the yield surface with a reduction in vertical and horizontal load (B→C). This implies work-softening of the sample. Model C simulates the elastic horizontal loading very well, predicting the yield surface at the same position (line segment A→B on Fig. 4.4(d)). However, it then predicts that work hardening will occur, with increasing vertical and horizontal load tracking up around the yield surface. This is consistent with, and entirely related to, Model C's prediction of the parallel point from a swipe at 1600 N. Nevertheless, it does indicate that Model C's flow rule will not always follow the experimental performance.

4.3.4 Constant Vertical Load Tests

The constant V tests as shown in Figs 4.5 and 4.6 are simulated with full load control to $V \approx 1600$ N, before the vertical load is held constant at around that value (with slight fluctuations according to the experimental data), whilst horizontal and moment displacement control models an excursion. The constant V tests model the expansion and then later contraction of the yield surface relative to the V_0 value. Figs 4.5(c) and 4.6(c) show that Model C models expanding yield surfaces reasonably well, reaching a similar peak for horizontal and moment load to the experimental values. Once the peak value has been reached, the Model C surfaces then contract back as predicted by the post-peak performance of the hardening law. Fig. 4.5(c) shows that for the predominately moment case this post-peak performance is adequately modelled, although the experimental data did not continue until $M/2R = 0$. However, in the horizontal constant V test the experiment did continue until $H = 0$, but this was not reproduced by the OXC simulation, with the unexpected result of increasing H occurring at the end of the test ($du > 4$ mm at point A in Fig. 4.6(c)). The cause of this rise in H in the numerical simulation is due to a rapid decrease in the experimentally recorded vertical load, which was used as input. Between point A and the end of the test, V

falls from approximately 1600 N to 1400 N. If V was held constant at 1600 N, Model C would simulate the horizontal load decreasing back to zero, as would be theoretically expected during a constant V test. This is a good example showing that prediction in Model C is very sensitive to the value of V near the peak value of capacity.

Figs 4.5(d) and 4.6(d) show that the flow rule satisfactorily predicts the vertical displacements when compared with the horizontal or rotational displacements, which are part of the input. Fig. 4.5(d) shows a slight over-prediction in vertical displacements, indicating that for this case the plastic potential's surface is too steep, or too normal when compared to the V' axis. However, with Fig. 4.6(d) showing a slight under-prediction, the flow rule is predicting balanced results.

4.3.5 Radial Displacement Tests

Constant gradients of moment to vertical and horizontal to vertical displacement were used as inputs to simulate horizontal and moment radial displacement tests. The resultant experimental moment and horizontal loads and Model C predictions are shown in Figs 4.7 and 4.8 respectively, noting that (a) represents the measured experimental data and (b) the Model C simulation. The simulations are of similar gradient, implying that the Model C flow rule is performing well. The noise that can be seen in Figs 4.7(b) and 4.8(b) is due to the fluctuations that occur in the real experimental input data.

4.4 Considering the Conical Shape of Spudcans

4.4.1 Vertical Bearing Capacity of Conical Footings

So far Model C has been derived for flat footings. In order to account for the conical shape of spudcans, a numerical study was performed to evaluate a comprehensive set of bearing capacity factors for various conical shapes, roughnesses and soil conditions. These factors

are used in section 4.4.2 to define a more realistic hardening law for spudcan footings. The investigation was carried out on Prof. G.T. Houlsby's existing FORTRAN program FIELDS, with lower bound collapse loads calculated for the axisymmetric problem using the Method of Characteristics. The theoretical methods used in FIELDS, as well as a sample numerical study of conical footings on clay, can be found in Houlsby (1982) and Houlsby and Wroth (1983). Within the study performed here, the sand was assumed to be rigid-plastic and to obey the Mohr-Coulomb yield criterion. Furthermore, change in geometry effects were not taken into account.

Fig. 4.9 defines the problem and notation used for the 360 combinations of the three dimensionless parameters investigated:

cone apex angle: $\mathbf{b} = 30^\circ, 60^\circ, 90^\circ, 120^\circ, 150^\circ, 180^\circ$

roughness factor: $\mathbf{a} = 0, 0.2, 0.4, 0.6, 0.8, 1.0$

friction angle: $\mathbf{f} = 5^\circ, 10^\circ, 15^\circ, 20^\circ, 25^\circ, 30^\circ, 35^\circ, 40^\circ, 45^\circ, 50^\circ$

A roughness factor of $\mathbf{a} = 0$ represents a smooth footing, whilst $\mathbf{a} = 1.0$ represents a rough one. For spudcans on dense sand a roughness factor close to one is appropriate, and the friction angle would lie in the range 40-50°. Fig. 4.10 shows a typical general shear failure mechanism generated by the program FIELDS. Lower bound bearing capacity factors for all combinations of the dimensionless parameters are shown in Fig. 4.11.

4.4.2 Adaptation of Model C for Conical Shape of Spudcans

The development of Model C was based on experiments on flat circular footings. Its strain hardening law differs from the load-penetration curve theoretically expected for flat plates. A new “combined” theory is needed to consider the differences in a manner consistent with both the experimental observations and the theoretical predictions.

4.4.2.1 Flat Plates

Theory: For a flat plate of radius R , as shown in Fig. 4.12(a), the theoretical vertical bearing capacity is considered constant with penetration as depicted in Fig. 4.12(b), and written as

$$V_{0m_{Theory}} = gN_g pR^3. \quad (4.12)$$

Experimental Evidence: For the same situation, with the experimental evidence used in the derivation of the strain hardening law of Model C, a different picture is seen. With increasing vertical penetration, vertical load increases with decreasing stiffness until a peak load is reached at a derived fraction of the footing diameter, as specified in Eqn 3.10 and shown in Fig. 4.12(d). With increasing penetration, work softening occurs in the sand and vertical load carrying capacity decreases. The peak vertical capacity in the model is defined as in the theoretical case as

$$V_{0m_{Exp}} = gN_g pR^3. \quad (4.13)$$

The experimental load penetration curve was derived for a flat footing with one set of surface roughness and soil condition values. For different values, the shape would be similar but with vertical load scaled according to an appropriate bearing capacity (from Fig. 4.11).

4.4.2.2 Conical Spudcans

Theory: The theoretical case of a conical footing, as depicted in Fig. 4.12(e), can be split into two parts: firstly, a conical section of varying radius (r) and penetration ($w_p < R/\tan(\mathbf{b}/2)$); and secondly, after full penetration of the conical section ($w_p \geq R/\tan(\mathbf{b}/2)$). Before full penetration of the conical section, theoretically the vertical

load is proportional to the cube of the current radius of the penetrated section. This is represented by segment A→B in Fig. 4.12(f), and written as:

$$V_{0Theory} = \mathbf{g}N_g \mathbf{p}r^3 = \mathbf{g}N_g \mathbf{p}(w_p \tan(\mathbf{b}/2))^3. \quad (4.14)$$

With the conical section of the footing fully penetrated, the footing is assumed to penetrate at a constant load according to Eqn 4.12, as shown between B→C on Fig. 4.12(f) (neglecting the geometrical effects of embedment).

A Combined Method: By combining these theoretical and experimental ideas, a more realistic strain hardening law can be derived for spudcans in dense sand. Figs 4.12(g) and (h) outline this new model. Using a N_g value (from Fig. 4.11) appropriate for the geometry¹ and roughness of the spudcans and friction angle of the sand, the experimental flat footing curve shape (Eqn 3.10) can be normalised by the theoretical maximum $V_{0mTheory}$, as shown in Fig. 4.12(g), and written as

$$\frac{V_{0Exp}}{V_{0mTheory}} = \frac{\frac{k w_p}{V_{0m}} + \left(\frac{f_p}{1 - f_p} \right) \left(\frac{w_p}{2R\mathbf{d}_p} \right)^2}{1 + \left(\frac{k w_p}{V_{0m}} - 2 \right) \frac{w_p}{2R\mathbf{d}_p} + \left(\frac{1}{1 - f_p} \right) \left(\frac{w_p}{2R\mathbf{d}_p} \right)^2} \quad (4.15)$$

where $V_{0mTheory} = V_{0mExp}$ (as given by Eqns 4.12 and 4.13). It should be noted that the plastic penetration has been normalised by the vertical penetration at peak load (Eqn 4.3).

Until full penetration of the conical footing, the appropriate value of $w_p/2R\mathbf{d}_p$ is a constant and equal to $1/2\mathbf{d}_p \tan(\mathbf{b}/2)$. From this value a constant factor $s_{fp} = V_{0Exp}/V_{0mTheory}$ can be

determined from Eqn 4.15, as indicated in Fig. 4.12(g). Before full penetration of the cone ($w_p < R/\tan(\mathbf{b}/2)$), the load penetration curve from the theoretical model is used, but scaled by s_{fp} , thereby consistently combining the two methods. This is shown as section A→B in Fig. 4.12(h) and can be written as

$$V_0 = s_{fp} \mathbf{g} N_g \mathbf{p}^3 = s_{fp} \mathbf{g} N_g \mathbf{p} (w_p \tan(\mathbf{b}/2))^3. \quad (4.16)$$

After full penetration of the conical section, Eqn 4.16 can still be applied; however, s_{fp} will now vary according to Eqn 4.15, thus following the original Model C experimental shape. If $w_{pm} \geq R/\tan(\mathbf{b}/2)$, the shape of the experimental hardening law will result in a peak load at $w_p = 2Rd_p$. This is illustrated as section B→C of Fig. 4.12(h). Conversely, if $w_{pm} < R/\tan(\mathbf{b}/2)$, the entire response after embedment is predicted from the post-peak section of the experimental curve. The maximum load occurs just as full embedment is reached, as shown in section B→D of Fig. 4.12(h). For realistic values of the parameters it appears that the latter case is more usual.

4.5 Implementation of Model C into JAKUP

Slight modification of the Model C numerical formulation described in section 4.2.2 (and implemented in OXC) allowed it to be independently incorporated into the dynamic structural analysis program JAKUP. The structural model within JAKUP uses a Eulerian approach where equilibrium, compatibility and stiffness equations are expressed in terms of the deformed geometry of the structure. JAKUP uses an incremental loading approach and Newton-Rhapson iteration to account for non-linearities (see Martin, 1994 and Thompson, 1996).

¹ The embedded part of the underside of the spudcan is treated as an “equivalent conical footing”, *i.e.* a conical footing with equal radius and volume as the embedded spudcan.

At the start of any new time increment the external applied loads (P_{ext}^t) are in equilibrium with the members' internal load state (P_{int}^t —these correspond to the deformation of the structure (x^t)), that is:

$$P_{ext}^t = P_{int}^t + P_{inertial}^t + P_{damping}^t \quad (4.17)$$

where $P_{inertial}$ and $P_{damping}$ represent the inertial and damping components of the dynamic equation of motion. With the application of a new load increment (dP), a new deformation (x^{t+dt}) needs to be defined such that the new internal and external loads are in equilibrium. This is achieved by summing the incremental displacement vector (dx —calculated by solving the dynamic equations of motion with a global stiffness matrix defined for the initial set-up) with the existing displacement vector. The new internal force vector corresponding to the internal state of stress can then be evaluated. Generally, P_{int}^{t+dt} does not satisfy the conditions of force equilibrium, and iteration is needed to correct the displacement vector. In order to do this, an out-of-balance force is evaluated as

$$P_{out-of-balance} = P_{ext}^{t+dt} - P_{int}^{t+dt} - P_{inertial}^{t+dt} - P_{damping}^{t+dt} \quad (4.18)$$

and used to find a new displacement correction vector (dx_{corr}). For each iteration step, a new tangent stiffness matrix is used, representing the latest configuration of the structural system. The iterative process is repeated until convergence of solution is achieved. The convergence criterion compares the size of the displacement correction vector with the actual displacement vector, and is as defined in Martin (1994) and Thompson (1996).

The contribution of the Model C foundations is included by combining their stiffness matrices with those of the general structural members when assembling the global stiffness

matrix. Furthermore, the reactions of the foundations are included when compiling the internal load conditions. To achieve the formulation outlined, Model C must operate in two modes:

- At the beginning of the timestep, the position of the spudcans is known and the footing stiffness matrix (3×3 in size) is evaluated. If the combined force state $(V, M/2R, H)$ at the beginning of the time increment lies within the current yield surface (“initially elastic”), an elastic footing stiffness matrix is returned; however, if the force state lies on the surface then an elasto-plastic stiffness matrix is calculated (“initially elasto-plastic”).
- During the iterations, due to incremental changes in footing displacement (displacement correction), the incremental changes in footing loads need to be evaluated. The spudcan displacements are extracted from the change in structural displacements at the footing node. The stiffness matrix used represents the current configuration. If the footing is initially elastic, an elastic matrix is used for the foundation stiffness component until yielding is detected, at which time an elasto-plastic configuration is used for all of the remaining iterations during that timestep. For the initially elasto-plastic case, the footing remains elasto-plastic unless it is calculated to lie within the yield surface (*i.e.* $f < 0$ using Eqn 3.19) for the first equilibrium iteration.

At the initial numerical set-up, all structural elements are assumed free of stress and all joints have zero displacement. The spudcans are embedded to the vertical plastic penetration corresponding to their initial vertical pre-load value. The load in the foundations is assumed to be zero, with the rotational and horizontal translations zero and the vertical displacement equal to $w_{p\ pre-load}$. The initial size of the yield surface is equivalent to the vertical pre-load per spudcan, *i.e.* $V_0 = V_{pre-load}$. The foundations are, therefore, in an elastic condition before the vertical weight of the hull is applied as the first step in a numerical analysis.

4.6 Concluding Remarks

An elasto-plastic model, entitled Model C, appropriate for the modelling of spudcan foundations for jack-up units on sand has been detailed. The major advantages of Model C in the analysis of jack-up response include:

- Its formulation is amenable to numerical analysis, allowing it to be implemented into structural analysis programs.
- It accounts for the non-linearities of combined loading on sand in a consistent manner.
- It provides a direct indication of yielding. Furthermore, movement of the spudcan footings can be evaluated, with differentiation between upwave and downwave leg behaviour possible. Sliding of spudcan footings, therefore, can be evaluated directly.
- A “realistic” interpretation of spudcan fixity allows for more accurate dynamic analysis. Model C gives significantly different dynamic response to pinned and fixed footing assumptions.

All of these advantages are highlighted in the following chapters of this thesis.

Chapter 5 - Application of NewWave Theory in the Analysis of Jack-Up Units

5.1 Introduction

Wave theories suitable for the analysis of jack-up platforms are discussed in this chapter. Emphasis is placed on NewWave theory as an alternative to widely used regular wave theories, such as Stokes' fifth-order waves. The theoretical basis of NewWave is described and verification of its implementation into JAKUP outlined. Appropriate stretching procedures and extensions of NewWave theory to account for second-order effects are discussed. Examples are shown to emphasise the differences in predicted extreme response due to various footing assumptions: pinned, linear springs and Model C.

5.2 Theoretical Background

5.2.1 Linear Random Wave Theory

By generating surface elevations and corresponding kinematics over short storm periods, for example three hours, the response of a jack-up to random wave loading may be analysed for that one sea-state. Analysis of wave data suggests the assumption that the ocean surface within a certain physical area is statistically a stationary Gaussian random process can generally be made. A description of this surface is given by the superposition of wavelets of different wavelengths, amplitudes and periods travelling at varying speeds and directions. For a uni-directional wave, the instantaneous surface elevation above the mean water-level $\mathbf{h}(t)$ at a point in space can be written as

$$\mathbf{h}(t) = \sum_{n=1}^N c_n \cos(\mathbf{w}_n t + \mathbf{f}_n) \quad (5.1)$$

where \mathbf{w}_n and \mathbf{f}_n are the frequency and random phase angle of the n^{th} wavelet respectively. The amplitudes of the individual wavelets c_n are described by the spectral decomposition of the ocean as

$$c_n = \sqrt{2S_{hh}(\mathbf{w}_n)d\mathbf{w}} \quad (5.2)$$

where $S_{hh}(\mathbf{w}_n)$ is the n^{th} component of the (one-sided) wave spectrum and $d\mathbf{w}$ the discrete frequency interval. This summation of all the coefficients (N in total) produces a wave record for a period $t = 0$ to T , where $T = 2\pi/d\mathbf{w}$. The random nature of the ocean surface is introduced by the phase angle \mathbf{f}_n associated with each sinusoidal component, with \mathbf{f}_n uniformly distributed between 0 and 2π . Further discussion of the generation of random surface elevations is given in Chapter 6 (section 6.2.1).

5.2.2 NewWave Theory

As an alternative to simulating many hours of random time domain simulation, Tromans *et al.* (1991) describe a first order wave that is deterministic but still accounts for the spectral composition of the sea. The method, entitled NewWave, involves the superposition of directional linear wavelets with an extreme crest associated with the superposition of all the wavelet crests at a specific point in space or time. The surface elevation around this extreme wave event is then modelled by the most probable wave shape conditional on this extreme crest. It is shown by Tromans *et al.* that the surface elevation is normally distributed about this most probable shape, with the surface elevation described by two terms, one deterministic and one random. As a function of time, the surface elevation can be written as

$$\mathbf{h}(\mathbf{t}) = \underset{(1)}{\mathbf{a}\mathbf{r}(\mathbf{t})} + \underset{(2)}{g(\mathbf{t})} \quad (5.3)$$

where $\mathbf{t} = t - t_1$, the time relative to the initial position of the crest (*i.e.* t_1 is the time when the wavelet forms). In Eqn 5.3, term₍₁₎ describes the most probable value, where \mathbf{a} is the crest elevation defined as the vertical distance between the wave maximum and the mean water-level, and $r(\mathbf{t})$ the autocorrelation function for the ocean surface elevation. For the random surface elevation, the autocorrelation function is defined as the mean value of the product $\mathbf{h}(t)\mathbf{h}(t + \mathbf{t})$, where \mathbf{t} is the time lag. For a stationary process this will depend only on \mathbf{t} . The autocorrelation function is proportional to the inverse Fourier Transform of the surface energy spectrum (known as the Wiener-Khintchine relationship), allowing the surface elevation to be determined efficiently. Further explanation is given below.

Term₍₂₎ of Eqn 5.3 is a non-stationary Gaussian process with a mean of zero and a standard deviation that increases from zero at the crest to \mathbf{s} , the standard deviation of the underlying sea at a distance away from the crest. Therefore, as the crest elevation increases, term₍₁₎ becomes dominant and can be used alone in the derivation of surface elevation and wave kinematics.

The continuous time autocorrelation function is defined as

$$r(\mathbf{t}) = \frac{1}{\mathbf{S}^2} \int_0^{\infty} S_{\mathbf{h}\mathbf{h}}(\mathbf{w}) e^{i\mathbf{w}\mathbf{t}} d\mathbf{w} \quad (5.4)$$

with the time history of the extreme wave group proportional to $r(\mathbf{t})$ at the region around $\mathbf{t} = 0$. An important property of $S_{\mathbf{h}\mathbf{h}}(\mathbf{w})$ for a time lag $\mathbf{t} = 0$ is that the autocorrelation function of Eqn 5.4 reduces to

$$r(\mathbf{t} = 0) = \frac{1}{\mathbf{S}^2} \int_0^{\infty} S_{\mathbf{h}\mathbf{h}}(\mathbf{w}) d\mathbf{w} \quad (5.5)$$

with the integral equal to the second moment of area of the wave data, *i.e.* $E[\mathbf{h}^2(t)]$.

Since the mean value of $\mathbf{h}(t)$ is zero, $r(\mathbf{t} = 0)$ is equal to one:

$$r(\mathbf{t} = 0) = \frac{1}{\mathbf{s}^2} E[\mathbf{h}^2(t)] = 1 \quad (5.6)$$

This allows the surface elevation of the NewWave to be scaled efficiently, as shown below in Eqn 5.7.

The NewWave shape as defined by the autocorrelation function (Eqn 5.4) can be discretised by a finite number (N) of wavelets. As there exists a unique relationship between wave number and frequency, spatial dependency can also be included, leading to the discrete form:

$$\mathbf{h}(X, \mathbf{t}) = \frac{\mathbf{a}}{\mathbf{s}^2} \sum_{n=1}^N [S_{hh}(\mathbf{w}_n) d\mathbf{w}] \cos(k_n X - \mathbf{w}_n \mathbf{t}) \quad (5.7)$$

where k_n is the wavenumber of the n^{th} wavelet. As defined previously, \mathbf{a} is the crest elevation, $S_{hh}(\mathbf{w}_n) d\mathbf{w}$ the surface elevation spectrum and \mathbf{s} the standard deviation corresponding to that wave spectrum. $X = x - x_1$ is the distance relative to the initial position with $X = 0$ representing the wave crest. This allows the positioning of the spatial field such that the crest occurs at a user-defined position relative to the structure, a useful tool for time domain analysis. The kinematics are then calculated as a function of time. Eqn 5.7 generates a NewWave as the summation of infinitesimal wavelets coming into phase, with their amplitudes proportional to $S_{hh}(\mathbf{w}_n) d\mathbf{w}$.

5.2.3 Wave Energy Spectrum

Appropriate choice of wave energy spectrum shape varies with location and conditions, depending on variables such as the wind duration and fetch length. The Pierson-Moskowitz (Pierson and Moskowitz, 1964) and the JONSWAP (Hasselmann *et al.*, 1973) spectra are widely used examples. The sea-states are usually described by just two terms, the significant wave height H_s and the mean zero crossing period T_z . The significant wave height is the average height of waves typically reported from usual observations. Such observations, however, are found to be biased towards the higher waves in a sea-state, and H_s can be defined more precisely as the mean of the highest third of the waves. The mean zero crossing period is defined as the average time between up-crossings of the surface elevation through the mean water-level.

The Pierson-Moskowitz spectrum derived from measured data for fully developed seas has the form

$$S_{hh}(\mathbf{w}) = \frac{A}{\mathbf{w}^5} e^{-\left(\frac{B}{\mathbf{w}^4}\right)} \quad (5.8)$$

where A and B are constants that can be evaluated for H_s and T_z , giving the one-sided wave spectrum

$$S_{hh}(\mathbf{w}) = \frac{1}{2\mathbf{p}} \frac{H_s^2}{4\mathbf{p}T_z^4} \left(\frac{2\mathbf{p}}{\mathbf{w}}\right)^5 e^{\frac{-(2\mathbf{p})^4}{\mathbf{p}T_z^4 \mathbf{w}^4}}. \quad (5.9)$$

Though developed from wave data in the North Sea, the Pierson-Moskowitz spectrum has the theoretical basis of wave energy spectrum formulated by Phillips (see, for instance, Phillips, 1958). Theoretically the spectrum frequency ranges between zero and ∞ , with the

zeroth spectral moment (the area under S_{hh}) equal to the mean square deviation of the water surface from the mean level. This is proportional to the wave energy in that sea-state.

It has been found that in the North Sea, with its limited fetch conditions and mainly wind-generated seas, the spectra are more “peaky” than the Pierson-Moskowitz shape (Hasselmann *et al.*, 1973). After measurements were taken in the North Sea, the JONSWAP spectrum was developed and can be described by adjusting the Pierson-Moskowitz spectrum. For an equivalent H_s and T_z , the JONSWAP spectrum gives a higher but narrower peak elevation, with the peak’s amplitude and frequency conditioned by a frequency dependent factor \mathbf{g} known as the peak enhancement factor. As the fetch length of the wind increases, the sea-state becomes fully developed and the JONSWAP spectrum approaches the Pierson-Moskowitz shape. Various authors have suggested formulations of the JONSWAP spectrum in terms of parameters commonly measured or predicted, usually wave height and period (see, for example, Houmb and Overvik, 1976 or Carter, 1982). Within this thesis, however, the JONSWAP spectrum described by Ochi (1979) has been implemented into JAKUP and used. Ochi suggested a mean value of the peak shape parameter \mathbf{g} of 3.3 with a standard deviation of 0.79. To describe the JONSWAP spectrum the following variables need to be defined:

$$\mathbf{g} = 3.3; \quad (5.10a)$$

$$k_b = 1.4085; \quad (5.10b)$$

$$k_p = 0.327e^{-0.315\mathbf{g}} + 1.17; \quad (5.10c)$$

$$k_g = 1 - 0.285 \ln(\mathbf{g}) \quad (5.10d)$$

where k_b is the value of T_p/T_z when $\mathbf{g} = 1$ (the Pierson-Moskowitz spectrum) and k_p defines the relationship between the mean zero crossing period and the period

corresponding to peak spectral frequency T_p , such that $T_p = k_p T_z$. The parameter k_g is a normalising factor. The JONSWAP spectrum, as described by Ochi, can therefore be written as

$$S_{hh}(\mathbf{w}) = \frac{1}{2\mathbf{p}} \frac{H_s^2 k_b^4 k_g}{4\mathbf{p} T_p^4} \left(\frac{2\mathbf{p}}{\mathbf{w}} \right)^5 e^{-\frac{1}{\mathbf{p}} \left(\frac{2\mathbf{p} k_b}{\mathbf{w} T_p} \right)^4} \mathbf{g}^a \quad \text{where } a = e^{-\frac{(\mathbf{w} - \mathbf{w}_p)^2}{2s^2 \mathbf{w}_p^2}} \quad (5.11)$$

and where \mathbf{w}_p represents the peak spectral frequency. As consistent with Hasselmann *et al.* (1973), \mathbf{s} has the numerical values 0.07 and 0.09 for $\mathbf{w} \leq 2\mathbf{p}/T_p$ and $\mathbf{w} > 2\mathbf{p}/T_p$ respectively.

5.3 Implementation of NewWave into JAKUP

NewWave theory has been implemented into JAKUP with the choice of either the Pierson-Moskowitz (Eqn 5.9) or JONSWAP (Eqn 5.11) as the wave energy spectrum. Fig. 5.1 shows the difference in the spectral shape for a sample sea-state characterised by $H_s = 12$ m and $T_z = 10$ s. The development of the extreme NewWave surface elevation in the time domain assuming a Pierson-Moskowitz spectrum is illustrated in Fig 5.2. In this example, the crest elevation \mathbf{a} has been set at 12m. A spectral bandwidth (\mathbf{e}) of 0.6 was achieved by cutting the tail of the spectral density function at $\mathbf{w} = 1.405$ rad/s. The bandwidth parameter characterises the frequency over which most of the wave energy exists, and for an unbounded spectrum $\mathbf{e} = 1$. The Nyquist frequency was assumed as $\mathbf{w} = 1.405$ rad/s and for frequencies larger than this a spectral density of zero was used for padding up to the maximum frequency of $\mathbf{w}_{\max} = 2\mathbf{w}_{ny} = 2.81$ rad/s. This ensures no corruption of the spectrum at high frequencies, a process known as aliasing. The number of frequency components (N) is user-defined; in this example $N = 512$, giving a $d\mathbf{w}$ component of 0.005488 rad/s. While describing a second-order theory, Jensen *et al.* (1995)

published the values of the surface elevation of a linear NewWave for the equivalent sea-state and spectral shape. Fig. 5.2 shows these values, which correspond to the profile evaluated by JAKUP. The wave profiles derived from the Pierson-Moskowitz and JONSWAP spectra for the same sea-state are shown in Fig. 5.3, with the JONSWAP spectrum showing evidence of a narrower banded spectrum as its autocorrelation decays less rapidly.

5.3.1 Wave Dispersion Relationship

A spatial profile of NewWave similar in shape to Fig. 5.2 can be obtained from the wave number spectrum. Due to the dispersive nature of ocean waves, however, a more rapid decay in the wave profile as a function of distance than as a function of time can be expected. Though a spatially variable NewWave at a constant time is not needed to analyse jack-ups, due to the substantial separation of their legs (51.96 m in the example structure used in this thesis), the ability to evaluate accurately the time varying surface elevation and kinematics at two spatial positions is significant. Therefore, the relationship between space and time will be further explored.

Angular frequency ω , and wave number k are related by the dispersion relation for plane waves, and in water of constant depth d this can be written as

$$\omega^2 = gk \tanh(kd). \quad (5.12)$$

The usual approach to solving Eqn 5.12 for the unknown wave number, when the frequency is specified, is to ‘guess’ a first approximation and iterate with an appropriate algorithm such as Newton’s method. However, this is a computational burden and care is required to ensure a robust algorithm for all values of ω . To avoid this calculation, the deep water approximation of $\omega^2 = gk$ is often used, but for JAKUP to be versatile under all conditions

this assumption was not deemed appropriate, and Eqn 5.12 is invariably used in the evaluation of wave number spectrum.

An approximate solution method of Eqn 5.12, as outlined by Newman (1990), has been implemented in JAKUP. Newman derived polynomial approximations valid for all water depths and accurate to seven or eight significant figures. Furthermore, with only two iterations of a conventional Newton-Rhapson approach, double precision accuracy (fourteen significant figures) can be achieved. The solution is separated into two water depth ranges, the first representing shallow water ($0 \leq kd \leq 2$) and the second deep water conditions ($kd \geq 2$), with Newman stating that the partition at $kd = 2$ is “somewhat arbitrary”.

In both cases, the solution of the water wave dispersion relationship can be found as a summation of known polynomial values. For the lower range, representing shallow water ($0 \leq kd \leq 2$), this can be written as

$$y_n \cong \frac{\sqrt{x_n}}{\sum_{i=0}^8 c_i \left(\frac{1}{2} x_n \right)^i} \quad (5.13)$$

where $y_n = k_n d$, $x_n = \mathbf{w}_n^2 d / g$. For the upper range representing deep water ($kd \geq 2$) it can be written as

$$y_n \cong x_n + \sum_{i=0}^5 b_i \left(\frac{1}{2} x_n e^{(4-2x_n)} \right)^i. \quad (5.14)$$

The values of c_i , $i = 0, 1, \dots, 8$ and b_i , $i = 0, 1, \dots, 5$ are presented in Table 5.1.

5.3.1.1 Implementation of NewWave in JAKUP - Dispersion Relationship

Fig. 5.4 shows the NewWave surface elevation profile evaluated by JAKUP for the upwave and downwave legs of the example structure for the same spectral conditions as used in Fig. 5.2. The co-ordinate x -axis has been defined as shown in Fig. 5.4, with $x = 0$ m and $x = 51.96$ m representing the upwave and downwave legs respectively. The peak crest of the NewWave has been focused on the upwave leg at $t = 0$ s. For all of the analyses in this thesis, the rig is orientated with two upwave legs and one downwave leg. From a series of simulations focussing the wave in various positions, this rig orientation and wave position was interpreted as the critical condition.

5.4 NewWave Kinematics

5.4.1 Theory

As NewWave is based on linear wave theory, the water particle kinematics can be easily obtained once the water surface is established. Though vertical kinematics can be derived, for the analysis of jack-up units only the horizontal kinematics are necessary and for unidirectional waves they can be written as

$$u(X, z, \mathbf{t}) = \frac{\mathbf{a}}{\mathbf{S}^2} \sum_{n=1}^N [S_{hh}(\mathbf{w}_n) d\mathbf{w}] \mathbf{w}_n F_n(z) \cos(k_n X - \mathbf{w}_n \mathbf{t}) \quad (5.15)$$

$$\dot{u}(X, z, \mathbf{t}) = \frac{\mathbf{a}}{\mathbf{S}^2} \sum_{n=1}^N [S_{hh}(\mathbf{w}_n) d\mathbf{w}] \mathbf{w}_n^2 F_n(z) \sin(k_n X - \mathbf{w}_n \mathbf{t}) \quad (5.16)$$

where u and \dot{u} are the horizontal water particle velocity and acceleration respectively. F_n is the horizontal attenuation factor and, as a function of depth z , is given by linear theory as

$$F_n(z) = \frac{\cosh(k_n(d+z))}{\sinh(k_n d)}. \quad (5.17)$$

As the kinematics in Eqns 5.15 and 5.16 are derived from linear wave theory, they have no theoretical validity above the mean water-level and care must be taken in describing their values in a crest. A number of extrapolation or stretching approaches are commonly used, such as delta stretching (Rodenbusch and Forristall, 1986) or Wheeler stretching (Wheeler, 1970).

Fig. 5.5 shows both extrapolation and stretching procedures widely used to evaluate wave kinematics in a crest. A straight extrapolation (linear extrapolation) above the mean surface can be used; however, this will over-predict wave kinematics. Vertical extrapolation uses linear theory up to the mean water-level and then uses the kinematics at the mean level up to the free surface. Wheeler stretching also uses the mean water-level kinematics as the free surface kinematics, but stretches the entire profile by modifying the depth attenuation function F_n to become

$$F_n(z) = \frac{\cosh\left(\frac{k_n(d+z)}{1+h/d}\right)}{\sinh(k_n d)} \quad (5.18)$$

where h is the instantaneous surface elevation. Wheeler stretching and linear extrapolation provide a lower and upper bound respectively for horizontal particle velocities in the crest of waves (Forristall, 1981). Delta stretching interpolates between the two, whilst maintaining some of the smooth non-linearities of a stretched profile (Rodenbusch and Forristall, 1986). This is achieved by stretching the vertical axis by replacing the depth z in the attenuation factor with z_s , at any height above half the significant wave height ($D_s = H_s/2$) below the mean water-level, according to

$$z_s = (z + D_s) \frac{(\nabla h + D_s)}{(h + D_s)} - D_s \quad \text{for } z > -D_s \text{ and } h > 0$$

$$z_s = z \quad \text{otherwise} \quad (5.19)$$

where ∇ is the stretching parameter (usually set as 0.3). All of these procedures are approximations and all break linear wave theory (namely the Laplace equation or the free surface boundary conditions).

In linear theory, a procedure for stretching (or extrapolation) is more important for steeper waves where the shorter wave components tend to over-predict wave kinematics in the crest. Compared with a single periodic model, NewWave being broad banded makes it less sensitive to over-prediction of wave kinematics; nevertheless, the difference in kinematics is significant and stretching (or extrapolation) should always be used with NewWave. Although there are numerous methods described in the literature, there is no clear preferred option. Stretching and extrapolation techniques with example calculations are further discussed in section 5.5.1.

5.4.2 Example of NewWave Kinematics in JAKUP

Fig. 5.6 shows the horizontal particle velocities calculated by JAKUP for an extreme wave under a crest for the example conditions used to generate the wave surface elevation in Fig. 5.2 (*i.e.* $H_s = 12$ m, $T_z = 10$ s and $\epsilon = 0.6$). The water depth was 200 m. The difference between the horizontal velocities with and without the use of Wheeler stretching is highlighted. The horizontal velocities below the first and largest trough (located at $x = \pm 5.62$ m) are also shown in Fig. 5.6. The horizontal velocities evaluated by JAKUP for the non-stretched case again correspond to the results published by Jensen *et al.* (1995) for the same conditions.

5.4.3 Example Response of a Jack-Up Subjected to NewWave Loading

The extended Morison equation (Eqn 2.2) is used in JAKUP to relate the horizontal kinematics to the hydrodynamic loads on the jack-up legs, as outlined in section 2.3.2. Fig. 5.8 indicates the wave forces calculated on each leg in the time domain for the NewWave used in the above example (the surface elevation at both legs is again shown in Fig 5.7). The example jack-up unit used here, and also for the rest of the thesis, is shown in Fig. 2.1. The forces at a given time are the sum of the loads applied at each node on the leg at that time. The rig is assumed to have two legs upwave, so for the 'upwave legs' the values shown are the total for two legs. For this example, the environmental force is purely wave loading, with no wind or current included. As the hydrodynamic loading includes relative velocity effects, it should be noted that Fig. 5.8 represents the Model C foundation case.

The corresponding horizontal deck displacements due to this NewWave are shown in Fig. 5.9, for three foundation cases: pinned, Model C and linear springs. Pinned footings represent infinite horizontal and vertical, but no rotational stiffness. Model C is the strain hardening plasticity model described in Chapters 3 and 4, whilst linear springs represents finite stiffness of equivalent formulation and values to the elastic region of the Model C case (Eqn 3.8). The parameters of Model C used are as outlined in Table 4.1 (an N_g value of 250 was used). Though only horizontal deck displacements have been shown, any measure of structural response can be determined by JAKUP. After the NewWave passes, the structure can be seen to be vibrating in its natural mode. With increased rotational fixity the natural periods decrease, with approximate values of 9, 5, and 5 seconds for the pinned, Model C and linear spring footings respectively. As expected, the pinned footings give the largest horizontal deck displacement over the time period. The pinned case for this example is rather conservative compared with the Model C footings, with a peak displacement close

to a factor of four greater (as would be expected from a quasi-static linear model of a simplified jack-up).

For the example in Figs 5.7 to 5.9, the load combinations on the Model C footings were contained entirely within the yield surface, giving a response equivalent to the linear spring case. By increasing the crest amplitude to $a = 15$ m or $a = 18$ m, as shown in Fig. 5.10, the increased loading caused plastic displacements in the Model C footings, shifting the entire foundations and leaving a permanent offset in the displacement of the deck. This yielding of the sand footings occurred during the peak of the NewWave. The natural period during this event may also be modified by the plastic behaviour. These examples have shown NewWave theory conveniently and efficiently implemented into a structural analysis program.

5.5 Discussion of NewWave

5.5.1 Calculation of Kinematics – Linear Stretching/Extrapolation

Procedures

For the analysis of jack-ups, interest lies not so much in the kinematics but the forces they translate onto the jack-up's legs, and then the dynamic response to them. To demonstrate the difference in the stretching procedures an example calculation was performed for wave conditions that a large jack-up in the North Sea could expect. Model C foundations were used, with the peak period of the sea-state chosen as three times the natural period of the structure (*i.e.* $T_p = 3T_{structure} \approx 15$ s). NewWave elevations were scaled to represent increasing wave steepness, with elevations given in Table 5.2.

The forces on the upwave leg and corresponding horizontal deck displacements are shown in Fig. 5.11 and Fig. 5.12 respectively. The linear extrapolation and Wheeler stretching give

upper and lower limits to the largest forces and dynamic response respectively, with similar response evaluated for delta stretching and vertical extrapolation. The choice of procedure is clearly more important with increasing wave steepness, with significant differences in deck displacements shown for the $k_p \mathbf{a} = 0.3$ case.

5.5.2 Second-Order NewWave Theory

Stokes (1847) demonstrated the non-linearity of finite amplitude water waves, and today design waves used to evaluate loads on offshore structures are usually Stokes' fifth-order waves (*i.e.* a deterministic non-linear regular wave). With the only free parameters being wave height and period, the spectral content of the waves is not considered. In NewWave, however, the spectral content is considered, but only by using linear waves. Second-order corrections to NewWave, which would account for both the spectral content and some non-linearities, have been suggested by several authors (Taylor, 1992; Jensen *et al.*, 1995; Jensen 1996); a discussion of these theories follows in sections 5.5.2.1 and 5.5.2.2. By accounting for the effects of short waves riding on longer waves, both the free surface elevation and the horizontal fluid velocities (within the extreme crest where the uncertainties are greatest) can be modelled to second-order.

5.5.2.1 The Second-Order Correction Suggested by Taylor (1992)

Taylor (1992) suggested a semi-empirical second-order extension to NewWave, making use of Longuet-Higgins and Stewart's (1964) theories about the effect of superposition of two sets of regular waves of different frequencies and wavelength. Longuet-Higgins and Stewart showed that there was a significant change in both the amplitude and the wavenumber of a short wave due to the presence of a long one, but not vice versa. They wrote this amplitude modulation and wave number variation as

$$\frac{\mathbf{a}}{\mathbf{a}_0} = \frac{k}{k_0} = 1 + AK \cos(Kx) \quad (5.20)$$

where \mathbf{a} and k are the varying amplitude and wavenumber of the shorter wave respectively, and \mathbf{a}_0 and k_0 are the shorter wave's amplitude and wave number in the absence of the longer wave. The parameters A and K are the amplitude and wave number of the longer wave. The modulations in Eqns 5.20 emphasise the physical causes of non-linearity, *i.e.* the vertical straining and horizontal propagation respectively.

In his second-order correction to NewWave, Taylor (1992) assumed that the mean wave-profile is identical with the profile obtained by taking all phase lags in the individual wave components to be equal to zero at the extreme wave crest, with the effects of Eqn 5.20 added to the formulation. With the individual wave component amplitudes being taken from the linear result, Taylor's formulation is only an empirical correction for second-order and does not have a well defined second-order stochastic definition. Just as the free surface is modified by second-order wave interaction, the velocity fields of the individual wavelets are affected, with Taylor also detailing a second-order extension for horizontal velocities.

5.5.2.2 Second-Order NewWaves Suggested by Jensen (1996)

Jensen (1996) has outlined explicit second-order formulae for the conditional mean value of the wave profile and the wave kinematics. These formulae are derived from Stokes' second-order unidirectional waves in deep water. However, any moderate non-linear wave theory could be used to generate the statistical moments needed to depict the conditional mean wave description. The mean values are determined for slightly non-Gaussian correlated processes and are conditional on both the value and slope of the surface elevation at a particular point. For the largest wave this is taken as being the extreme wave

crest with a slope of zero. Explicit details will not be given here; however, their development and formulation can be found in Jensen *et al.* (1995) and Jensen (1996).¹

5.5.2.3 Comparisons of the Second-Order Formulations with Linear Kinematics

Both Taylor's (1992) and Jensen's (1996) formulations have been independently implemented in JAKUP, allowing surface elevations and kinematics (at both legs) to be evaluated to second-order. For the steepest condition in Table 5.2 ($T_p = 15$ s and linear NewWave amplitude = 16.79 m), the surface elevations for linear NewWave theory, Taylor's second-order extension and Jensen's formulation are shown in Fig. 5.13. The horizontal particle kinematics are also shown in Fig. 5.14, with comparisons with Wheeler and delta stretching of the linear profile given. Both Wheeler stretching and Jensen's second-order formulation give a smooth velocity profile, whereas delta stretching and Taylor's second-order formulation are disjointed at or just below the mean water-level.

The second-order surface elevation profile developed by Jensen (1996) gives steeper slopes above the still water level and shallower troughs than those predicted by linear NewWave theory and also Taylor's (1992) second-order correction. The predictions also reduce the horizontal velocity of the wave kinematics, a result which is consistent with the conventional Stokes' fifth-order wave (Jensen, 1996). Furthermore, the kinematics can be evaluated without the need for stretching; therefore, no further assumptions are introduced. The kinematics are, however, sensitive to the bandwidth parameter (or cut-off frequency).

For the same conditions, Fig. 5.15 shows the horizontal deck displacements estimated by JAKUP for the second-order theories and compares them with a linear NewWave with delta and Wheeler stretching. For this example, Taylor's (1992) second-order formulation

¹ Jensen (1996) is an extension of the second-order formulation of Jensen *et al.* (1995). Taking the formulation further, it assumes that the wave elevation at a particular point in space or time is actually a

gives a similar response to the delta stretching method. Although there are significant differences in the kinematics and predicted forces at different depths on the jack-up legs, *i.e.* Taylor's second order is predicting larger forces around the crest but lower below the mean sea-level, these differences have averaged out over the entire leg. Jensen's (1996) second-order formulation has given the smallest response, though it is similar to Wheeler stretching. Fig. 5.15 shows that there is as much difference in response caused by the choice of stretching procedure in a linear theory as by choosing a second-order formulation.

In Chapter 6 linear NewWaves are constrained within a random background to evaluate extreme response statistics of jack-ups in random seas. It is possible to constrain second-order waves in a similar way; however, considering the additional computational burden, this was not performed in this thesis.

Chapter 6 - Evaluation of Extreme Response Statistics using Constrained NewWave

6.1 Introduction

Much computation is needed to evaluate extreme response statistics using full random time domain simulations with only a few of the waves in each time series capable of producing the extreme result. In contrast to this, by constraining a NewWave with a predetermined large crest in an arbitrary random time series, Taylor *et al.* (1995) devised a method that allows for the calculation of extreme statistics without the same degree of computational burden.

This chapter is concerned with the evaluation of extreme response statistics of jack-up units using the Constrained NewWave methodology. Firstly, the theoretical derivations and implementation of both full random simulation and Constrained NewWave are detailed, with example calculations highlighting the importance of a random background in the analysis of jack-ups. Following this, a method of generating short- and long-term response statistics using JAKUP is examined. The short-term is based on individual sea-state activity over a short discrete time period, whilst the long-term is based on the response to many sea-states over extended periods of time. The term sea-state as used here defines the set of parameters that describe statistically the wave conditions at a given time (typically three hours) and location. An example calculation based on a jack-up located in the central North Sea is detailed.

6.2 Theoretical Background

6.2.1 Numerical Random Wave Simulation

The numerical method widely used to evaluate a random instantaneous elevation of the sea surface from a given wave energy spectrum is based on the summation of a finite number of Fourier components, as described by Eqns 5.1 and 5.2. This method, however, only correctly simulates a Gaussian random process at the limits $d\mathbf{w} \rightarrow 0$ and $N \rightarrow \infty$ (see Rice, 1944 and Tucker *et al.*, 1984), *i.e.* when the summation becomes an integration. For finite values of N , by using deterministic values of the amplitude components c_n , $n = 1, 2, \dots, N$, the variability of a Gaussian random process is not truly modelled. Tucker *et al.* suggest an alternative method where the amplitude components are themselves random variables.

For use in this procedure, Eqn 5.1 can alternatively be written as

$$\mathbf{h}(t) = \sum_{n=1}^{N/2} (a_n \cos(\mathbf{w}_n t) + b_n \sin(\mathbf{w}_n t)) \quad (6.1)$$

where a_n and b_n are Fourier components which are themselves independent Gaussian random variables with zero mean and a variance related to the wave energy spectrum at the corresponding discrete frequency:

$$s_{\mathbf{h}\mathbf{h},n}^2 = S_{\mathbf{h}\mathbf{h}}(\mathbf{w}_n) d\mathbf{w} . \quad (6.2)$$

Therefore, a_n (and b_n) can be easily simulated by finding the product of a standardised normally distributed random variable rn_{a_n} (or rn_{b_n}) with zero mean and the standard deviation $s_{\mathbf{h}\mathbf{h},n}$ as

$$a_n = rn_{a_n} \sqrt{S_{hh}(\mathbf{w}_n) d\mathbf{w}} \quad \text{and} \quad b_n = rn_{b_n} \sqrt{S_{hh}(\mathbf{w}_n) d\mathbf{w}} \quad (6.3)$$

noting that rn_{a_n} and rn_{b_n} are independent.

6.2.1.1 Implementation in JAKUP

The method of evaluating a random surface elevation established by Tucker *et al.* (1984) has been implemented into JAKUP, allowing the capability of full random time domain analysis. As an example of this implementation, the calculation of one random surface elevation for the sea-state characterised by $H_s = 12$ m and $T_z = 10$ s will be described. The JONSWAP spectrum with the frequency cut at $\mathbf{w} = \pi/2$ rad/s is used with 512 summation components. Fig. 6.1 shows the randomly generated Fourier coefficients a_n and b_n for a typical realisation, whilst Fig. 6.2 illustrates the surface elevation for these components. The timesteps are marked by crosses with $dt = 2\mathbf{p}/\mathbf{w}_{max}$. The unsmoothed power spectral density of this realisation is shown in Fig. 6.3 for comparison with the standard JONSWAP spectrum for the same sea-state. The variance of the JONSWAP spectrum was calculated as 8.979 compared with 8.750 for this random realisation. By repeating the process and averaging the ensembled realisations, or by smoothing a single realisation, a closer fit to the JONSWAP spectrum would be achieved.

6.2.2 Constraining a NewWave into a Random Background

It is important when constraining a NewWave into a random sequence that the constrained sequence is statistically indistinguishable from the original random sequence. The details of a procedure achieving this (as outlined by Taylor *et al.* (1995)) follow. The constrained surface elevation $\mathbf{h}_c(t)$ could be considered as

$$\mathbf{h}_c(t) = \mathbf{h}_r(t) + Qe(t) + Rf(t) \quad (6.4)$$

where $\mathbf{h}_r(t)$ is the random surface of Eqn 6.1 and $e(t)$ and $f(t)$ are two non-random functions of the form

$$e(t) = \sum_{n=1}^{N/2} c_n \cos(\mathbf{w}_n t) \quad \text{and} \quad f(t) = \sum_{n=1}^{N/2} d_n \sin(\mathbf{w}_n t) \quad (6.5)$$

where c_n and d_n at $t=0$ have the same statistical properties as a_n and b_n in Eqn 6.1.

The values of c_n and d_n , and the forms of Q and R , are selected to constrain $\mathbf{h}_c(t)$ at $t=0$ to the criteria $\mathbf{h}_c(0) = \mathbf{a}$ and $\dot{\mathbf{h}}_c(0) = \dot{\mathbf{a}}$, where \mathbf{a} is the predetermined crest elevation and $\dot{\mathbf{a}}$ the gradient. For a crest $\dot{\mathbf{a}}$ is naturally set to zero. Therefore, Q and R can be evaluated as

$$Q = \frac{1}{c} \left[\mathbf{a} - \sum_{n=1}^{N/2} a_n \right] \quad \text{where} \quad c = \sum_{n=1}^{N/2} c_n, \quad \text{and} \quad (6.6a)$$

$$R = \frac{1}{d} \left[\dot{\mathbf{a}} - \sum_{n=1}^{N/2} \mathbf{w}_n b_n \right] \quad \text{where} \quad d = \sum_{n=1}^{N/2} \mathbf{w}_n d_n. \quad (6.6b)$$

As stated by Taylor *et al.*, there is an infinite set of solutions of $e(t)$ and $f(t)$ that can constrain this process to satisfy the criteria. However, the desired choice should minimise the variance of the constrained process, allowing the profile $\mathbf{h}_c(t)$ to be as similar as possible to the expected profile $E[\mathbf{h}_c(t)]$, where

$$E[\mathbf{h}_c(t)] = E[\mathbf{h}_r(t)] + e(t).E[Q] + f(t).E[R] = \frac{\mathbf{a}e(t)}{c} + \frac{\dot{\mathbf{a}}f(t)}{d}. \quad (6.7)$$

The one solution which achieves this is

$$\frac{e(t)}{c} = r(t) \quad \text{and} \quad \frac{f(t)}{d} = \frac{-\dot{r}(t)}{\mathbf{I}^2} \quad (6.8)$$

where $r(t)$ is the autocorrelation function (or the unit NewWave), and $\dot{r}(t)$ the differentiation of the autocorrelation function with respect to time (or the slope of the unit NewWave). I^2 is obtained from the second spectral moment of the wave energy spectrum ($m_2 = I^2 S^2$).

By substituting these solutions into Eqn 6.4, the solution of the constrained surface elevation is derived as

$$\mathbf{h}_c(t) = \mathbf{h}_r(t) + r(t) \cdot \left[\mathbf{a} - \sum_{n=1}^{N/2} a_n \right] + \left(\frac{-\dot{r}(t)}{I^2} \right) \left[\dot{\mathbf{a}} - \sum_{n=1}^{N/2} \mathbf{w}_n b_n \right] \quad (6.9)$$

(1) (2) (3) (4) (5) (6) (7)

where the terms have the following meanings:

term (1) - the original random surface elevation;

term (2) - the unit NewWave;

term (3) - the predetermined constrained amplitude (\mathbf{a});

term (4) - the original random surface elevation at $t = 0$ (or $\mathbf{h}_r(0)$);

term (5) - the slope of the unit NewWave;

term (6) - the predetermined constrained slope; for a crest, $\dot{\mathbf{a}} = 0$;

term (7) - the original random surface's slope at $t = 0$ (or $\mathbf{h}_r(0)$).

6.2.2.1 Example Response of a Jack-Up Subjected to a Constrained NewWave

Fig. 6.4 illustrates the surface elevation of a NewWave with a crest elevation of 15 m embedded in a random sea-state characterised by $H_s = 12$ m and $T_z = 10$ s. The wave has been constrained such that at about 59.34 s its peak collides with the upwave leg of the jack-up. It is shown in Fig. 6.4 that, for this example, the influence of the NewWave on the surface elevation is contained to within 40 s of the constrained peak. The surface elevation for the downwave as well as the upwave leg, as evaluated in JAKUP, is

displayed in Fig. 6.5. The corresponding deck displacements with time are shown in Fig. 6.6 for the linear springs, Model C and pinned foundation assumptions. For this example embedment, the peak displacements have been increased compared with just the equivalent NewWave (Fig. 5.10). This is due to the random background and the structural memory caused, indicating that for dynamically sensitive structures, such as jack-ups, the response is not only conditional on the present applied load, but also on the load history. As was the case for a jack-up loaded exclusively by a NewWave, the assumption of pinned footings is clearly illustrated in Fig. 6.6 as overly conservative. The linear springs can be seen to yield lower displacements than the Model C footing due to the greater stiffness exhibited. In addition, Model C indicates a permanent horizontal displacement occurring in the jack-up.

6.3 Using Constrained NewWave in the Evaluation of Response Statistics of Jack-Ups

6.3.1 Overview

Though only one Constrained NewWave example has so far been shown here, one of the main benefits of the constraining technique is that the probability distribution of the extreme response can be estimated without the need to simulate many hours of real time, most of which is of no interest. For a storm associated with one sea-state, shorter time periods can be used with a logical combination of crest elevations to simulate responses for the expected wave sizes within that sea-state. Convolution with the probability of occurrences of crest elevations allows for the compilation of response statistics. With knowledge of long-term sea conditions, long-term extreme exceedence probabilities for response design properties of interest in the reliability of jack-ups (for example lower leg-guide moments or deck displacement) can be evaluated.

6.3.2 Methodology Adopted for the Evaluation of Short-Term Statistics

Within this thesis, simulations of 75 s duration, with the crests constrained at 60 s, are used to estimate the time history response associated with one crest height. A lead time of 60 s was considered to have the same statistical response properties due to the crest when compared with longer time periods. For five discrete crest elevations representative of the full range of wave heights in a three hour storm, 200 simulations per crest elevation were performed using JAKUP. The largest response caused by the constrained peak was recorded for each simulation. The extreme response distributions were evaluated by convolving responses from the five constrained crest elevations with the Rayleigh distribution of crest heights. This was accomplished numerically using Monte Carlo techniques. The steps followed are outlined below and are also shown in Fig. 6.7:

Step 1: For a short time period (for example three hours), crest heights may be randomly derived assuming a Rayleigh distribution.¹ One crest elevation is predicted as

$$\mathbf{a}_{pred} = \sqrt{-(2\mathbf{s}^2) \cdot \ln(1 - rn)} \quad (6.10)$$

where rn is a random number generated from a uniform distribution between 0 and 1. Therefore, a set of wave crests \mathbf{a}_i , $i = 1, 2, \dots, N_{crest}$, can be estimated from a Monte Carlo simulation (N_{crest} is the number of wave crests, assumed as the time period divided by T_2).

Step 2: Using the response information from the 5 sets of 200 JAKUP runs, lines of constant probability are constructed by firstly sorting the response at each of the five

¹ This is based on the assumption of a Gaussian sea and a narrow-banded process (see Longuet-Higgins (1952)). The Gaussian sea assumption depends on the water depth of the jack-up and for many shallow water cases it would not be appropriate.

NewWave crest elevations into order from the lowest (or 1st) response to the highest (or 200th) response. Following this, polynomial curve fitting of the five responses representing the five NewWave elevations at each response level (1 → 200) gives 200 lines of constant probability.² These lines allow response values to be estimated for crest elevations between the five NewWave amplitudes used in JAKUP. Construction of the lines of constant probability will be shown in an example in section 6.3.3.

For each crest elevation in *step 1*, i.e. \mathbf{a}_i , $i = 1, 2, \dots, N_{crest}$, a response corresponding to its elevation is “randomly” chosen. By simulating a number between 1 → 200 (the number of JAKUP runs per NewWave crest elevation), interpolation along that number’s line of constant probability gives the “random” response for that one crest. Repeating for all N_{crest} elevations completes a set of responses for that time period. This is shown in *step 2* of Fig. 6.7. Therefore, for one random three-hour event, the distribution of responses within that sea-state have been calculated and the extreme event can be extracted.

Step 3: By repeating *steps 1* and *2*, responses for different three-hour events are evaluated and, by using the maximum of each, the distribution of extreme response can be compiled. This is shown in *step 3* of Fig. 6.7. In the numerical experiments in this thesis, distributions are based on 2500 of these samples.

6.3.3 Example Numerical Results for One Sea-State ($H_s = 12\text{ s}$ and $T_z = 10.805\text{ s}$)

An example of the methodology described in section 6.3.2 to compile short-term extreme response statistics is outlined here. The sea-state described by the JONSWAP wave

² The 200 lines of constant probability need to be constructed only once and contain all of the response

energy spectrum with parameters $H_s = 12$ m and $T_z = 10.805$ s has been chosen. This is the base condition on which the long-term numerical experiments in section 6.4 are contingent and is assumed to be representative of the 100 year sea-state in a central North Sea location.

Fig. 6.8 shows the deck displacements calculated by JAKUP for the five crest elevations: 3.5, 7, 10, 12 and 15 m. Though Fig. 6.8 seems to illustrate larger variation of deck displacements as the NewWave crest elevation increases, this is not the case. When the coefficient of variation is calculated, defined in the usual way as

$$CoV_x = \frac{\mathbf{s}_x}{\mathbf{m}_x} \quad (6.11)$$

where \mathbf{s}_x and \mathbf{m}_x are the standard deviation and mean of set x respectively, there is actually a reduction in CoV with increasing elevation. This implies that as the crest elevations become higher, they also become more dominant in the calculation of global response, thereby reducing the response's variation.

Constructed by simple polynomial curve fitting, Fig. 6.9 shows five example lines of constant probability between the levels of evaluated response. This was performed using standard MATLAB functions and was necessary for the interpolation of intermediate crests. The actual number of lines of constant probability used is not five, as implied in Fig. 6.9, but is the number of simulations at each crest elevation performed by JAKUP (in this case 200).

The extreme response distribution for deck displacement, evaluated using the convolution procedure described in section 6.3.2, is shown in Fig. 6.10. The mean and 50% exceedence values are 0.251 and 0.241 m respectively and the distribution has a CoV of 22.26%.

6.3.4 Verification of Short-Term Extreme Response Results

The accuracy of this method has been examined by repeating the calculations. Four new sets of 200 extreme responses per crest elevation were evaluated by JAKUP and the convolution procedures repeated. With little difference between the resulting statistics, uniformity in successive tests is shown in Fig. 6.11. The question of whether 200 responses per crest elevation is a large enough sample has also been answered. With convolution performed on all the data (1000 JAKUP responses per crest elevation), the extreme response statistics evaluated are consistent with results evaluated from the 200 JAKUP response data. This is shown in Fig. 6.11 and validates the use of only 200 extreme responses per crest elevation.

Consistency is also shown in Fig. 6.11 for a more extreme sea-state, $H_s = 16.45$ m and $T_z = 12.66$ s (the 1 in 10^6 year sea-state used in the long-term calculations of section 6.4). This is an important outcome, as the method used is validated for large amounts of plasticity and non-linearities in the Model C calculation and, moreover, the results for the more ‘linear’ pinned and linear spring cases can therefore also be accepted.

The results have also been verified by “brute force” random wave simulation for both sea-states. As shown in Fig. 6.12, one hundred full three-hour simulations correspond well with the Constrained NewWave results.

Comparisons of the values for the maximum horizontal force on the jack-up legs for the repeated calculations and the full random domain simulation are shown in Fig. 6.13. Again, the Constrained NewWave procedure used with a sample of 200 response data for five crest elevations is satisfactory.

6.4 Evaluation of Long-Term Statistics: A Numerical Experiment on an Example Jack-Up

6.4.1 Overview

An understanding of long-term meteorological and oceanographic (met-ocean) conditions is needed before any convolution of short-term statistics into long-term probabilities can be performed. Difficulties arise, however, in extrapolating measured or hindcast time series data, which in the North Sea are usually only of length 5-25 years, to longer return periods. A short review of extrapolation methods used will be given here, and then the approach taken for the numerical experiments in this chapter will be highlighted.

6.4.1.1 Review of Extrapolation Methods

In an effort to derive long-term design conditions, one widely used method is to derive a “design wave”, an individual wave with a height which is exceeded on average only once in a specified return period (for example, 100 years) (see Durning (1971), Hogben (1990) or Tucker (1991)). The design wave is evaluated by finding the 100-year return value of H_s from either a measured or predicted cumulative distribution (usually log-normal, Weibull or Fisher Tippett Type 1) and then for that 100-year H_s , the most probable maximum wave height in a three-hour period (Tucker, 1991). Wind and current are assumed to act independently and similar procedures are used to calculate design wind and current velocities for the return period in question. This is unnecessarily conservative as the extreme events are not expected to occur at precisely the same time (Forristall *et*

al., 1991). Uncertainty in the extreme wave in a sea-state is neglected, with only most probable values calculated. As sea-state is defined as the independent variable, correlation between successive sea-states is also neglected.

For dynamically sensitive structures, the design wave does not always represent the situation producing the greatest force on the structure, making the design wave approach inadequate in reliability calculations of jack-up units. As an alternative, Tromans and Vanderschuren (1995) demonstrated a method for the prediction of extreme waves and long-term load statistics based on the assumption of “storms” as individual events. Here a storm is defined as a continuous period of severe sea with H_s at over 30-40% of the peak H_s in the database record for the particular location. In the North Sea the NESS hindcast database can be used (Peters *et al.*, 1993). Typically lasting from 12 to 36 hours, a storm has a period of increasing H_s , a peak and then a decaying phase. For a typical location several hundred storms might be extracted from 25 years of data (Tromans and Vanderschuren, 1995), and these results can be used to develop short- and long-term statistics.

Short-term: By characterising each storm in the database by its most probable extreme individual wave, a model for the uncertainty of an extreme within a short time scale (or storm) can be achieved.

Long-term: Compiling all the most probable extreme wave heights for each individual storm provides a picture of the long-term distribution of that variable. However, with limited data available, extrapolation to large values of most probable extreme wave height requires an assumption of the distribution the data follows. Convolution of the short- and long-term models provides a complete storm-based long-term distribution, accounting for uncertainty of the extreme within a storm and the uncertainty in storm severity.

6.4.1.2 Response-Based Design Conditions

Using generic load models (for drag-dominated quasi-static structures) that combine the environmental variables into a structural response, such as base shear force, Tromans and Vanderschuren (1995) describe a method of evaluating response-based joint ocean design conditions. By using a similar procedure to that of wave height (see section 6.4.1.1), Tromans and Vanderschuren deduce the distribution of long-term extreme loads (for instance base shear force and overturning moment). For any return period, therefore, the design wave parameters of interest (crest elevation, current and wind) can be evaluated as the solutions which equate the same loads in the generic model. This approach has the advantage of accounting for joint probabilities of occurrence and evaluating design conditions based on the response of a structure. Example normalised load versus return period for the northern, central and southern North Sea, as well as the Gulf of Mexico, produced by Tromans and Vanderschuren, are shown in Fig. 6.14 (the loads have been normalised by the 100-year result). The central North Sea results presented here are used as the basis for scaling of sea-states in the long-term evaluations in this chapter (see section 6.4.2 below).

6.4.2 Example Calculations for a Central North Sea Jack-Up

To describe the long-term behaviour of the jack-up in this investigation, assumptions about the condition of the wave environment had to be made. The three major assumptions were:

1. The 1 in 100 year value of H_s was assumed to be 12 m. This is a value which could be derived from NESS for a specific site; however, for most positions in the central North Sea it is believed to be reasonable.

2. From this base condition, H_s was scaled to other return periods ranging between 1 year and 10^6 years. The scaling is based on the normalised load versus return period of Fig. 6.14 for the central North Sea, *i.e.* a 22% increase in load per factor of 10 on return period. With load approximately estimated as proportional to the crest elevation squared (\mathbf{a}^2) in drag-dominated structures, and with \mathbf{a} proportional to H_s , H_s was scaled by $\sqrt{1.22}$ per factor of 10 on return period. This can be written as

$$H_s(r.p.) = H_{s_{100\text{-year}}} \sqrt{1 + 0.22(\log_{10}(r.p.) - 2)} \quad (6.12)$$

where $r.p.$ is the return period and $H_{s_{100\text{-year}}}$ the 100 year return period value of H_s (*i.e.* 12m). Table 6.1 outlines the return periods and corresponding H_s values used. It is acknowledged that this assumption is based on a curve derived on a generic quasi-static structure; however, the H_s values deduced will give reasonable results to study long-term jack-up response.

3. For all the experiments, wave steepness was assumed constant at $k_p H_s = 0.25$, with values of T_z and T_p also given in Table 6.1

These conditions are a simplification of a real environment. With a known location and access to a hindcast database a more accurate analysis could be performed in practice. The methodology of determining long-term statistics, however, would be the same as the procedure detailed in this chapter. Two numerical experiments were performed, one excluding and one including wind and current effects. As mentioned previously, Fig. 2.1 shows the example jack-up used in a water depth of 90 m.

6.4.3 First Long-Term Numerical Experiment - Wave Loading Only

For the first numerical experiment, wave loading was the only environmental force, with no wind or current applied. For seven return periods, Table 6.1 outlines the sea-states and five crest elevations at which the NewWave peak was constrained.

Implicit in this statistical approach is the assumption that it is not possible to determine a meaningful upper limit of sea-state wave conditions. However, the limiting size of a sea-state in the North Sea must depend on the geographical fetch limits and wind duration. Therefore, the physical possibility of the larger sea-states should be questioned. For example, is the 1 in 10^6 year sea-state used here possible? Moreover, even if it is possible, for the results to be credible all of the components of the analysis (*i.e.* the structural, foundation and wave models) must remain accurate at this sea-state severity. The contribution of this sea-state, however, to probability levels of interest ($10^{-4} \rightarrow 10^{-6}$) is negligible.³ Nonetheless, it has been included to complete the trends occurring, and to show what might be expected in extrapolation to very low levels of probabilities (for instance 10^{-9}). The reality of a sea-state of this severity and the physical bounds of any analysis, however, must be kept in mind in the interpretation and discussion of the results presented.

Following the procedures in section 6.3.3, seven short-term extreme response distributions were evaluated. The distributions of maximum deck displacement for Model C footings are shown in Fig. 6.15. With increasing severity of the short-term conditions, Fig. 6.15 indicates increasing variation in the levels of response. Hypotheses explaining

³ Fjeld (1977) in a summary of probabilities of failure used in recognised codes quotes an accepted failure level of 10^{-4} - 10^{-6} in the offshore industry compared with a level of 10^{-6} - 10^{-7} onshore. The Canadian Standards Association sets the target annual probability of failure at 10^{-3} when there is a small

this are investigated here. As the sea-states become more severe, the CoVs of load increase. This is because drag loading on the jack-up will be increasingly dominant compared with inertia loading and, due to the horizontal particle velocity squared term in the drag component of the Morison equation (Eqn 2.2), CoVs also increase. This is shown in Figs 6.16(a) and (b), where the values of maximum force CoVs exemplify this well. However, this does not fully explain the higher levels of variation found in the deck displacement extreme response distributions, and other factors must be contributing.

With increasing severity, the amount of plasticity in the Model C calculation must add to the variation in the levels of extreme deck displacement response. The amount of plasticity in any simulation can be represented by the V_0 value to which the yield surface has expanded. In Model C, as the loading on a footing reaches the yield surface, it expands according to the hardening law, with its size described by V_0 . Therefore, the V_0 value normalised by the initial $V_{0_{pre-load}}$ can be used as a descriptive measure of the level of plasticity in the calculation. The extreme response $V_0/V_{0_{pre-load}}$ values for the upwave and downwave footings are shown in Figs 6.17(a) and (b) respectively. For the 1 in 1 year sea-state in both footings, $V_0/V_{0_{pre-load}} = 1$, indicating that all loading was within the initial yield surface and only elastic behaviour occurred. However, as the sea-states became more severe, the levels of $V_0/V_{0_{pre-load}}$ and their variation both increase. This must contribute to the variation of global response of the jack-up as indicated in the increasing CoVs of deck displacement.

risk to life and a low potential for environmental damage, and at 10^{-5} for situations of great risk to life or high potential for environmental damage (Sharples *et al.*, 1989).

Both the mean and CoV values of $V_0/V_{0_{pre-load}}$ are larger for the downwave footing than for the upwave footing. This is due to the combination of larger vertical loads pushing the downwave footing into the sand, and the sliding occurring in the upwave footing due to the NewWave's peak being focussed on the upwave leg.

6.4.3.1 Methodology Adopted to Numerically Scale Short-Term Extreme Response Distributions

With the extreme response distribution evaluated for each sea-state (*i.e.* 1 in 10^j year, $j = 0, 1, \dots, 6$), convolution with the logarithmic distribution of sea-state occurrences gives long-term probability predictions of response. However, as sea-states do not occur in discrete intervals, the extreme response distribution of any intermediate sea-state must be adequately estimated to evaluate this convolution numerically. Though numerous techniques would be satisfactory, a method based on the scaling of the “normalised” 1 in 100 year distribution has been chosen here due to its ease of implementation.

By normalising each curve by its 50% exceedence value ($R_{50\%}$), a point common in all short-term sea-states is achieved. This is shown for all three footing assumptions in Fig. 6.18. Two scale factors, $sf_{0.8}$ and $sf_{0.2}$ —one for the upper tail ($0.5 \leq Q(x) \leq 1.0$) and one for the lower tail ($0 \leq Q(x) < 0.5$)—are evaluated at $Q(x) = 0.8$ and $Q(x) = 0.2$ respectively. The scale factors represent the difference in normalised response (at $Q(x) = 0.8$ and $Q(x) = 0.2$) between each return period and the 100 year sea-state. Each return period distribution is weighted according to its relation in logarithmic time to the 1 in 100 year ($j = 2$) distribution, *i.e.* each integer increase in j (for example 1 in $10^0 \rightarrow$ 1 in 10^1 or 1 in $10^3 \rightarrow$ 1 in 10^4) is equivalent to one order of magnitude of the scale factor. Therefore, $sf_{0.8}$ is evaluated as the sum of the difference between all of the normalised

curves compared with the 100 year curve at $Q(x) = 0.8$, scaled according to the number of integers in logarithmic time (values of j) they are from the 100 year curve ($j = 2$). In numerical form this can be written as:

$$sf_{0.8} = \frac{\sum_{j=0}^6 [R/R_{50\% \ j} - R/R_{50\% \ j=2}]}{\sum_{j=0}^6 |j - 2|} \quad (6.13)$$

where $R/R_{50\%}$ is the normalised measured response at $Q(x) = 0.8$ and j the power integer describing the sea-state occurrence. The numerator represents the sum of the difference in the normalised curves' response values at $Q(x) = 0.8$ and the denominator the sum of the integer differences (remembering that $sf_{0.8}$ represents one step of the power integer). This calculation is also summarised in Fig. 6.19. A similar calculation can be performed on the lower tail to evaluate $sf_{0.2}$. Fig. 6.20 shows the 50% response exceedence values ($R_{50\%}$) used in the normalisation process for each sea-state. The curves of best fit indicate the 50% exceedence values to be used to re-scale at any intermediate level.

With the scale factors calculated, the extreme response can be estimated for any return period and cumulative probability value ($Q(x)$). For the return period of value j , using the appropriate $R_{50\%}$ value and the normalised 1 in 10^2 distribution (*i.e.* $[R/R_{50\%}]_{j=2}$), the extreme response can be evaluated at the $Q(x) = 0.8$ level as

$$x_j = [R_{50\%}]_j \cdot \left([R/R_{50\% \ Q(x)=0.8}]_{j=2} + (j-2).sf_{0.8} \right) \quad \text{for } Q(x) = 0.8. \quad (6.14a)$$

Assuming a linear scaling of $sf_{0.8}$ from $Q(x) = 0.5$ to $Q(x) = 1.0$ (i.e. at $Q(x) = 0.5$, $sf_{0.8} = 0$ and at $Q(x) = 0.8$, $sf_{0.8} = sf_{0.8}$), at any value of $Q(x)$ the extreme response can be evaluated as

$$x_j = [R_{50\%}]_j \cdot \left([R/R_{50\%}]_{j=2} + \left(\frac{Q(x) - 0.5}{0.3} \right) (j - 2) \cdot sf_{0.8} \right) \text{ for } Q(x) \geq 0.5 \quad (6.14b)$$

For the lower tail, the formulation of Eqn 6.14 is the same, except that $sf_{0.2}$ replaces $sf_{0.8}$. For the Model C case, the equivalent scaled values for $j = 0, 1, \dots, 6$ are shown in Fig. 6.21, for comparison with the original distributions. Throughout the distributions, the scaled curves approximate the original curves closely.

6.4.3.2 Monte Carlo Sampling of Long-Term Extreme Exceedence Probabilities

Using the scaling and convolution procedures described in section 6.4.3.1, long-term extreme exceedence probabilities for the horizontal deck displacement have been evaluated for the example jack-up and are shown in Fig. 6.22. All three foundation cases are presented, with the additional variation in the short-term Model C distributions creating a more non-linear long-term curve. As expected, for large annual exceedence probabilities ($10^0 \rightarrow 10^{-1}$), the linear springs and the Model C cases are equivalent. However, as the probabilities get smaller, the Model C deck displacements become relatively larger and there is a significant difference between the Model C and linear spring displacements. For annual exceedence values of 10^{-4} and 10^{-5} (probability levels of interest in an offshore reliability analysis), the Model C displacements are 33% and 50% greater respectively; this indicates the importance of the plasticity component of the model to the level of response.

The pinned case is again shown to be conservative compared to Model C for all annual probabilities of exceedence, although with enough extrapolation the Model C curve could be expected to cross the pinned curve. This is possible as horizontal plastic displacements are accounted for in the Model C formulation. In this analysis with no wind or current, however, this would not occur at any significant level of probability.

There is a little less than a factor of four difference between the pinned and the linear springs cases. This is expected as non-linearities in both the structure and loading are included, and the linear springs case, though very stiff, is not fully fixed. Theoretically, if non-linear and dynamic amplification effects were not considered, there would be a factor of four difference between a pinned and fixed case for a jack-up with a very stiff hull.

6.4.3.3 Long-Term Loads on the Jack-Up Legs

Fig. 6.23 shows the long-term annual probabilities of exceedence for forces on the legs of a jack-up. It is of interest to compare these results with the initial assumption upon which the scaling of H_s was based (Eqn 6.12). Rather than giving a steady linear increase in force of 22% per factor of 10 on the return period (as in Fig. 6.14), the loads increase non-linearly. The assumption that force is proportional to wave amplitude squared, and thus H_s^2 , is overestimating the force due to the NewWaves. This could be due to the fact that:

- The force on the legs is not completely drag-dominated, as the assumption suggests, with the level of inertia compared with drag loading changing the CoVs for each short-term sea-state. The inclusion of other non-linearities in the loading also changes the results from the initial “linear” assumption.
- Force is not only proportional to H_s , but as T_z increases with more extreme sea-states, loading varies in a non-linear manner. This is due to changes in the wave energy spectrum influencing the wave kinematics formulation, the depth dependency function

and also the load on the downwave legs (affected because of the dispersive nature of waves).

It has been shown that the initial assumption, which was based on a generic load model of a quasi-static structure, has not held for the non-linearities associated with the analyses in JAKUP. However, as discussed in section 6.4.2, the sea-states and associated return periods are not for a specific location, but a general assumption of what could occur in the central North Sea. Therefore, though not consistent with Fig. 6.14, the long-term loads on the legs are still representative of the example location described by Table 6.1.

6.4.4 Second Long-term Numerical Experiment - All Environmental Forces

During a second numerical experiment with the same wave loading, wind and current loading was applied as outlined in Table 6.2. The wind force was assumed as point loads on the nodes of the deck with two thirds applied at the upwave and one third at the downwave node. The wind loading was assumed as 15% of the constrained NewWave loading on all legs at the 100-year condition (as shown in Table 6.3) and then scaled for the other sea-states according to Fig. 6.14.⁴ A uniform current of 0.8 m/s was chosen for the base 100-year case and also scaled to give the same force ratio per time of occurrence as the wave and wind loading.

The value of current is similar to values used in previous studies of jack-up response (see, for example, Morandi *et al.* (1997) and Karunakaran *et al.* (1994)). It is assumed here to be an independent variable and its level might be highly conservative if joint contributions were considered. Peters *et al.* (1993) suggest that widely used current values based on

⁴ The proportion of 15% was chosen as a representative level of wind load that could be expected on the jack-up (see, for instance, Patel (1989))

guidance notes (such as SNAME) could be more than double the magnitude of currents associated with extreme waves based on NESS.

Fig. 6.24 shows the maximum deck displacement distributions normalised by their 50% exceedence values for three hour periods of the seven sea-states. As was the case for the experiment with no wind or current loading, all three foundation cases exhibit an increase in variation with sea-state severity, with the increase larger for the Model C case. However, the magnitudes of all the CoVs are less than they are with no wind or current (see Fig. 6.18). This is to be expected as the wind and current do not act with any variation. In the numerical experiments detailed here, wind is a steady force which for each realisation causes a consistent deck offset. Moreover, current adds to the magnitude of horizontal particle velocity by the same amount for each realisation. Therefore, both wind and current reduce the CoVs of the force and deck displacement calculations; Table 6.3 outlines the magnitude and variation of force both with and without wind and current.

The predicted long-term horizontal deck displacements are shown in Fig. 6.25. The difference in Model C and the linear springs is evident and more significant with the additional wind and current loading. At the 10^{-4} and 10^{-5} levels, the increase in deck displacement is about 75% and 100% respectively. Furthermore, this difference increases to 233% for an annual probability of exceedence of 10^{-9} , where the Model C case has nearly crossed the pinned footing curve.

6.4.5 Measuring the Relative Importance of the Random Background

It has been shown for one realisation in Fig. 6.6 that the random background in which a NewWave is constrained affects the force on and response of the jack-up. It is therefore significant to evaluate the relative importance of this background and determine if there is

a need to perform random time domain analysis in the calculation of long-term statistics of jack-up response.

To address this, the two long-term numerical experiments were repeated for the same environmental conditions, except that the NewWaves were not constrained in a random sea, but acted on their own. For all the NewWave elevations, the results of horizontal deck displacement are shown in Fig. 6.26. Although only results for Model C are shown, similar trends occur for the linear spring and pinned cases. Using the same convolution and scaling procedures, short-term maximum response distributions and long-term probability estimates were evaluated.

Table 6.4 contains the mean and CoV values for the three-hour maximum deck displacement distributions, and Table 6.3 presents the respective force results. Assuming a fixed relation between wave force and wave height (H), an estimate of a CoV for the extreme wave force can be calculated from the Rayleigh distribution ($R(H)$) of wave heights raised to the power of the number of waves (N_{crest}) in the sea state:

$$P(H_{extr.} / H_s) = [R(H / H_s)]^{N_{crest}} . \quad (6.15)$$

By assuming that the extreme force is proportional to H for inertia-dominated structures and H^2 for drag-dominated, Harland *et al.* (1997) estimated CoVs of 8.5% and 17% respectively in a single three-hour sea-state. On this basis, the force CoVs in Table 6.3 are clearly more drag-dominated. The additional variation is probably due to the assumptions made by Harland *et al.* and the use of the extended Morison equation in JAKUP.

In Fig. 6.27 the long-term deck displacement estimates are compared with the fully constrained results. For all annual probability of exceedence levels, the random

background sea increases the deck displacement response. The percentage increase at a number of levels is shown in Table 6.5. The linear spring and pinned cases have similar differences, steady for the range of probabilities at around 6% to 8%. However, for Model C, rather than maintaining a constant difference, the estimates of response for the Constrained NewWave case become proportionately larger relative to just the NewWave case. At the $10^{-4} \rightarrow 10^{-5}$ probability levels, they are around double that of the linear and pinned case, and at the more unreliable 10^{-8} level, they have increased to a multiple of around two and a half. This implies that the random background noise is more significant when using plasticity footing models than when using linear springs or pinned footings. In general, however, for all three foundation assumptions investigated, the levels of difference are high enough to necessitate the need for full random analysis, especially as they are non-conservative in nature.

The comparison of the force applied to the jack-up due to the Constrained NewWave and just the NewWave is shown in Fig. 6.28 for the cases without and with wind and current respectively. As for hull displacement, the Constrained NewWave gives a significantly larger probability of exceedence level.

6.4.6 Further Discussion of Long-Term Results

Although jack-up leg forces and deck displacement have been the only responses shown so far, the same methodology could be used to evaluate long-term statistics for any jack-up response variable. One design property of interest in the reliability of jack-ups is lower leg-guide moment. From JAKUP this is estimated as the moment at the node linking the deck element and the highest leg element (one for each leg). Fig. 6.29 shows the long-term probability of exceedence for lower leg-guide moments for the same example conditions. As expected, the results follow the same trends as for the horizontal deck displacement,

and the benefits of using Model C are evident. For example, if a critical design bending moment was set at 1.0 GNm, using the overly conservative pinned footing assumption, an annual exceedence probability of around 10^{-4} would be calculated. Conversely, using Model C as a more realistic interpretation of spudcan fixity, this value is reduced to around 10^{-6} . This could result in the difference between acceptance and non-acceptance of the rig.

Chapter 7 - Application of Probabilistic Models in the Response Analysis of Jack-Ups

7.1 Introduction

In chapter 6 the probabilistic response of jack-up units was introduced through the random nature of wave loading. The rest of the model was deterministic; *i.e.* its material properties, geometric properties and its actions were uniquely specified. It is known, however, that there are parameters within the models presented that are not unique, but have a range of possibilities. For example, if the mass of the deck could be measured it would vary in value. Furthermore, if experimental testing of the structural, wave loading and foundation models of JAKUP could be performed, they too would give a variable response, even for the same input conditions. Therefore, by using a probabilistic formulation of one or more of the material properties, geometric dimensions or even the action of the structure, the likelihood that the jack-up behaves in a certain way can be more “realistically” evaluated.

This probabilistic approach is an extension of any deterministic analysis, but with a number of previously deterministic quantities randomly interpreted with specified distributions. Within this chapter, probabilistic methods are used to develop understanding of the response behaviour of jack-ups. Variables which influence the dynamic response are addressed and probabilistic distributions attributed to them. These are known as random variables. A sensitivity study is described of the important random variables involved in the evaluation of extreme dynamic response of an example jack-up, using JAKUP and the Model C foundation model. Within this study, not only has the significance of parameters within an elasto-plastic foundation model been evaluated, but their relative importance compared with other random variables commonly used in reliability analyses has also been calculated.

7.2 Literature Review

7.2.1 General Reliability Theory

Probabilistic response of jack-up units is most commonly encountered during reliability evaluations. In structural reliability theory, the failure probability of one component is defined as

$$P_f = P[G(X) \leq 0] = \int_{G(X) \leq 0} f_X(X) dx \quad (7.1)$$

where $G(X)$ is the failure function ($G(X) \leq 0$ is a failure state and $G(X) > 0$ a safe state) and X is a set of k random basic variables, *i.e.* $[X] = [X_1, X_2, \dots, X_k]$ (further details of random variables used in jack-up analyses can be found in section 7.5). $f_X(X)$ is the multi-variant density function of X . For a component reliability analysis, failure criteria are usually set on the limiting factors of strength or behaviour of the jack-up and are of the form:

$$G(X) = R - S \quad (7.2)$$

where R is the component's resistance (or upper limit of strength/behaviour) and S its serviceability (or calculated response distribution from load effects). This failure region is shown in Fig 7.1 in a diagrammatic comparison of a deterministic and a probabilistic analysis.

Confidence in this probabilistic approach depends on the following factors:

- The ability to evaluate the integral in Eqn 7.1 accurately. Techniques to achieve this are described in section 7.2.2.
- The accuracy of the failure function. In any reliability analysis, the results can only be judged by the accuracy of the individual modelling components used in the analysis.

This is especially true for highly interactive and non-linear processes, as seen in jack-ups. With inappropriate and highly conservative assumptions, such as pinned footings, not only are the reliability results inaccurate, but the level of uncertainty in them can be unacceptably high. It is, therefore, important to have confidence in the failure function derived.

- The probabilistic modelling of the uncertainty in the basic random variables. The statistical spread assumed for random variables needs to reflect their inherent variability, and this will be investigated for application to jack-up dynamic response in section 7.5.

7.2.2 Reliability Calculation Techniques

One method of calculating the integral in Eqn 7.1 is by Monte Carlo simulation. For each simulated vector of random variables X , a complete numerical experiment needs to be performed. As the majority of structural analysis problems are complex and computationally time-consuming, this requires a prohibitively large number of complete runs to produce a result with statistical confidence. This is especially true for small probabilities of failure.

Alternate methods requiring less computational effort include:

- *Response Surface Methods* (RSM): If the computational effort is large for each response calculation in a Monte Carlo simulation, then this calculation can be replaced by a response surface (RS) that is of simple mathematical form and can be solved more efficiently. Once the RS is determined it is used to predict the required response, avoiding the former complicated numerical procedure. In this chapter response surfaces are used to estimate jack-up horizontal deck displacements (based on results evaluated by JAKUP); these are further described in section 7.4.
- *First Order Reliability Methods* (FORM): The failure function (or the RS) is approximated by a first order function in standardised Gaussian space at the most probable failure point. In standardised Gaussian space this is the point physically

closest to the origin (the mean point). More details of FORM, along with a practical example, are given in section 7.6.1.5.

- *Second Order Reliability Methods (SORM)*: Similar to FORM except that curvature is considered by fitting a second order function. SORM has not been used in this chapter.
- *Importance Sampling in Monte Carlo Simulations*: Monte Carlo techniques can be optimised by organising the sampling procedure around the most probable failure area. This minimises the amount of sampling required. Though not used here, examples of importance sampling techniques in structural analysis can be found in Melchers (1989) or Karunakaran (1993).

7.2.3 Use of Reliability Theory for the Analysis of Jack-Up Units

Difficulties arise when attempting reliability calculations of jack-up platforms, due to their highly non-linear dynamic response. Dynamic effects change for different response quantities and sea-states, and various approaches have been used in published studies to account for the dynamic contribution. For example, in a comparative study of the reliability of jack-ups and jackets designed according to design assessment procedures (SNAME (1994) and API (1993) respectively), Morandi *et al.* (1997) used an additional load set to account for dynamic effects, *i.e.* they used a DAF to scale the forces of one “design wave” from a quasi-static analysis. The design wave was calculated by finding the return period H_s required from a long-term probability distribution of H_s , and then the short-term most probable highest wave from the Rayleigh distribution. This method is arguably unconservative as it assumes the dynamic contribution to response is the same for all sea-states and response characteristics. Short-term force variability is accounted for by Morandi *et al.* as a basic random variable with a COV of 18% (perhaps a little low when compared with the COVs calculated for short-term force variation in Chapter 6).

A method which calculates DAFs for short-term sea-states and then applies each in a long-term evaluation was outlined by Daghigh *et al.* (1997). Using a simplified jack-up model, for each short-term sea-state the largest stress response was evaluated in each of the following three analyses:

- three hours of random sea using a dynamic analysis,
- the same three hours of sea using a quasi-static analysis, and
- a short-term design wave (based on the most probable highest wave from the Rayleigh distribution) for a quasi-static analysis.

A DAF was then calculated to scale the quasi-static design wave force to a short-term three-hour dynamic force, through the intermediary three-hour quasi-static analysis. To calculate short-term reliability values of a more detailed jack-up, Daghigh *et al.* proceeded to use simple quasi-static design waves, but with their forces scaled by the DAFs calculated. Long-term reliability values were calculated by ‘adding the reliabilities for various short-term sea-states in accordance with the scatter diagram for the area of operation’ (Daghigh *et al.*, 1997). This method, while accounting for differences in long-term sea-state dynamics, does not correctly account for the variation within the short-term seas. As shown in Chapter 6, the variation of force for three-hour short-term seas is considerable; however, the method used by Daghigh *et al.* results in only one value for short-term dynamic force per sea-state.

In both Morandi *et al.* (1997) and Daghigh *et al.* (1997), extremely complex finite element models were used but, with the simplest of foundation assumptions. In the latter the structural model consisted of 1800 nodes, yet the foundations were assumed to be pinned. It has been shown in this thesis that the foundation model used can affect the long-term probability of exceedence of response by an order of magnitude; thus these reliability results must be interpreted in light of that consideration. The study detailed by Morandi *et al.* is, however, part of an ongoing investigation commissioned by the U.K. Health and

Safety Executive, and will include Martin's (1994) Model B elasto-plastic model for spudcans on clay at a later stage.

Karunakaran (1993), in a study of the non-linear dynamic behaviour of jack-up units, proposed a reliability procedure accounting for long-term response. Noting that traditional design wave methodology in combination with dynamic amplification factors, as used, for example, by Morandi *et al.* (1997), is not capable of predicting the extreme dynamic response correctly and may even give unconservative results, Karunakaran fit three-parameter Weibull distributions to maxima calculated for short-term sea-states. However, he used only 10-20 samples of 45-60 minutes length in the evaluation of these distributions. By dividing an example scatter diagram of the location into regions of similar dynamic response and fitting short-term distributions to these blocks, Karunakaran then calculated long-term reliability values in a consistent manner by convolution of the short-term distributions and their long-term probabilities of occurrence (as can be determined from the scatter diagram).

Similarly, the long-term reliability experiments in this chapter will be based upon the combination of short-term distributions with their long-term expectance. The long-term sea-states used for the example experiments in Chapter 6 will again be utilised.

7.3 Aims of Numerical Experiments

The aims of the numerical experiments discussed in this chapter are:

- to ascertain and incorporate probabilistic distributions for random variables which influence the response analysis of jack-up units;
- for short-term sea-states, to fit response surfaces which adequately model an example jack-up response (in this chapter horizontal deck displacement is investigated);

- to evaluate the significance of each random variable to this extreme jack-up response;
- for long-term conditions, to compare the probability of exceedence estimates for deck displacement using probabilistic random variables with the values calculated using just their deterministic mean values (previously evaluated in Chapter 6). This comparison will be made for NewWaves without any random background.

7.4 Use of the Response Surface Method (RSM)

As shown in Chapter 6, the calculation of jack-up response probabilities of exceedence using Monte Carlo techniques requires a significant sample size. For numerical experiments with probabilistic distributions of random variables, the use of one JAKUP run per response calculation would be computationally prohibitive. Therefore, to estimate probability of exceedence values in this chapter, JAKUP is replaced by a RS which can predict extreme response efficiently.

To create a RS, a suitable mathematical form is chosen with a finite set of parameters to be uniquely fixed. If there are k free parameters, for instance, then it only requires k different experiments to fit the surface (or in this case k JAKUP runs). However, with only k experiments no information is given about error of fit and the possible random error; therefore, it is usual to make more than k experiments when fitting the surface. In this case, the surface parameters are chosen by a regression method based on the minimisation of the total misfit error.

Within this chapter the form of the response surface chosen to model extreme jack-up response is the versatile second-order polynomial with mixed terms:

$$\hat{S}(X) = a + \sum_{i=1}^k b_i X_i + \sum_{i=1}^k c_i X_i^2 + \sum_{i<j}^k \sum_{j=1}^k d_{ij} X_i X_j + \mathbf{e} \quad (7.3)$$

where X_i and X_j are the i^{th} and j^{th} components respectively of the set of random variables, a , b_i , c_i and d_{ij} the free parameters needing evaluation (a total of $1 + 2k + k(k-1)/2$ parameters) and \mathbf{e} the error of fit. The term \hat{S} represents the service response predicted by the RS. This form was chosen for its ability to model response with significant system curvature. Unfortunately, it carries no formal resemblance to the actual surface resulting from the mechanical modelling of jack-ups; however, with further developments a surface shape resembling the physical processes more closely could be identified.

The free parameters are evaluated by systematic numerical experiments using the central composite design method (see, for instance, Myers and Montgomery, 1995). There are three main sets of random variables (X) used to fit the surface, as depicted in Fig. 7.2 (for the $k = 2$ case). They are:

- The axial points, which largely contribute to the estimation of the quadratic terms, but not to the interaction terms. There are $2k$ axial points.
- The factorial points, which contribute to the estimation of linear terms, but also are the sole contributors to evaluation of the interaction terms. The number of factorial points is equal to 2^k .
- The central runs, which contribute to the estimation of the quadratic terms and provide an evaluation of pure error. The number of central runs is user-defined, as discussed below.

Fig. 7.2 depicts an axial “distance”¹ of $\sqrt{2}$ and gives the number of central runs as three. These are the only components of the method that allow flexibility in the design and both are important to the RS accuracy. The axial distance chosen is usually in the range of 1 to \sqrt{k}

(for a factorial distance of ± 1 standard deviations from the mean), and these points define the experimental design region (Myers and Montgomery, 1995). The latter forms an equal distance from the centre, with the factorial points creating a “spherical” design region, whilst the former creates a ‘cubic’ region. If one chooses an axial distance of \sqrt{k} and an appropriate number of centre runs (Myers and Montgomery recommend three to five runs), the prediction variance has the same value at any two locations that are the same distance from the design centre—a notion developed by Box and Hunter (1957) and known as “rotatability”. Centre runs also reduce the prediction variance within the design region and can give an estimate of pure error. However, in JAKUP, for NewWaves not constrained in a random background, all central runs give an equivalent response. For the response surfaces developed in this chapter the spherical design is used.

As an alternative to regression analysis, “interpolating polynomials” could be used to fit a RS (Bucher and Bourgund, 1990). Once a first attempt at evaluating an equivalent RS has been performed, a design point (defined as the point on the failure surface closest to the mean of the normalised set of basic variables) can be established. This point represents the set of basic variables most likely to breach the ‘failure’ criteria. As the response surface’s accuracy might be questionable (the design point could be a distance from the central point where the surface was fit), further iteration is used to refine the response surface around this area of ‘most probable failure’. This technique is powerful when evaluating one failure point rather than a region of values (where re-runs of the iterations for every new failure point would be required). Interpolating polynomials were used by Morandi *et al.* (1997) in a reliability investigation of jack-ups; however, they will not be used here.

¹ All distances quoted here are in standardised Gaussian space and, therefore, need to be multiplied by \mathbf{S} , the standard deviation of the random variable. In this case all variables are assumed to be normally distributed.

7.5 Choice of Random Variables and their “Predicted” Variability

To quantify uncertainty in the modelling of jack-ups it is necessary to define a set of *basic* variables which govern the dynamic response of the structure. The term basic is used to emphasise that these quantities represent the most fundamental variables in the analysis calculation. This process of defining values for all input variables is also performed in a deterministic calculation with single values attributed. In a probabilistic approach, however, the uncertainty in the basic variables is specified.

There are distinctive types of uncertainty in the basic random variables to be considered.

These include:

- *Physical uncertainty*: due to inherent variability of the properties in nature. Loads, material properties and dimensions are all examples of basic variables which, if measured, would exhibit physical fluctuation which could be described in terms of a probabilistic distribution or stochastic process.
- *Statistical uncertainty*: as the physical variability can only be quantified from example data, which is often of small sample size, uncertainty arises due to the inferences drawn from these limited observations.

Besides the randomness and uncertainty associated with the input variables, uncertainty exists in the mechanical model set up to formulate the response. This *modelling uncertainty* includes not only uncertainty of model components, but also the response of the complete model.

7.5.1 Random Variables Influencing the Dynamic Response of Jack-Ups

Before a set of basic random variables was chosen to represent the loading and physical uncertainties in JAKUP, an investigation of random variables used in the literature was undertaken. The aim was to determine which variables might be important in the response analysis of jack-ups. Table 7.1 outlines the results and gives some indication of possible

distributions, mean values and CoVs. For clarity the basic random variables have been divided into four categories: environmental loading, geometric/structural, foundation and modelling.

Environmental Loading: Many studies formulate this variation in loading as a variation in the applied load calculated with deterministic values, as opposed to uncertainty in the individual components of the Morison equation; see, for instance, Morandi *et al.* (1997) and Lacasse and Nadim (1994). However, as one of the aims of these experiments is to compare the components of the models that are used in JAKUP, and not just to reach a probability of failure answer for one particular case, the most basic components were used.

In experiments, despite the attempt to maintain constant conditions, such as steady flow, viscosity, temperature, roughness and geometry, the measured values of the Morison drag and inertia coefficients exhibit considerable scatter (see, for example, Kim and Hibbard, 1975). With even greater complexities in the conditions for offshore jack-ups, such as interaction of members, marine growth and unsteady flow, any scaled experimental values would be invalid when applied to a real jack-up. There is therefore considerable uncertainty in the application of C_d and C_m arising from a large number of effects that are not fully understood (Thoft-Christensen and Baker, 1982). This uncertainty is reflected in values previously used in the literature, with CoVs of 20-25%; the drag coefficient is usually considered to have a larger variation than the inertia coefficient. Distributions used to describe the effect of marine growth on jack-ups have also been listed in Table 7.1. This uncertainty could also be included as a component of the uncertainty within the Morison coefficients.

Wind and current are other variables influencing the force on a jack-up. In reliability studies, wind can be described either in terms of wind velocity (Thoft-Christensen and

Baker, 1982) or as a wind force (Morandi *et al.*, 1997). As the wind loading in Chapter 6 was described as a force, the latter approach will be used here.

Geometric/Structural: Important variables found in the literature for the response of jack-ups are the mass of the deck and the structural damping ratio. Deck mass influences the dynamic response and geometric non-linearities, as well as the pre-load applied to the foundations. As Model C is very dependent on the pre-load level (as it determines the initial yield size), in the numerical experiments described later in this chapter these two effects have been separated into two variables: deck mass and pre-loading factor.

Foundation: Due to limited data (in terms of both quantity and quality) there is a large measure of subjective judgement when determining geotechnical uncertainty (Gilbert and Tang, 1995). In the literature surveyed, jack-up analyses (and reliability studies) generally contain complex structural or wave models, whilst using simplistic assumptions for the foundations. When probabilistic methods for geotechnical models have been used, it has often been as an overall uncertainty on the deterministic model's results (see for example Nadim and Lacasse (1992)). There are, however, a number of studies which used probabilistic distributions for the stiffness of the linear spring representation of spudcans, with variations shown in Table 7.1.

Modelling: Some typical examples of the types of statistical variations which are placed on jack-up models in reliability studies are shown in Table 7.1. Modelling uncertainty is incorporated by introducing variability (and often bias) to represent the ratio between the "actual" and predicted model response. Use of modelling uncertainty is discussed further in section 7.5.2.

7.5.2 Distributions of Random Variables used in Numerical Experiments

Based on the experience of previous studies (Table 7.1) and knowledge gained from the results of Chapter 5 and 6, eleven basic random variables have been chosen for an initial numerical experiment using JAKUP. Table 7.2 outlines these variables, their distribution type (formulations can be found in Appendix A), mean values and CoVs. There are three types of basic random variables used: environmental loading (current (u), C_d , C_m , $wind$), structural modelling (*structural damping*, *mass of hull*) and Model C (g , m_0 , N_g , $f - \mathbf{d}_p$, *pre-load*). All of these variables have been used previously, except the last two Model C parameters, with further explanation given here.

The basic variable $f - \mathbf{d}_p$ is a combination of the parameters f (the initial plastic stiffness factor) and \mathbf{d}_p (the dimensionless plastic penetration at peak), both of which affect the hardening law of Eqn 3.10. The initial stiffness is proportional to f (Eqn 4.2), and \mathbf{d}_p affects the location of the peak in plastic vertical displacement (Eqn 4.3). If f is reduced, to keep the peak at the same vertical load, \mathbf{d}_p must increase in proportion; therefore, the product of f and \mathbf{d}_p must remain constant. The basic variable $f - \mathbf{d}_p$ represents the f value used, with \mathbf{d}_p calculated as

$$\mathbf{d}_p = \frac{f_{mean} \times \mathbf{d}_{pmean}}{(f - \mathbf{d}_p)_{random}} = \frac{4.55 \times 10^{-3}}{(f - \mathbf{d}_p)_{random}}. \quad (7.4)$$

The hardening law's shape is changed by the range of $f - \mathbf{d}_p$ values, but with the peak of the vertical load remaining at the same level, as depicted in Fig. 7.3. The *pre-load factor* determines the amount of vertical pre-load applied to the foundations before operation (or numerically, before any wave loading is applied). The vertical pre-load per footing is

determined by the multiplication of this factor and the weight of the hull distributed to each leg.

Modelling uncertainty has been included as variation in the model's components (for instance, the variables g , m_0 and $f - \mathbf{d}_p$ in the Model C category) rather than uncertainty in the model itself. The idea of incorporating an uncertainty or bias to the calculated response due to a whole model, for example, Model C, is extremely difficult to quantify and reduces any attempt to reflect the physical processes occurring. Uncertainty in the fit of the RS has not been included as it is expected to be minimal (tests of this are described in section 7.6.1.3)

The statistical distributions ascribed to the Model C parameters should be considered as best judgements for an example numerical experiment, not as definitive results. Part of the motivation for these probabilistic numerical experiments is the identification of Model C parameters that are significant for jack-up response. It is hoped that a judgement on parameters needing more careful consideration in further research (to determine more representative distributions) and ones which can be thought of as deterministic (as they do not notably affect the response) will be resolved.

7.6 Short-Term Analysis (100-year return period)

7.6.1 NewWave with Most Probable Highest Amplitude (i.e. $\mathbf{a} = 0.93H_s$)

To test the application of a second-order polynomial as a RS for the random variable distributions outlined in Table 7.2, the 1 in 100 year sea-state of Chapter 6 is used with a NewWave amplitude held constant at its *most probable* highest wave elevation. There are two definitions of most probable highest elevation that could be used: the modal and the mean. Both will be investigated for the 100-year sea-state, starting with the modal.

For a narrow-banded sea, where the number of waves is N_{crest} , the modal extreme amplitude ($\bar{a}_{mod.}$) can be evaluated as

$$\bar{a}_{mod.} = \sqrt{2 \ln(N_{crest})} \sqrt{m_{0h}} \quad (7.5)$$

where m_{0h} is the zeroth spectral moment (the area under the wave spectrum).² For a narrow-banded spectrum this can be estimated as

$$m_{0h} = \left(\frac{H_s}{4.01} \right)^2 \quad (7.6)$$

Therefore, for three-hours of the example 100-year sea-state (characterised by $H_s = 12$ m, $T_z = 10.805$ m and with $N_{crest} = 1000$), using Eqns 7.5 and 7.6, $\bar{a}_{mod.} = 11.16$ m. This was the NewWave amplitude used in the first numerical experiment. The composite design method described in section 7.4, with 2071 different sets of random input variables, was used to fit the polynomial. The largest deck displacement was extracted from the displacement time series for each JAKUP run, and by minimising the error squared, polynomial coefficients for an extreme deck displacement RS were estimated. Their values are shown in Table 7.3.

7.6.1.1 Calculating Probability of Exceedence Results from a Monte Carlo Simulation of the RS

Using the distributions in Table 7.2, a random set of basic variables (X) can be selected and the corresponding deck displacement calculated from the extreme deck displacement RS. By

² h has been placed as a subscript on the zeroth spectral moment of the wave spectrum in this chapter to distinguish it from the dimension of the Model C yield surface in the moment direction (m_0).

repeating this process an extreme response distribution for deck displacement can be formulated, as shown in Fig. 7.4 for a NewWave amplitude of 11.16m in the 100-year sea-state. The number of random variable sets sampled for Fig. 7.4 was 10 000. The 50% exceedence value was evaluated as 0.369 m and the mean as 0.387 m. As expected, the 50% exceedence value approximates the deck displacement of 0.363 m calculated by JAKUP when all random variables equal their mean value.

7.6.1.2 The Mean Most Probable Highest Amplitude

For the same sea-state, another RS was evaluated for the mean highest amplitude in a three-hour sea-state. The NewWave was again held constant, with the same procedure used to approximate the RS and extreme response statistics. Barltrop and Adams (1991) estimate the mean extreme wave amplitude (\bar{a}_{mean}) for sea-states with over 100 crests as

$$\bar{a}_{mean} = \left(\sqrt{2 \ln(N_{crest})} + \frac{0.5772}{\sqrt{2 \ln(N_{crest})}} \right) \sqrt{m_{0h}}. \quad (7.7)$$

Fig. 7.5 compares the extreme response distributions of deck displacement for the modal highest wave with the mean highest wave. In the latter the NewWave amplitude was calculated from Eqn 7.7 as 11.60 m. A CoV of 30.32% for the mean distribution is similar to the modal value of 29.16%. The difference in deck displacements between the mean and modal distributions is greater in the middle region of the cumulative distribution than at both the high and low extremes. This indicates that the NewWave amplitude (and the additional force created) is not as important as the other basic random variables at these extremes.

7.6.1.3 How Precise is the Response Surface Fit?

To investigate the fit of the RS (for $\bar{a}_{mod.}$), retrospective simulations of sets of random variables were performed using JAKUP. The sets of basic variables were recorded from

the Monte Carlo calculation performed in section 7.6.1.1 and can be divided into two categories:

1. The first 1000 sets of random variables evaluated irrespective of the displacement calculated by the RS.
2. Three groups of 200 sets each, where the deck displacement calculated by the RS was between $0.2 \text{ m} < \mathbf{d}_{deck} \leq 0.4 \text{ m}$, $0.4 \text{ m} < \mathbf{d}_{deck} \leq 0.6 \text{ m}$ and $0.6 \text{ m} < \mathbf{d}_{deck}$.

This division was made so that the general random accuracy as well as the accuracy within bands of response could be gauged. Fig. 7.6 shows the deck displacements calculated by JAKUP against the predicted response of the RS for the first 1000 random variable sets. By inspection, the response surface seems to be accurately predicting the JAKUP evaluated displacements, with no bias evident. Fig. 7.7 has been divided into the response sections being retrospectively simulated; again the RS surface is indicating a good fit. For both large and small displacements, the RS is not as accurate as it is around the mean response level; this is expected as accuracy of the RS decreases as the set of basic variables move away from the initial central run (in this case $\mathbf{d}_{deck} = 0.363 \text{ m}$).

A quantitative measure of relative error ($\mathbf{e}_{rel.}$) has been evaluated as

$$\mathbf{e}_{rel.} = \frac{\hat{\mathbf{d}}_{deck} - \mathbf{d}_{deck}}{\mathbf{d}_{deck}} \cdot 100\% \quad (7.8)$$

where $\hat{\mathbf{d}}_{deck}$ and \mathbf{d}_{deck} are the deck displacements evaluated by the RS and JAKUP respectively. As shown in Figs 7.6 and 7.7, the relative error for the first 1000 runs was 2.08%, and for the three sets of 200: 2.47%, 1.04% and 2.15%. The relative error calculations confirm the observation that there is more accurate RS prediction surrounding the mean value.

7.6.1.4 Sensitivities of the Basic Random Variables

The relative importance of the random variable X_i can be calculated as $\partial P_f / \partial \mathbf{m}_{X_i}$ (Karunakaran, 1993). Within a Monte Carlo calculation this sensitivity measure denoted $S_{\mathbf{m}_{X_i}}$ can be evaluated as

$$S_{\mathbf{m}_{X_i}} = \frac{P_f(\mathbf{m}_X + d\mathbf{m}_{X_i}) - P_f(\mathbf{m}_X)}{d\mathbf{m}_{X_i} / \mathbf{m}_{X_i}} \quad (7.9)$$

where $d\mathbf{m}_{X_i}$ is a small change in the mean value of the random variable X_i . In this thesis this small change was assumed as a 1% increase (or decrease, depending on which change enlarged the response).

Table 7.4 outlines the sensitivity values calculated at three response levels ($\mathbf{d}_{deck} = 0.3, 0.5$ and 0.7 m) for the RS evaluated. The random variables have also been ranked in Table 7.4 according to their $S_{\mathbf{m}_{X_i}}$ value. The drag coefficient (C_d) can be interpreted as the most influential random variable at all levels of response, with current, hull mass, and the Model C parameters m_0 and the pre-load factor all consistently showing high sensitivity values. The two Model C variables change in rank at different response levels, and this warrants further explanation.

At $\mathbf{d}_{deck} = 0.3$ m, a low displacement for this NewWave amplitude (as indicated by the high exceedence P_f value), the pre-load factor is ranked higher than m_0 (third versus fifth respectively). As the response level becomes larger, the pre-load factor falls in the rankings (at $\mathbf{d}_{deck} = 0.7$ m it is ranked 5-7); however, m_0 becomes more important, moving up the rankings to be nearly as sensitive as C_d at the $\mathbf{d}_{deck} = 0.7$ m level. This shows the influence of plasticity in the calculation of deck displacement. As the pre-load factor determines the

initial yield surface size according to the Model C formulation, it directly influences whether a load combination produces plastic conditions at the footing, and thus the extreme response. In contrast to this, although m_0 does influence the yield surface shape (it determines the peak size on the $M/2R$ axis), it is not as influential in determining whether plasticity occurs. If the load combination does not reach (and expand) the initial Model C yield surface, the value of m_0 is insignificant. These factors are reflected in the rankings at $\mathbf{d}_{deck} = 0.3$ m. The opposite is true for the $\mathbf{d}_{deck} = 0.7$ m level, as a calculation including a plastic component is expected and the influence of m_0 on the surface shape is more important than whether the surface is reached.

7.6.1.5 Calculations Using First Order Reliability Methods (FORM)

As a practical method of evaluating probabilities of failure, FORM is widely used in offshore structural applications (see, for example, Baker and Ramachandran (1981), Nadim and Lacasse (1992) and Morandi *et al.* (1997)). Its main advantage is the simplification of computationally difficult analyses. Using the second-order RS outlined, Monte Carlo simulation is computationally efficient for large samples. Therefore, FORM is not specifically required in this chapter, but it will be outlined here and used to evaluate P_f and sensitivity values as a comparative method.

The RS of Eqn 7.3 can be mapped into standardised Gaussian space (of k dimensions) by replacing all uncorrelated normally distributed basic random variables X_i with their standardised value Z_i , where:

$$Z_i = \frac{X_i - \mathbf{m}_{X_i}}{\mathbf{s}_{X_i}}. \quad (7.10)$$

An important characteristic of the z -coordinate system is rotational symmetry with respect to the standard deviations. Therefore, the point on the RS with the highest probability of occurrence is the point on the surface closest to the origin (the origin represents the mean set (\mathbf{m}_x) in a normalised set of basic variables). This point is called the design point and is shown in Fig. 7.8. Another term commonly used is the reliability index \mathbf{b} , which Hasofer and Lind (1974) defined as the distance between the origin and the design point in standardised Gaussian space:

$$\mathbf{b} = \min \left(\sqrt{\sum_{i=1}^k Z_i^2} \right). \quad (7.11)$$

As shown in Fig. 7.8, the original RS is replaced in a FORM calculation by a first-order surface of the same gradient as the RS at the design point. The probability of failure can therefore be estimated as

$$P_f = \Phi(-\mathbf{b}) \quad (7.12)$$

where Φ is the standard normal distribution function (see appendix A). In most circumstances this alternative estimate could be seen as a conservative estimate of P_f .

Iterative solution techniques for finding the reliability index and the design point were used on the RS of section 7.6.1.1 for the failure condition of deck displacements exceeding 0.5 m, *i.e.* $S = \hat{S} > 0.5$ m. Details of these techniques will not be given here but can be found in Thoft-Christensen and Baker (1982). The log-normal distributions of g and N_g were incorporated by finding equivalent normal distributions at the design point, as is recommended in Thoft-Christensen and Baker (1982). In finding the design point the unit vector \mathbf{a} was defined as the direction of the design point from the origin. As shown in Fig. 7.8, the vector from the origin to the design point is therefore

$$\overline{OA} = \mathbf{ba} \quad (7.13)$$

where O represents the origin and A the design point. The individual components of \mathbf{a} allow for a sensitivity measure of the basic random variables. Firstly, \mathbf{a}_i^2 is the fraction of the variance of the safety margin that originates from X_i . Another measure used is the omission sensitivity factor (\mathbf{z}_i), which expresses the relative error in the geometric reliability index (\mathbf{b}) if an input variable was replaced by a fixed value (Ditlevsen and Madsen, 1996). For the calculation here, \mathbf{z}_i can be interpreted as the percentage change in the reliability index when variable i is replaced by its mean value and is evaluated as

$$\mathbf{z}_i = \frac{1}{\sqrt{1 - \mathbf{a}_i^2}}. \quad (7.14)$$

Table 7.5 shows the results calculated for the RS of section 7.6.1.1 using FORM. The reliability index was evaluated as $\mathbf{b} = 1.03$, giving an estimated P_f of 0.1515; as could be expected, this value is larger than the value of 0.1479 estimated for the 10 000 samples using Monte Carlo simulation. Furthermore, the sensitivities to individual random variables have similar ranking to those given in Table 7.4. The drag coefficient is again dominating the response, with its proportion of \mathbf{a}_i^2 at 0.67. Moreover, if it was replaced by just its mean value, the reliability index would change by a very significant 74.71%.

7.6.1.6 Using Only 7 Basic Random Variables – Repeat Calculation

As some of the random variables originally chosen were not significantly influencing the extreme deck displacement—as indicated by low $S_{m_{x_i}}$ values—the number of random variables was reduced from eleven to seven in order to abridge the computational effort for the rest of the numerical experiments. Naturally the most influential were left in the experiments and they are described in Table 7.6. Following the same procedure as in

sections 7.6.1 to 7.6.1.4, a RS was estimated and a distribution of extreme deck displacements formulated (from Monte Carlo sample sets of 10 000 random variables). Fig. 7.9 shows a comparison between the eleven- and seven- variable extreme response distributions. As would be expected for fewer random variables, the seven-variable distribution shows less variation than the eleven-variable distribution; however, the difference is small enough to justify using the lower number of random variables.

7.6.2 Short-Term Sea-States with Variable Wave Amplitudes

For short-term conditions, random wave amplitudes follow the Rayleigh distribution as employed in Chapter 6. Therefore, in this section the variation in wave amplitudes will be considered, rather than using the most probable maximum wave amplitude.

7.6.2.1 Methodology Adopted

The method adopted to incorporate the variability of extreme wave amplitudes, as well as the probabilistic occurrence of the random variables in the evaluation of extreme response distributions, follows these steps:

Step 1: For the five NewWave crest elevations (described for each sea-state in Table 7.7), a separate RS is estimated using the central composite design and regression analysis. For k number of random variables this requires $(1 + 2k + 2^k)$ JAKUP runs per crest elevation.

Step 2: In a Monte Carlo calculation, for the same set of random variables (X) a response is calculated for each of the five NewWave elevations and a line of best fit is evaluated for these five responses. This allows interpolation for intermediate crests.

Step 3: With an extreme wave elevation randomly calculated,³ one extreme response can be estimated from the random-set best-fit polynomial of *Step 2*.

By repeating *Step 2* and *Step 3* for many sets of X , a statistical distribution of the extreme response can be formulated. This method adds another random component to the distribution compared with the calculations using the most probable extreme elevation in section 7.6.1, *i.e.* the extreme elevation in a short-term sea-state.

7.6.2.2 Numerical Experiment for 100-Year Return Period

An example of the methodology described in section 7.6.2.1 to compile short-term extreme response statistics for probabilistic random variables is outlined here. The 100-year sea-state characterised by the JONSWAP spectrum with parameters $H_s = 12$ m and $T_z = 10.805$ s is used again. For each of the five NewWave crest elevations, 3.5, 7, 10, 12 and 15 m (as utilised in Chapter 6), 143 JAKUP runs were performed (for $k = 7$) and the maximum deck displacements extracted. With the five RS polynomials estimated, 10 000 sets of basic random variables were simulated and 10 000 extreme wave amplitudes used to evaluate the distribution of extreme deck displacements. Fig. 7.10 shows this distribution and compares it with the distribution of extreme deck displacements calculated with variable NewWave amplitudes, but with basic variables at their mean value (as evaluated in Chapter 6). The additional variation caused by the uncertainty in the basic random variables is clearly shown. Two more observations from Fig. 7.10 can be made:

- The increase in displacement caused by the basic random variables at large deck displacements is greater than the reduction at low deck displacement levels. It is believed this is due to the non-linear response of the basic random variables, and this is discussed further in section 7.7.1.

³ Evaluated by Monte Carlo simulation of the number of waves in the short-term time period (N_{crest}) using

- The two curves intersect below the 50% exceedence level, at about $Q(x) \approx 0.38$ when $d_{deck} \approx 0.36$ m. Again, reasons for this are explored in section 7.7.1.

In Fig. 7.11 a comparison of the extreme deck displacement distributions for variable NewWave amplitudes and for the mean most probable highest wave amplitude shows the importance of varying the wave elevations. The extra variation is reflected by the CoV increasing from 30.32% to 35.66%. The curves cross at around $Q(x) \approx 0.5$, the expected mean value (the slight difference might be due to the ‘most probable’ curve being estimated from eleven random variables as opposed to seven).

7.7 Long-Term Numerical Experiment with Probabilistic Random Variables

7.7.1 Short-Term Results

Six short-term extreme response distributions have been evaluated based on the long-term conditions used in Chapter 6 and described again in Table 7.7. The experiments include wind and current, with their mean and standard deviations also shown in Table 7.7. The mean values are those used in Chapter 6 and the CoVs are those used in the example 1 in 100 year sea-state previously detailed in this chapter.

Fig. 7.12 shows the extreme deck displacement distributions evaluated with statistical variation in the basic random variables (or ‘random-variable’ distributions) and compares them with the short-term distributions calculated for the mean values of the basic variables (or ‘mean-variable’ distributions). Table 7.8 outlines all of the extreme response distributions’ statistical properties (mean values and CoVs). A considerable increase in

the Rayleigh distribution of wave elevations (see Eqn 6.10).

CoVs for the random-variable distributions is observed for all sea-states. Although for a return period of 1-year the mean deck displacement is the same (for the random-variable and mean-variable curves), there is a steady increase in the mean response for the random-variable extreme deck displacement distributions for longer return periods, as is shown by the percentage increases in Table 7.8.

For the 1-year return period, the intersection of the mean-variable and the random-variable distributions on the cumulative distribution plot of Fig. 7.12 is at approximately $Q(x) \approx 0.5$. For the other short-term distributions, however, as the sea-states become less probable the intersection is at progressively lower $Q(x)$ values, crossing at around $Q(x) \approx 0.26$ for the 10^5 year sea-state. An explanation considering the linearity of the response to each of the random variables is explored further here.

Firstly, assume the change in response to all of the random variables is linear, *i.e.* for the same probability of occurrence of the random variable's value at a "distance" from its mean, either lower or higher, the reduction in response is the same as the increase. This is shown in Fig. 7.13(a). For this case, the mean-variable and the random-variable extreme response distributions should intersect at $Q(x) = 0.5$. Furthermore, as shown in Fig. 7.13(b), the variation of the random-variable curve away from the mean-variable extreme response distribution should be of the same magnitude for both $Q(x) < 0.5$ and $Q(x) > 0.5$. On the other hand, if the response to a random variable is non-linear, the random-variable extreme response distribution becomes skewed. If, as in Fig. 7.13(c), the additional response is relatively larger for the same probability away from the mean as it is smaller, then the distributions should intersect at $Q(x) < 0.5$ (assuming more than one random variable). Additionally, the random-variable distribution will not have the same difference in variability, but will show a larger change in response at high $Q(x)$ values, as indicated

in Fig. 7.13(d). This is a simplistic explanation and one which becomes more complex with competing non-linearities and cross-term effects.

For the 1-year sea-state the majority of runs used to evaluate the RS were within the initial Model C yield surface (only a few of the runs for the highest NewWave elevation of 11m caused expansion of the yield surface). Therefore, the runs were all within the foundation's elastic region and the footings were acting as linear springs. In this situation, the Model C parameters m_0 and the *pre-load* factor had no effect on the response. The remaining parameters, especially C_d and *wind load*, have a more linear effect on the horizontal deck displacement, and this is reflected in the extreme response distribution for the 1-year sea-state shown in Fig. 7.12.

As the sea-states become harsher, the Model C parameters become more important and more non-linear. For example, with all of the other variables at their mean level and only m_0 varied for the 10^5 sea-state and a NewWave amplitude of 19 m, the deck displacement calculated by JAKUP is increased by 0.219m for m_0 at two standard deviations below its mean, but only decreased by 0.122 m for m_0 at two standard deviations above its mean. This influence would be increased when cross terms are considered, especially due to the increase in load caused by higher C_d values. It is these non-linear effects which are thought to create the skewed curves described by Fig. 7.12.

7.7.2 Long-Term Results

As discussed in section 6.4.3.1, the convolution of the short-term distribution with the logarithmic distribution of sea-state occurrence gives long-term probability predictions of response. The same method of scaling the normalised (by the 50% exceedence value) 1 in

100 year distribution as described in section 6.4.3.1 was used to estimate values in intermediate sea-states.

Long-term extreme exceedence probabilities have been calculated for the horizontal deck displacement of the example jack-up for the statistical distributions of random variables outlined in Table 7.7, and are shown in Fig. 7.14. The estimates are significantly larger than the annual probability of exceedence values calculated in Chapter 6 for the mean deterministic values of the basic random variables. This can be explained by the increased variability observed in the short-term random-variable extreme response distributions. For all sea-states (apart from the 1-year return period) the variations in the basic random variables caused larger mean deck displacements for the short-term distributions (as outlined in Table 7.8). This, as well as the fact that the short-term response is relatively larger at high $Q(x)$, and that the curves cross at lower $Q(x)$ levels as the sea-state return period increases, means that the long-term exceedence prediction is significantly increasing. For the reasons discussed in section 7.7.1, it is believed that if a linear foundation model was used, the difference in long-term exceedence estimates would not be as large.

Chapter 8 – Concluding Remarks

8.1 Introduction

This thesis is concerned with the modelling of jack-up units on sand when subjected to random ocean waves. Analysis techniques have been developed in the three main areas outlined in the research aims: foundation modelling, random wave loading and the probabilistic approach to developing extreme response statistics. In this chapter the main findings of the thesis are summarised, conclusions drawn, and some possible directions for future work presented.

8.2 Conclusions – Main Findings

8.2.1 Foundation Modelling

Based on a series of experiments performed at the University of Oxford by Gottardi and Houlsby (1995), an incremental work hardening plasticity model entitled Model C has been developed to represent spudcan footings in the analysis of jack-up units on sand. The yield surface, flow rule and hardening law of Model C are all empirically determined to fit the experimental data. Stiffness factors derived from three-dimensional finite element analyses performed by Bell (1991) are used to describe elastic behaviour within the yield surface.

A complete incremental numerical formulation of Model C describing the combined loading on spudcan footings was outlined. This was implemented in the FORTRAN program OXC, which was used to perform retrospective simulations of several footing experiments. The capability of OXC to simulate the original test data for both load and displacement controlled stages was demonstrated.

Using the Method of Characteristics, a theoretical study of the vertical bearing capacity of conical footings on sand was conducted. Lower bound solutions were evaluated for a range of cone angles, footing roughness and the angle of friction of sand. Using the results of this study, a method accounting for the conical shape of spudcan footings in Model C was suggested. The hardening law relating the size of the yield surface was defined by a combination of an empirical fit to experimental data for flat circular footings on dense sand and a theoretical bearing capacity approach for the conical section of the footing.

Model C represents a significant advance to the response analysis of jack-up units. When compared with techniques widely used in the jack-up industry, a significantly different response is found, and this was shown in examples in this thesis.

8.2.2 Numerical Modelling of Random Wave Loading

The numerical formulation of Model C was implemented into the plane frame structural analysis program JAKUP, which is suitable for the dynamic analysis of jack-up units. NewWave, Constrained NewWave and second-order NewWave theories have all been independently implemented into JAKUP to consider the random, spectral and non-linear aspects of wave loading. The following conclusions can be drawn from the numerical experiments performed:

- Due to the interpretation of spudcan fixity in Model C, a significantly different dynamic response from the pinned footing assumption was found. Predicted response was shown for NewWave and Constrained NewWave examples according to various footing assumptions: pinned, linear springs (using the elastic stiffness matrix of Model C) and Model C. For the cases shown, the pinned response was arguably over-conservative.

- The importance of the random background for the dynamic analysis of jack-up units was shown by comparing an example NewWave with the same NewWave constrained within a random background.

8.2.3 Probabilistic Approach to Developing Extreme Response Statistics

The probabilistic response of jack-ups was investigated through the random nature of wave loading. Using an example structure and central North Sea location, a series of numerical experiments designed to evaluate short- and long-term extreme response statistics produced the following findings:

- A method for determining short-term extreme response statistics using the Constrained NewWave was demonstrated. The peak responses due to five Constrained NewWave elevations (for 200 random backgrounds each) were used to evaluate numerically the short-term extreme statistics of that sea-state using Monte Carlo methods. This was found to be computationally efficient and the results comparable with 100 full three-hour simulations of random seas, even with the inclusion of significant amounts of foundation non-linearities.
- For the example jack-up, for increasing sea-state severity there was an increasing variation in the short-term extreme horizontal deck displacements. It was suggested that more drag-dominant loading behaviour contributed to the increasing CoVs of response. For the Model C case, increasing levels of yielding of both the upwave and downwave foundations was also influential.
- For long-term conditions, Model C displayed significantly different extreme response from both the pinned and linear spring assumptions. For annual failure probability levels of interest in the offshore industry ($10^{-4} \rightarrow 10^{-6}$), there was over an order of magnitude difference for the equivalent pinned and Model C deck displacements. It is conceivable that in certain situations this could be the difference between acceptance or non-

acceptance of the rig. The benefit to the jack-up industry of the more realistic interpretation of spudcan behaviour in Model C, combined with an efficient long-term response evaluation method, has been displayed.

- For the three foundation models presented, Model C footings displayed higher variation in the short-term statistics and a comparatively more non-linear long-term annual probability of exceedence curve.
- It was found that it is possible for Model C to give larger long-term probability of exceedence results than pinned footings. This is due to horizontal plastic displacements being accounted for in the Model C formulation, demonstrating that the indication of yielding is a major benefit of using a plasticity formulation for spudcan load:displacement behaviour.
- For long-term probability of exceedence levels, the random background sea significantly increases the extreme (deck displacement) response, confirming the need for random time domain analysis of jack-ups.

The influence of a probabilistic analysis approach, as an extension of the deterministic analysis, was investigated using the response surface methodology. It was found that accounting for the uncertainty in the values of a set of basic random variables affected the extreme response statistics. The following conclusions can be drawn:

- For one sea-state investigated (the example 100-year condition), the drag coefficient used in the extended Morison equation was the most significant basic random variable. Others, including current, hull mass, m_0 and the amount of pre-load, also notably affected the extreme deck displacement results. It can therefore be concluded that for future experimental development of plasticity models, the terms m_0 and the effect of pre-load (*i.e.* the vertical loading level) should be modelled accurately.

- For short-term statistics there was an increase in CoV values. Furthermore, for increasing sea-state severity, the 50% exceedence response value increased in comparison with the equivalent deterministic approach. Both of these affected long-term estimates, giving increased annual probability of exceedence results. Accounting for the probabilistic distributions of random variables was therefore shown to be important.

8.3 *Directions for Future Work*

8.3.1 **Extension to Three Dimensions**

In this thesis JAKUP was used for analyses of plane frames, with wave loading applied along the axis of symmetry of the jack-up. With much of the structural and wave loading theory available,¹ an extension to a three-dimensional analysis is possible and would represent a significant advance.

Model C was developed for behaviour constrained within a single vertical plane, *i.e.* a three degree of freedom problem. For inclusion in a three-dimensional structural analysis program, the extension of Model C to six degrees of freedom is required, with the six loading conditions being horizontal and moment loading in two orthogonal directions, vertical load and torque. The likely theoretical form of the yield surface for the extension of Model B to six dimensions was detailed by Martin (1994). However, an experimental program designed to fit this surface shape (and to develop a suitable flow rule) for the new Model C would be challenging to perform in the laboratory.

¹ For details of accounting for geometric non-linearities in space frames see Oran (1973[b]) and Chan and Kitipornchai (1987) for example. Extension of NewWave to spread seas is possible using the theory set out by Tromans *et al.* (1991).

8.3.2 Foundation Theories for Spudcan Footings

Model C has been developed from monotonic loading tests on sand. However, for the analysis of offshore structures, loading rates and cyclic loading are both important. The strength of the sand foundation is related to the rate of the applied load and the degree of drainage of developed pore pressures. Furthermore, reversal of load paths and cyclic behaviour (as can be expected in an ocean environment) can cause reduction of the strength in the soil. The next step in formulating a more advanced plasticity model is to account for these effects.

8.3.3 Physical Validation of Model C

Model C has been used as a macro-model in a numerical analysis to evaluate the response of a jack-up unit. It would therefore be desirable to substantiate this use with physical experiments involving both the structural and foundation components. Two types of experiments could be undertaken:

1. Through the use of a scaled model, including the physical structural components, a comparison of Model C's numerically predicted load:displacement path of the spudcans in service conditions with a physical test could be achieved. Furthermore, response levels (of lower leg-guide moment, for instance) would help verify the numerical models used.
2. At the University of Oxford, a Structural Dynamics Laboratory has been built to test physically a structural element when coupled in real time to a numerical model of the surrounding structure (see Williams *et al.*, 1997). This equipment could be used with the overall jack-up numerically modelled in JAKUP, but with one (or both) of the foundations replaced by a physical model of the spudcan. In the time domain, JAKUP would calculate the displacements to be applied by the actuators to the physical test spudcan. The reaction forces generated would then be used as input into the JAKUP

model for the next displacement increment. Use of the control capacity in the Oxford University Structural Dynamics Laboratory with this substructure approach offers the following advantages:

- Not only could verification of the use of Model C for drained cases be investigated; comparisons with realistic transient loading cases are also feasible. Use of Constrained NewWave in conjunction with the structural and wave loading non-linearities included in a JAKUP calculation would allow for a more realistic random load path to use in laboratory testing of model foundations.
- Performance of various foundation types could be investigated; for instance, varying cone angles of spudcans and the use of skirts on spudcans.
- The testing for Model C used a footing radius of 50 mm. Through use of larger size actuators and footing radii, scale effects could also be investigated.

8.3.4 Wave Models

The Constrained NewWave technique provides a powerful tool for numerically analysing jack-up problems. In this thesis, the effect of only one large peak was investigated as the basis for development of extreme response statistics. However, there are conceivable examples of problems caused by a number of large waves following each other. For instance, if a large wave horizontally displaces the downwave spudcan, less force needs to be applied to further displace the downwave spudcan due to $P - \Delta$ effects. A detrimental situation can occur with increasingly smaller waves displacing the footing. This type of problem could be investigated by constraining a number of successive NewWaves. Constrained NewWave has the ability to investigate different combinations of waves in a numerically simple manner (with the inclusion of random backgrounds).

In further investigation of higher-order NewWave theory, the wave models used to analyse jack-ups could be refined. However, considering the level of rigour for other components of the model, this may be overly sophisticated at this time.

8.4 *Conclusion*

The modelling of jack-ups is challenging due to its complexity in a number of different areas. Only with confidence in each modelling component can one have confidence in the final result. In this thesis, several techniques have been combined to achieve what is believed to be a realistic modelling of a jack-up.

Appendix A: Statistical Distributions Used

This appendix contains the statistical distributions used to represent the probabilistic variability of the basic random variables in the numerical experiments of Chapter 7.

Normal Distribution

probability density function:

$$f_X(x) = \frac{1}{s\sqrt{2p}} \exp\left[-\frac{1}{2}\left(\frac{x-m}{s}\right)^2\right] \quad \text{where } -\infty < x < \infty \quad (\text{A-1})$$

cumulative distribution function:

$$F_X(x) = \int_{-\infty}^x \frac{1}{s\sqrt{2p}} \exp\left[-\frac{1}{2}\left(\frac{t-m}{s}\right)^2\right] dt \quad \text{where } -\infty < x < \infty \quad (\text{A-2})$$

This integral can not be evaluated in closed form, however, by using the substitution $s = (t - m)/s$ and $dt = s ds$, Eqn A-2 becomes

$$F_X(x) = \int_{-\infty}^{\frac{x-m}{s}} \frac{1}{\sqrt{2p}} \exp\left[-\frac{1}{2}s^2\right] ds \quad (\text{A-3})$$

The standard normal distribution function used is defined by:

$$\Phi_X(x) = \int_{-\infty}^x \frac{1}{\sqrt{2p}} \exp\left[-\frac{t^2}{2}\right] dt \quad (\text{A-4})$$

Log-Normal Distribution

If the random variable $Y = \ln(X)$ is normally distributed (and m_Y is a real number and $s_Y > 0$) then X is log-normally distributed.

probability density function:

$$f_X(x) = \frac{1}{s_Y\sqrt{2p}} \frac{1}{x} \exp\left[-\frac{1}{2}\left(\frac{\ln(x)-m_Y}{s_Y}\right)^2\right] \quad \text{where } 0 \leq x < \infty \quad (\text{A-5})$$

cumulative distribution function:

$$F_X(x) = \Phi\left(\frac{\ln(x) - m_Y}{s_Y}\right) \quad (\text{A-6})$$

where Φ is the standard normal distribution of Eqn A-4.

REFERENCES

- Ackland, D.F. (1949). Moving Heaven and Earth, R.G. LeTourneau. *Marshall, Morgan and Scott*, London.
- Al-Bermani, F.G.A. and Kitipornchai, S. (1990). Elasto-plastic large deformation analysis of thin-walled structures. *Engng Struct.* Vol. 12, pp. 28-36.
- American Petroleum Institute (1993). Recommended practice for planning, designing and constructing fixed offshore platforms - load and resistance factor design. RP 2A-LRFD, *American Petroleum Institute*, 1st ed., Washington DC.
- Baerheim, M., Manschot, D. and Nortvedt, T. (1997). Use of a jack-up as a permanent installation for the marginal Siri field. *Proc. of 6th Int. Conf. Jack-Up Platform Design, Construction and Operation*, City University, London.
- Baker, M.J. and Ramachandran, K. (1981). Reliability analysis as a tool in the design of fixed offshore platforms. *Proc. of 2nd Int. Symp. on The Integrity of Offshore Structures*, Glasgow, pp. 135-153.
- Barltrop, N.D.P. and Adams A.J. (1991). Dynamics of fixed marine structures. *Butterworth Heinemann*, 3rd ed., Oxford.
- Bell, R.W. (1991). The analysis of offshore foundations subjected to combined loading. *M.Sc. Thesis*, University of Oxford.
- Bennett, W.T. and Sharples, B.P.M. (1987). Jack-up legs to stand on?. *Mobile Offshore Structures*, Elsevier, London, pp. 1-32.
- Bolton, M.D. and Lau, C.K. (1993). Vertical bearing capacity factors for circular and strip footings on Mohr-Coulomb soil. *Canadian Geotechnical Journal*, Vol. 30, pp. 1024-1033.
- Boon, B., Vrouwenvelder, A., Hengst, S., Boonstra, H., and Daghigh, M. (1997). System reliability analysis of jack-up structures: possibilities and frustrations. *Proc. of 6th Int. Conf. Jack-Up Platform Design, Construction and Operation*, City University, London.
- Box, G.E. and Hunter, J.S. (1957). Multifactor experimental designs for exploring response surfaces. *The Annals of Mathematical Statistics*, Vol. 28, pp. 195-241.
- Bradshaw, I.J. (1987). Jack-up structural behaviour and analysis methods. *Mobile Offshore Structures*, Elsevier, London, pp. 125-155.
- Brekke, J.N., Campbell, R.B., Lamb, W.C. and Murff, J.D. (1990). Calibration of a jackup structural analysis procedure using field measurements from a North Sea jackup. *Proc. 22nd Offshore Technology Conference*, Houston, pp. 357-368, OTC 6465.
- Brinch Hansen, J. (1961). A general formula for bearing capacity. *Danish Geotechnical Institute Bulletin*, No. 11, pp. 38-46.
- Brinch Hansen, J. (1970). A revised and extended formula for bearing capacity. Bull. No. 98, *The Danish Geotechnical Institute*, Copenhagen, pp. 5-11.

References

- Bucher, C.G. and Bourgund, U. (1990). A fast and efficient response surface approach for structural reliability problems. *Structural Safety*, Vol. 7, pp. 57-66.
- Butterfield, R., Houlsby, G.T. and Gottardi, G. (1997). Standardized sign conventions and notation for generally loaded foundations. *Geotéchnique*, Vol. 47, No. 5, pp. 1051-1054.
- Butterfield, R. and Ticof, J. (1979). Design parameters for granular soils (discussion contribution). *Proc. 7th European Conf. Soil Mech. Fndn Engng*, Brighton, Vol. 4, pp. 259-261.
- Carlsen, C.A., Kjeøy, H. and Eriksson, K. (1986). Structural behaviour of harsh environment jack-ups. *The Jack-up Drilling Platform Design and Operation*, Collins, London, pp. 90-136.
- Carter, D.J.T. (1982). Prediction of wave height and period for a constant wind velocity using the JONSWAP results. *Ocean Engineering*, Vol. 9, pp. 17-33.
- Cassidy, M. J. (1996). The behaviour of jack-up platforms. *First Year Report*, University of Oxford.
- Chan, S.L. and Kitipornchai, S. (1987). Geometric nonlinear analysis of asymmetric thin-walled beam-columns. *Engng Struct.* Vol. 9, No. 4, pp. 243-254.
- Chen, Y.N., Chen, Y.K. and Cusack, J.P. (1990). Extreme dynamic response and fatigue damage assessment for self-elevating drilling units in deep water. *SNAME Transactions*, Vol. 98, pp. 143-168.
- Chiba, S., Onuki, T. and Sao, K. (1986). Static and dynamic measurement of bottom fixity. *The Jack-up Drilling Platform Design and Operation*, Collins, London, pp. 307-327.
- Daghigh, M., Hengst, S., Vrouwenvelder, A. and Boonstra, H. (1997). System reliability analysis of jack-up structures under extreme environmental conditions. *Proc. of BOSS'97 Behaviour of Offshore Structures*, Vol. 3, Delft University of Technology, pp. 127-143.
- Dean, E.T.R., James, R.G., Schofield, A.N., Tan, F.S.C. and Tsukamoto, Y. (1993). The bearing capacity of conical footings on sand in relation to the behaviour of spudcan footings of jack-ups. *Proc. Wroth Memorial Symp. "Predictive Soil Mechanics"*, Oxford, pp. 230-253.
- Ditlevsen, O. and Madsen, H.O. (1996). Structural reliability methods. *John Wiley & Sons*, Chichester.
- Durning, P.J. (1971). Prediction of maximum wave height from historical data. *Proc. 3rd Offshore Technology Conference*, Houston, pp. 165-176, OTC 1343.
- Elzinga, T. and Tromans, P.S. (1992). Validation of 'NewWave' theory and RDWF predictions against measured global loading on a North Sea jacket. *6th Int. Conf. on the Behaviour of Off-Shore Structures (BOSS)*, University of London, London, pp. 495-505.
- Fjeld, S. (1977). Reliability of offshore structures. *Proc. 9th Offshore Technology Conference*, Houston, pp. 459-471, OTC 3027.
- Forristall, G.Z. (1981). Kinematics of directionally spread waves. *Proc. Conference on Directional Wave Spectra Applications*, ASCE, Berkeley, pp. 129-146.
- Forristall, G.Z., Larrabee, R.D. and Mercier, R.S. (1991). Combined oceanographic criteria for deepwater structures in the Gulf of Mexico. *Proc. 23rd Offshore Technology Conference*, Houston, pp. 377-386, OTC 6541.

References

- Frieze, P.A., Bucknell, J., Birkenshaw, M., Smith, D. and Dixon, A.T. (1995). Fixed and jack-up platforms: basis for reliability assessment. *Proc. 5th Int. Conf. on Jack-Up Platform Design, Construction and Operation*, City University, London.
- Gilbert, R.B. and Tang, W.H. (1995). Model uncertainty in offshore geotechnical reliability. *Proc. 27th Offshore Technology Conference*, Houston, pp. 557-567, OTC 7757.
- Gottardi, G. and Butterfield, R. (1993). On the bearing capacity of surface footings on sand under general planar loads. *Soils and Foundations*, Japanese Society of Soil Mech. and Fndn Engng, Vol. 33, No. 3, pp. 68-79.
- Gottardi, G. and Butterfield, R. (1995). The displacements of a model rigid surface footing on dense sand under general planar loading. *Soils and Foundations*, Japanese Society of Soil Mech. and Fndn Engng, Vol. 35, No. 3, pp. 71-82.
- Gottardi, G. and Houlsby, G.T. (1995). Model tests of circular footings on sand subjected to combined loads. *Report No. 2071/95*, Oxford University Engineering Laboratory.
- Gottardi, G., Houlsby, G.T. and Butterfield, R. (1997). The plastic response of circular footings on sand under general planar loading. *Report No. 2143/97*, Oxford University Engineering Laboratory.
- Grenda, K.G. (1986). Wave dynamics of jackup rigs. *Proc. 18th Offshore Technology Conference*, Houston, pp. 111-116, OTC 5304.
- Grundlehner, G.J. (1989). The development of a simple model for the deformation behaviour of leg to hull connections of jack-up rigs. *M.Sc. Thesis*, Delft University of Technology.
- Hambly, E.C., Imm, G.R. and Stahl, B. (1990). Jackup performance and foundation fixity under developing storm conditions. *Proc. 22nd Offshore Technology Conference*, Houston, pp. 369-380, OTC 6466.
- Hambly, E.C. and Nicholson, B.A. (1991). Jackup dynamic stability under extreme storm conditions. *Proc. 23rd Offshore Technology Conference*, Houston, pp. 261-272, OTC 6590.
- Harland, L.A. (1994). On the simulation of jack-up dynamics. *Student Thesis Report*, Delft University of Technology.
- Harland, L.A., Taylor, P.H. and Vugts, J.H. (1997). The variability of extreme forces on offshore structures. *Proc. of BOSS'97 Behaviour of Offshore Structures*, Vol. 2, Delft University of Technology, pp. 221-235.
- Hasofer, A.M. and Lind, N.C. (1974). Exact and invariant second-moment code format. *J. Engng Mech. Div.*, ASCE, Vol. 100, No. EM1, pp. 111-121.
- Hasselmann, K., Barnett, T.P., Bouws, E., Carlson, H., Cartwright, D.E., Enke, K., Ewing, J.A., Gienapp, H., Hasselmann, D.E., Kruseman, P., Meerburgh, A., Muller, P., Olbers, D.J., Richter, K., Sell, W. and Walden, H. (1973). Measurements of wind wave growth and swell decay during the JONSWAP project. *Deutsches Hydrographisches Zeitschrift Reihe*, Suppl. A., 8, No 12.

References

- Hattori, Y., Ishihama, T., Matsumoto, K., Arima, K., Sakata, N. and Ando, A. (1982). Full-scale Measurement of natural frequency and damping ratio of jackup rigs and some theoretical considerations. *Proc. 14th Offshore Technology Conference*, Houston, pp. 661-670, OTC 4287.
- Hogben, N. (1990). Long term wave statistics. in *The Sea*, Vol. 9, Pt A, *Ocean Engineering Science*, Wiley, New York, pp. 293-333.
- Houlsby, G.T. (1982). Theoretical analysis of the fall cone test. *Geotéchnique*, Vol. 32, No. 2, pp.111-118.
- Houlsby, G.T. and Martin, C.M. (1992). Modelling of the behaviour of foundations of jack-up units on clay. *Proc. Wroth Memorial Symp. "Predictive Soil Mechanics"*, Oxford, pp. 339-358.
- Houlsby, G.T. and Wroth, C.P. (1983). Calculation of stresses on shallow penetrometers and footings. *Report No. 1503*, Oxford University Engineering Laboratory.
- Houmb, O.G. and Overvik, T. (1976). Parameterization of wave spectra and long term joint distribution of wave height and period. *An Int. Conf. on the Behaviour of Off-Shore Structures (BOSS)*, Vol. 1, Norwegian Institute of Technology, Trondheim, pp. 144-169.
- Hoyle, M.J.R. (1992). Jack-up dynamics - a review of analysis techniques. *Recent Developments in Jack-Up Platforms*, Elsevier, London, pp. 176-200.
- Hoyle, M.J.R. and Snell, R.O. (1997). Jack-up sliding probability in the context of current assessment practice. *Proc. of 6th Int. Conf. Jack-Up Platform Design, Construction and Operation*, City University, London.
- Jensen, J.J. (1996). Second-order wave kinematics conditional on a given wave crest. *Applied Ocean Research*, Vol. 18, pp. 119-128.
- Jensen, J.J., Baatrup, J. and Mansour, A.E. (1995). A conditional mean second-order wave theory. *Proc. 14th Int. Conf. on Offshore Mechanic and Arctic Engineering (OMAE)*, Vol. 1-A, pp. 347-355.
- Karunakaran, D. (1993). Nonlinear dynamic response and reliability analysis of drag-dominated offshore structures. *Dr. ing Thesis*. Div. of Marine Structures, NTH, Norway.
- Karunakaran, D., Leira, B.J. and Spidsø, N. (1992). Effect of nonlinear behaviour on long term extreme response of a dynamically sensitive jack-up platform. *Recent Developments in Jack-Up Platforms*, Elsevier, London, pp. 201-227.
- Karunakaran, D., Leira, B.J., Svano, G., and Moan, T. (1994). Foundation reliability of a jack-up platform. *Proc. 13th Int. Conf. on Offshore Mechanic and Arctic Engineering (OMAE)*, Vol. 2, pp. 111-120.
- Kassimali, A. (1983). Large deformation analysis of elastic-plastic frames. *J. Struct. Engng*, ASCE, Vol. 109, No. 8, pp. 1869-1886.
- Kim, Y.Y. and Hibbard, H.C. (1975). Analysis of simultaneous wave force and water particle velocity measurements. *Proc. 7th Offshore Technology Conference*, Houston, pp. 461-470, OTC 2192.
- Kjeøy, H., Bø, N.G. and Hysing, T. (1989). Extreme-Response analysis of jack-up platforms. *Proc. of 2nd Int. Conf. on the Jack-Up Drilling Platform*, City University, London, pp. 125-154.

References

- Lacasse, S. and Nadim, F. (1994). Reliability issues and future challenges in geotechnical engineering for offshore structures. *7th Int. Conf. on the Behaviour of Off-Shore Structures (BOSS)*, M.I.T., Boston, pp. 1-30.
- Lade, P.V. (1977). Elasto-plastic stress-strain theory for cohesionless soil with curved yield surfaces. *Int. J. Solids and Structures*, Vol. 13, pp. 1019-1035.
- Leijten, S.F. and Efthymiou, M. (1989). A philosophy for the integrity assessment of jack-up units. *Proc. Society of Petroleum Engrs Conf "Offshore Europe 89"*, Aberdeen, SPE 19236.
- Lewis, D., Maison, J. and Mobbs, B. (1992). Analysis of a jack-up unit using super-element techniques. *Recent Developments in Jack-up Platforms*, Blackwell Scientific Publications, London, pp. 1-40.
- Longuet-Higgins, M.S. (1952). On the statistical distribution of the heights of sea waves. *J. Marine Res.*, 11, 3, pp. 245-66.
- Longuet-Higgins, M.S. and Stewart, R.W. (1964). Radiation stresses in water waves; a physical discussion, with applications. *Deep-Sea Research*, Vol. 11, pp. 529-562.
- Løseth, R. and Bjerager, P. (1989). Reliability of offshore structures with uncertain properties under multiple load processes. *Proc. 21st Offshore Technology Conference*, Houston, pp. 107-114, OTC 5969.
- Løseth, R. and Hauge, L. (1992). Probabilistic methods in calibration of partial safety factors. *In Recent Developments in Jack-up Platforms*, Blackwell Scientific Publications, London, pp. 228-245.
- Manuel, L. and Cornell, C.A. (1996). The influence of alternative wave loading and support modeling assumptions on jack-up rig response extremes. *J. of Offshore Mechanics and Arctic Engineering (OMAE)*, Vol. 118, pp. 109-114.
- Martin, C.M. (1994). Physical and numerical modelling of offshore foundations under combined loads. *D.Phil. Thesis*, University of Oxford.
- Melchers, R.E. (1989). Importance sampling in structural systems. *Structural Safety*, Vol. 6, pp. 3-10.
- Meyerhof, G.G. (1951). The ultimate bearing capacity of foundations. *Geotechnique*, Vol. 2, No. 4, pp. 301-332.
- Meyerhof, G.G. (1953). The bearing capacity of foundations under eccentric and inclined loads. *Proc. 3rd ICSMFE*, Zurich, Vol. 1, pp. 440-445.
- Mommaas, C.J. and Gründlehner, G.J. (1992). Application of a dedicated stochastic non-linear dynamic time domain analysis program in design and assessment of jack-ups. *Recent Developments in Jack-Up Platforms*, Elsevier, London, pp. 152-175.
- Morandi, A.C., Frieze, P.A., Birkinshaw, M., Smith, D. and Dixon, A.T. (1997). Reliability of fixed and jack-up structures: a comparative study. *Proc. of BOSS'97 Behaviour of Offshore Structures*, Vol. 3, Delft University of Technology, pp. 111-126.
- Myers, R.H. and Montgomery, D.C. (1995). Response surface methodology: Process and product optimization using designed experiments. *John Wiley & Sons*, New York.

References

- Nadim, F. and Lacasse, S. (1992). Probabilistic bearing capacity analysis of jack-up structures. *Canadian Geotechnical Journal*, Vol. 29, No. 4, pp. 580-588.
- Naess, A. and Pisano, A.A. (1997). Frequency domain analysis of dynamic response of drag dominated offshore structures. *Applied Ocean Research*, Vol. 19, Elsevier, London, pp. 251-262.
- Newman, J.N. (1990). Numerical solutions of the water-wave dispersion relation. *Applied Ocean Research*, Vol.12, No. 1, pp. 14-18.
- Nielsen, L.P., Friis Hansen, P., Jensen, J.J., Baatrup, J. and Terndrup Pedersen, P. (1994). Reliability based inspection planning of a jack-up rig. *Proc. 7th Int. Conf. on the Behaviour of Off-Shore Structures (BOSS)*, M.I.T., Boston, pp. 377-399.
- Ngo-Tran, C.L. (1996). The analysis of offshore foundations subjected to combined loading. *D.Phil. Thesis*, University of Oxford.
- Noble Denton and Associates. (1987). Foundation fixity of jack-up units: a joint industry study. *Noble Denton and Associates*, London.
- Norris, V.A. and Aldridge, T.R. (1992). Recent analytical advances in the study of the influence of spudcan fixity on jack-up unit operations. *Recent Developments in Jack-Up Platforms*, Elsevier, London, pp. 424-450.
- Nova, R. and Montrasio, L. (1991). Settlements of shallow foundations on sand. *Geotechnique*, Vol. 41, No. 2, pp. 243-256.
- Ochi, M.K. (1979). A series of JONSWAP wave spectra for offshore structure design. *Proc. 2nd Int. Conf. on the Behaviour of Off-Shore Structures (BOSS)*, University of London, London, pp. 75-86.
- Offshore Technology (1999). web site: <http://www.offshore-technology.com/projects/>, *Net Resources Int. Ltd.*
- Oran, C. (1973[a]). Tangent stiffness in plane frames. *J. Struct. Engng Div*, ASCE, Vol. 99, No. ST6, pp. 973-985.
- Oran, C. (1973[b]). Tangent stiffness in space frames. *J. Struct. Engng Div*, ASCE, Vol. 99, No. ST6, pp. 987-1001.
- Osborne, J.J., Trickey, J.C., Houlsby, G.T. and James, R.G. (1991). Findings from a joint industry study on foundation fixity of jackup units. *Proc. 23rd Offshore Technology Conference*, Houston, pp. 517-533, OTC 6615.
- Patel, M.H. (1989). Dynamics of offshore structures. *Butterworths*, London.
- Peters, D.J., Shaw, C.J., Grant, C.K., Heideman, J.C. and Szabo, D. (1993). Modelling the North Sea through the Northern European Storm Study. *Proc. 25th Offshore Technology Conference*, Houston, pp. 479-493, OTC 7130.
- Phillips, O.M. (1958). The equilibrium range in the spectrum of wind-generated waves. *J. Fluid Mech.*, Vol. 4, pp. 426-434.

References

- Pierson, W.J. and Moskowitz, L. (1964). A proposed spectral form for fully developed wind seas based on the similarity theory of S.A. Kitaigorodskii. *J. Geophys. Res.*, Vol. 69, No. 24, pp. 5181-90.
- Poulos, H.G. and Davis, E.H. (1974). Elastic solutions for soil and rock mechanics. *John Wiley*, New York.
- Puskar, F.J., Aggarwal, R.K., Cornell, C.A., Moses, F. and Petruskas, C. (1994). A comparison of analytically predicted platform damage to actual platform damage during Hurricane Andrew. *Proc. 26th Offshore Technology Conference*, Houston, pp. 41-53, OTC 7473.
- Reardon, M.J. (1986). Review of the geotechnical aspects of jack-up unit operations. *Ground Engineering*, Vol. 19, No. 7, pp. 21-26.
- Rice, S.O. (1944). Mathematical analysis of random noise. *Bell System Tech. J.*, Vol. 23, 1945, Vol. 24. (Reprinted in: *Selected papers on noise and stochastic processes*, Wax, N., ed., *Dover Publications*, New York, 1954, pp. 133-294).
- Rodenbusch, G. (1986). Random directional wave forces on template offshore platforms. *Proc. 18th Offshore Technology Conference*, Houston, pp. 147-156, OTC 5098.
- Rodenbusch, G. and Forristall, G.Z. (1986). An empirical model for random directional wave kinematics near the free surface. *Proc. 18th Offshore Technology Conference*, Houston, pp. 137-146, OTC 5097.
- Rodenbusch, G. and Kallstrom, C. (1986). Forces on a large cylinder in random two-dimensional flows. *Proc. 18th Offshore Technology Conference*, Houston, pp. 127-136, OTC 5096.
- Roscoe, K.H. and Schofield, A.N. (1956). The stability of short pier foundations in sand. *British Welding Journal*, August, pp. 343-354.
- Schotman, G.J.M. (1989). The effects of displacements on the stability of jack-up spud-can foundations. *Proc. 21st Offshore Technology Conference*, Houston, pp. 515-524, OTC 6026.
- Sharples, B.P.M., Bennett Jr, W.T. and Trickey, J.C. (1989). Risk analysis of jack-up rigs. *Proc. of 2nd Int. Conf. on the Jack-Up Drilling Platform*, City University, London, pp. 101-123.
- Shetty, N.K., Gierlinski, J.T., Smith, J.K. and Stahl, B. (1997). Structural system reliability considerations in fatigue inspection planning. *Proc. of BOSS'97 Behaviour of Offshore Structures*, Vol. 3, Delft University of Technology, pp. 161-175.
- Sigurdsson, G., Skjong, R., Skallerud, B. and Amdahl, J. (1994). Probabilistic collapse analysis of jackets. *Proc. of 13th Int. Conf. on Offshore Mechanics and Arctic Engineering (OMAE)*, Vol. 2, pp. 367-379.
- SNAME (1994). Guidelines for site specific assessment of mobile jack-up units. *Society of Naval Architects and Marine Engineers*, Technical and Research Bulletin 5-5A, New Jersey.
- Spidsø, N. and Karunakaran, D. (1993). Non-linear dynamic behaviour of jack-up platforms. *Proc. of 4th Int. Conf. Jack-Up Platforms Design*, City University, London.
- Stiff, J.J., Sharples, B.P.M. and Bowie, R.D. (1997). Jack-ups: classification past, present, and future. *Proc. of 6th Int. Conf. Jack-Up Platform Design, Construction and Operation*, City University, London.

References

- Stokes, G.G. (1847). On the theory of oscillatory waves. *Trans. Camb. Philos. Soc.*, Vol. 8, pp. 441-455.
- Tan, F.S.C. (1990). Centrifuge and theoretical modelling of conical footings on sand. *Ph.D. Thesis*, University of Cambridge.
- Taylor, P.H. (1992). On the kinematics of large ocean waves. *Proc. 6th Int. Conf. on the Behaviour of Off-Shore Structures (BOSS)*, University of London, London, pp. 134-145.
- Taylor, P.H., Jonathan, P. and Harland, L.A. (1995). Time domain simulation of jack-up dynamics with the extremes of a Gaussian process. *Proc. 14th Int. Conf. on Offshore Mechanic and Arctic Engineering (OMAE)*, Vol. 1-A, pp. 313-319.
- Thoft-Christensen, P. and Baker, M.J. (1982). Structural reliability theory and its applications. *Springer-Verlag*, New York.
- Thompson, R.S.G. (1996). Development of non-linear numerical models appropriate for the analysis of jack-up units. *D.Phil. Thesis*, University of Oxford.
- Tromans, P.S., Anaturk, A.R. and Hagemeyer, P. (1991). A new model for the kinematics of large ocean waves -applications as a design wave-. *Proc. 1st Int. Offshore and Polar Engng Conf.*, Edinburgh, Vol. 3, pp. 64-71.
- Tromans, P.S. and Vanderschuren, L. (1995). Response based design conditions in the North Sea: application of a new method. *Proc. 27th Offshore Technology Conference*, Houston, pp. 387-397, OTC 7683.
- Tromans, P.S. and van de Graaf, J.W. (1992). A substantiated risk assessment of a jacket structure. *Proc. 24th Offshore Technology Conference*, Houston, pp. 651-662, OTC 7075.
- Tucker, M.J. (1991). Waves in ocean engineering. *Ellis Horwood*, New York.
- Tucker, M.J., Challenor, P.G. and Carter, D.J.T. (1984). Numerical simulation of a random sea: a common error and its effect upon wave group statistics. *Applied Ocean Research*, Vol. 6, No. 2, pp. 118-122.
- Veldman, H. and Lagers, G. (1997). 50 years offshore. *Foundation for Offshore Studies*, Delft, The Netherlands.
- Vesic, A.S. (1975). Bearing capacity of shallow foundations. In *Foundation Engineering Handbook (ed. Winterkorn, H.F. and Fang, H.Y.)*, Van Nostrand, New York, pp. 121-147.
- Vugts, J.S. (1990). Environmental forces in relation to structure design or assessment -a personal view towards integration of the various aspects involved-. *Keynote paper presented at the SUT Int. Conf. on Environmental Forces on Offshore Structures*, London.
- Weaver, T.O. and Brinkmann, C.R. (1995). Calibration of a dynamic analysis procedure using measurements from a North Sea jack-up in a severe storm. *Proc. 27th Offshore Technology Conference*, Houston, pp. 333-341, OTC 7840.
- Wheeler, J.D. (1970). Method for calculating forces produced by irregular waves. *J. Petroleum Technology*, March, pp. 359-367.

References

Wroth, C.P. and Houlsby, G.T. (1985). Soil mechanics – property characterization and analysis procedures. *Proc. 11th Int. Conf. on Soil Mech. and Fndn Engng*, San Francisco, Vol. 1, pp. 1-55.

Williams, M.S., Blakeborough, A., Houlsby, G.T. and Williams, D.M. (1997). Development of a real-time hybrid dynamic testing system. *Proc. 6th SECED Conf. on Seismic Design Practice*, Oxford.

Winterstein, S.R., Torhaug, R. and Kumar, S. (1998). Design seastates for extreme response of jack-up structures. *J. of Offshore Mechanics and Arctic Engineering (OMAE)*, ASME, Vol. 120, pp. 103-108.

Young, A.G., Remmes, B.D. and Meyer, B.J. (1984). Foundation performance of offshore jack-up drilling rigs. *J. Geotech Engng Div.*, ASCE, Vol. 110, No 7, pp. 841-859, Paper No. 18996.

Zaharescu, E. (1961). Sur la stabilité des fondations rigides. *Proc. 5th Int. Conf. Soil Mech. Fndn Engng*, Paris, Vol. 1, pp. 867-871.

Table 2.1 - Level of complexity used in the analysis of jack-up units

		structural				foundations				dynamic				wave loading			
degree of complexity		→				→				→				→			
assessment grade		<i>g</i>	<i>b</i>	<i>b</i>	<i>a</i>	<i>g</i>	<i>b</i>	<i>b</i>	<i>a</i>	<i>g</i>	<i>b</i>	<i>b</i>	<i>a</i>	<i>g</i>	<i>b</i>	<i>b</i>	<i>a</i>
Author	Year	linear elastic	non-linear effects as correction factors		non-linear structural algorithm	pinned	linear springs	non-linear springs	plasticity theory	quasi static	DAF	frequency domain	time domain	point loads	regular wave theory	random wave theory with extrapolation	full random wave theory
			P-Δ	Euler													
Grenda	86	✓				✓					✓		✓				✓ ¹
Bradshaw	87		✓	✓			✓ ²				✓	✓					✓ ³
Schotman	89	✓							✓	✓				✓			
Kjeøy <i>et al.</i>	89				✓	✓							✓		✓	✓ ⁴	
Brekke <i>et al.</i>	90	✓					✓						✓		✓		
Chen <i>et al.</i>	90		✓	✓		✓							✓				✓ ⁵
Mommas & Grundlehner	92		✓	✓		✓					✓		✓				✓ ⁶
Karunakaran <i>et al.</i>	92				✓		✓	✓					✓			✓	
Spidsø & Karunakaran	93		✓			✓							✓				✓
Harland	94	✓ ⁷				✓							✓				✓ ⁸
Martin	94				✓				✓	✓				✓			
Taylor <i>et al.</i>	95	✓ ⁷				✓							✓				✓ ⁸
Manuel & Cornell	96	✓				✓	✓	✓					✓				✓ ⁹
Thompson	96				✓				✓				✓		✓		
Hoyle & Snell ^(R)	97				✓			✓ ¹⁰					✓			✓ ¹¹	
Morandi <i>et al.</i> ^(R)	97				✓	✓					✓			✓			
Daghigh <i>et al.</i> ^(R)	97				✓	✓				✓	✓ ¹²		✓				✓ ¹²
Cassidy ¹³	99				✓				✓				✓				✓

1. investigated DAFs for different levels of damping for 1000 waves (representing one 3hr event)
 2. uncoupled springs
 3. for random time domain simplified the structure to a stick model
 4. fitted extreme response of 3hr storm with 3 parameter Weibull distribution from one 40min and two 20min simulations
 5. ten 2.3hr simulations
 6. ten 3hr simulations
 7. used single degree of freedom stick model
 8. used Constrained NewWave
 9. six 0.57hr simulations
 10. implemented the non-linear stiffness model recommended in the SNAME (1994) procedures
 11. used a 200-second segment of one 3hr storm to scale and represent the extreme case
 12. used dynamic analysis of a simplified stick model to evaluate DAFs at specific H_s values for use in a quasi static push over analysis
 13. this thesis
- (R) studies on jack-up reliability

Table 2.2 - Calculation of equivalent hydrodynamic diameter (D_{Eh}) and area (A_{Eh})

$s = 5.16 \text{ m} = \text{bay height}$

Member	Number	Diameter (m)	Marine growth (m)	Area (m ²)	Length (m)	$\Sigma(\text{Vol.})$ (m ³)	Drag				Inertia			
							C_d	a degrees	b degrees	a.c.d.	C_{dei}	C_m	$C_m \cdot \text{Vol}/s$ (m ²)	
1	3	0.900	0.01	0.664	5.160	10.285	2	90	90	1	2.557	1	1.993	
2	1	0.356	0.01	0.111	6.377	0.706	1	90	44.254	1	0.215	1	0.137	
	2	0.356	0.01	0.111	6.377	1.412	1	30	44.254	0.48257	0.208	1	0.274	
3	1	0.356	0.01	0.111	6.377	0.706	1	90	44.254	1	0.215	1	0.137	
	2	0.356	0.01	0.111	6.377	1.412	1	30	44.254	0.48257	0.208	1	0.274	
4	1	0.406	0.01	0.143	9.700	1.384	1	90	0	1	0.371	1	0.268	
	2	0.406	0.01	0.143	9.700	2.769	1	30	0	0.125	0.093	1	0.537	
5	1	0.114	0.01	0.014	4.712	0.067	1	90	0	1	0.057	1	0.013	
	2	0.114	0.01	0.014	4.712	0.133	1	30	0	0.125	0.014	1	0.026	
$D_E = (4 \cdot \Sigma(\text{Area} \cdot \text{Length} / (\pi s)))^{0.5} = 2.159$											ΣC_{de}	3.937	$\Sigma C_m \cdot \text{Vol}/s$	3.658

note: Both C_d and C_m in this table are unit values (*i.e.* to be scaled later in the Morison equation)

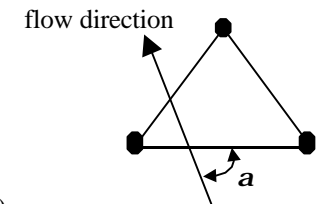
The drag coefficient of the chord member has been estimated as twice that of other circular members.

Assuming a marine growth of 10mm.

a is the angle of the flow direction (see inserted figure); flow is assumed to be perpendicular to the triangular face (see Fig. 2.2).

b is the angle of vertical inclination of the members (90 degrees is vertical and 0 horizontal)

a.c.d. = angular correction for drag = $(\sin^2 \mathbf{b} + \cos^2 \mathbf{b} \sin^2 \mathbf{a})^{1.5}$; therefore for each member $C_{de} = (\text{Number} \cdot C_d \cdot (\text{a.c.d.}) \cdot \text{Vol}) / (D_E \cdot s)$



Equivalent $D_{Eh} = (\Sigma C_{de} \cdot D_E) = \mathbf{8.50 \text{ m}}$

Equivalent $A_{Eh} = \Sigma(C_{me} \cdot \text{Vol})/s = \mathbf{3.66 \text{ m}^2}$

Table 4.1 - Parameters for Model C

Constant	Dimension	Explanation	Constraints	Typical value	Notes
R	L	Footing radius		(various)	
γ	F/L ³	Unit weight of soil		10kN/m ³	Saturated sand
g	-	Shear modulus factor		4000	
k_1	-	Elastic stiffness factor (vertical)		2.65	
k_2	-	Elastic stiffness factor (moment)		0.46	
k_3	-	Elastic stiffness factor (horizontal)		2.3	
k_4	-	Elastic stiffness factor (horizontal/moment coupling)		-0.14	
h_0	-	Dimension of yield surface (horizontal)		0.116	Maximum value of H/V_0 on $M = 0$
m_0	-	Dimension of yield surface (moment)		0.086	Maximum value of $M/2RV_0$ on $H = 0$
a	-	Eccentricity of yield surface	$-1.0 < a < 1.0$	-0.2	
b_1	-	Curvature factor for yield surface (low stress)	$b_1 \leq 1.0$	0.90	$b_1 = b_2 = 1$ gives parabolic section
b_2	-	Curvature factor for yield surface (high stress)	$b_2 \leq 1.0$	0.99	$b_1 = b_2 = 1$ gives parabolic section
b_3	-	Curvature factor for plastic potential (low stress)	$b_3 \leq 1.0$	0.55	
b_4	-	Curvature factor for plastic potential (high stress)	$b_4 \leq 1.0$	0.65	
a_h	-	Association factor (horizontal)		1.0-2.5	Variation according to Eqn 3.32 and $a_{h\infty} = 2.5$
a_m	-	Association factor (moment)		1.0-2.15	Variation according to Eqn 3.33 and $a_{m\infty} = 2.15$
$k\dot{c}$	-	Rate of change in association factors		0.125	
f	-	Initial plastic stiffness factor		0.144	
N_γ	-	Bearing capacity factor (peak)		150-300	
δ_p	-	Dimensionless plastic penetration at peak		0.0316	

Table 5.1 - Coefficients used in Eqns 5.13 and 5.14 (after Newman, 1990)

i	c_i (for Eqn 5.13)	b_i (for Eqn 5.14)
0	1.00000000	0.000000122
1	-0.33333372	0.073250017
2	-0.01109668	-0.009899981
3	0.01726435	0.002640863
4	0.01325580	-0.000829239
5	-0.00116594	-0.000176411
6	0.00829006	
7	-0.01252603	
8	0.00404923	

Table 5.2 - NewWave amplitudes used in the sea-state characterised by $T_p = 15$ s

steepness [$k_p a$] (rad ² /(ms))	NewWave amplitude [a] (m)
0.1	5.60
0.2	11.19
0.3	16.79

Table 6.1 - Sea-state characteristics and NewWave elevations used in the long-term numerical experiments

Return Period	H_s (m)	T_z (s)	T_p (s)	a_1 (m)	a_2 (m)	a_3 (m)	a_4 (m)	a_5 (m)
1	8.98	9.35	12.02	2.5	4.5	6.5	8.5	11
1E1	10.60	10.16	13.06	3.0	5.5	7.5	10	14
1E2	12.00	10.81	13.90	3.5	7	10	12	15
1E3	13.25	11.36	14.61	4.0	7.5	10.5	13	17
1E4	14.40	11.84	15.22	4.5	8	11	15	18
1E5	15.46	12.27	15.78	4.75	10	13	16	19
1E6	16.45	12.66	16.27	5.0	12	15	17.5	21

Table 6.2 - Wind and current values used in the long term numerical experiments

Return Period	Wind Force (MN)	Current (m/s)
1	0.756	0.599
1E1	1.053	0.707
1E2	1.350	0.800
1E3	1.647	0.884
1E4	1.944	0.960
1E5	2.241	1.031
1E6	2.538	1.097

Table 6.3 - Statistical properties of the extreme force distributions

(a) no wind or current

probability of occurrence (year)	Force on upwave legs				Total force on all legs			
	just NewWave		Constrained NewWave		just NewWave		Constrained NewWave	
	m (MN)	CoV (%)	m (MN)	CoV (%)	m (MN)	CoV (%)	m (MN)	CoV (%)
1 in 1E0	3.867	16.81	4.103	17.16	4.292	15.84	4.517	16.43
1 in 1E1	5.637	17.42	5.957	17.72	6.180	16.43	6.653	16.90
1 in 1E2	7.530	17.47	7.985	18.18	8.354	17.03	9.043	17.42
1 in 1E3	9.741	17.66	10.250	18.54	10.954	17.45	11.844	17.64
1 in 1E4	11.986	17.87	12.560	18.31	13.837	17.65	14.988	17.65
1 in 1E5	14.308	18.12	14.849	18.68	17.060	18.09	18.164	18.14
1 in 1E6	16.944	18.53	17.871	19.22	20.673	18.21	22.543	18.37

(b) with wind and current

probability of occurrence (year)	Force on upwave legs				Total force on all legs			
	just NewWave		Constrained NewWave		just NewWave		Constrained NewWave	
	m (MN)	CoV (%)	m (MN)	CoV (%)	m (MN)	CoV (%)	m (MN)	CoV (%)
1 in 1E0	6.029	12.96	6.251	13.66	6.804	12.61	7.125	12.60
1 in 1E1	8.824	13.57	9.197	14.04	9.998	12.54	10.644	12.86
1 in 1E2	11.607	13.84	12.361	14.33	13.642	13.02	14.771	13.31
1 in 1E3	14.986	14.04	15.700	14.77	18.002	13.35	19.038	13.47
1 in 1E4	18.607	14.24	19.317	14.97	22.657	13.60	24.375	13.61
1 in 1E5	22.173	14.49	22.932	15.30	27.860	14.19	29.366	14.35
1 in 1E6	26.041	14.84	27.283	15.71	33.351	14.63	36.001	14.81

Table 6.4 - Statistical properties of the extreme deck displacement distributions for just the NewWave

(a) no wind or current

probability of occurrence (year)	linear springs		Model C		pinned	
	$m(m)$	CoV (%)	$m(m)$	CoV (%)	$m(m)$	CoV (%)
1 in 1E0	0.104	16.97	0.104	16.92	0.472	14.91
1 in 1E1	0.159	18.41	0.161	19.29	0.638	15.72
1 in 1E2	0.225	18.54	0.233	20.99	0.823	16.32
1 in 1E3	0.290	18.73	0.326	24.54	1.019	16.97
1 in 1E4	0.356	18.93	0.427	25.64	1.249	17.25
1 in 1E5	0.431	19.03	0.560	27.70	1.478	17.76
1 in 1E6	0.509	19.13	0.703	29.05	1.751	17.91

(b) with wind and current

probability of occurrence (year)	linear springs		Model C		pinned	
	$m(m)$	CoV (%)	$m(m)$	CoV (%)	$m(m)$	CoV (%)
1 in 1E0	0.175	12.99	0.175	12.99	0.672	12.85
1 in 1E1	0.257	13.82	0.278	17.81	0.898	13.22
1 in 1E2	0.349	14.13	0.400	20.58	1.137	13.33
1 in 1E3	0.451	14.29	0.596	22.15	1.441	13.52
1 in 1E4	0.547	14.57	0.857	22.68	1.816	13.61
1 in 1E5	0.654	14.62	1.141	22.86	2.205	13.70
1 in 1E6	0.773	14.71	1.503	23.08	2.670	13.64

Table 6.5 - Percentage increase in expected deck displacement at three levels of annual probability of exceedence due to the random background in the Constrained NewWave analysis

probability of exceedence	no wind or current			with wind and current		
	linear springs (%)	Model C (%)	pinned (%)	linear springs (%)	Model C (%)	pinned (%)
1.0E-4	7.5	13.0	7.5	6.0	12.0	7.0
1.0E-5	8.0	16.0	8.0	6.5	15.0	7.5
1.0E-8	8.5	21.0	8.0	7.0	16.0	8.0

Table 7.1 – Basic random variables of interest in the probabilistic modelling of jack-up units (table continues over page)

	Basic Variable	Mean Value	Distribution	CoV (%)	Reference	Notes	
Env. Loading	C_d	0.75	normal	30	Thoft-Christensen and Baker (1982)	used in an example calculation of a jacket structure	
		1.0	normal	20	Løeth and Bjerager (1989)	for example deep water jacket (over 300m water depth)	
		1.0	log-normal	20	Løeth and Hauge (1992) ¹	for example jack-up calculation	
		1.0	normal	20	Karunakaran (1993) and Karunakaran <i>et al.</i> (1994)	values used for three-legged jack-up with triangular-trussed legs	
		0.75	log-normal	25	Sigurdsson <i>et al.</i> (1994)	for example jacket located in the North Sea	
		0.61		24	Kim and Hibbard (1975)	full scale tests on 325mm diameter smooth piles (consistent for $H_s = 0.8-3.0\text{m}$)	
	marine growth			log-normal	20	Løeth and Hauge (1992)	for central North Sea jack-up in 83.7m water depth
		25 – 50 mm		log-normal	50	Sigurdsson <i>et al.</i> (1994)	values are depth dependent and for a jacket platform (indicating higher values than for a jack-up)
		varies		normal	10	Shetty <i>et al.</i> (1997)	for a jacket structure in North Sea conditions
	C_m	1.8		normal	15	Thoft-Christensen and Baker (1982)	used in an example calculation of a jacket structure
		2.0		normal	10	Løeth and Bjerager (1989)	for example deep water jacket (over 300m water depth)
		1.75		log-normal	10	Løeth and Hauge (1992)	for example jack-up calculation
		2.0		normal	20	Karunakaran (1993) and Karunakaran <i>et al.</i> (1994)	values used for three-legged jack-up with triangular-trussed legs
		1.7		log-normal	25	Sigurdsson <i>et al.</i> (1994)	for example jacket located in the North Sea
		1.2			22	Kim and Hibbard (1975)	full scale tests on 325mm diameter piles
	wind				12-13	Thoft-Christensen and Baker (1982)	CoV for annual max. mean-hourly extreme wind levels at Lerwick (a reasonable representation of the Northern North Sea)
		42.40 m/s 40.45 m/s		normal	8 (of force)	Morandi <i>et al.</i> (1997) ²	based on 50-year return-period based on 20-year return-period variation is included with dead and live loads
	current (u)	0.85 m/s		log-normal	20.0	Karunakaran (1993)	based on observed current data in a central North Sea location (varies with H_s)
0.2, 0.4, 0.7 m/s			log-normal	20.0	Karunakaran <i>et al.</i> (1994)	uniform current with value related to increasing H_s	
			log-normal	15	Puskar <i>et al.</i> (1994)	error in current values used for comparison of predicted platform damage due to a hurricane in the Gulf of Mexico in 1992	

	Basic Variable	Mean Value	Distribution	CoV (%)	Reference	Notes
		0.86 m/s 0.42 m/s	normal	15	Morandi <i>et al.</i> (1997)	based on 50-year return-period based on 20-year return-period variation included with wave loading
		0.44 m/s	log-normal	15	Shetty <i>et al.</i> (1997)	based on a 50-year return current in the North Sea
Geometry / Structural	deck mass		normal	5 (10)	L�seth and Bjerager (1989)	top mass (distributed mass in legs and braces) values are for a jacket and have been included for comparison
		16.9E6 kg	log-normal	10	Karunakaran (1993)	for ‘MSC CJ62’ jack-up platform designed for operation in 108m water depth
			normal	8 15	Morandi <i>et al.</i> (1997)	for application as gravity dead load for application as inertia load set
	damping ratio (structural)	0.03	normal	33.3	Baker and Ramachandran (1981)	for an example jacket structure (included for comparison)
		0.025	log-normal	25.0	Karunakaran (1993)	included as Rayleigh damping with hydrodynamic damping accounted for in relative Morison equation
		0.02	log-normal	25.0	Karunakaran <i>et al.</i> (1994)	included as Rayleigh damping with hydrodynamic damping accounted for in relative Morison equation
		0.055		21.8	Weaver and Brinkman (1995)	total damping estimated from acceleration record from a jack-up in the central North Sea (depth = 75m & $H_s = 11.7$ m)
Foundation	linear spring stiffness		log-normal	20	L�seth and Hauge (1992)	on uncorrelated linear springs for vertical, horizontal and rotation directions
			normal	30	Karunakaran (1993)	on uncorrelated linear springs (for jack-up in dense sand)
Modelling	wave kinematics		normal	10	Karunakaran (1993)	After using Wheeler stretching on the Airy wave model, a variation on the kinematics of 10% with a bias of 1.05 is applied. The reason stated is the under-prediction of wave kinematics in the crest compared to laboratory experiments.
	extreme mudline forces (global CoVs)			15-30 20-25	Lacasse and Nadim (1994)	CoVs quoted for extreme mudline forces in jackets and jack-ups respectively
	pushover analysis		normal	12	Morandi <i>et al.</i> (1997)	once the failure point is found by push-over analysis, an additional variation is applied

Notes:

1. L seth and Hauge (1992) used normal distributions for current and wind velocities based upon H_s values. Deterministic values were used for structural damping (1%) and hull mass.
2. In modelling forces Morandi *et al.* (1997) place a normal distribution with CoVs of 15% on the [wave + current] loading and 8% on the [wind + dead + live] loading.

Table 7.2 – Set of eleven basic random variables used in short-term numerical experiments

Random variable number (X_i)	Basic variable	Category	Mean value (m_x)	Distribution	Standard deviation (s_x)	CoV (%)
1	u	loading	0.8 m/s	normal	0.16	20
2	C_d	loading	1.1	normal	0.22	20
3	C_m	loading	2.0	normal	0.3	15
4	$wind$	loading	1.35E6 N	normal	0.135E6 N	10
5	$structural\ damping$	structural	0.02	normal	0.004	20
6	$mass\ of\ hull$	structural	16.1E6 kg	normal	1.61E6 kg	10
7	g	Model C	8.228 (4000)	log-normal	0.363 (1500)	37.5
8	m_0	Model C	0.086	normal	0.0129	15
9	N_g	Model C	5.502 (250)	log-normal	0.198 (50)	20
10	$f\text{-}d_p$	Model C	0.144	normal	0.0288	20
11	$pre\text{-}load\ factor$	Model C	1.925	normal	0.1925	10

Table 7.3 – Polynomial coefficients for a RS of deck displacements

X_i	a	b_i	c_i	$d_{ij} (X_i = \dots)$										
				1	2	3	4	5	6	7	8	9	10	11
1	-9.97E-3	2.72E-1	9.93E-2	-	3.76E-1	-2.28E-2	1.06E-7	-3.307	-1.12E-8	-1.32E-5	-2.844	-2.05E-4	-3.24E-1	-4.61E-2
2		1.192	1.47E-1	-	-	-9.08E-3	-7.04E-9	-2.997	-2.31E-8	-1.78E-5	-5.919	-1.18E-4	-4.58E-1	-1.31E-1
3		2.06E-1	-5.23E-4	-	-	-	-1.84E-8	2.91E-1	-4.14E-9	-4.73E-6	-1.97E-1	-5.66E-5	-2.32E-1	-1.20E-3
4		2.47E-7	-1.7E-15	-	-	-	-	2.75E-7	-8.2E-16	-7.1E-12	-1.01E-6	7.0E-11	-1.35E-7	-5.43E-8
5		-5.578	-4.680	-	-	-	-	-	5.31E-7	-1.41E-4	1.87E1	-3.28E-3	1.20E1	-5.36E-1
6		-1.48E-8	3.2E-16	-	-	-	-	-	-	-3.3E-13	2.71E-7	7.3E-12	-1.91E-8	3.65E-9
7		4.08E-5	4.9E-10	-	-	-	-	-	-	-	9.61E-5	-1.04E-8	-9.92E-6	1.16E-6
8		-1.11E1	6.40E1	-	-	-	-	-	-	-	-	1.47E-3	5.788	1.015
9		4.17E-5	-5.00E-8	-	-	-	-	-	-	-	-	-	6.27E-4	3.69E-5
10		-2.94E-1	-1.30E-1	-	-	-	-	-	-	-	-	-	-	5.65E-1
11		-2.69E-1	5.93E-2	-	-	-	-	-	-	-	-	-	-	-

Table 7.4 – Sensitivity values evaluated at three response levels

$N = 10\ 000$ $\Delta m_{x_i} = 1\%$			$R = d_{deck} = 0.3\ m$ $P_f = 0.7756$			$R = d_{deck} = 0.5\ m$ $P_f = 0.1479$			$R = d_{deck} = 0.7\ m$ $P_f = 0.0131$		
X_i	Type	+/-	$P_f(\Delta m_{x_i})$	$S_{m_{x_i}}$	Rank	$P_f(\Delta m_{x_i})$	$S_{m_{x_i}}$	Rank	$P_f(\Delta m_{x_i})$	$S_{m_{x_i}}$	Rank
1	u	+	0.7794	0.38	2	0.1524	0.45	4	0.0134	0.03	3-4
2	C_d	+	0.7886	1.3	1	0.1575	0.96	1	0.0147	0.16	1
3	C_m	+	0.7759	0.03	7-8	0.1481	0.02	10	0.0131	-	8-11
4	$wind$	+	0.7777	0.21	6	0.1494	0.15	6	0.0132	0.01	5-7
5	$damping$	-	0.7758	0.02	9-10	0.1486	0.07	8	0.0132	0.01	5-7
6	$hull\ mass$	-	0.7785	0.29	4	0.1527	0.48	3	0.0134	0.03	3-4
7	g	-	0.7759	0.03	7-8	0.1487	0.08	7	0.0131	-	8-11
8	m_0	-	0.7780	0.24	5	0.1549	0.70	2	0.0145	0.14	2
9	N_g	-	0.7757	0.01	11	0.1480	0.01	11	0.0131	-	8-11
10	$f\text{-}d_p$	-	0.7758	0.02	9-10	0.1485	0.06	9	0.0131	-	8-11
11	$pre\text{-}load\ factor$	-	0.7786	0.30	3	0.1513	0.34	5	0.0132	0.01	5-7

note: +/- indicates whether the basic variable's mean is being changed by + Δm_{x_i} or - Δm_{x_i}

Table 7.5 – Results from FORM calculation for a response of $d_{deck} = 0.5$ m

The reliability index was evaluated as $\beta = 1.03$ giving an estimated P_f of 0.1515.

X_i	Type	a_i	$X_{\text{design point}}$	a_i^2	z_i (%)	Rank	Rank from Monte Carlo
1	u	0.35	0.8577	0.1225	6.75	3	4
2	C_d	0.82	1.2858	0.6724	74.71	1	1
3	C_m	0.0046	2.0014	2.12E-5	0.0011	10	10
4	$wind$	0.066	1.3592E6	0.004356	0.22	6	6
5	$damping$	-0.032	0.0199	0.001024	0.051	9	8
6	$hull\ mass$	-0.18	15.8015E6	0.0324	1.66	4	3
7	g	-0.061	3656.8	0.003721	0.19	7	7
8	m_0	-0.38	0.0810	0.1444	8.11	2	2
9	N_g	-0.0004	245.16	1.6E-7	8.0E-6	11	11
10	$f \cdot d_p$	-0.042	0.1428	0.001764	0.088	8	9
11	$pre-load\ factor$	-0.13	1.8992	0.0169	0.86	5	5

Table 7.6 - Set of seven basic random variables used in numerical experiments

Random variable number (X_i)	Basic variable	Category	Mean value (m_k)	Distribution	Standard deviation (s_x)	CoV (%)
1 (1)	u	loading	0.8 m/s	normal	0.16	20
2 (2)	C_d	loading	1.1	normal	0.22	20
3 (4)	$wind$	loading	1.35E6 N	normal	0.135E6 N	10
4 (6)	$mass\ of\ hull$	structural	16.1E6 kg	normal	1.61E6 kg	10
5 (7)	g	Model C	8.228 (4000)	log-normal	0.363 (1500)	37.5
6 (8)	m_0	Model C	0.086	normal	0.0129	15
7 (11)	$pre-load\ factor$	Model C	1.925	normal	0.1925	10

() indicate previous random variable number for 11 random variable experiment

Table 7.7 – Sea-states and NewWave elevations used in the long-term numerical experiments

Return period	H_s (m)	T_z (s)	T_p (s)	a_1 (m)	a_2 (m)	a_3 (m)	a_4 (m)	a_5 (m)	m_{wind} (MN)	s_{wind} (MN)	$m_{current}$ (m/s)	$s_{current}$ (m/s)
1	8.98	9.35	12.02	2.5	4.5	6.5	8.5	11	0.756	0.0756	0.599	0.1198
1E1	10.60	10.16	13.06	3.0	5.5	7.5	10	14	1.053	0.1053	0.707	0.1414
1E2	12.00	10.81	13.90	3.5	7.0	10	12	15	1.350	0.1350	0.800	0.16
1E3	13.25	11.36	14.61	4.0	7.5	10.5	13	17	1.647	0.1647	0.884	0.1768
1E4	14.40	11.84	15.22	4.5	8.0	11	15	18	1.944	0.1944	0.960	0.1920
1E5	15.46	12.27	15.78	4.75	10	13	16	19	2.241	0.2241	1.031	0.2062

Table 7.8 – Statistical properties of the short-term extreme deck displacement distributions

Return period	All X_i with mean values (Ch. 6)		All X_i include statistical variability		Percentage increase in $m_{(d_{deck})}$
	$m_{(d_{deck})}$ (m)	CoV (%)	$m_{(d_{deck})}$ (m)	CoV (%)	
1	0.175	12.99	0.176	22.38	0.5
1E1	0.278	17.81	0.291	31.59	4.7
1E2	0.400	20.58	0.433	35.66	8.3
1E3	0.596	22.15	0.660	36.67	10.7
1E4	0.857	22.68	0.952	36.82	11.1
1E5	1.141	22.86	1.294	38.72	13.4

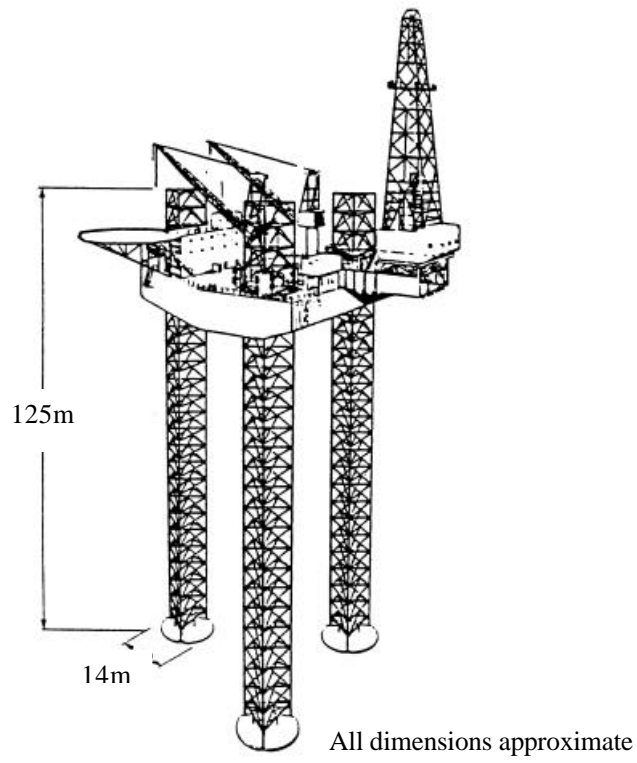


Figure 1.1 - Typical three legged jack-up unit (after Reardon, 1986)

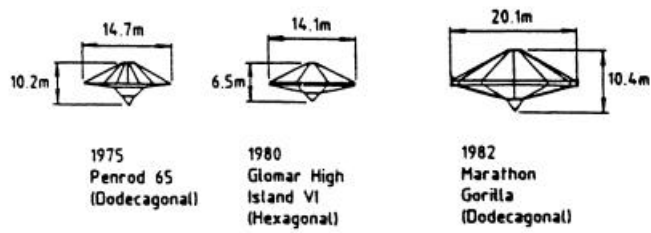


Figure 1.2 - Examples of jack-up spudcan footings (after Young *et al.*, 1984)

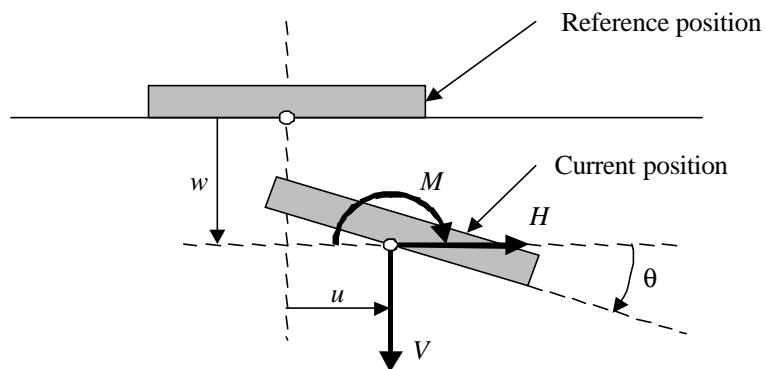


Figure 1.3 - Loads and displacements defined in a three-dimensional foundation model (after Butterfield *et al.*, 1997)

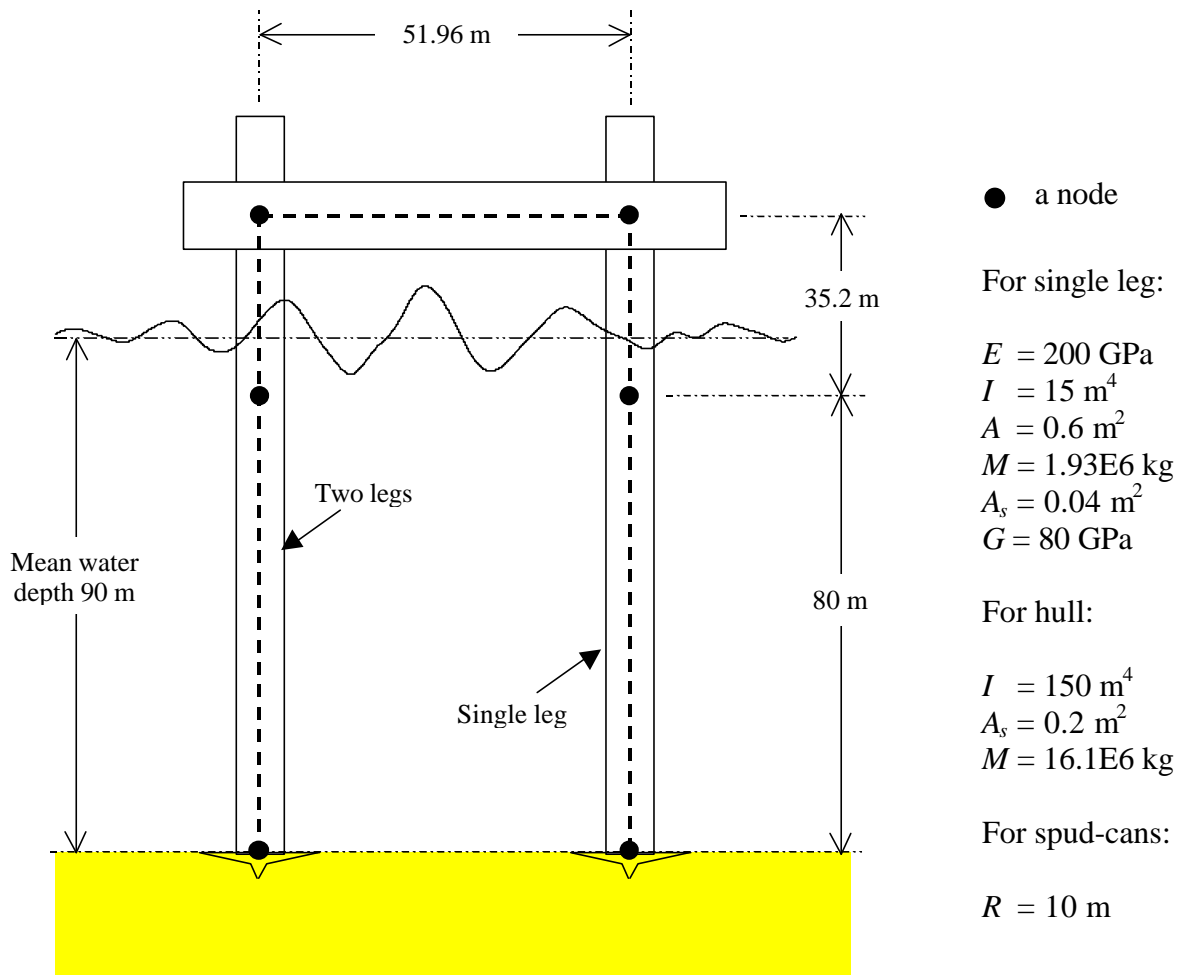
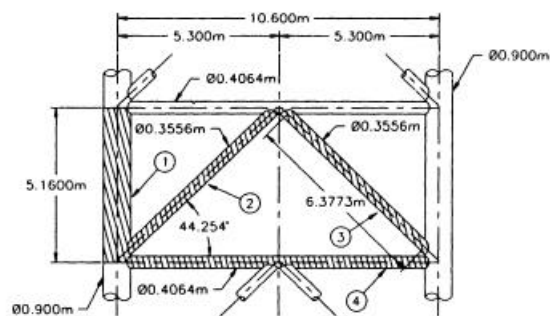
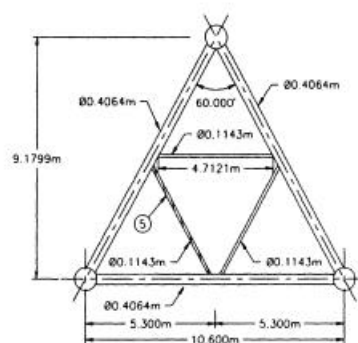


Figure 2.1 - General schematic of the idealised jack-up unit used in the analyses



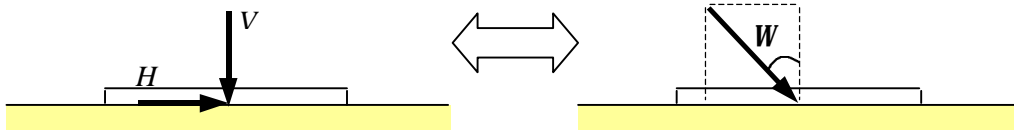
Elevation



Plan

Figure 2.2 - Detailed leg section used in the idealised jack-up unit (after Nielsen *et al.*, 1994)

(a) simultaneous horizontal and vertical loading



(b) simultaneous moment and vertical loading

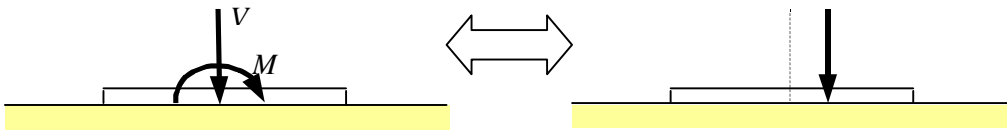
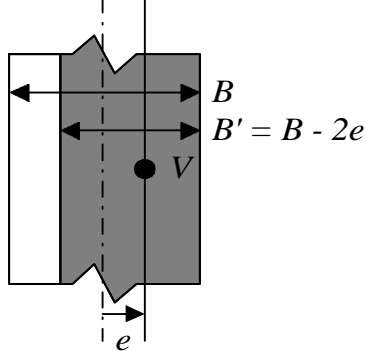


Figure 3.1 – Representations of inclined and eccentric loading

(a) strip footing



(b) circular footing

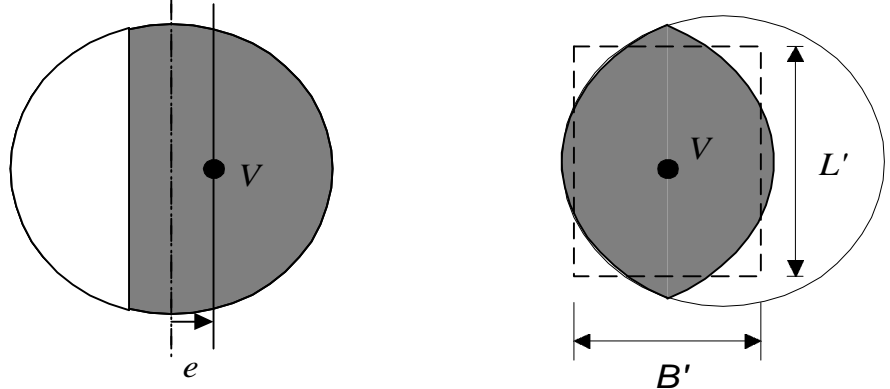
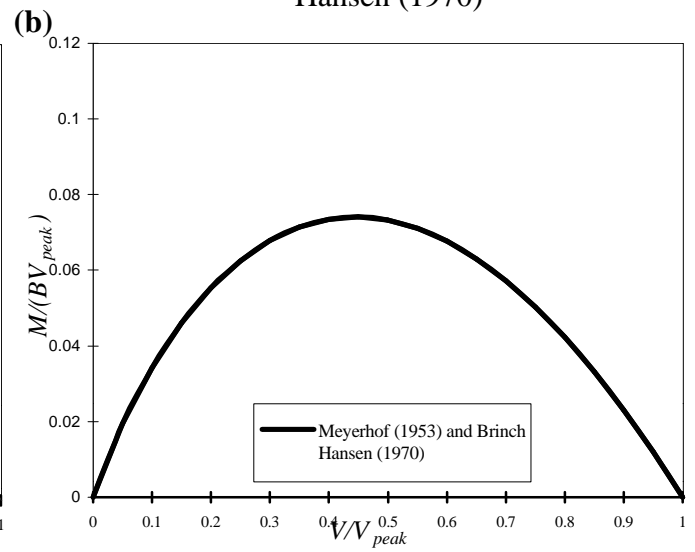
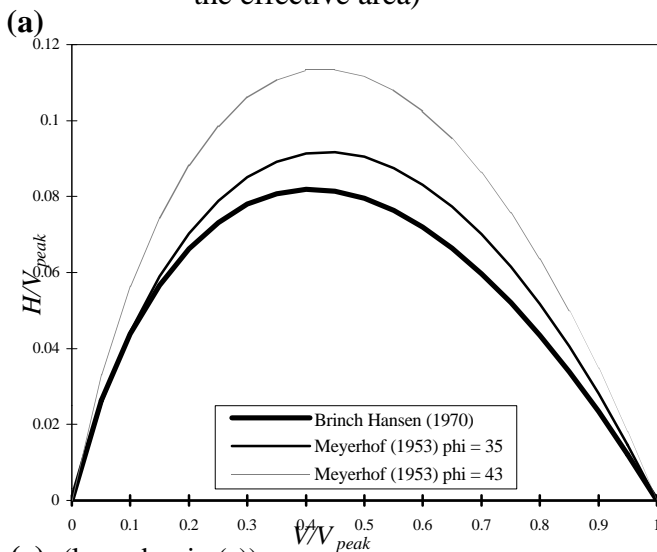


Figure 3.2 - Effective area concept as defined by Meyerhof (1953) (shaded area represents the effective area)

Figure 3.3 - Effective area for a circular footing as defined by Brinch Hansen (1970)



(c) (legend as in (a))

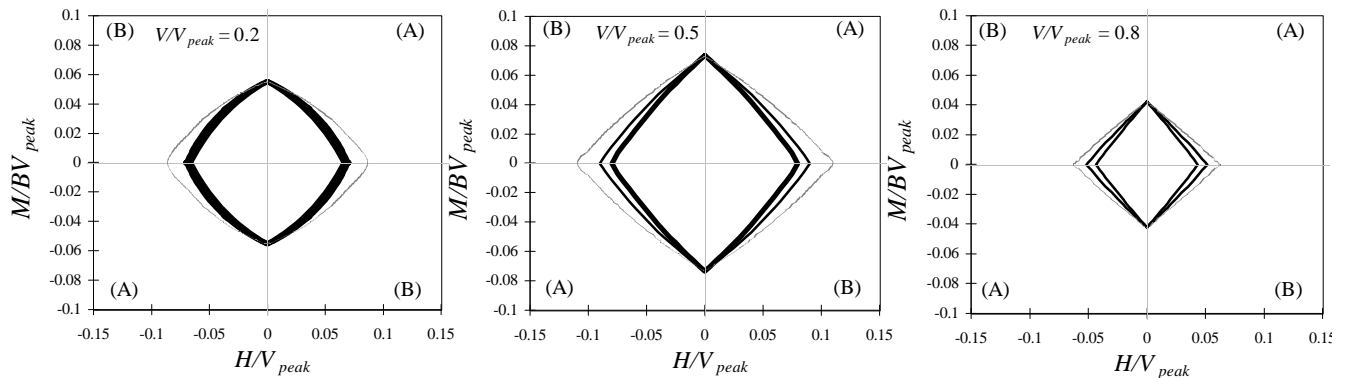
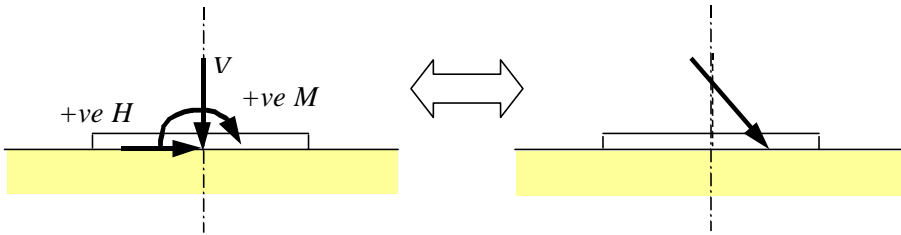


Figure 3.4 - Bearing capacity interaction surfaces derived from Meyerhof (1953) and Brinch Hansen (1970)

(a) positive eccentricity



(b) negative eccentricity

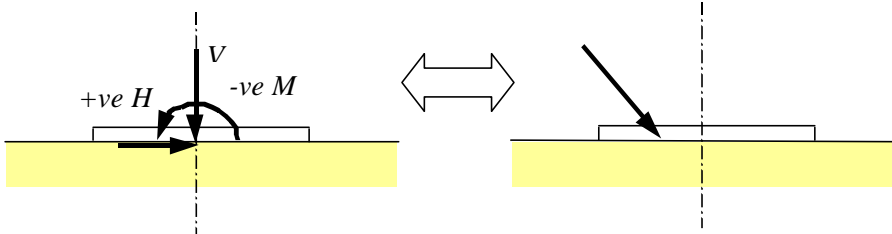


Figure 3.5 – Representations of positive and negative eccentricity

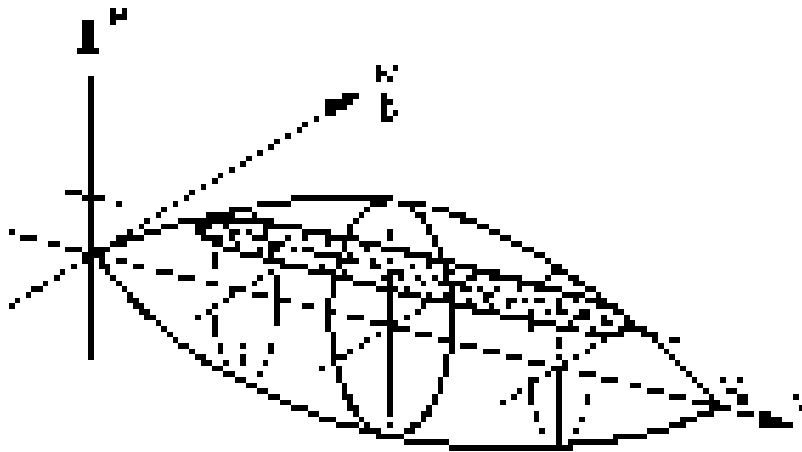


Figure 3.6 - Cigar-shaped yield surface (after Butterfield and Ticof, 1979)

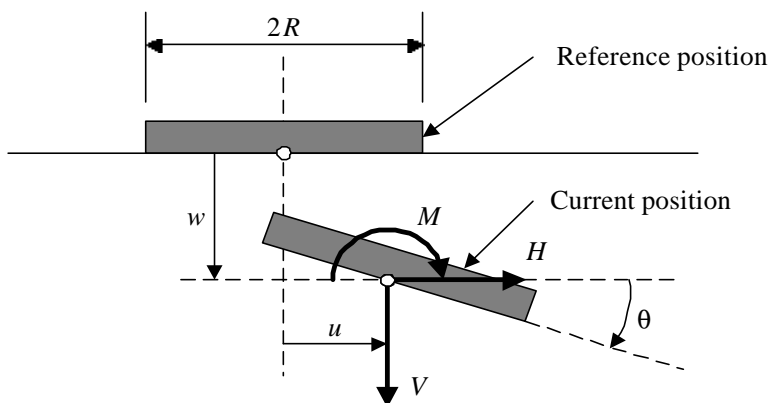


Figure 3.7 - Sign convention for positive loads and displacements (after Butterfield *et al.*, 1997)

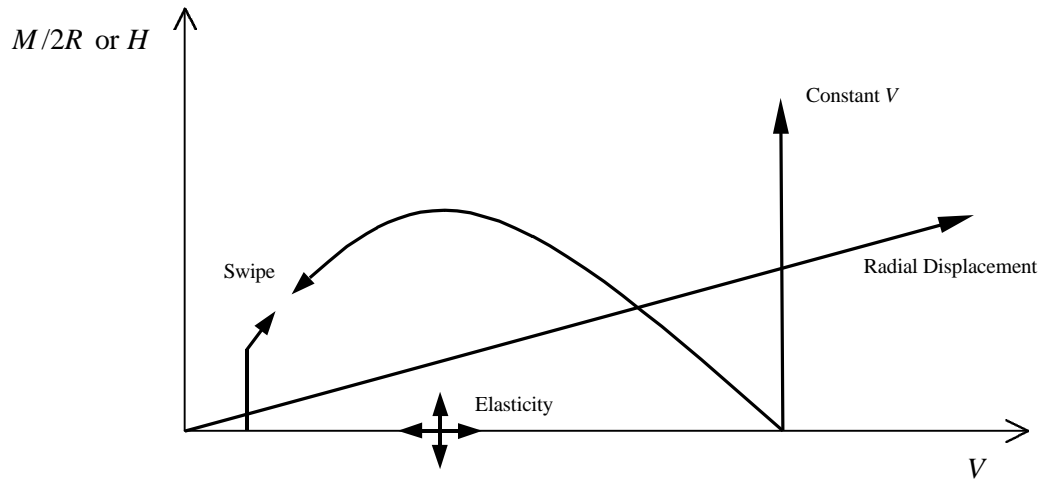


Figure 3.8 - Expected load paths for the experimental plasticity tests

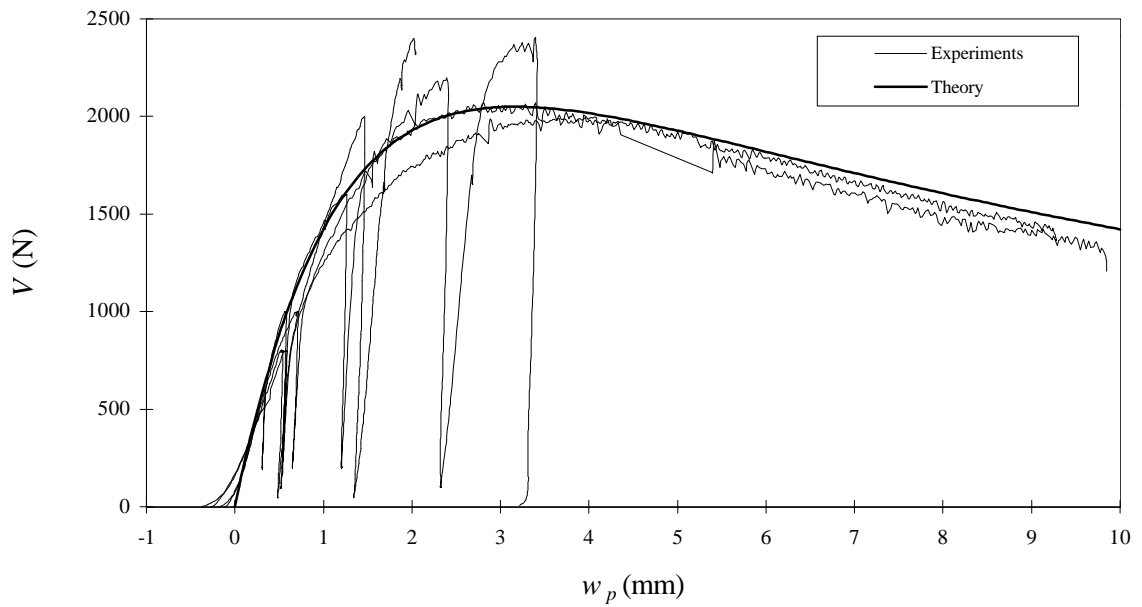


Figure 3.9 - Theoretical fit of the vertical load tests

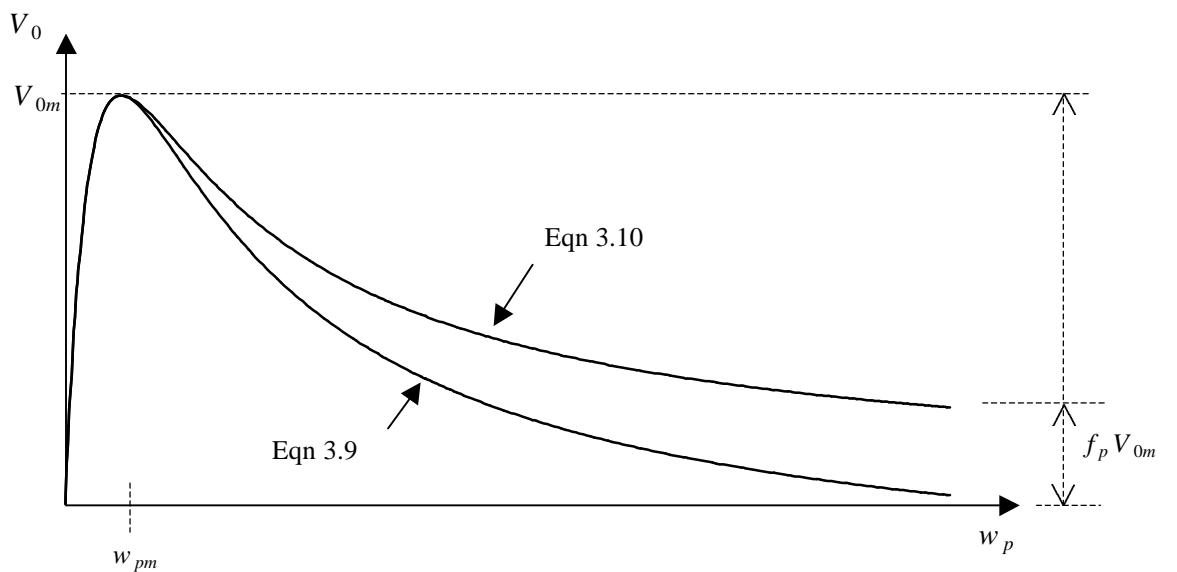


Figure 3.10 - Comparison of hardening law of Eqn 3.9 and Eqn 3.10 as w_p approaches infinity

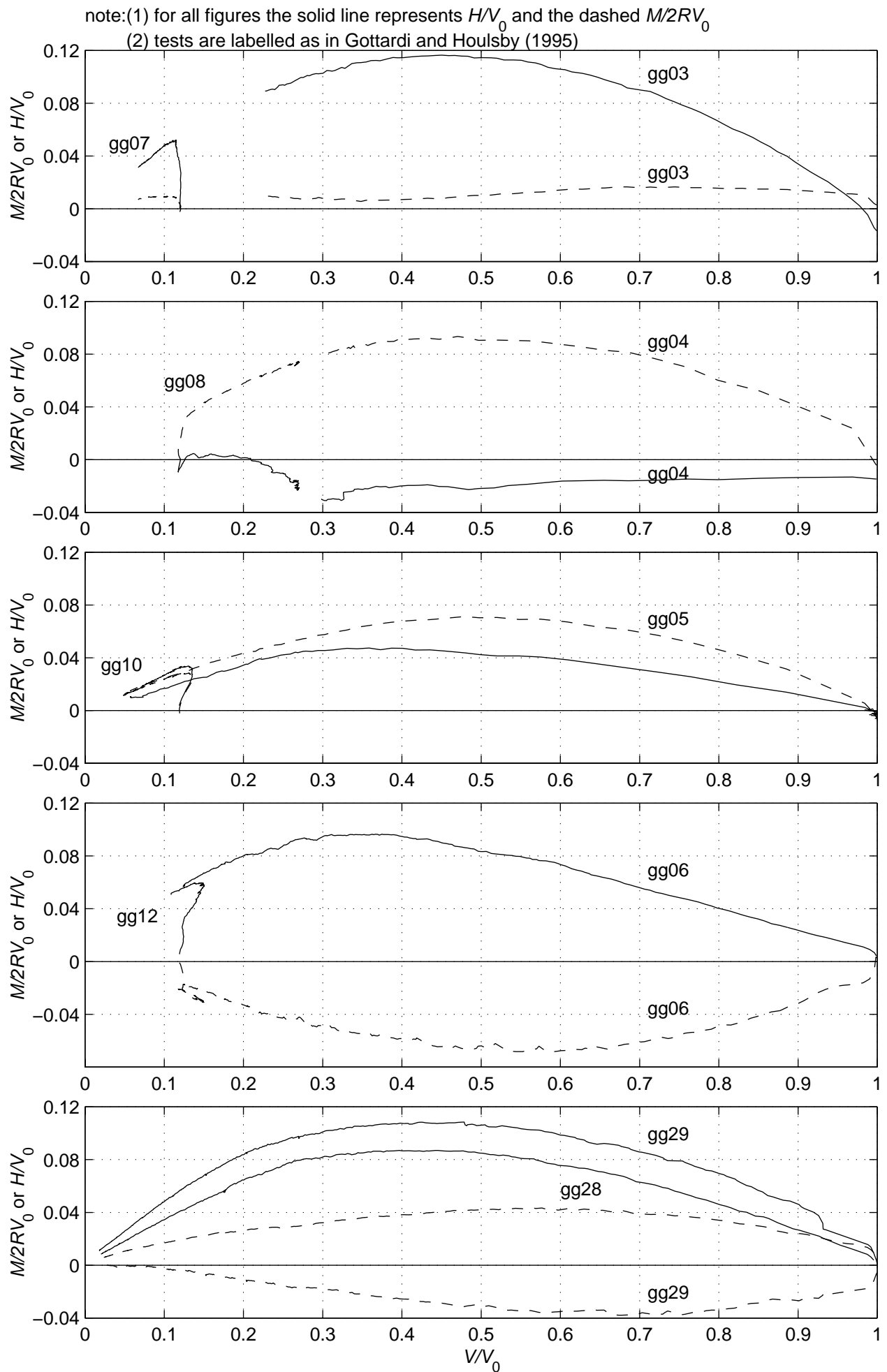


Figure 3.11 – Swipe test load paths mapped onto the deviatoric/normal plane

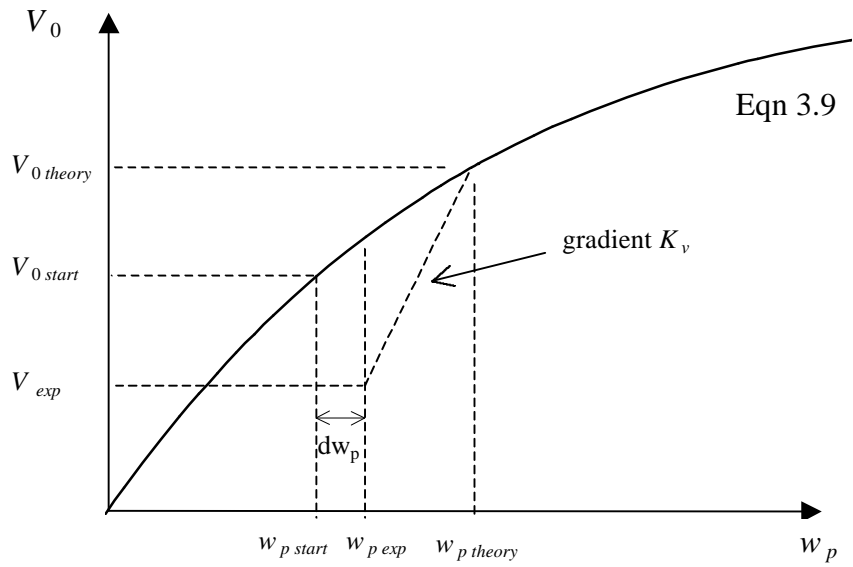


Figure 3.12 - Description of correction of V_0 in swipe tests

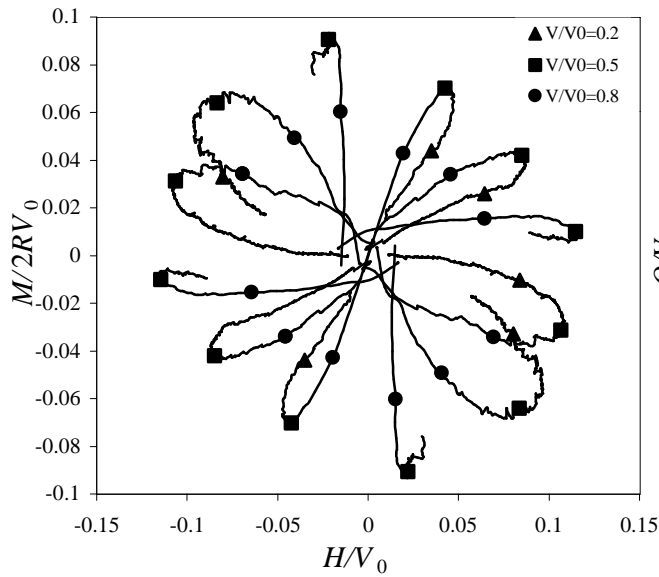


Figure 3.13 - Yield points of swipe tests in the π plane

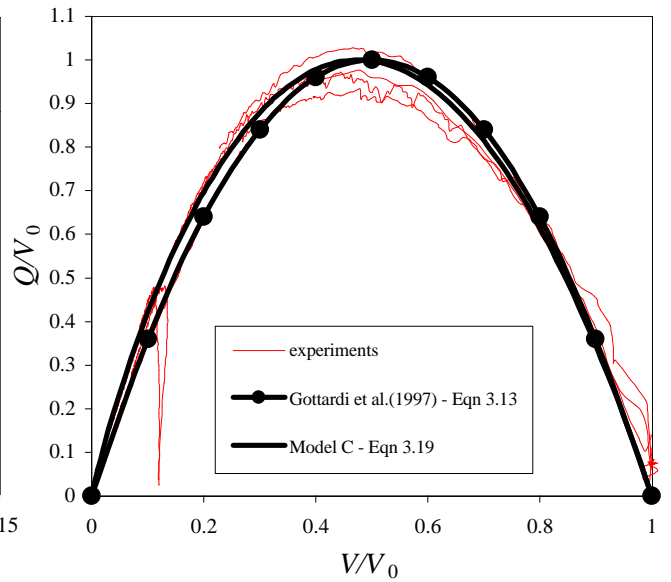


Figure 3.14 - Comparison of experimental yield points and theoretical curves

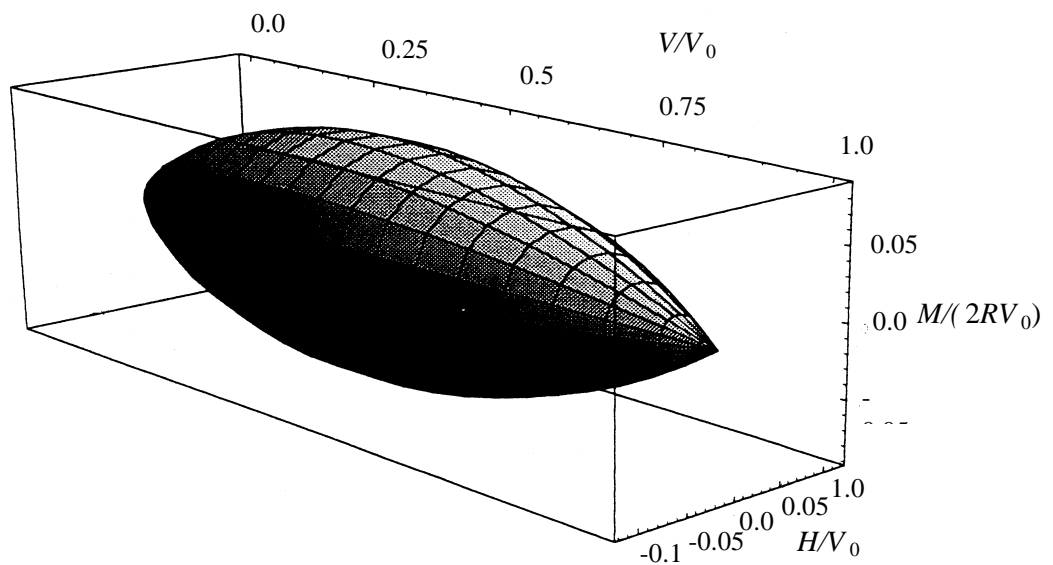


Figure 3.15 - Shape of yield surface in Model C

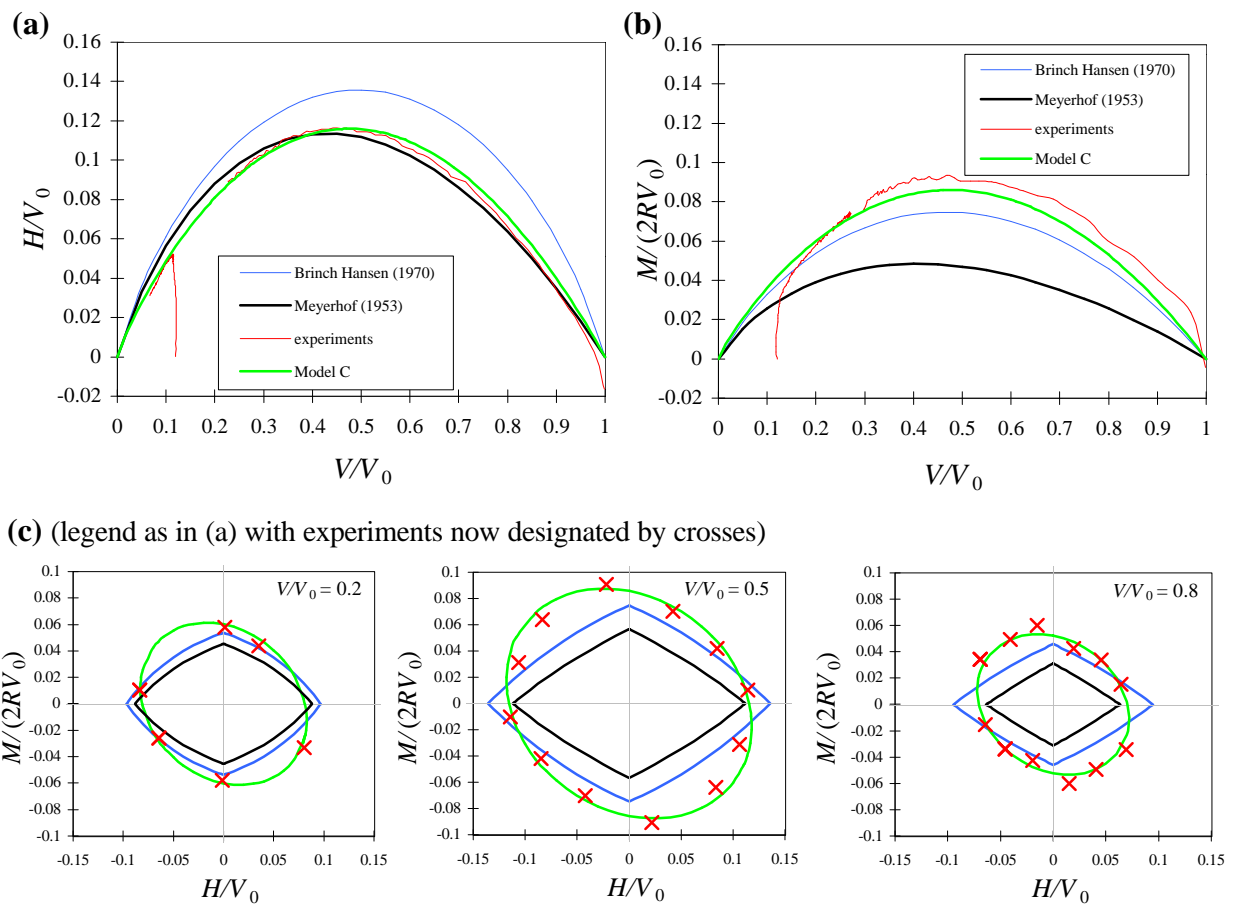


Figure 3.16 - Comparisons of the Model C yield surface with bearing capacity interaction surfaces (for $\phi = 43$)

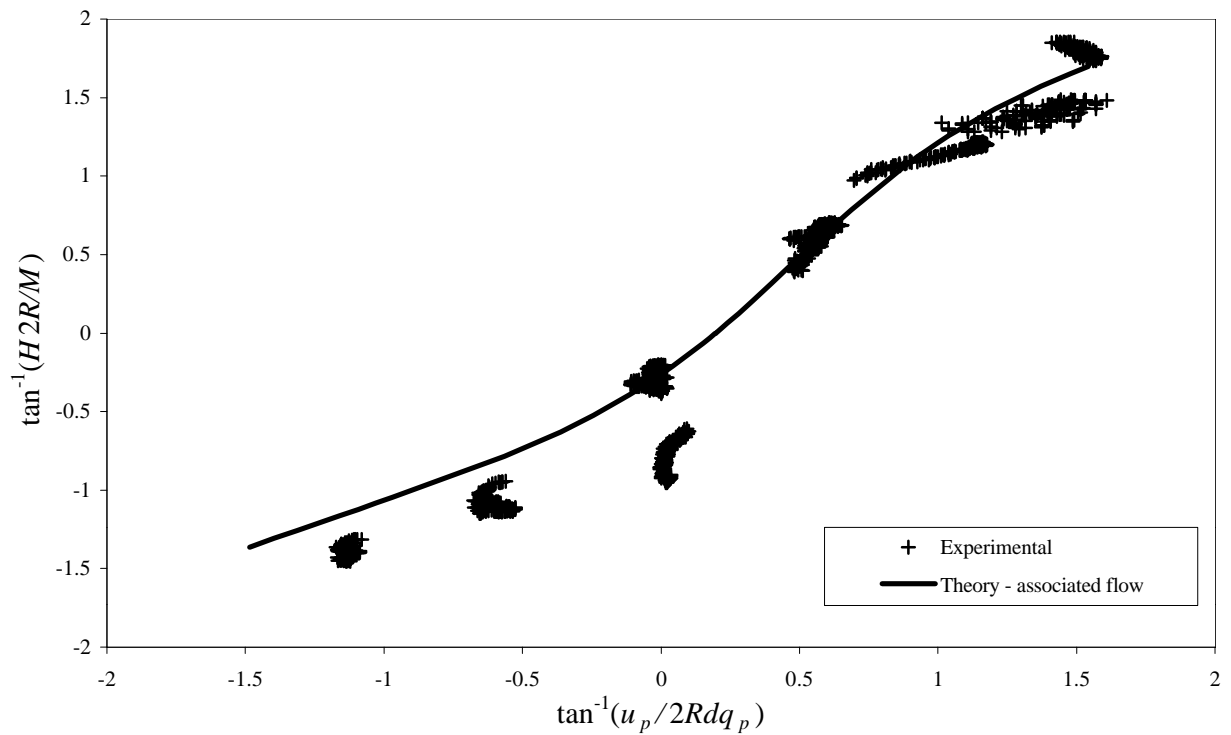


Figure 3.17 - Incremental plastic displacement ratios in the π plane

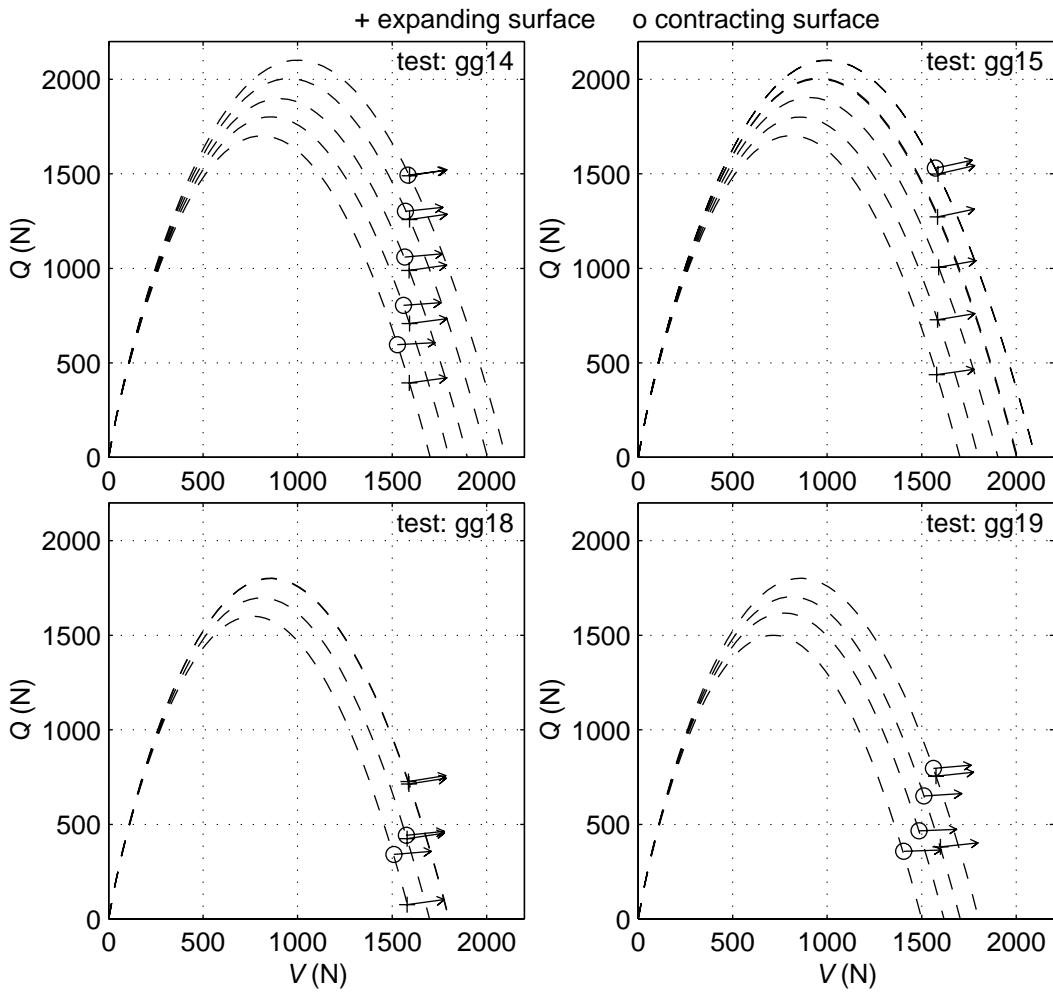


Figure 3.18 – Incremental plastic displacement directions for constant V tests

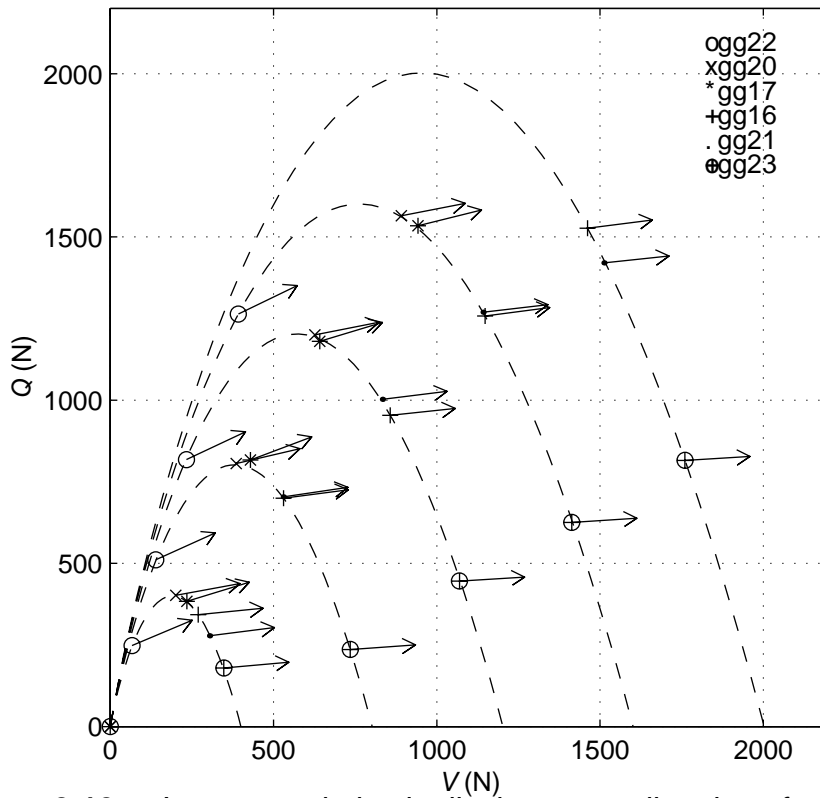


Figure 3.19 – Incremental plastic displacement directions for radial displacement tests

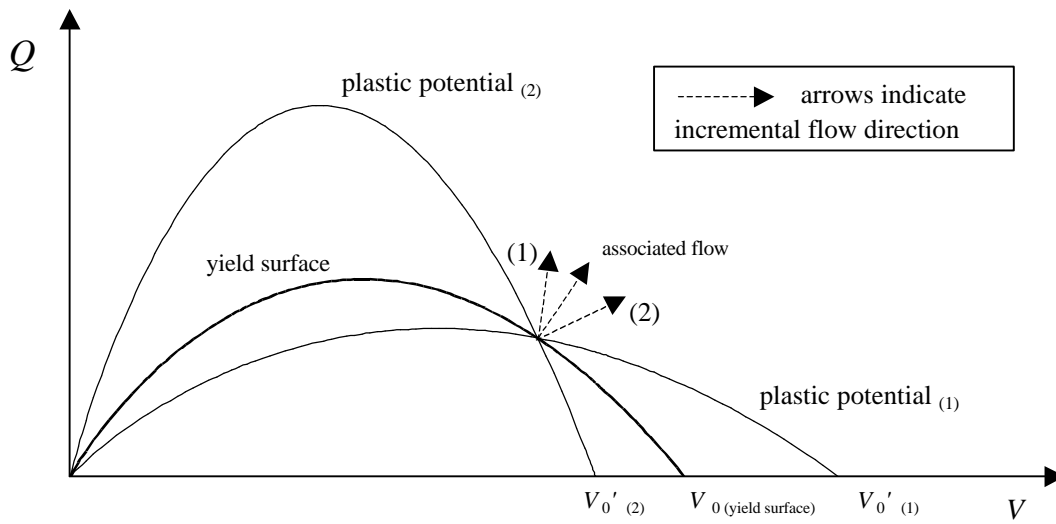


Figure 3.20 - Theoretical plastic potential shapes in the $Q:V$ plane

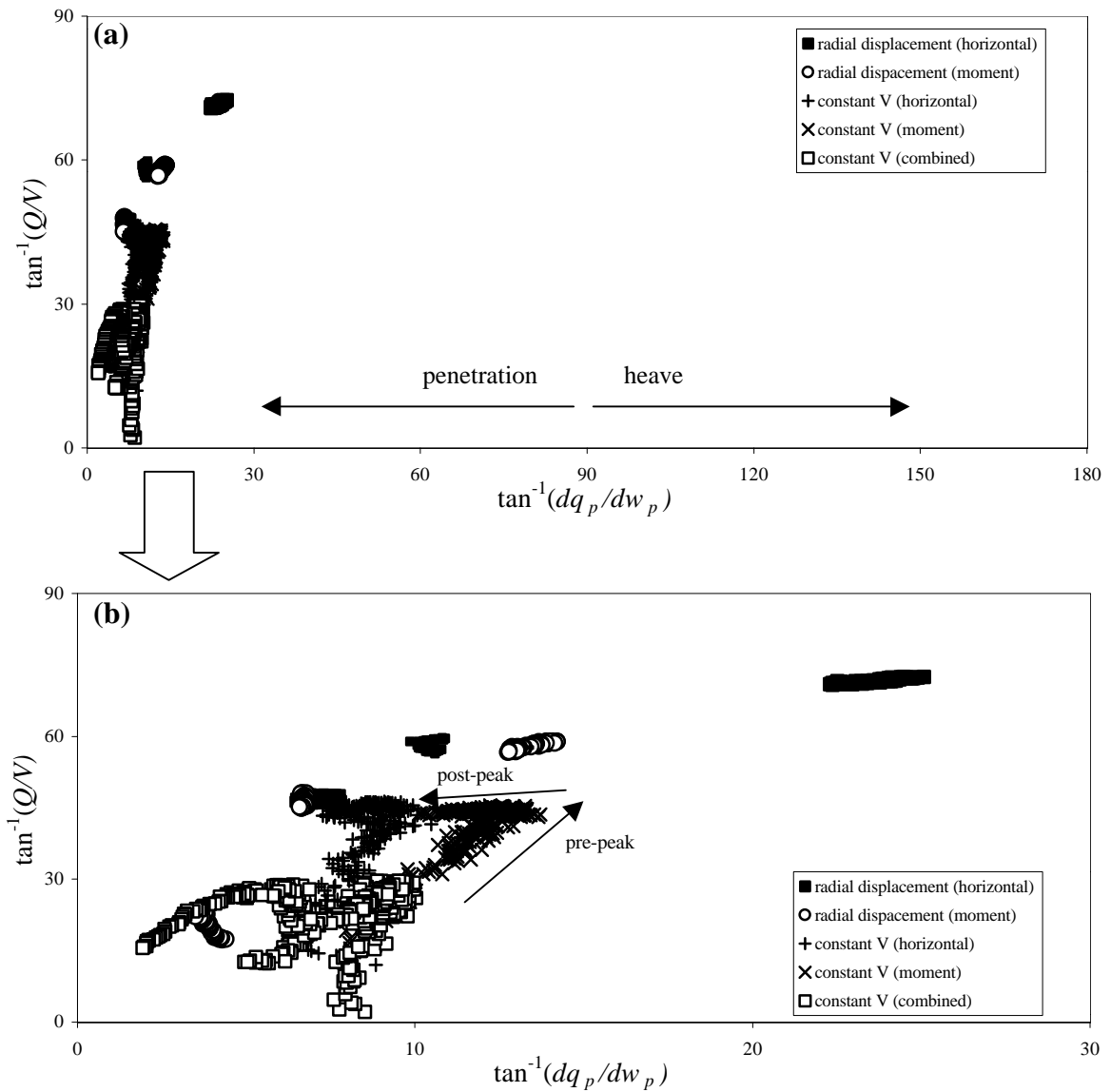


Figure 3.21 - Force ratio $\tan^{-1}(dQ/dV)$ vs displacement ratio $\tan^{-1}(dq_p/dw_p)$ for all constant V and radial displacement tests

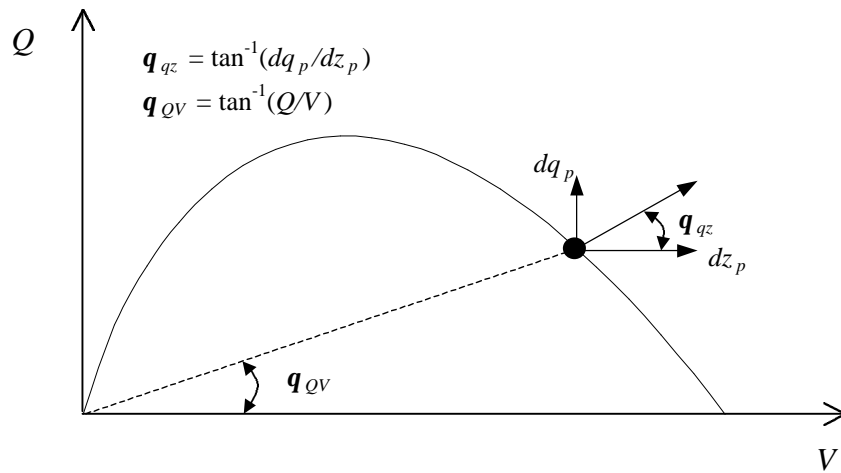


Figure 3.22 - Definition of angle of force and angle of plastic displacement ratios (q_{QV} and q_{qz} respectively)

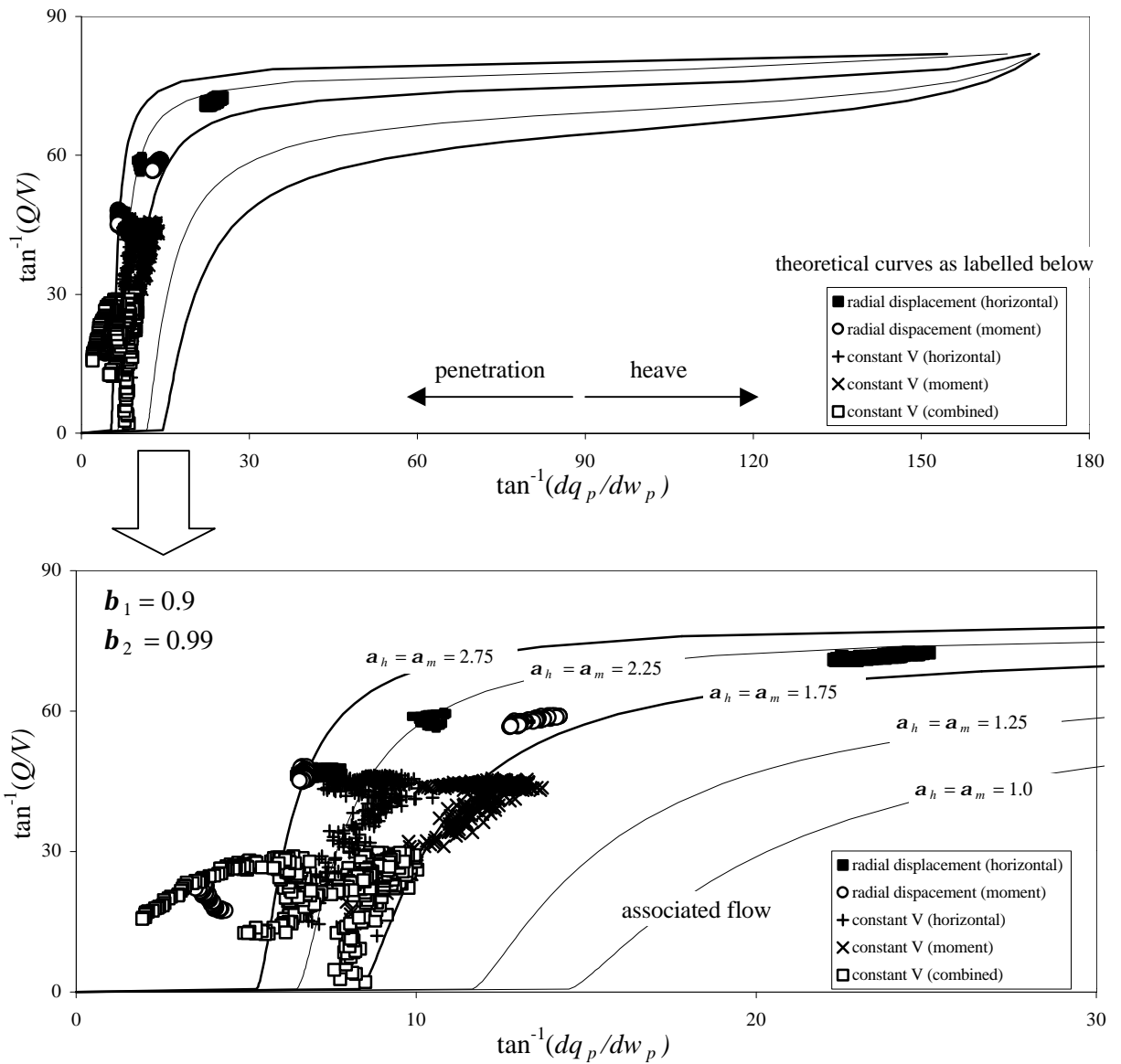


Figure 3.23 - Theoretical predictions of $\tan^{-1}(dq_p/dw_p)$ with various degrees of non-association from the yield surface

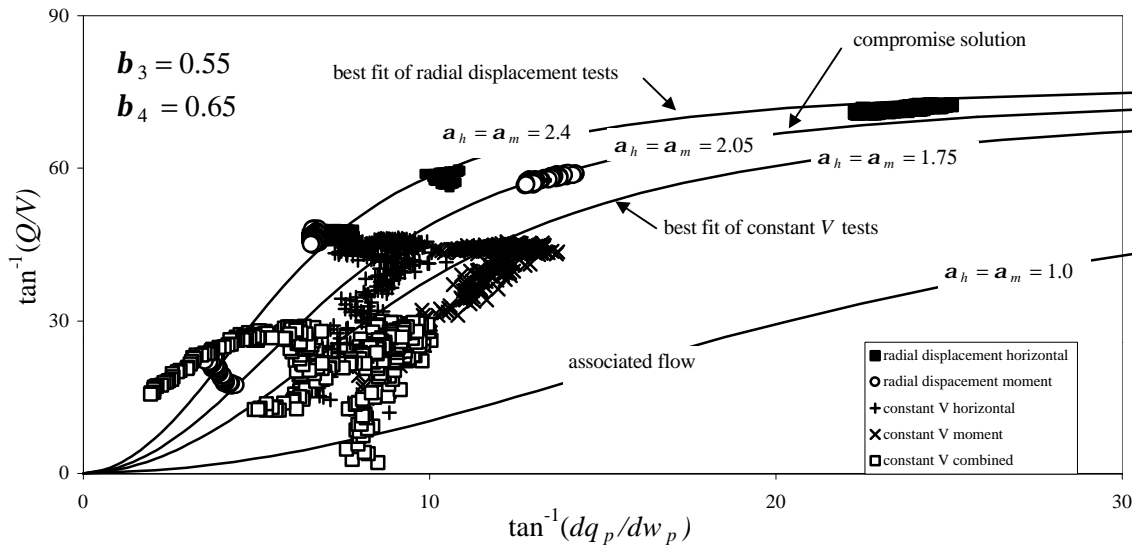


Figure 3.24 - Comparison of experimental displacement directions and theoretical predictions

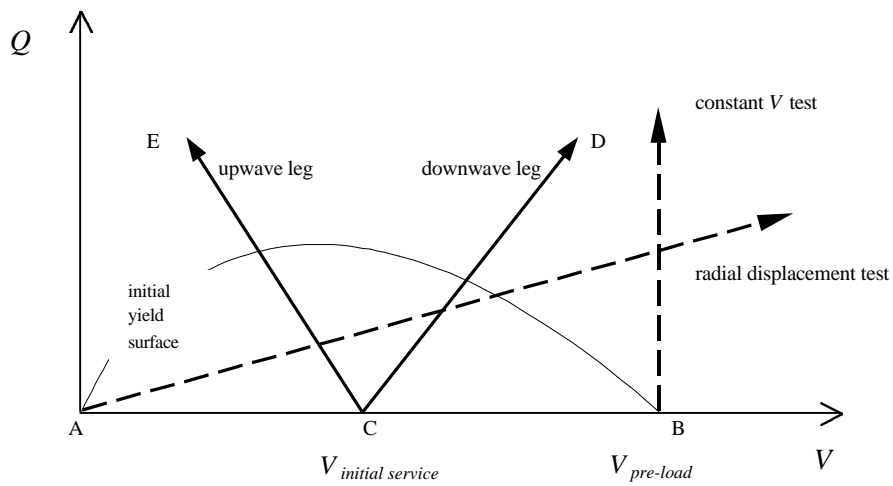


Figure 3.25 - Expected load paths of a jack-up unit in service

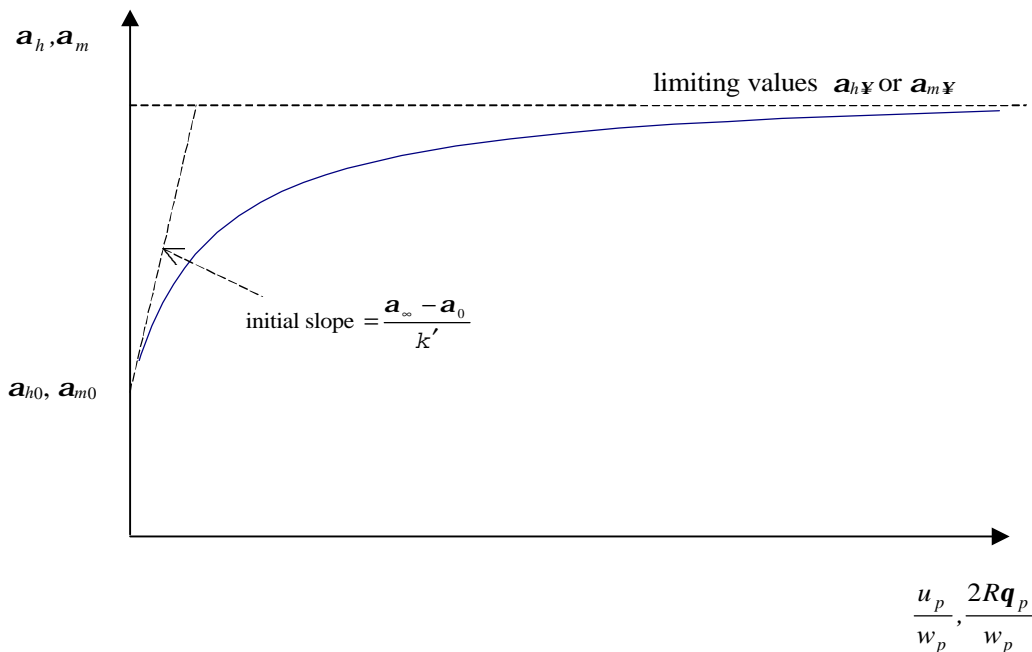
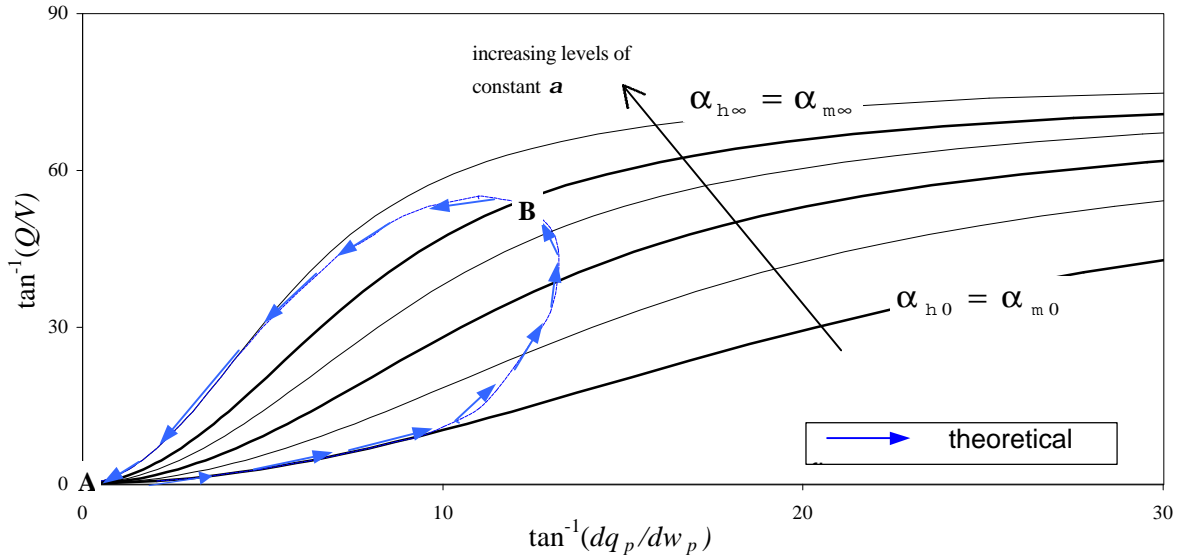


Figure 3.26 - Variation of association factors

(a) Constant V tests



(b) Radial displacement tests

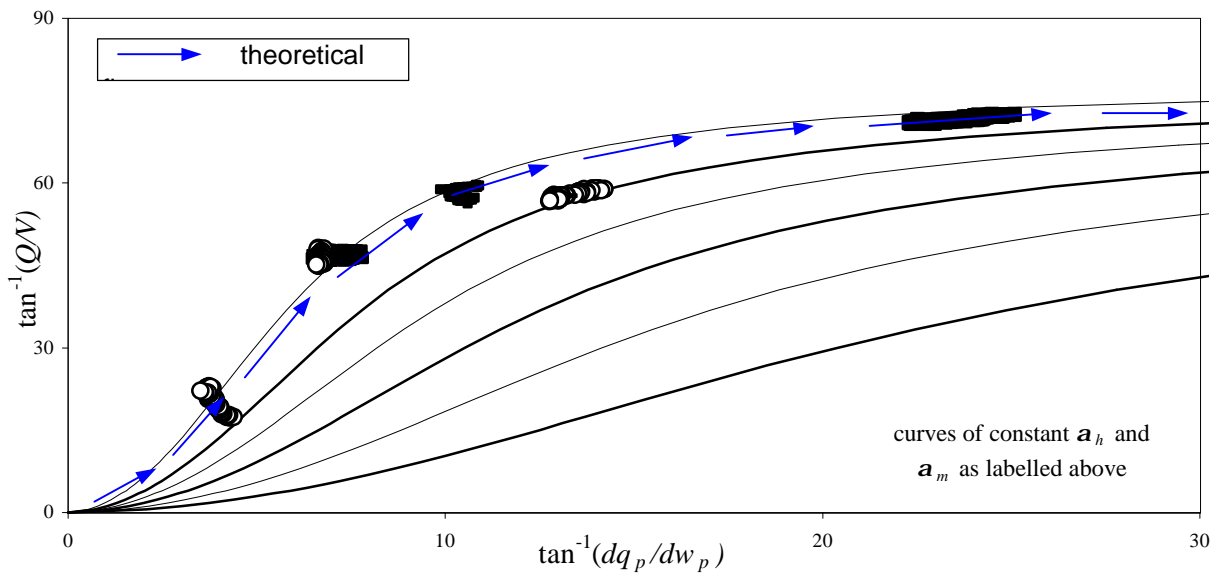


Figure 3.27 - Theoretical concept of modelling experiments with varying association factors

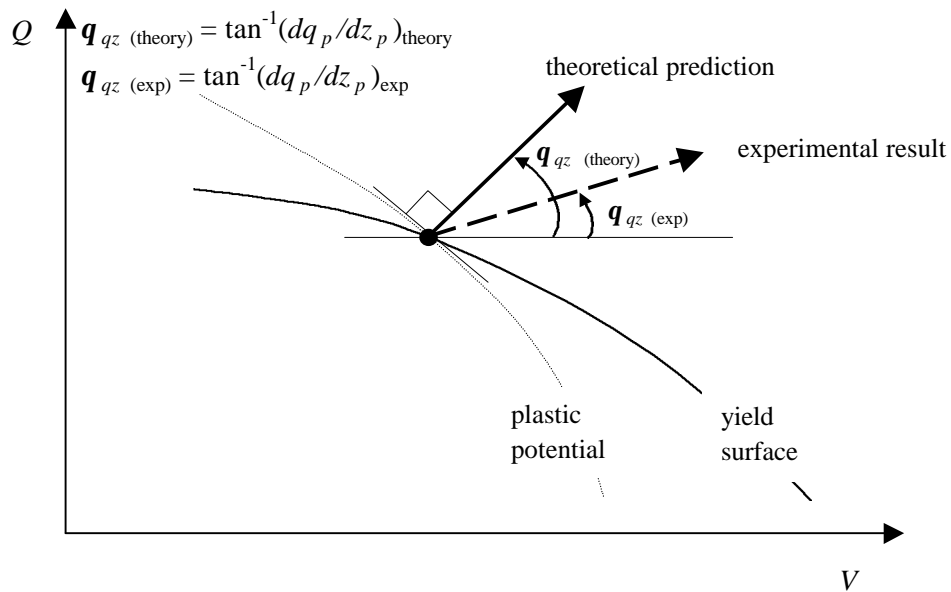


Figure 3.28 - Definition of the experimental and theoretical angular plastic displacement in the deviatoric/normal plane

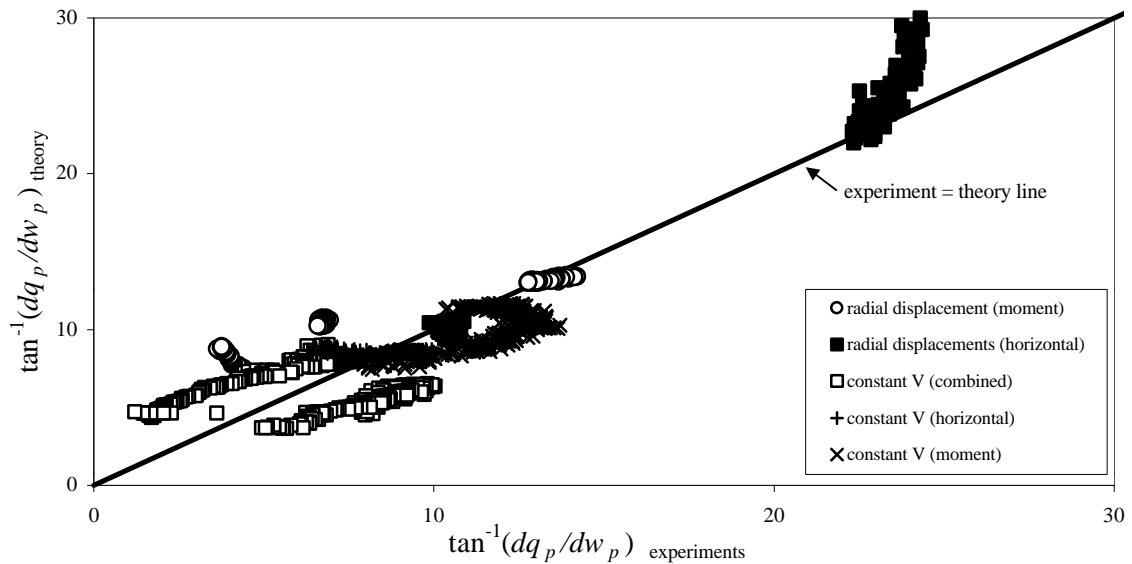


Figure 3.29 - Comparison of theoretical and experimental plastic displacement directions

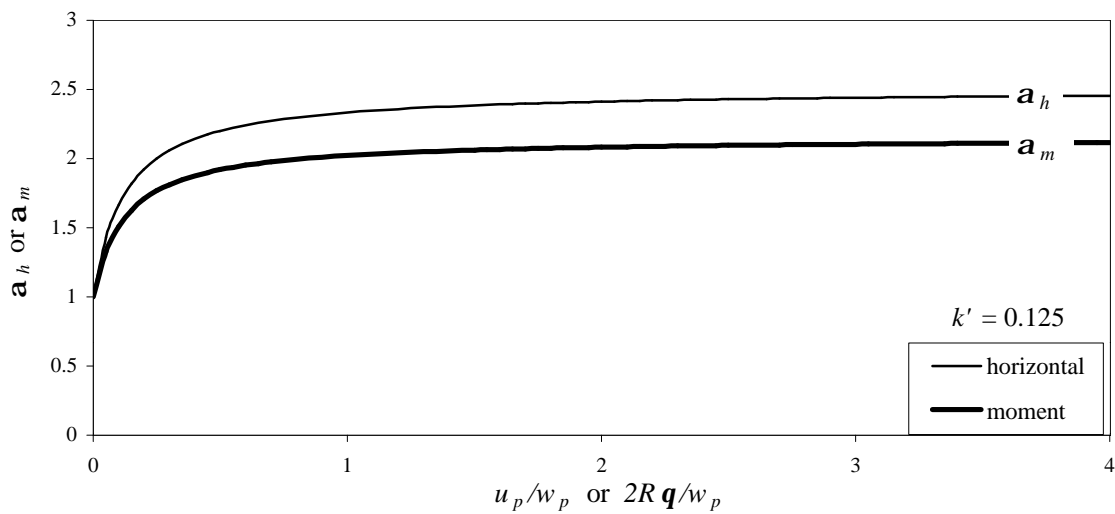


Figure 3.30 - Rates of variation of a_h and a_m

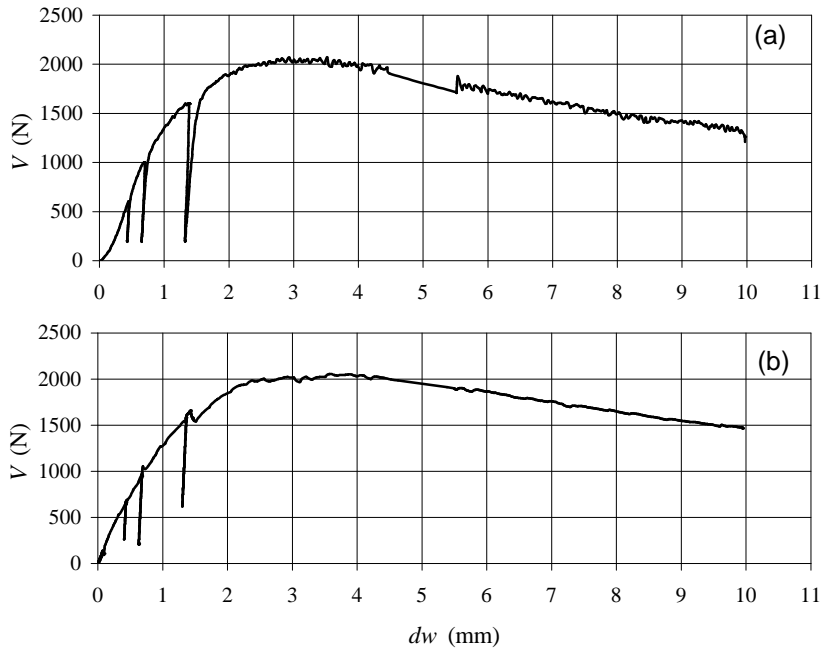


Figure 4.1 - Retrospective simulation of vertical penetration test

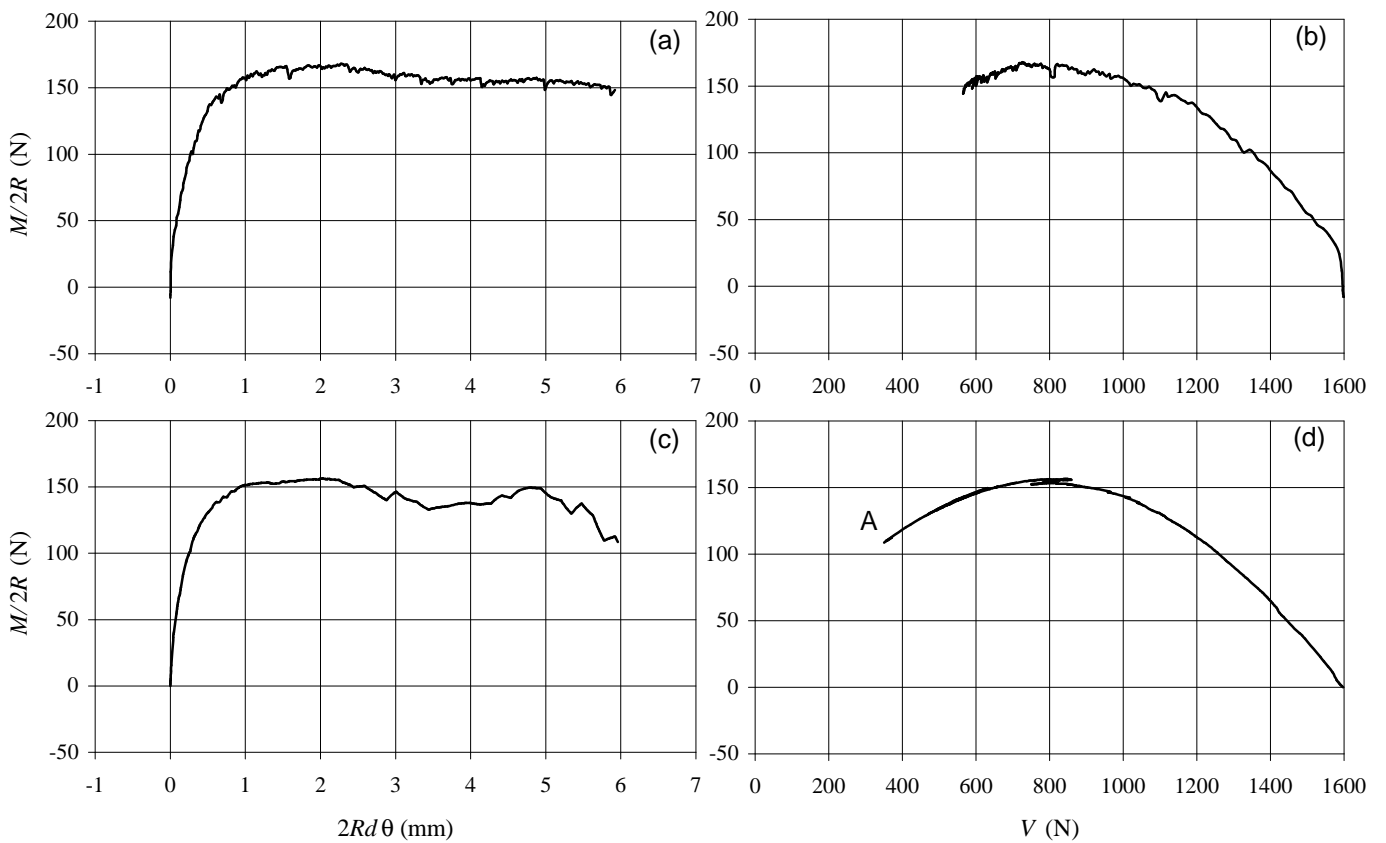


Figure 4.2 - Retrospective simulation of moment swipe test

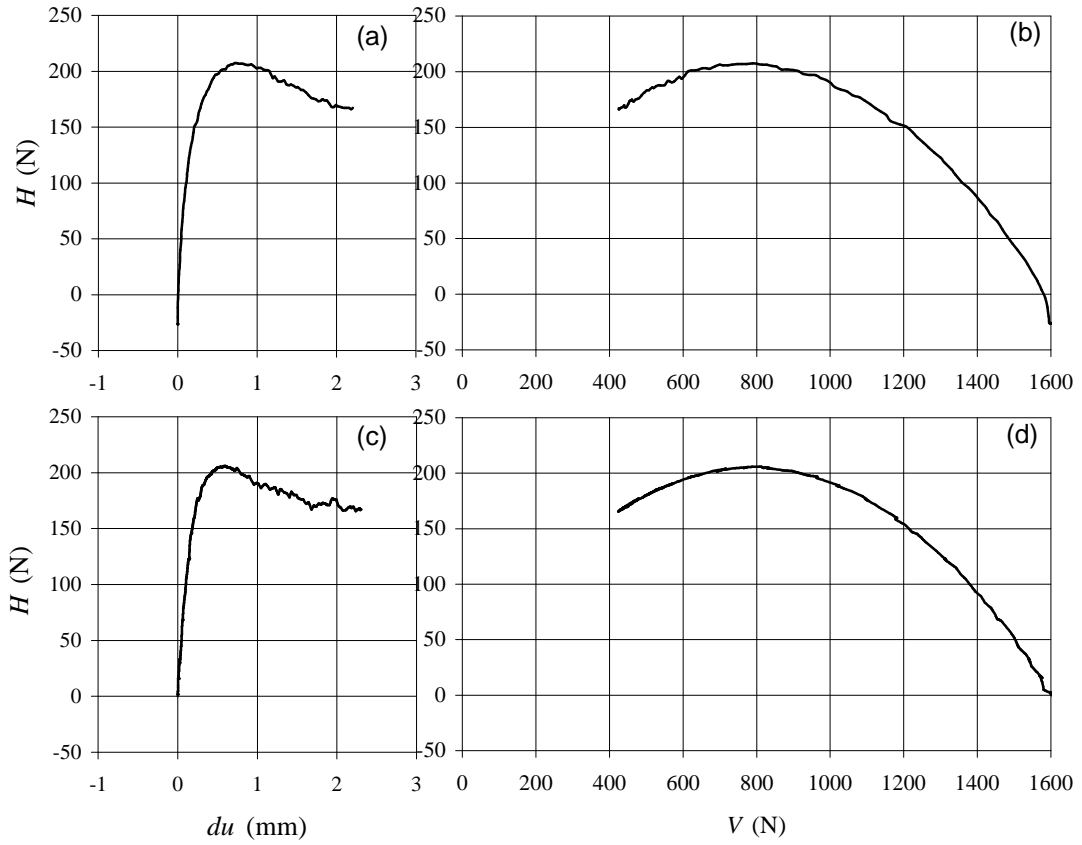


Figure 4.3 - Retrospective simulation of horizontal swipe test

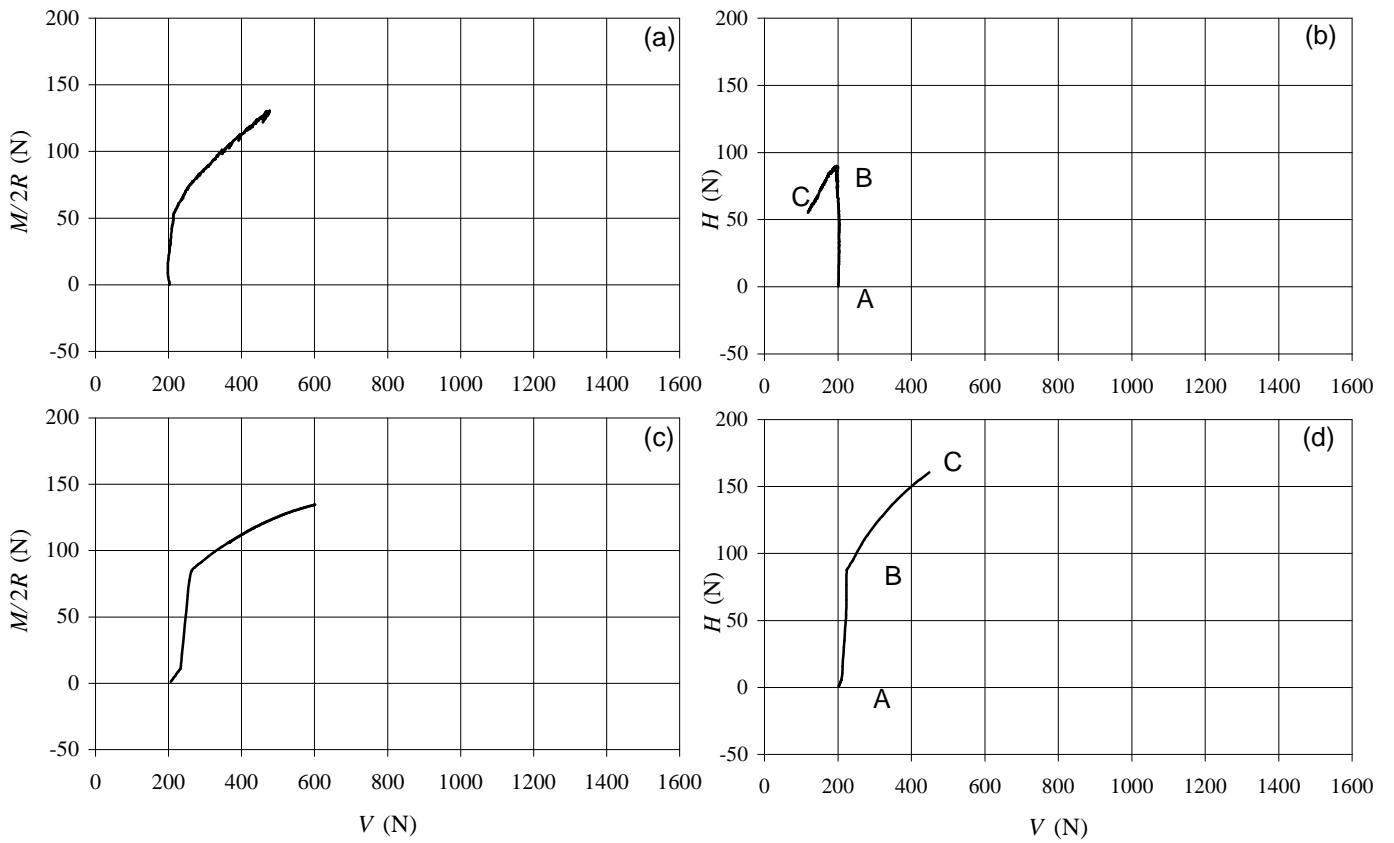


Figure 4.4 - Retrospective simulation of swipe test from $V =$

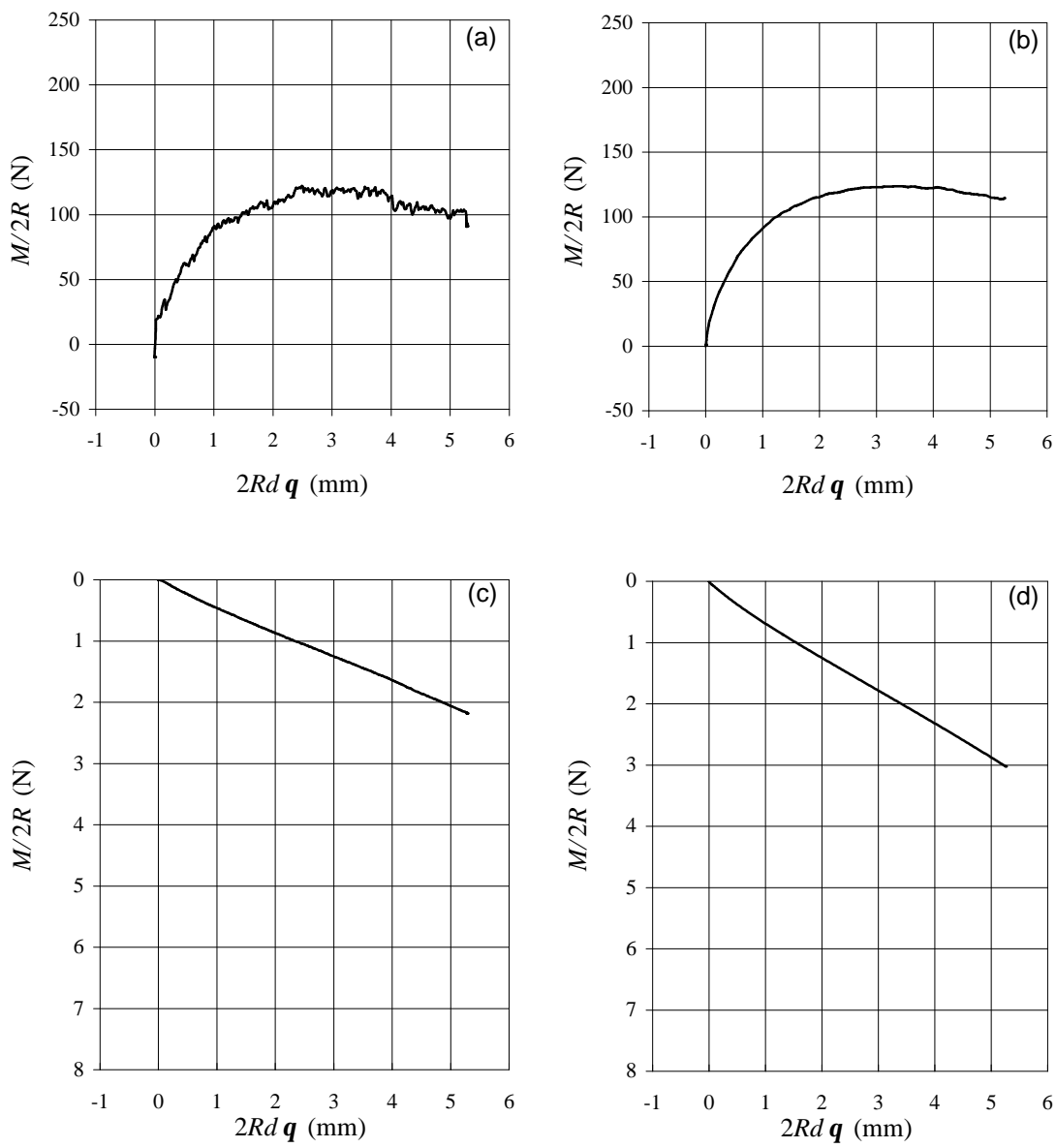


Figure 4.5 - Retrospective simulation of constant V test

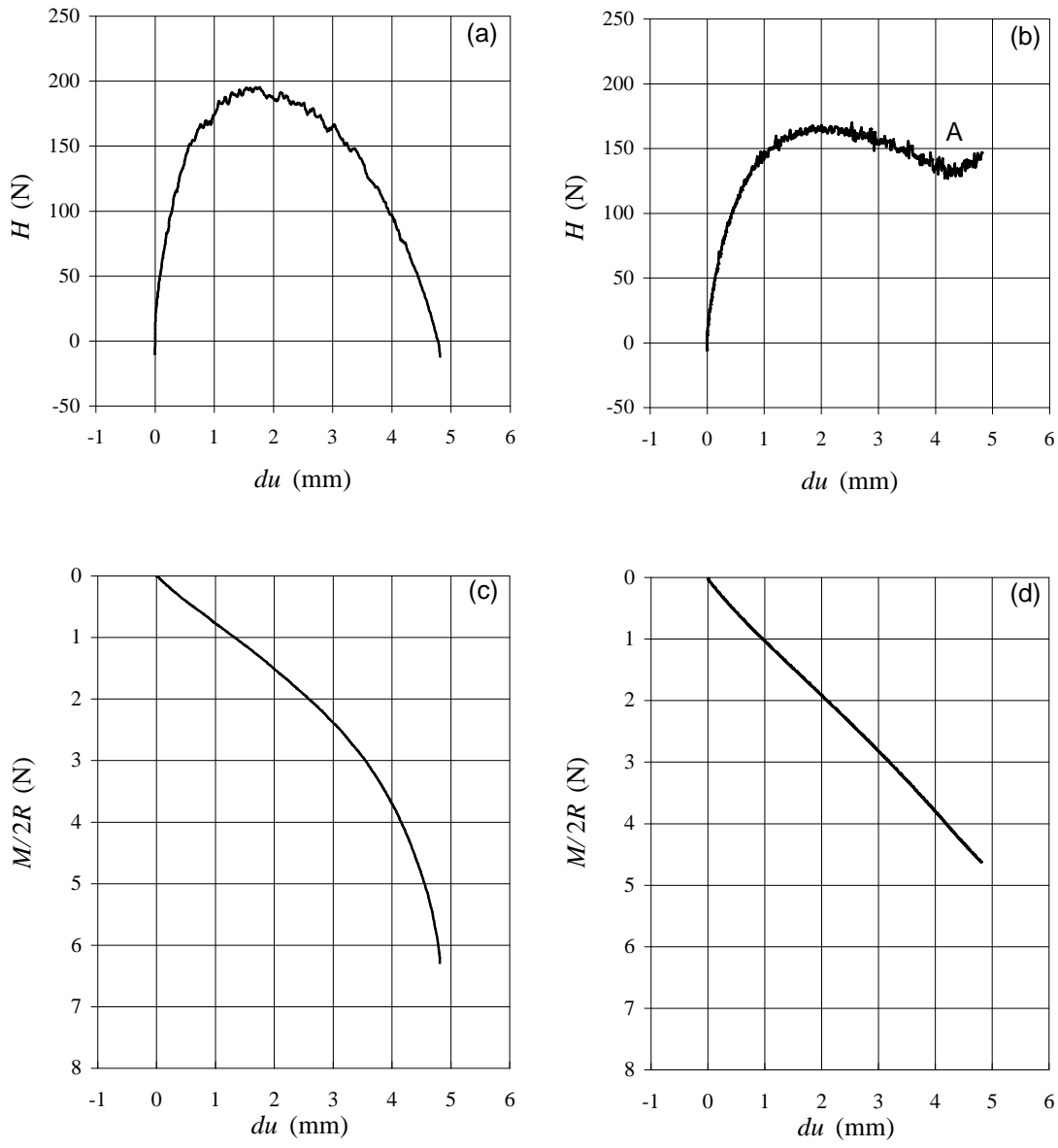


Figure 4.6 - Retrospective simulation of constant V test

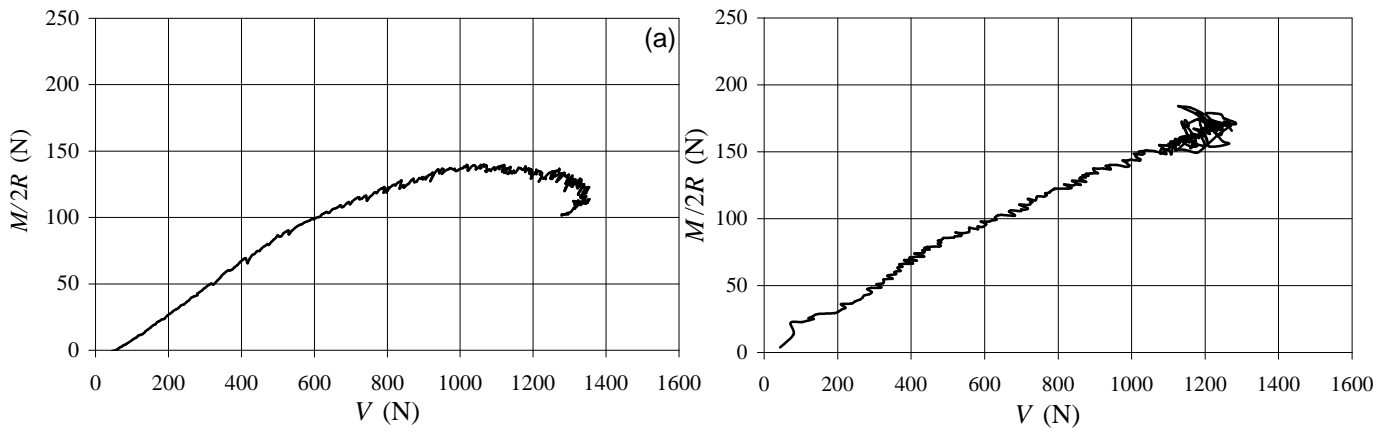


Figure 4.7 - Retrospective simulation of radial displacement test

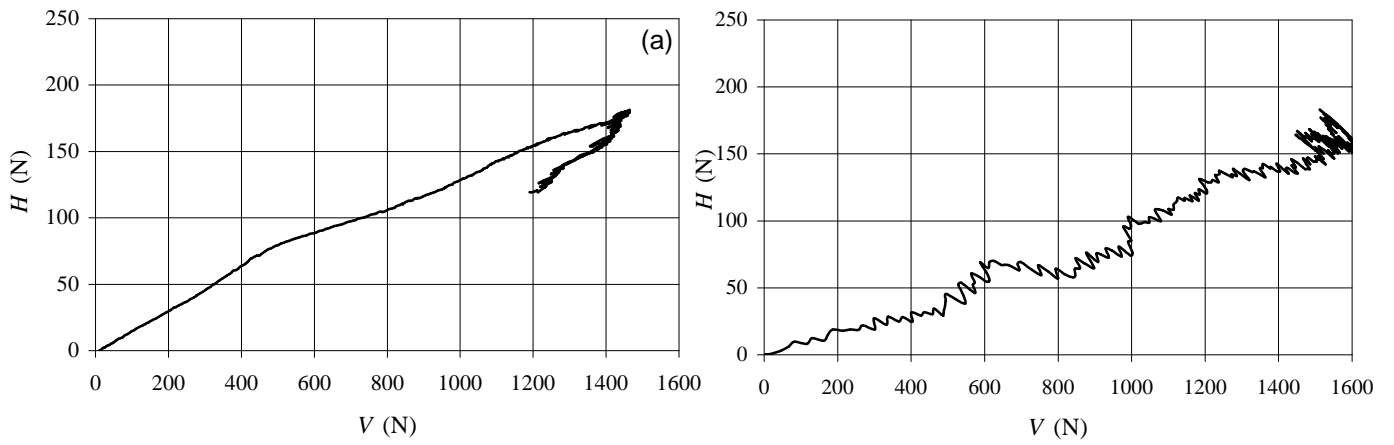


Figure 4.8 - Retrospective simulation of radial displacement test

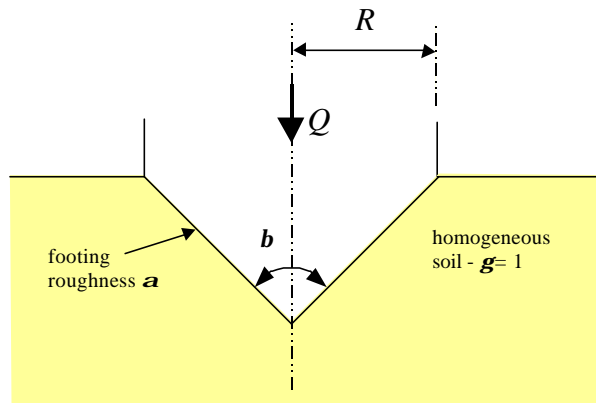


Figure 4.9 - Problem definition and notation

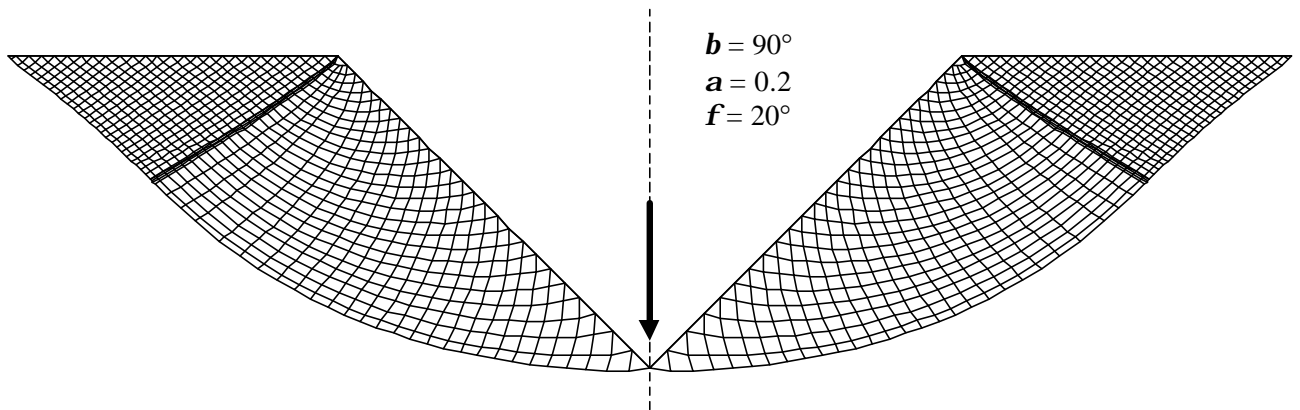


Figure 4.10 - Example general shear failure mechanism generated by program FIELD5

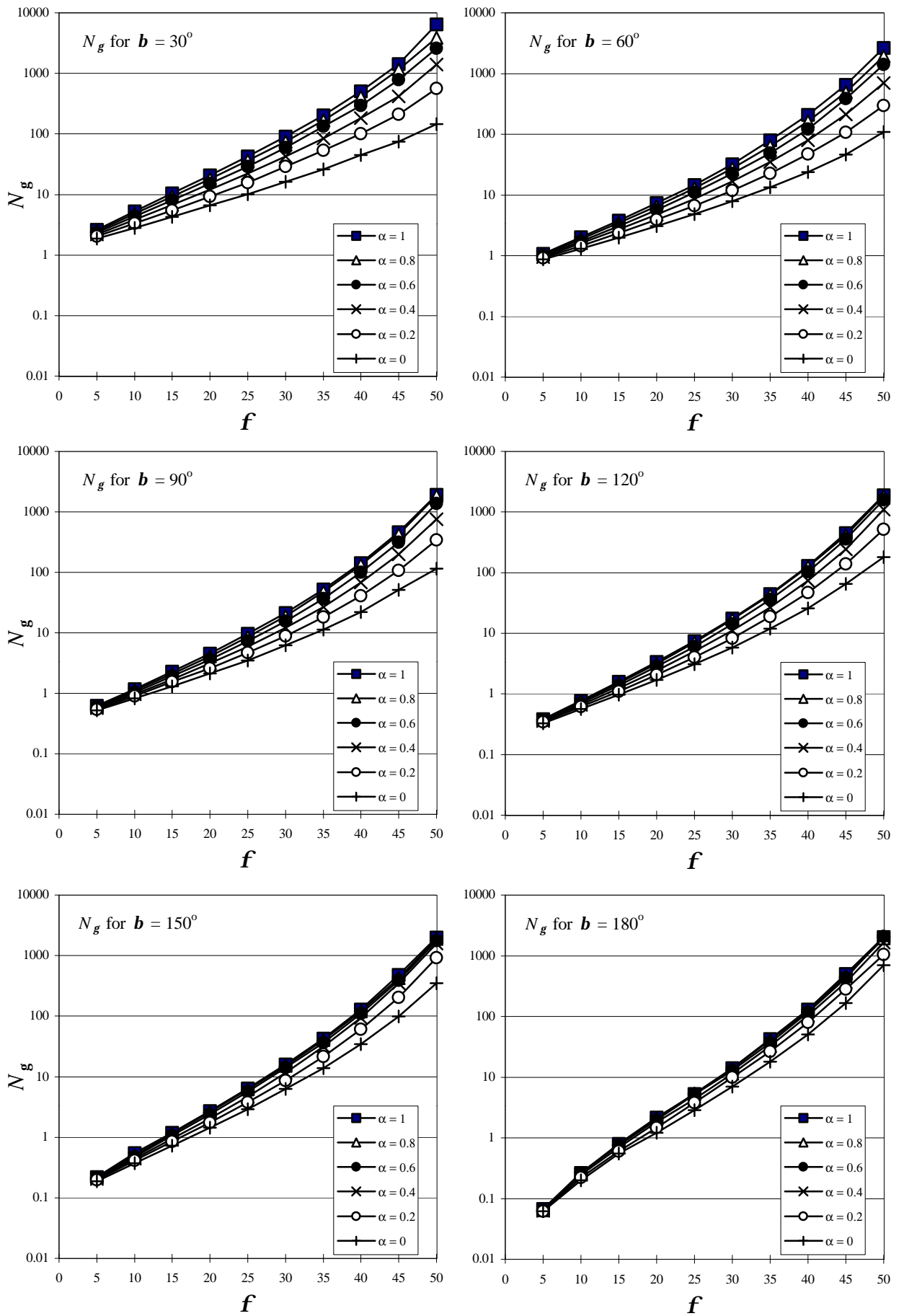


Figure 4.11 - Bearing capacity factors (N_g)

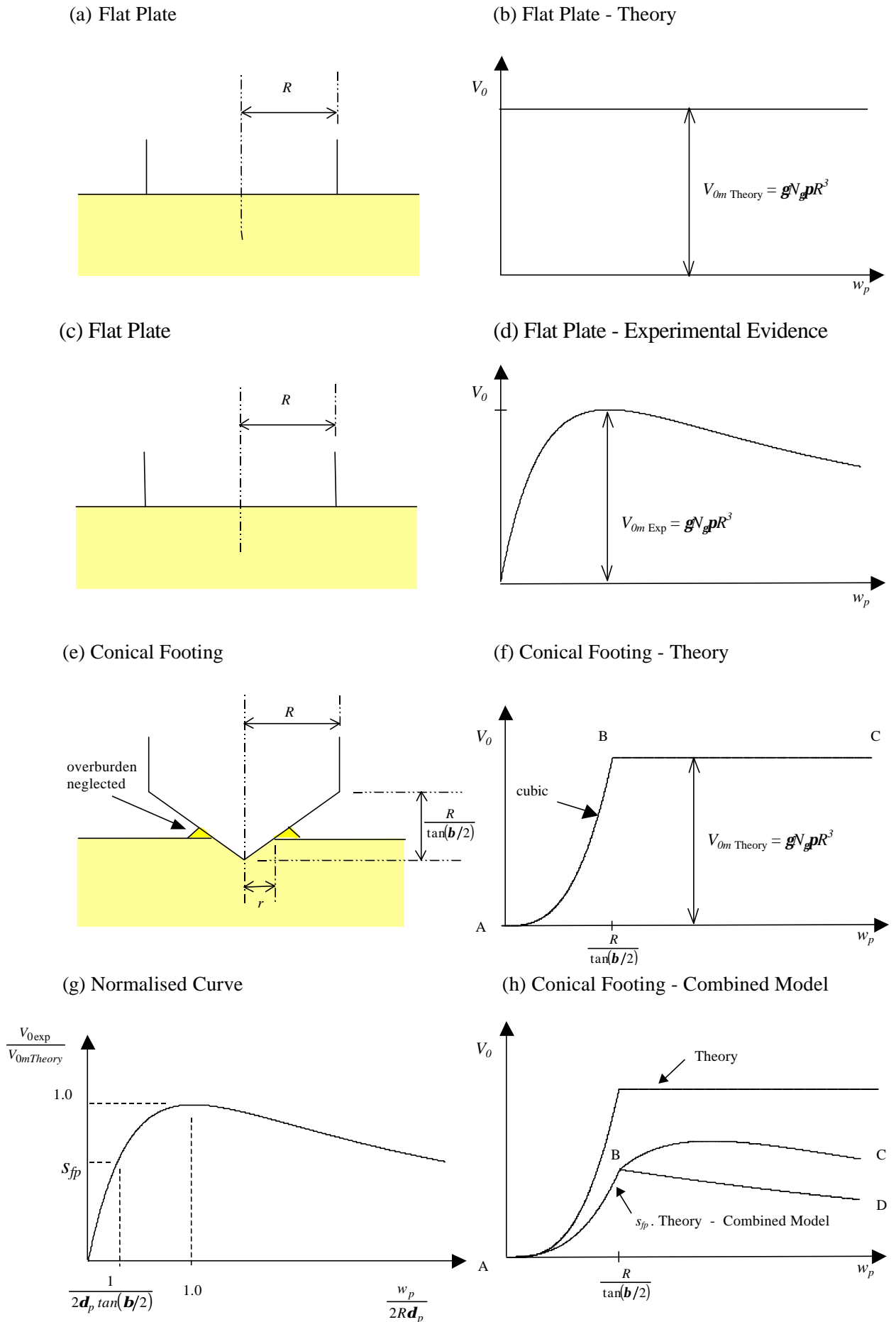


Figure 4.12 - Adaptation of Model C for conical shape of spudcans

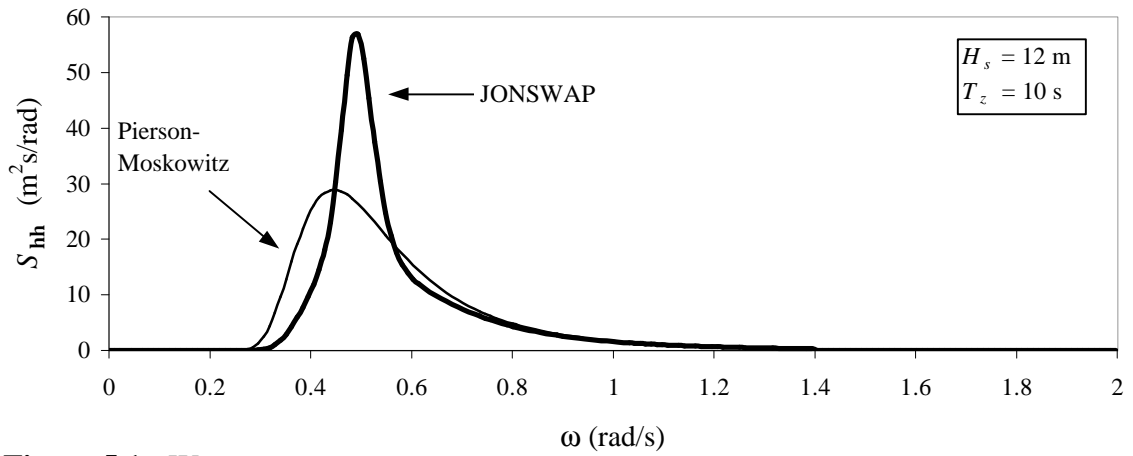


Figure 5.1 - Wave energy spectrum

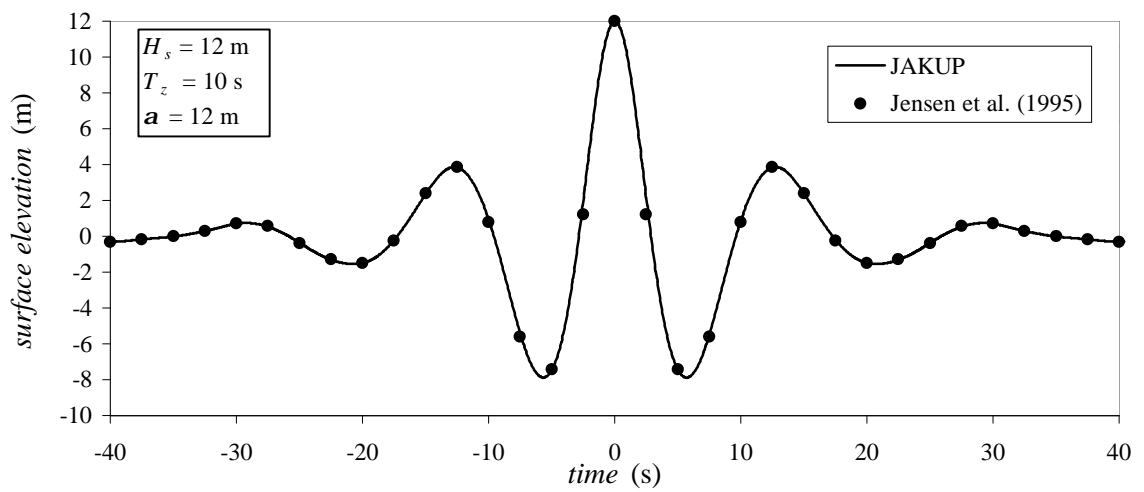


Figure 5.2 - NewWave surface elevations evaluated by JAKUP

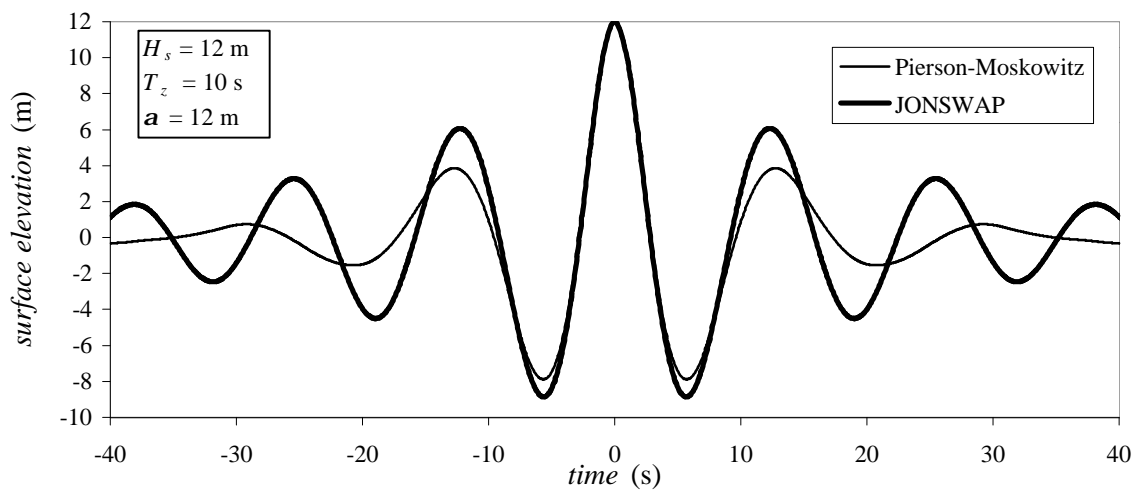


Figure 5.3 - NewWave surface elevations for the Pierson-Moskowitz and JONSWAP spectrum

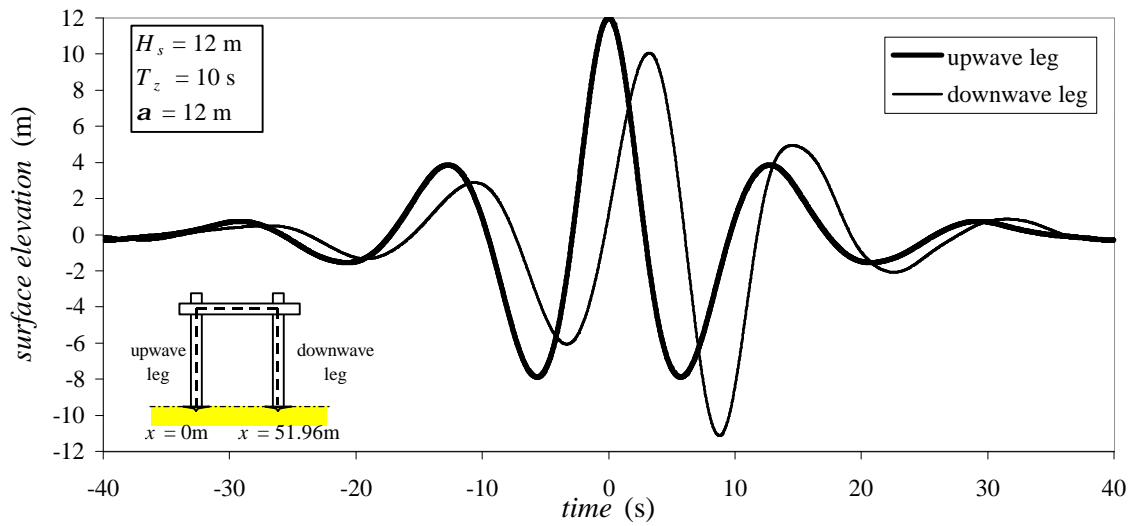


Figure 5.4 - NewWave surface elevations at $x = 0$ m (upwave leg) and $x = 51.96$ m (downwave leg)

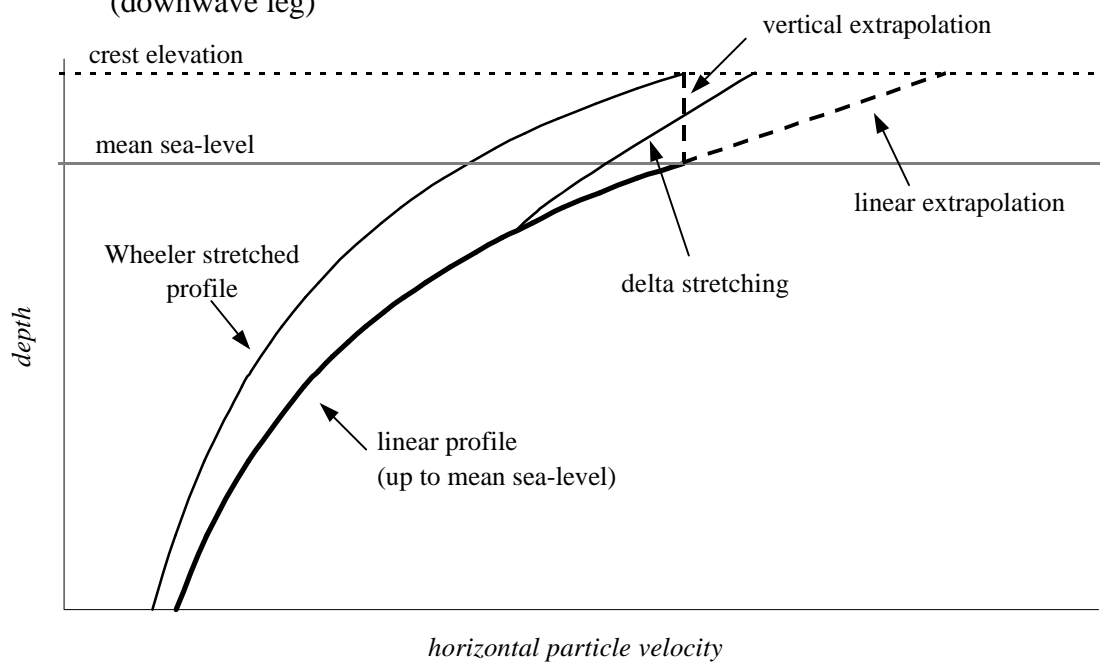


Figure 5.5 - Commonly used stretching and extrapolation procedures in linear theory

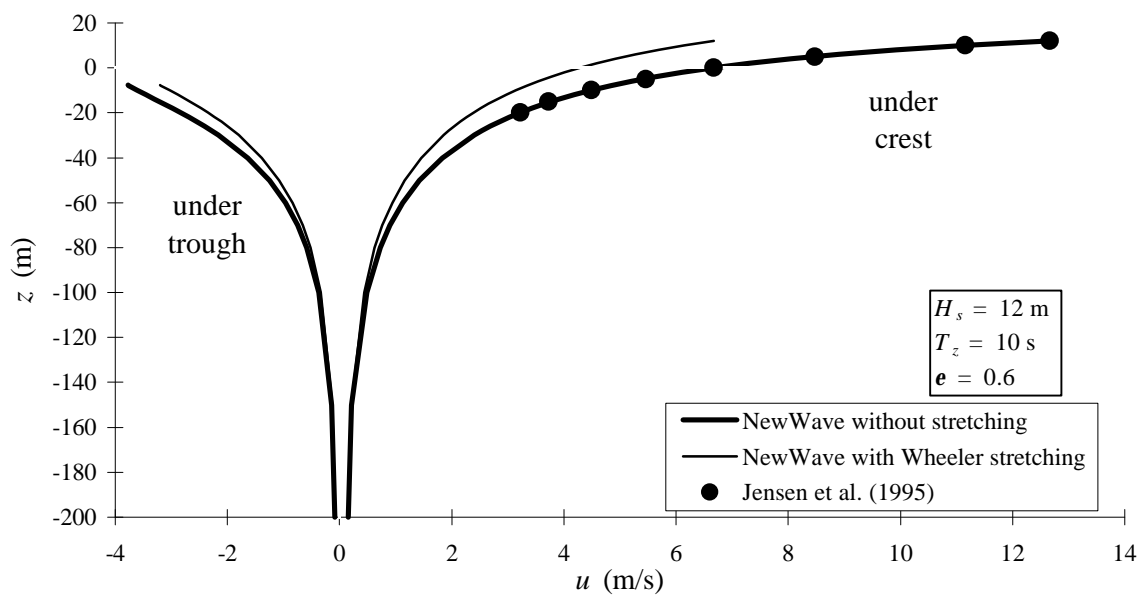


Figure 5.6 - Horizontal wave particle velocities evaluated by JAKUP

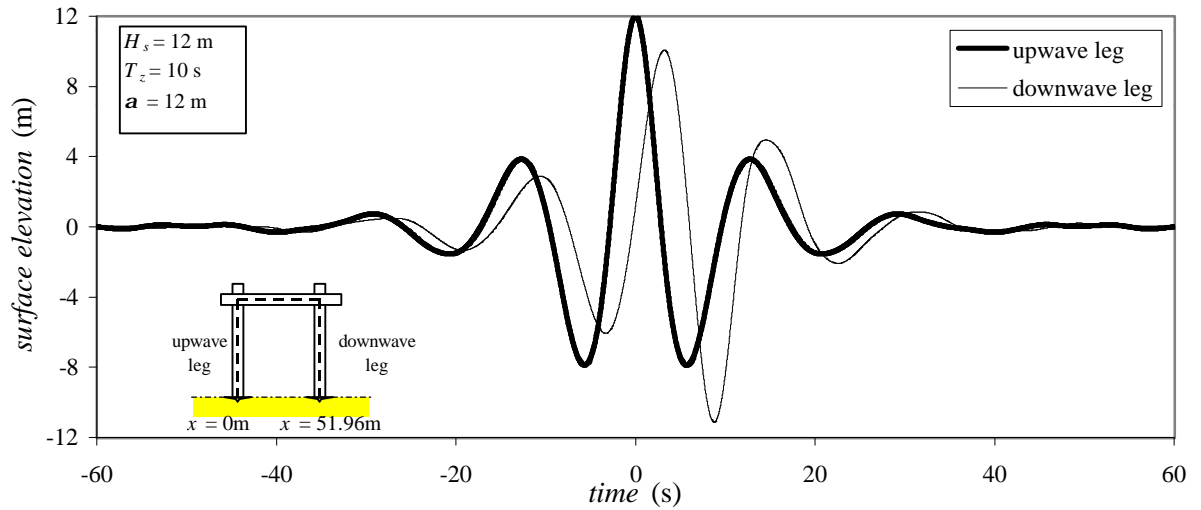


Figure 5.7 - NewWave surface elevation at the upwave and downwave legs

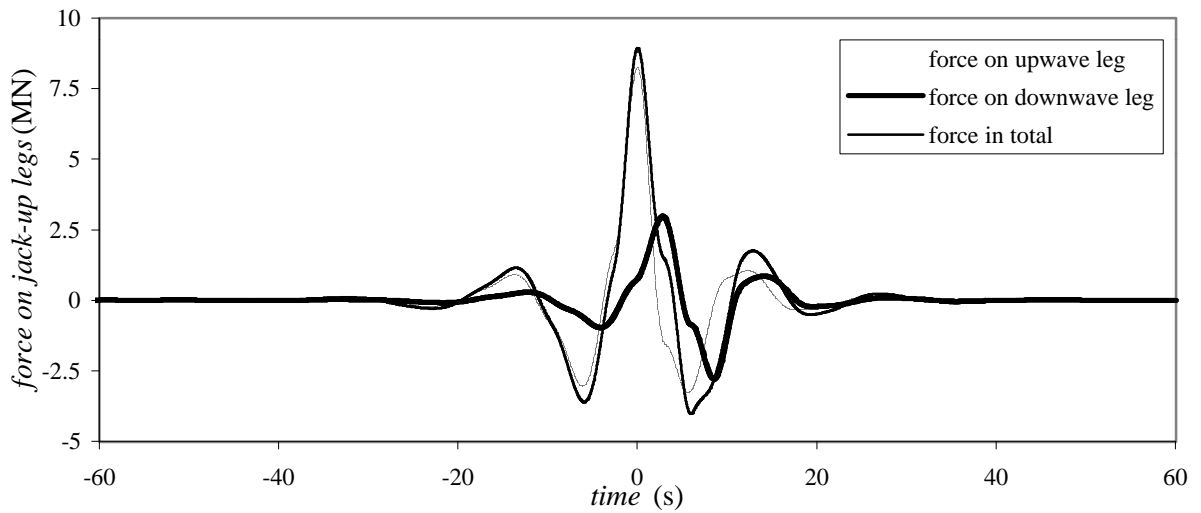


Figure 5.8 - Horizontal force on the jack-up's legs due to the NewWave loading

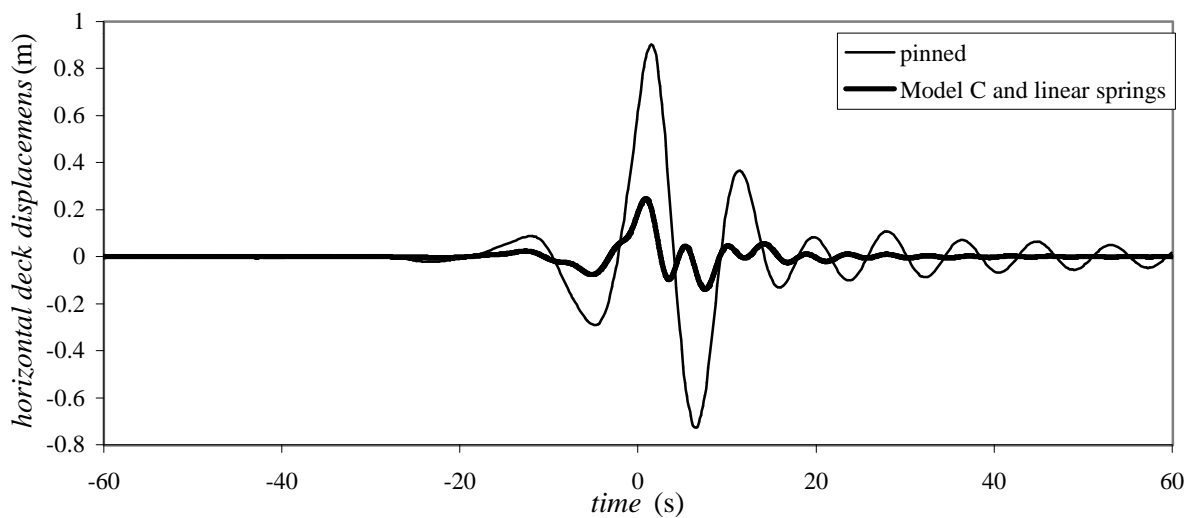


Figure 5.9 - Horizontal deck displacements due to the NewWave loading

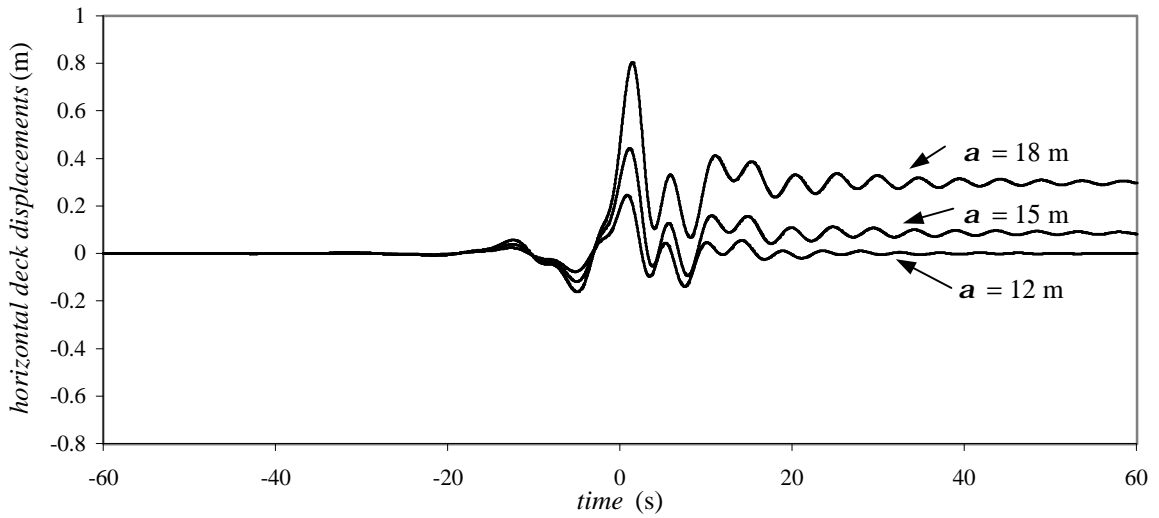


Figure 5.10 - Horizontal deck displacements due to increasing amplitude NewWaves

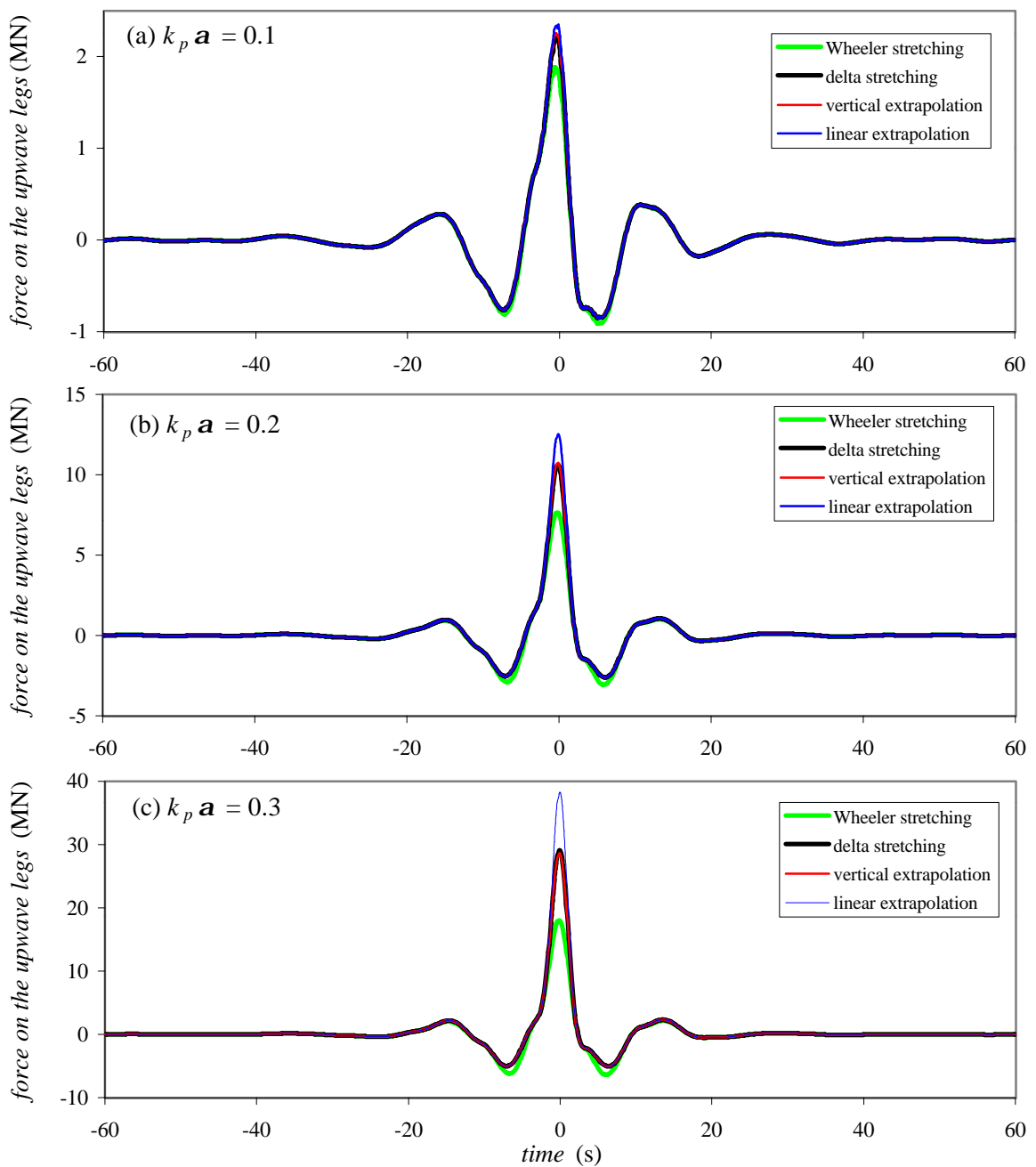


Figure 5.11 - Force on the upwave leg for different stretching/extrapolation assumptions

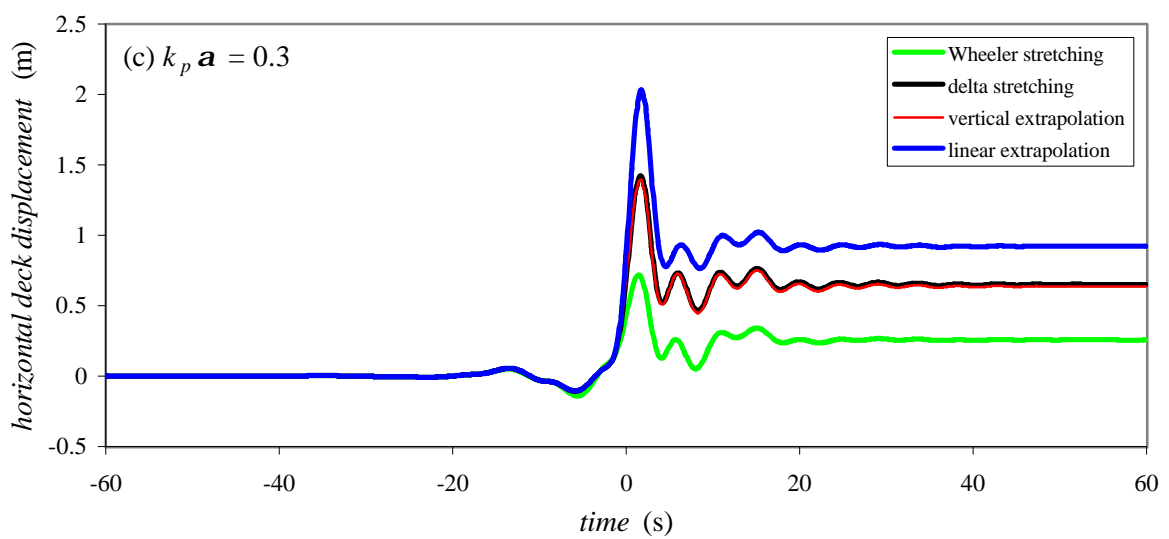
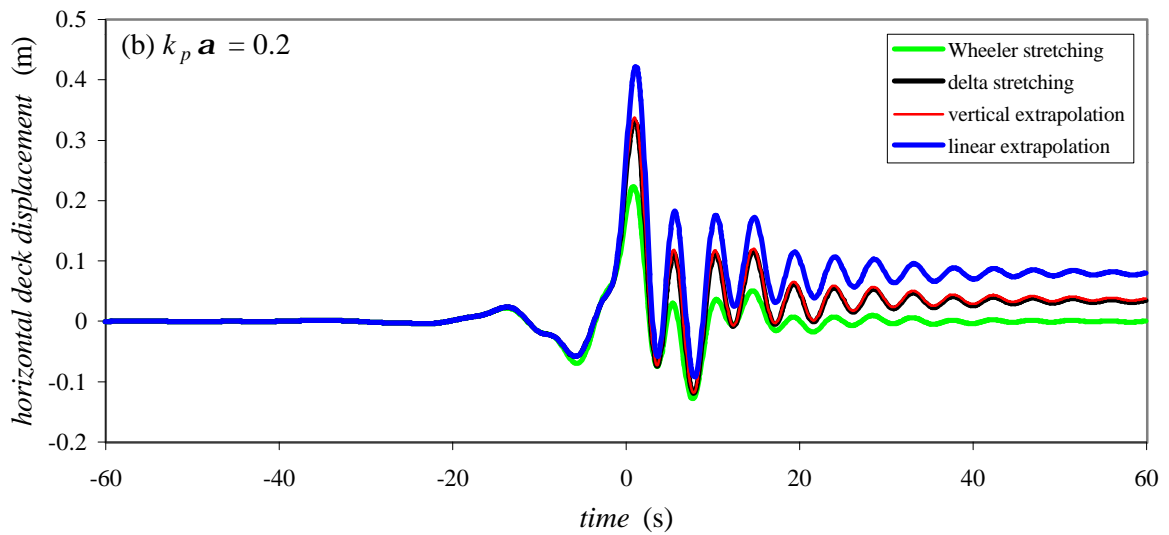
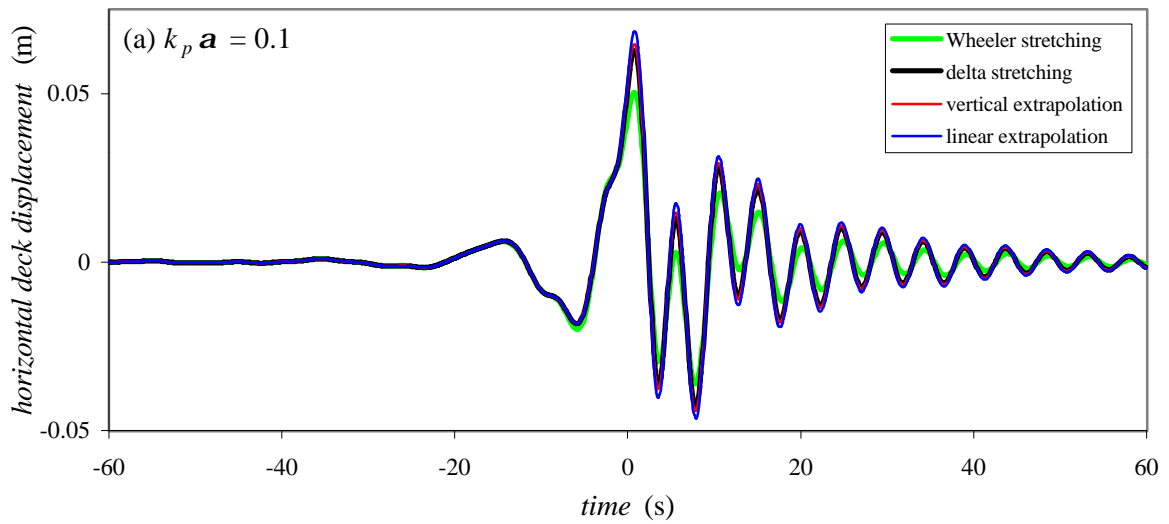


Figure 5.12 - Deck displacements calculated in JAKUP for different stretching/extrapolation assumptions

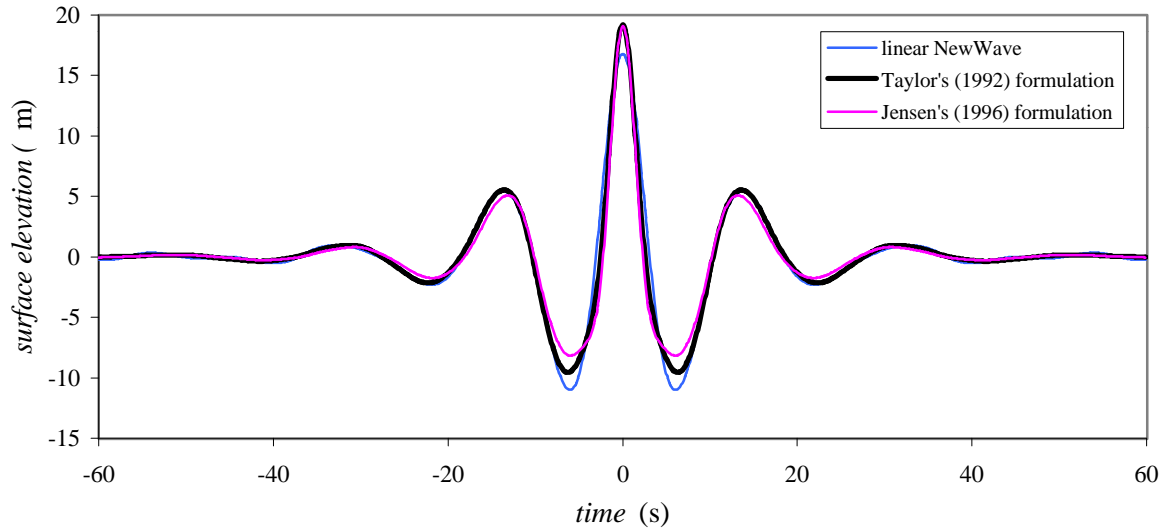


Figure 5.13 - Surface elevations calculated in JAKUP for second-order formulations

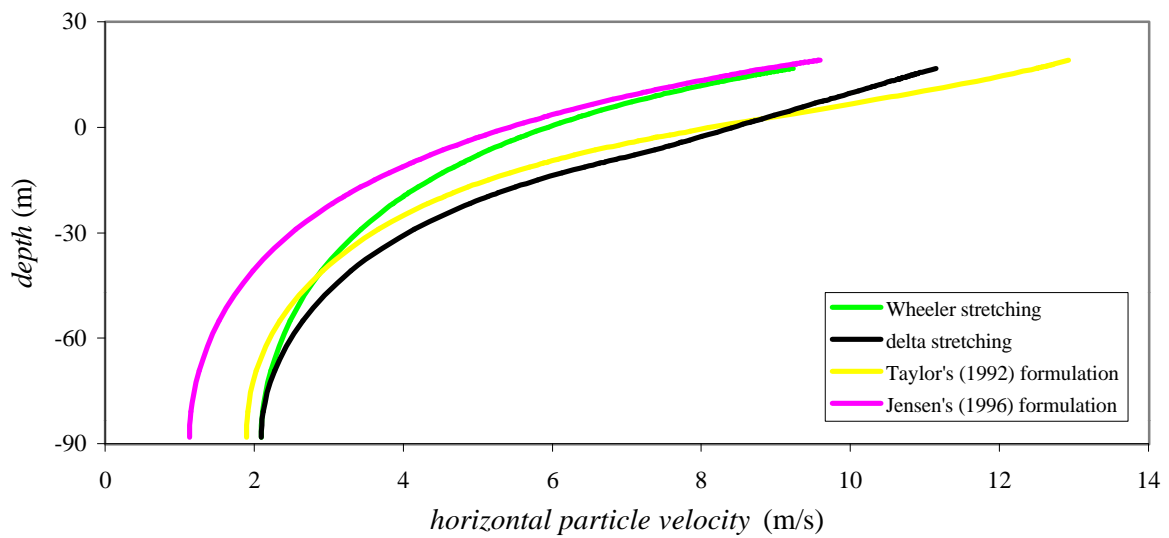


Figure 5.14 - Wave kinematics under the crest calculated in JAKUP for second-order formulations

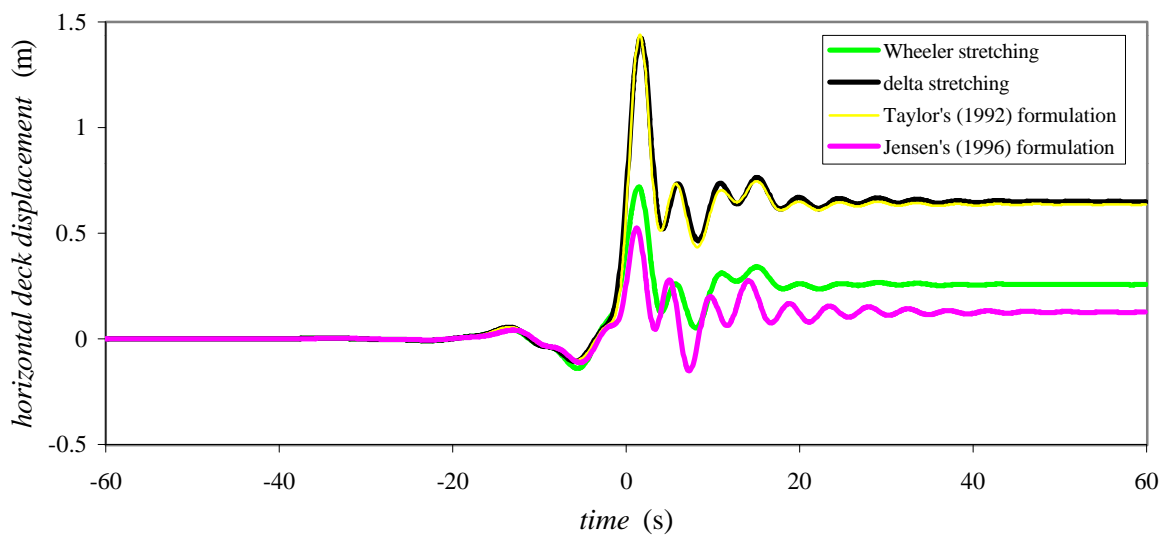


Figure 5.15 - Deck displacements calculated in JAKUP for second-order formulations

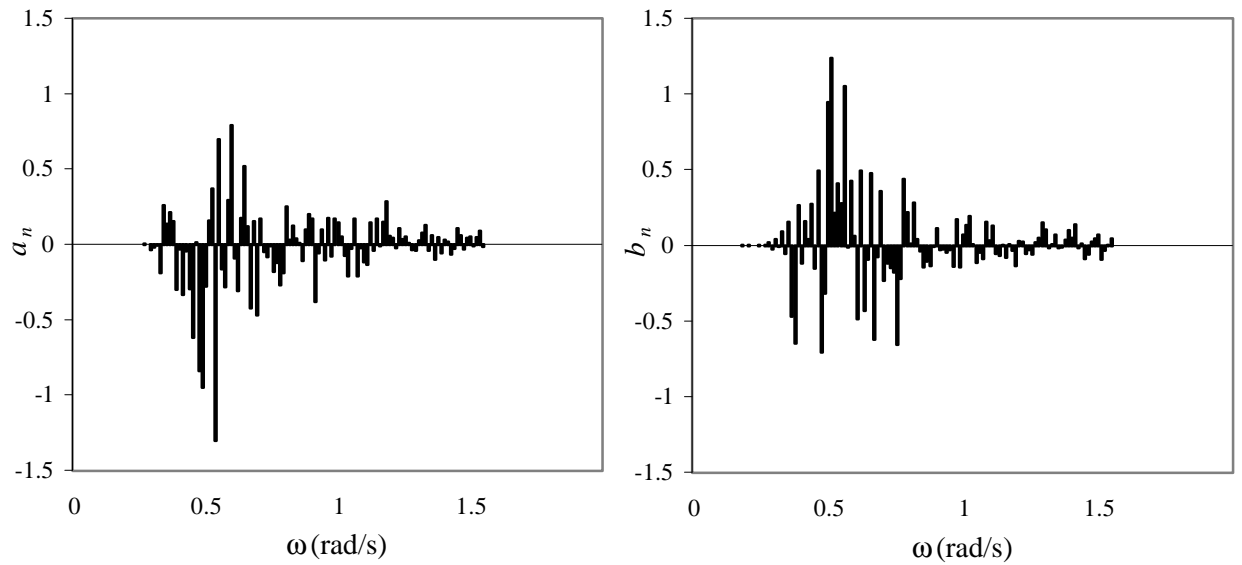


Figure 6.1 - Randomly generated Fourier coefficients

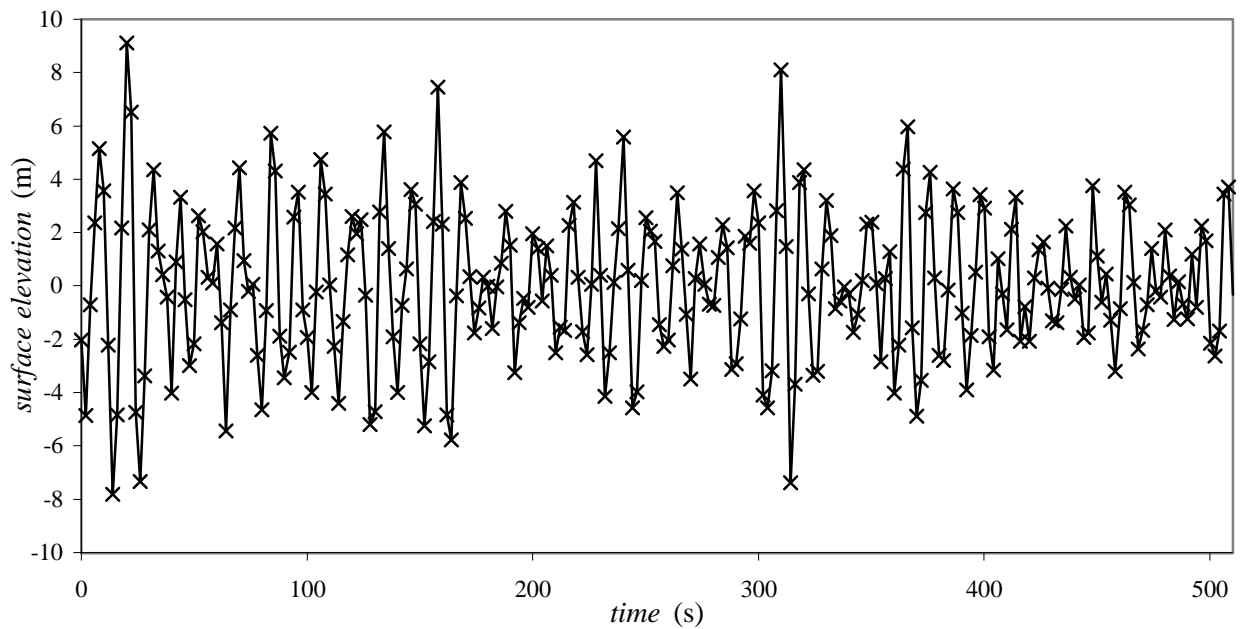


Figure 6.2 - Time history of surface elevation

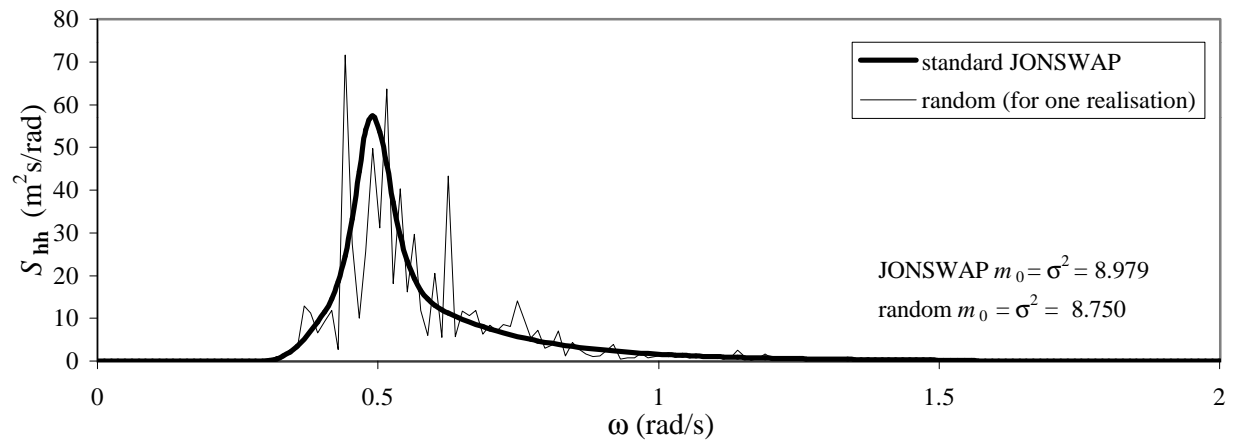


Figure 6.3 - Spectral density estimate for one realisation of the JONSWAP wave energy spectrum

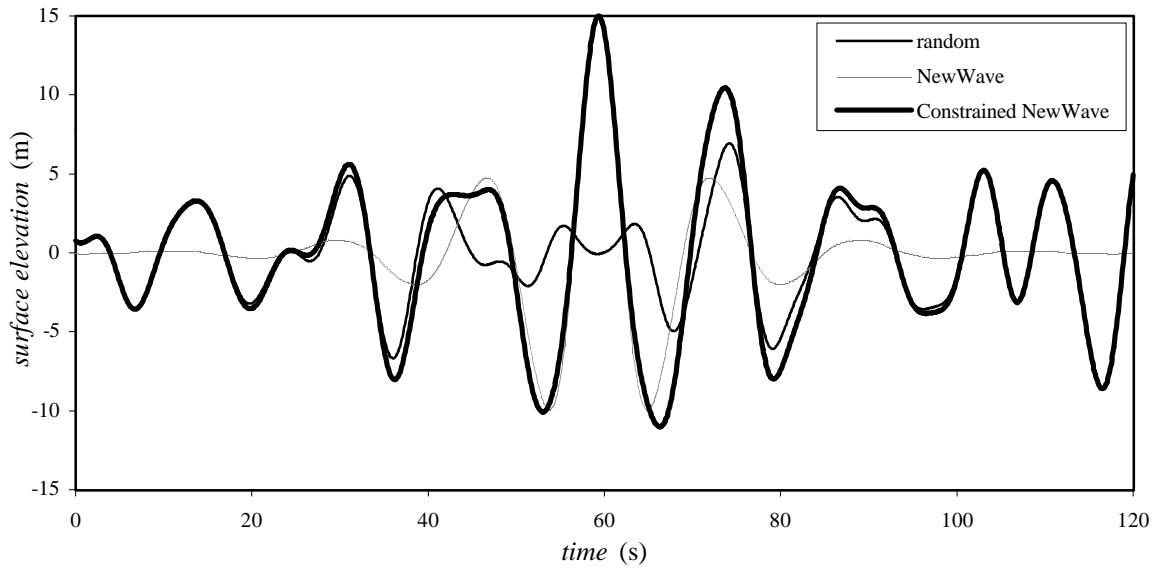


Figure 6.4 - Surface elevation of a NewWave of 15m elevation constrained within a random background

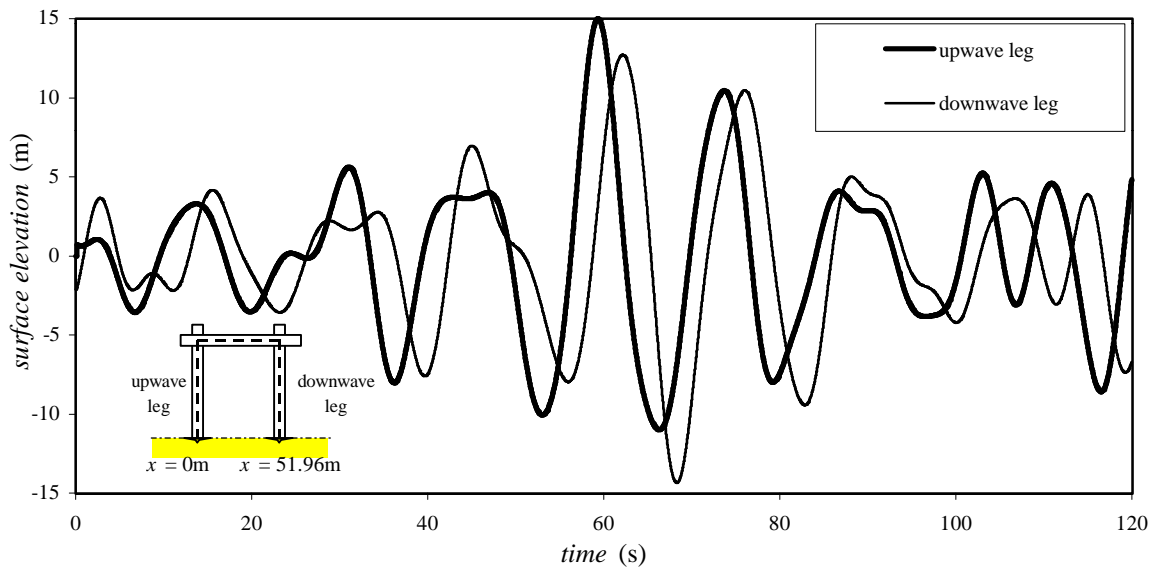


Figure 6.5 - Surface elevation at the upwave and downwave legs

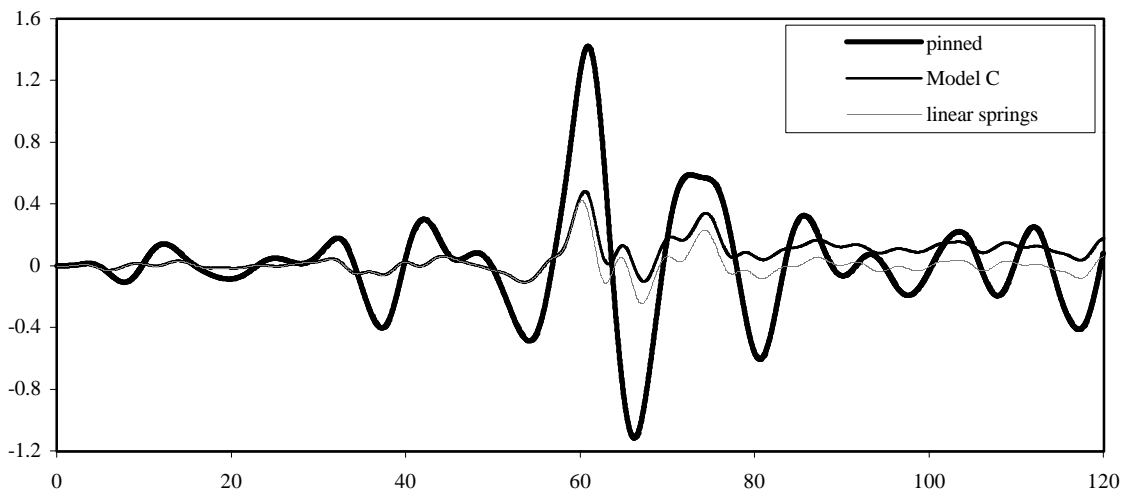
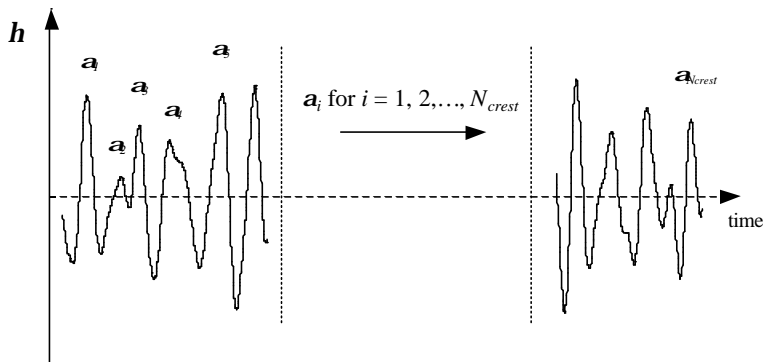


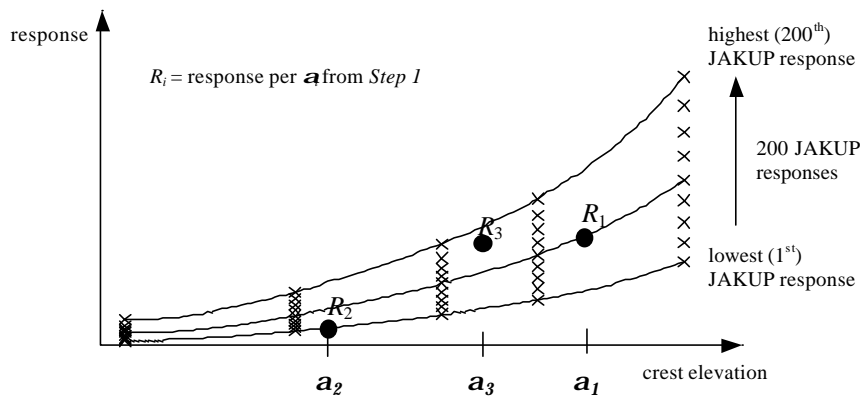
Figure 6.6 - Horizontal deck displacements due to the Constrained NewWave

Step 1



For a narrow banded Gaussian sea, crest elevations are Rayleigh distributed. A set of elevations (a_i) can be generated from a Monte Carlo simulation.

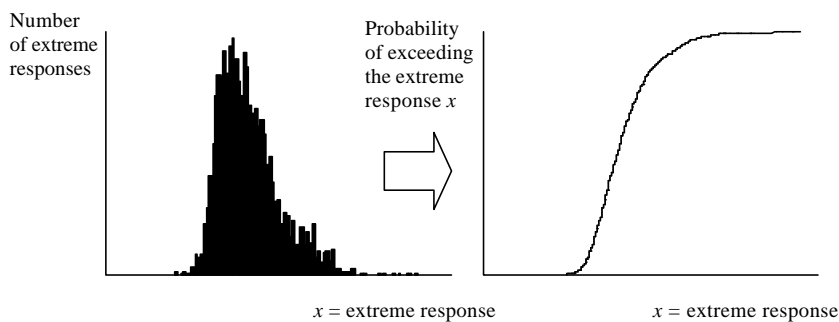
Step 2



The crosses represent the 5 sets of 200 JAKUP runs (sorted into ascending order) from which lines of constant probability are constructed.

For each set of a_i , a set of responses R_i is generated by selecting the response value for each elevation from a randomly generated number (between 1 \rightarrow 200) and then its line of constant probability.

Step 3



One Monte Carlo simulation of steps 1 and 2 produces one extreme response (the largest in the set R_i). Repeating the steps gives an expected distribution of extreme response for the period in that sea-state.

Figure 6.7 - Explanation of methodology adopted to evaluate the extreme response statistics for one short-term sea-state

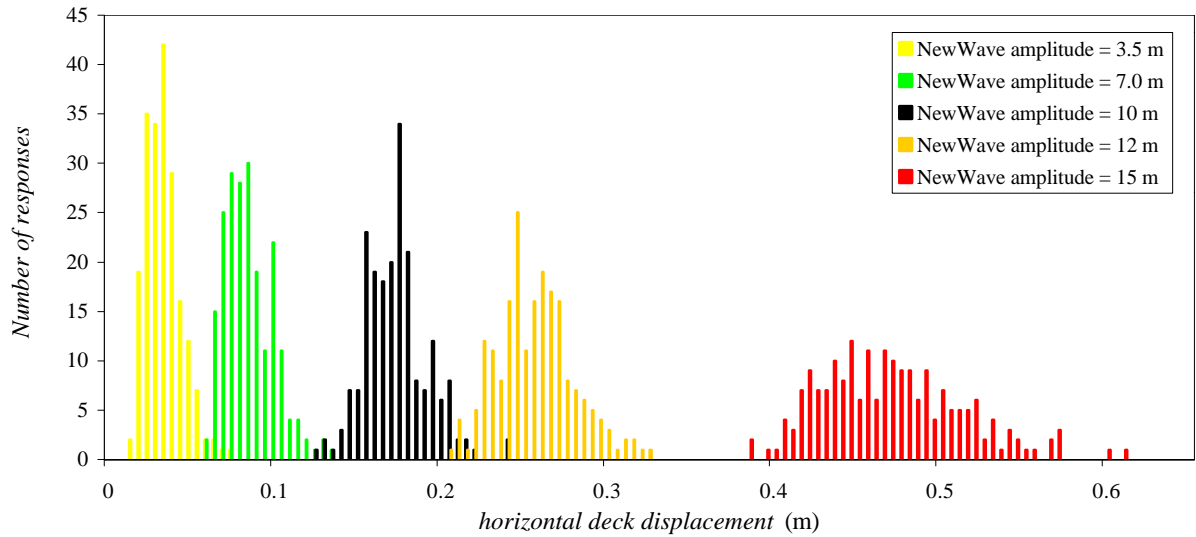


Figure 6.8 - Deck displacements calculated by JAKUP for five Constrained NewWave elevations

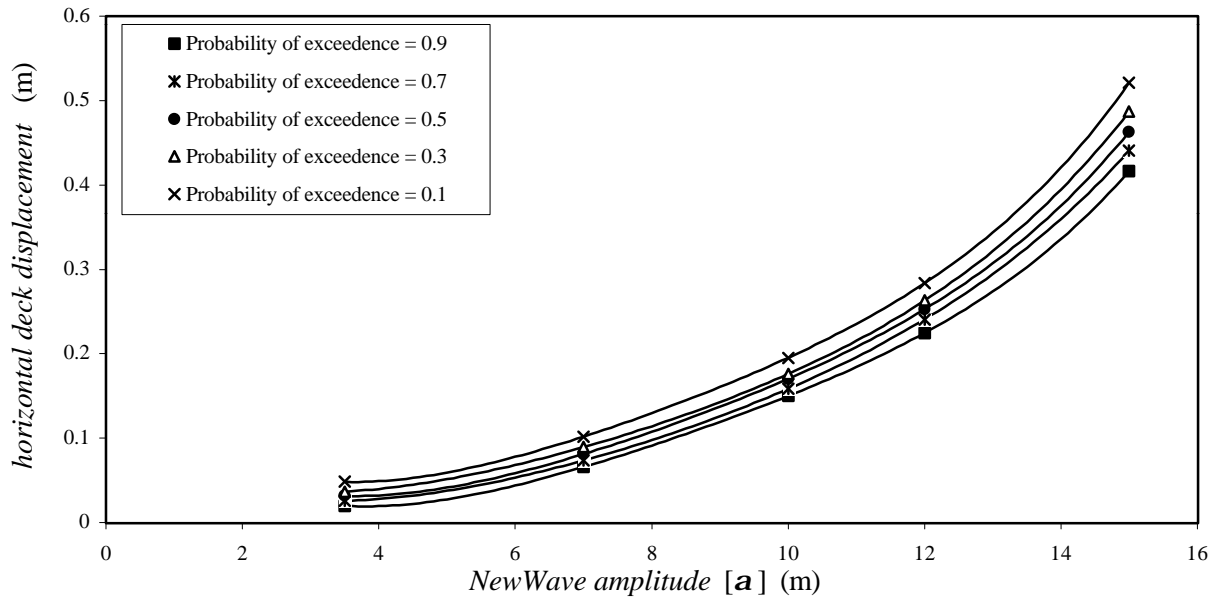


Figure 6.9 - Lines of constant probability

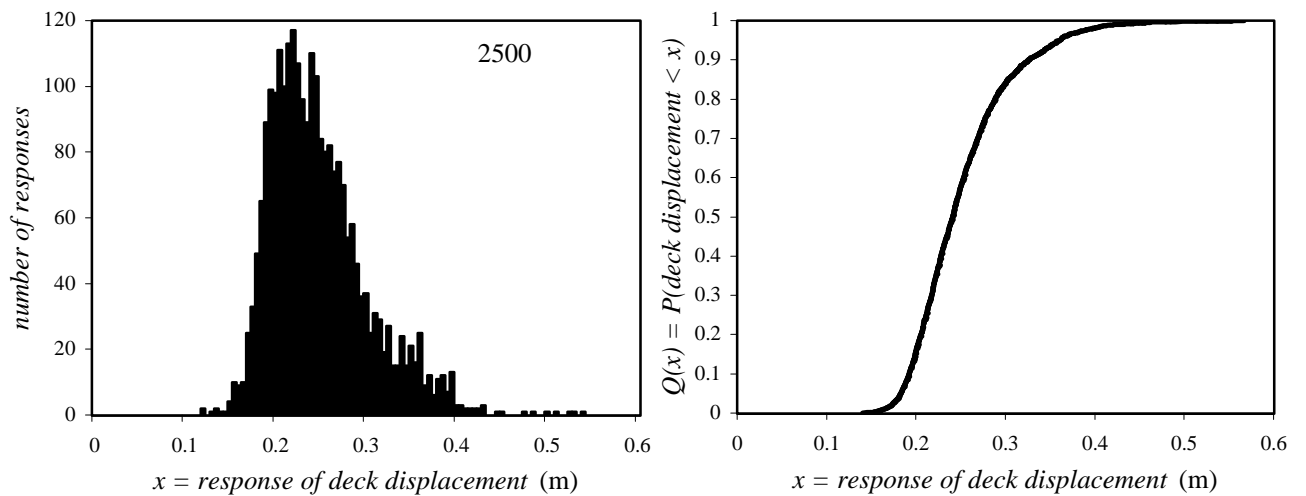


Figure 6.10 - Extreme deck displacement distributions for a three hour period of a sea-state represented by $H_s = 12$ m and $T_z = 10.805$ s

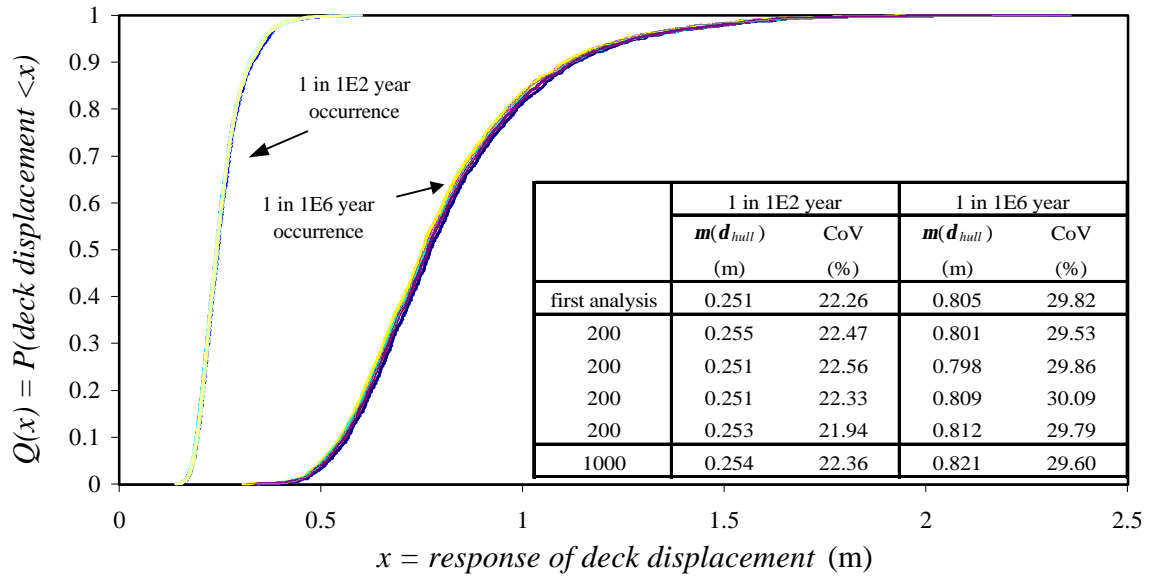


Figure 6.11 - Repetition of the calculation of extreme response statistics

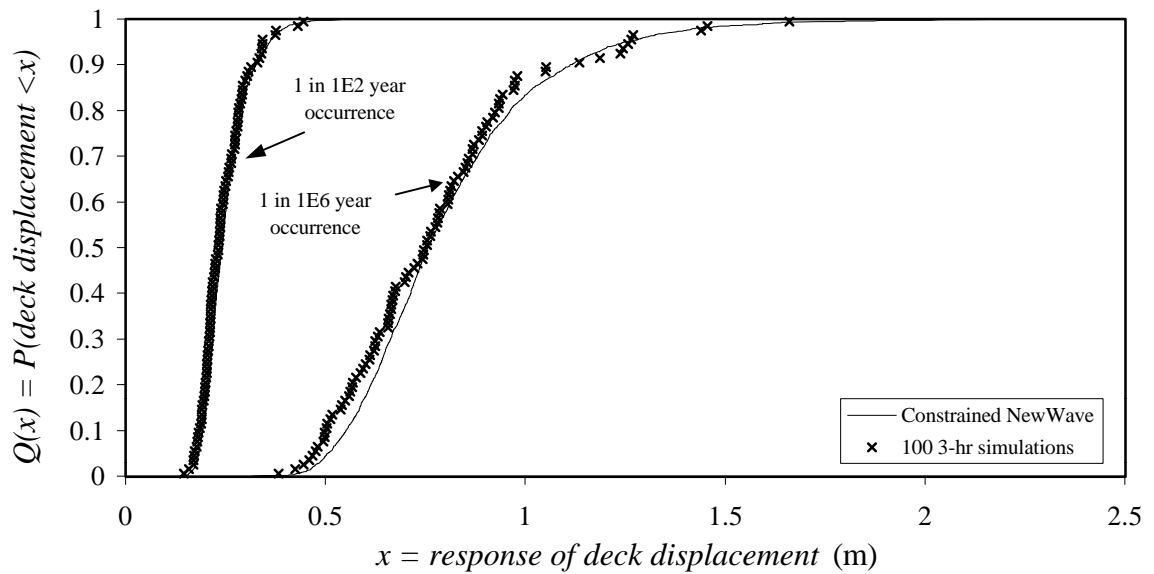
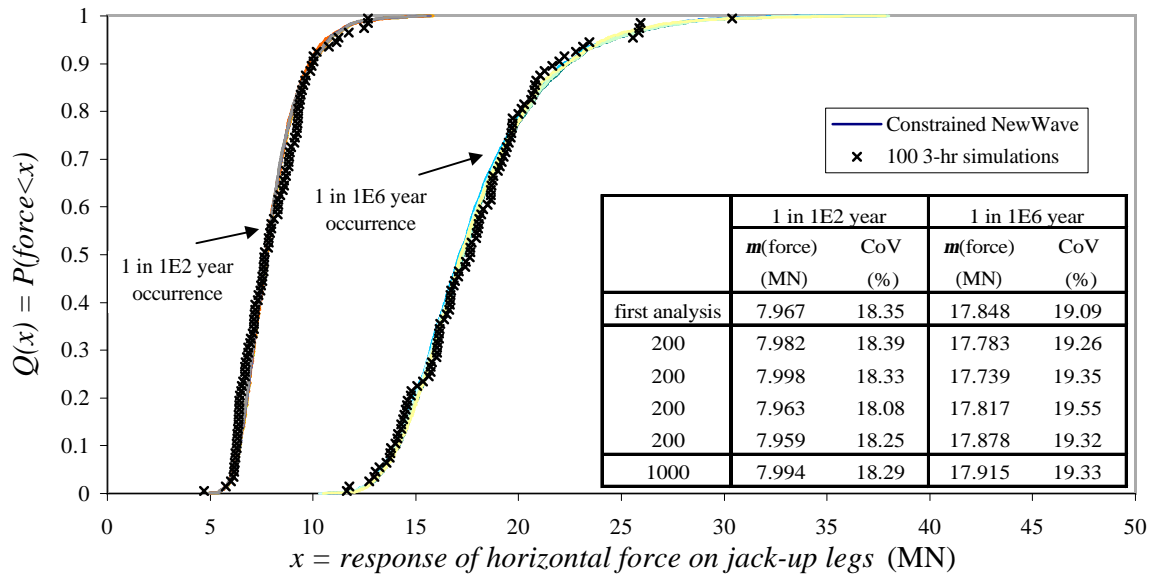


Figure 6.12 - Comparison of extreme response statistics evaluated using the Constrained NewWave method with 100 three-hour random simulations

(a) force on upwave legs



(b) total force on all legs

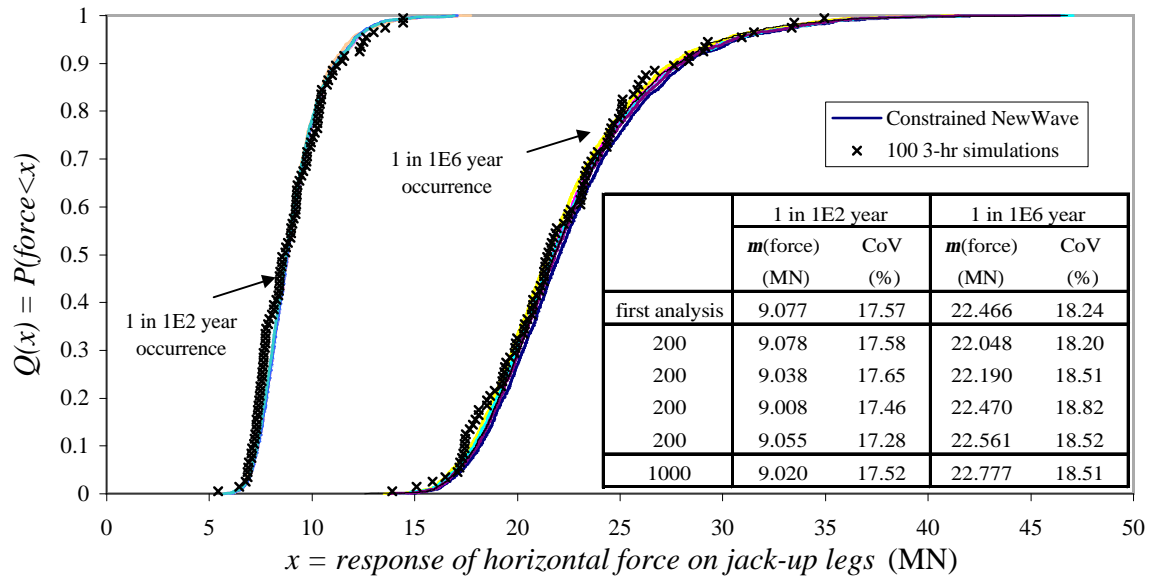


Figure 6.13 - Repetition of the calculation of force on the legs of the jack-up

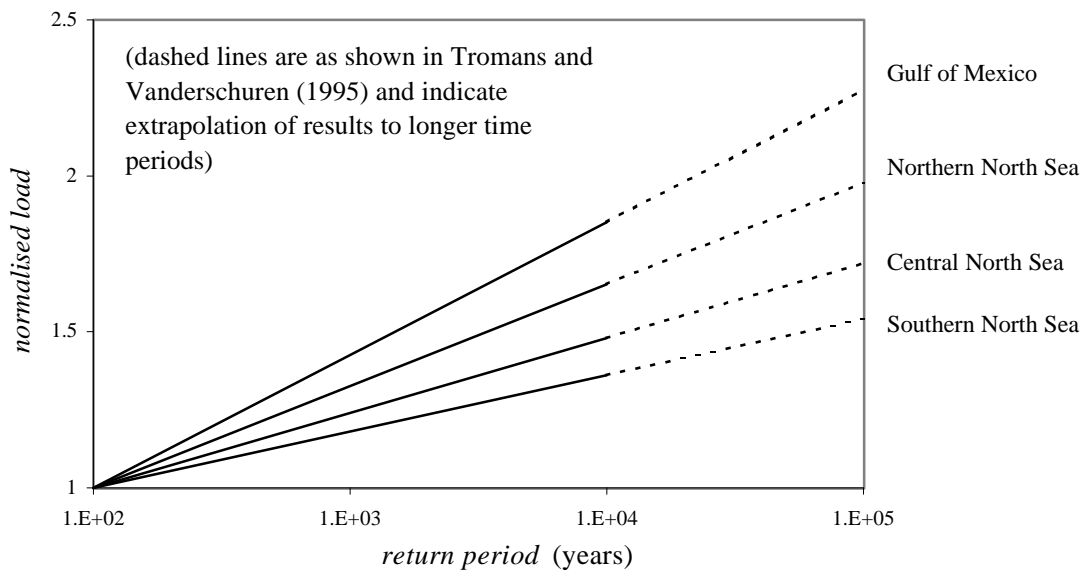


Figure 6.14 - Normalised load versus return period for different areas (after Tromans and Vanderschuren, 1995)

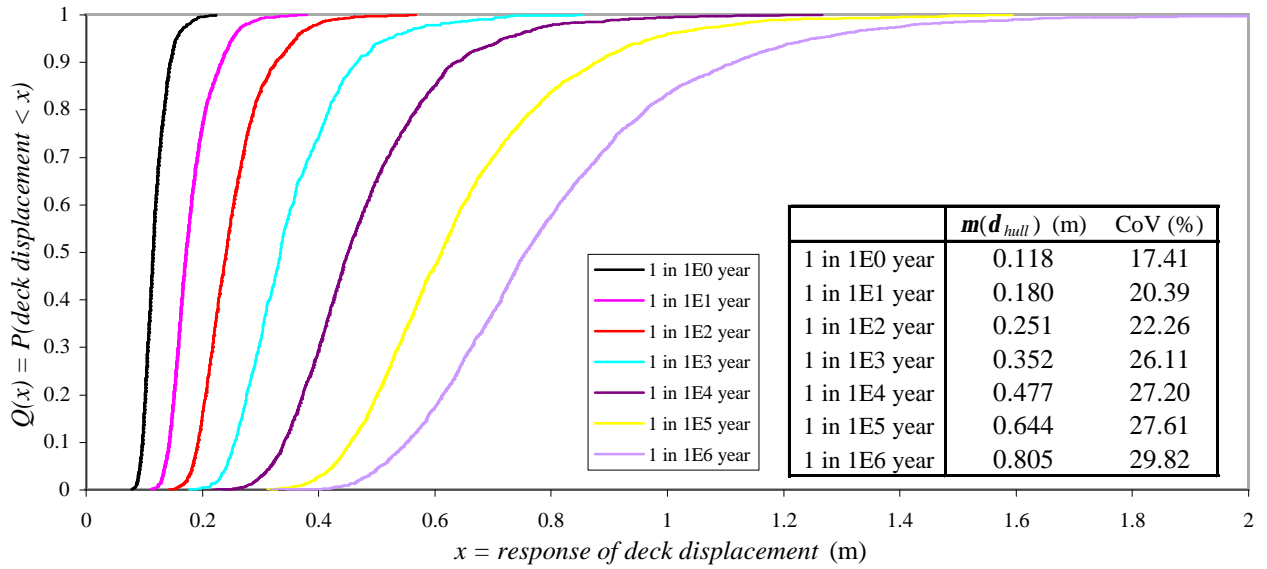
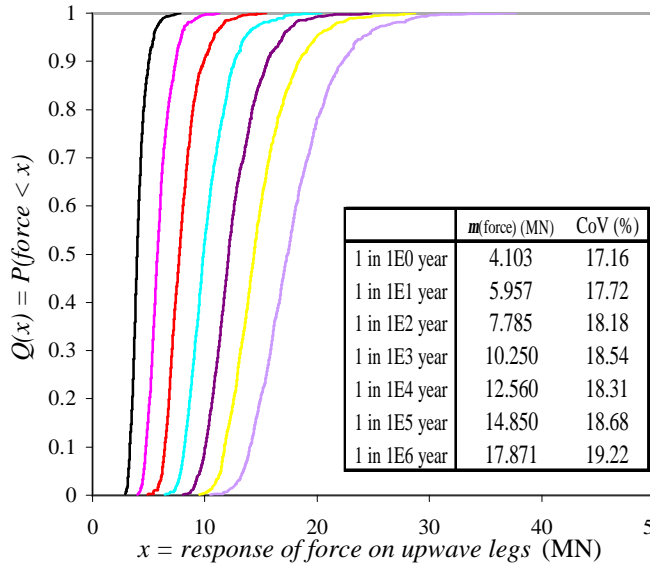


Figure 6.15 - Seven short-term extreme deck displacement response distributions for Model C footings

(a) force on upwave legs



(b) total force on all legs

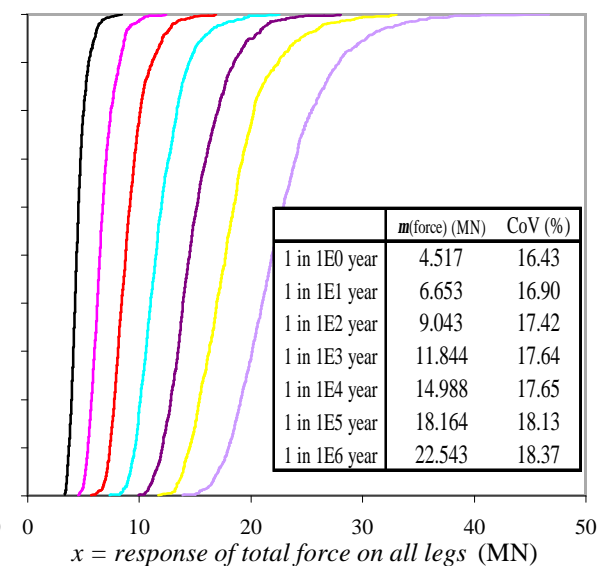
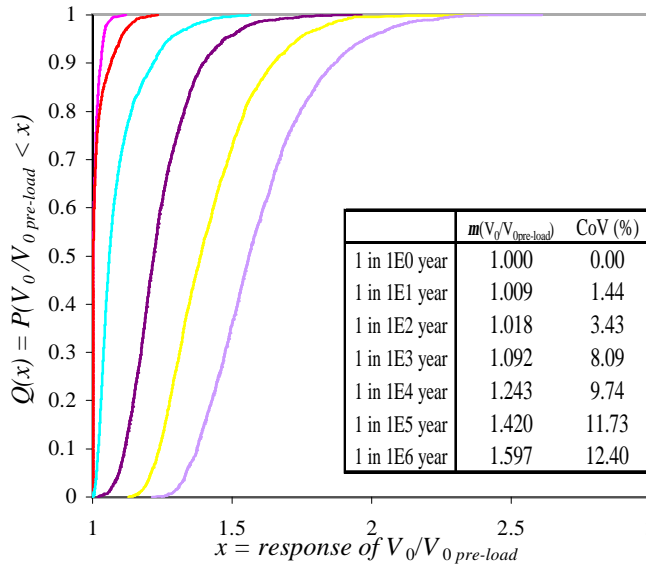


Figure 6.16 - Extreme force distributions (legend as in Fig. 6.15)

(a) upwave footing



(b) downwave footing

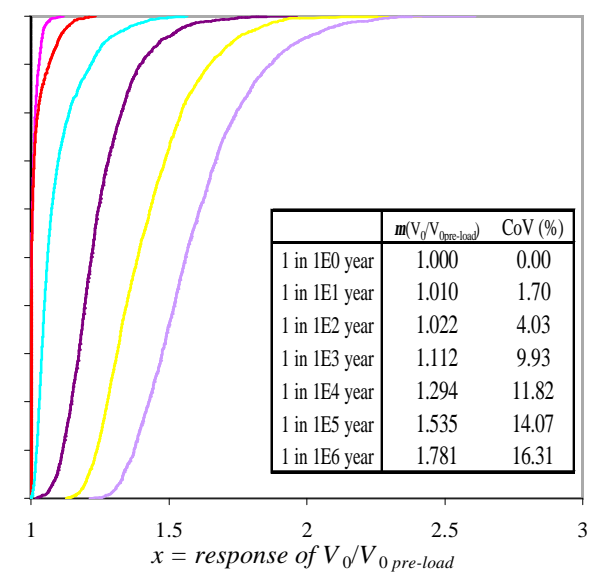


Figure 6.17 - Distribution of the level of plasticity in the Model C short-term calculations (legend as in Fig. 6.15)

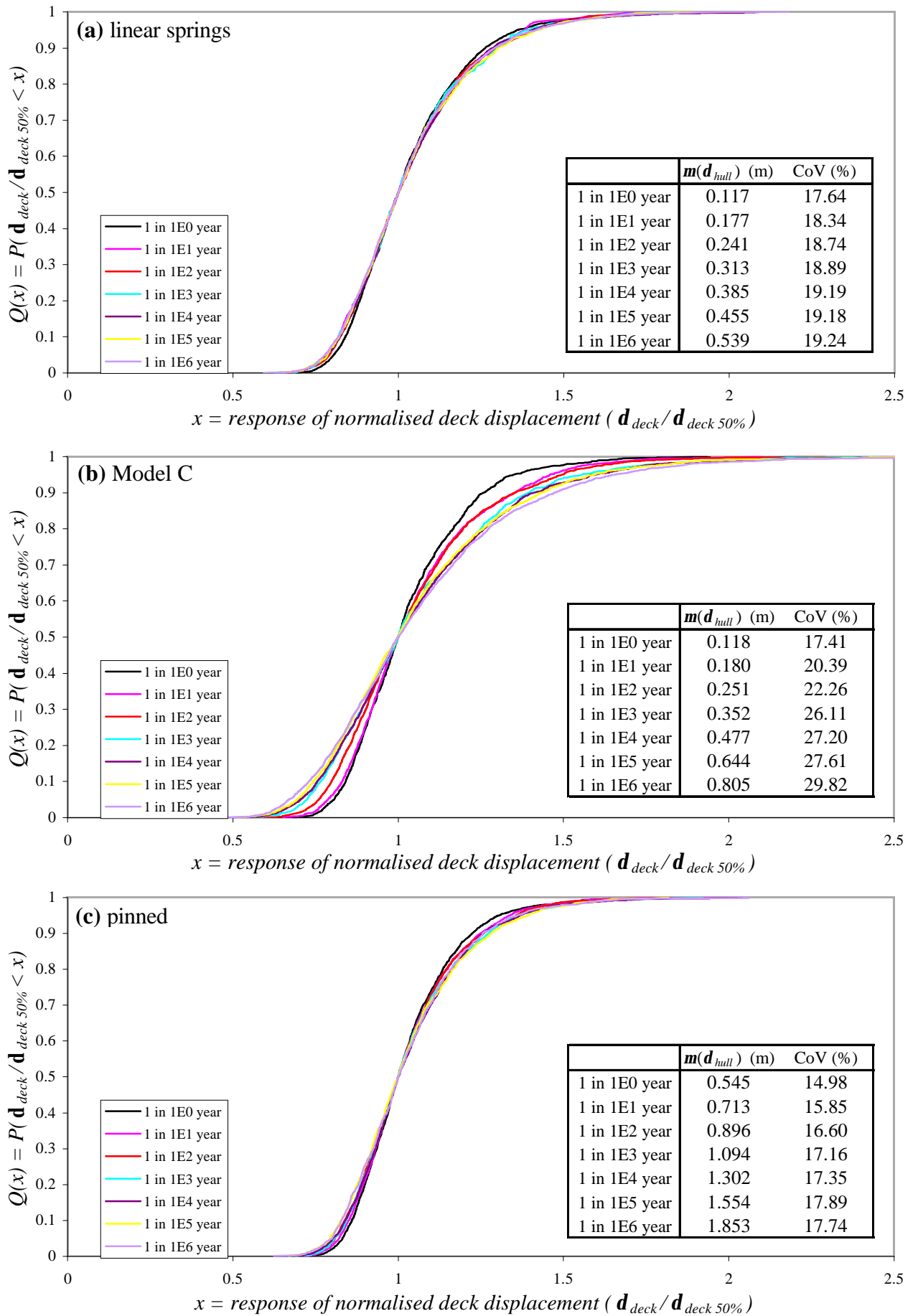


Figure 6.18 - Normalised extreme response distributions

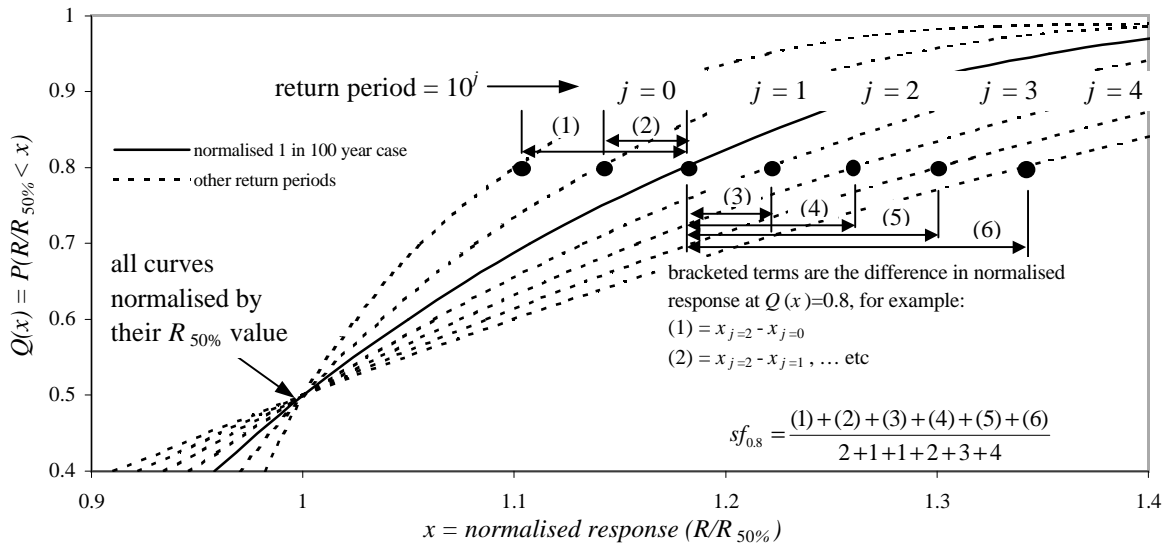


Figure 6.19 - Description of the calculation of short-term scaling factors (this diagram is for $sf_{0.8}$)

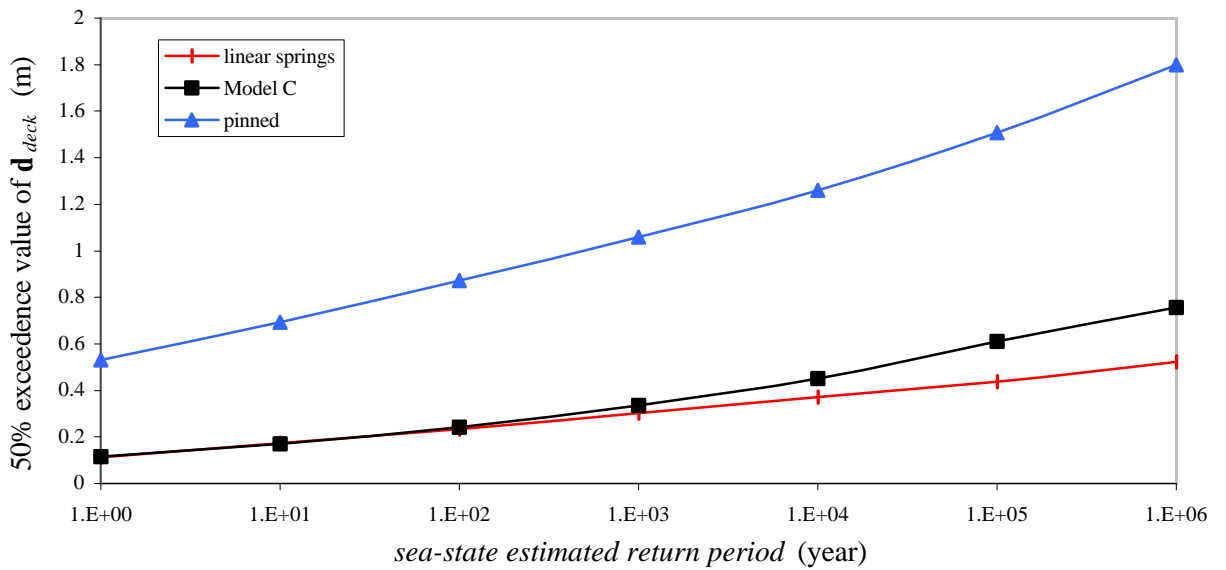


Figure 6.20 - 50% exceedence values used to normalise the extreme deck displacement response distributions

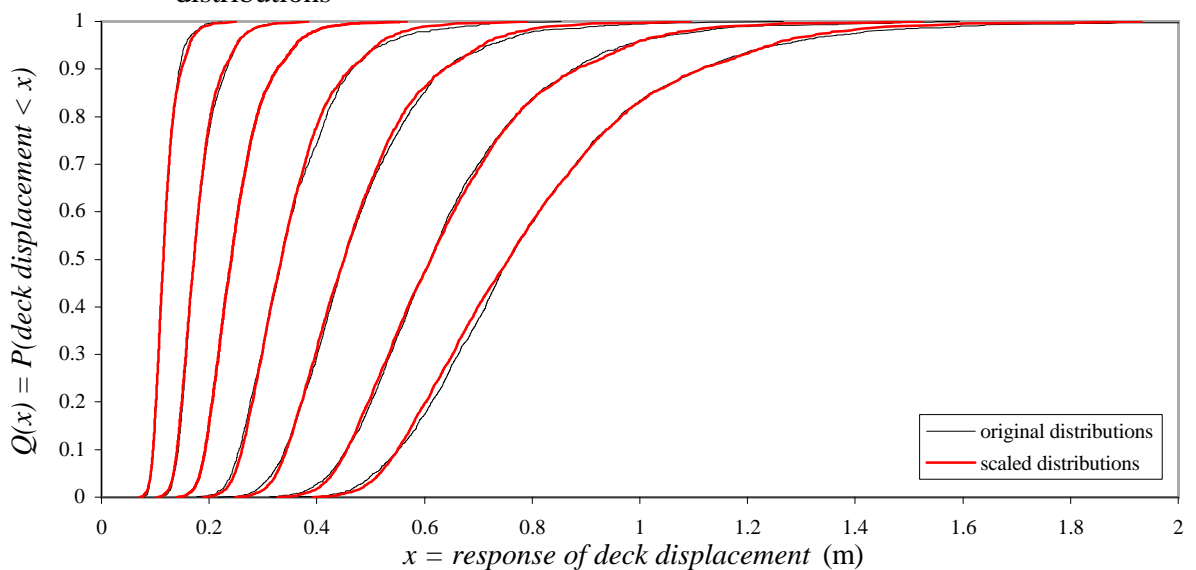


Figure 6.21 - Comparisons of the scaled and original extreme deck displacement distributions for Model C with no wind or current

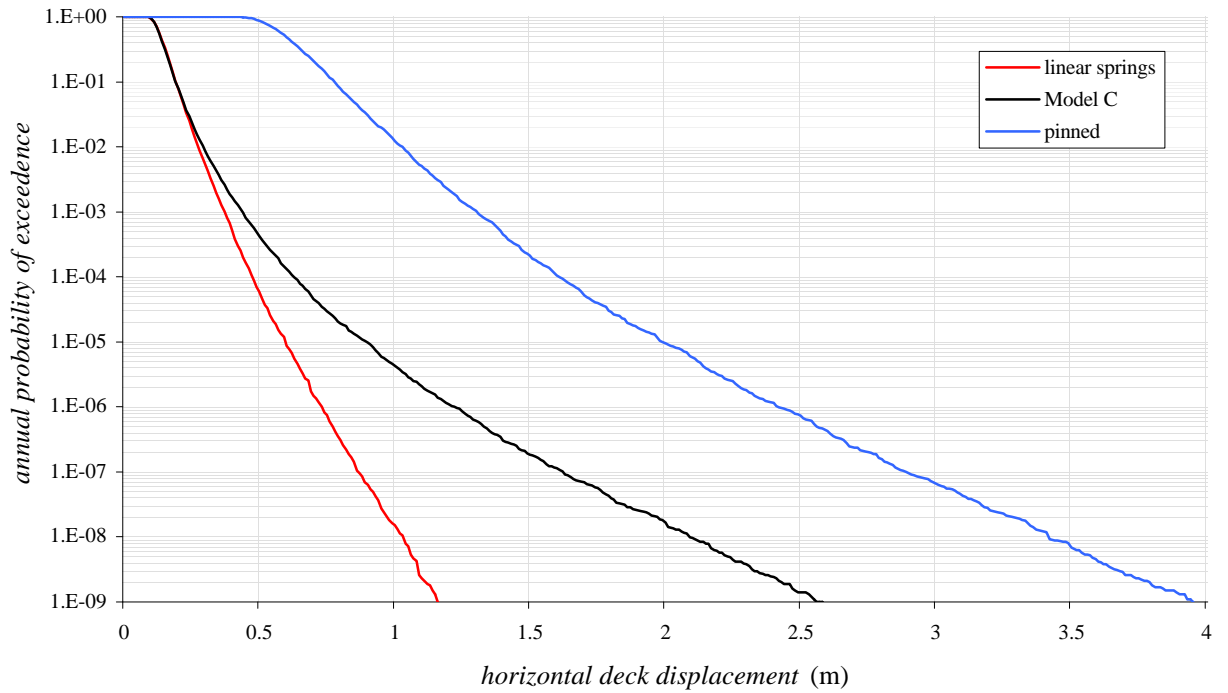


Figure 6.22 - Annual probabilities of exceedence of deck displacements under various foundation assumptions

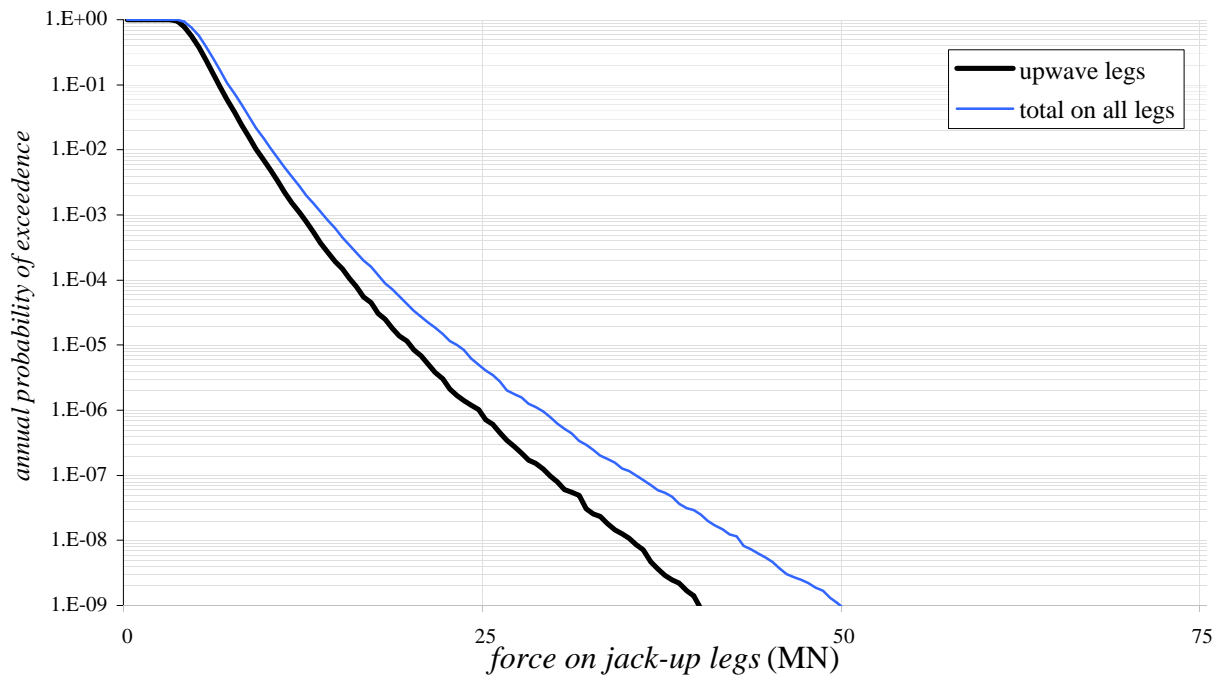


Figure 6.23 - Annual probabilities of exceedence of force on the jack-up legs

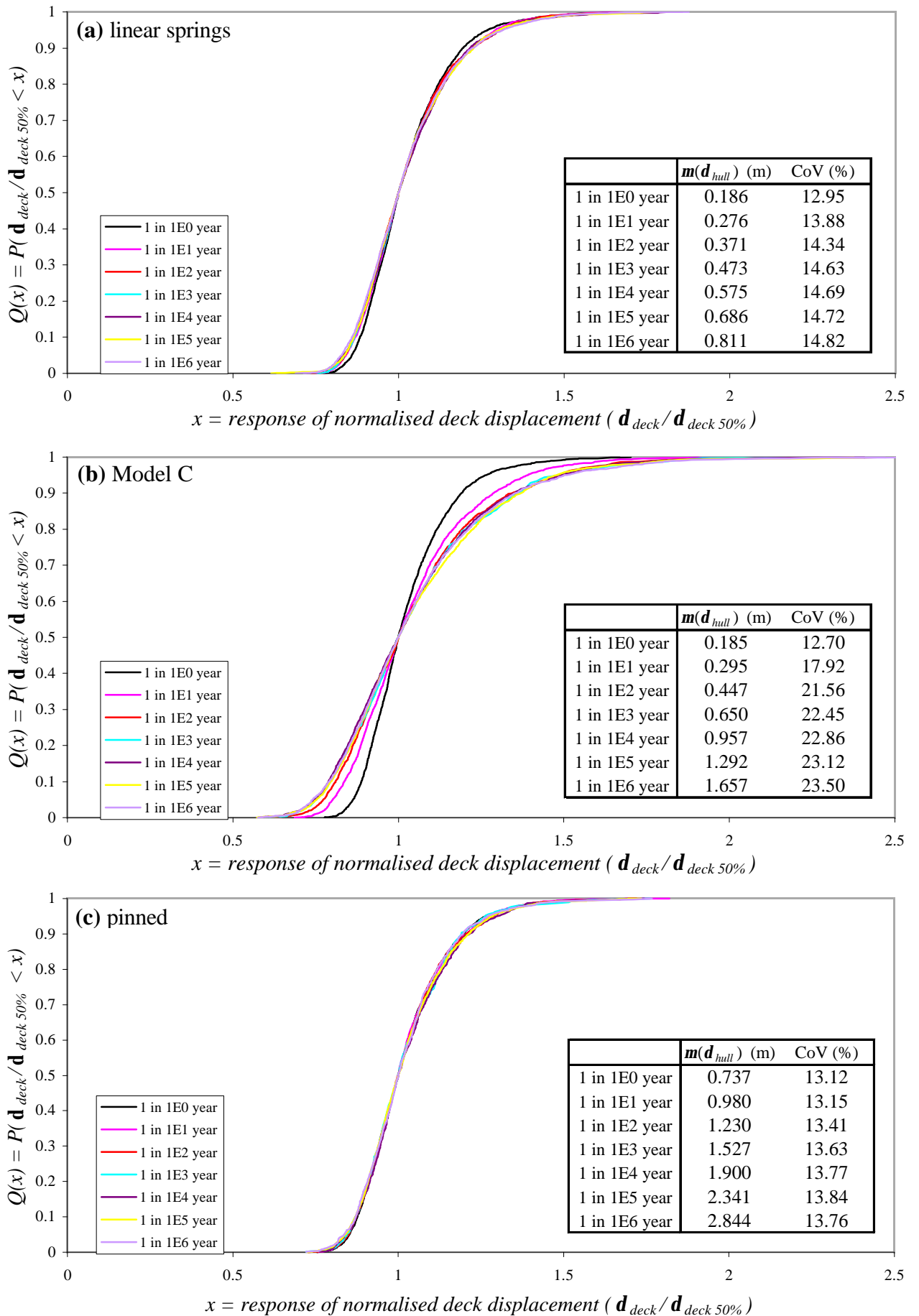


Figure 6.24 - Normalised extreme response distributions (including wind and current in the analysis)

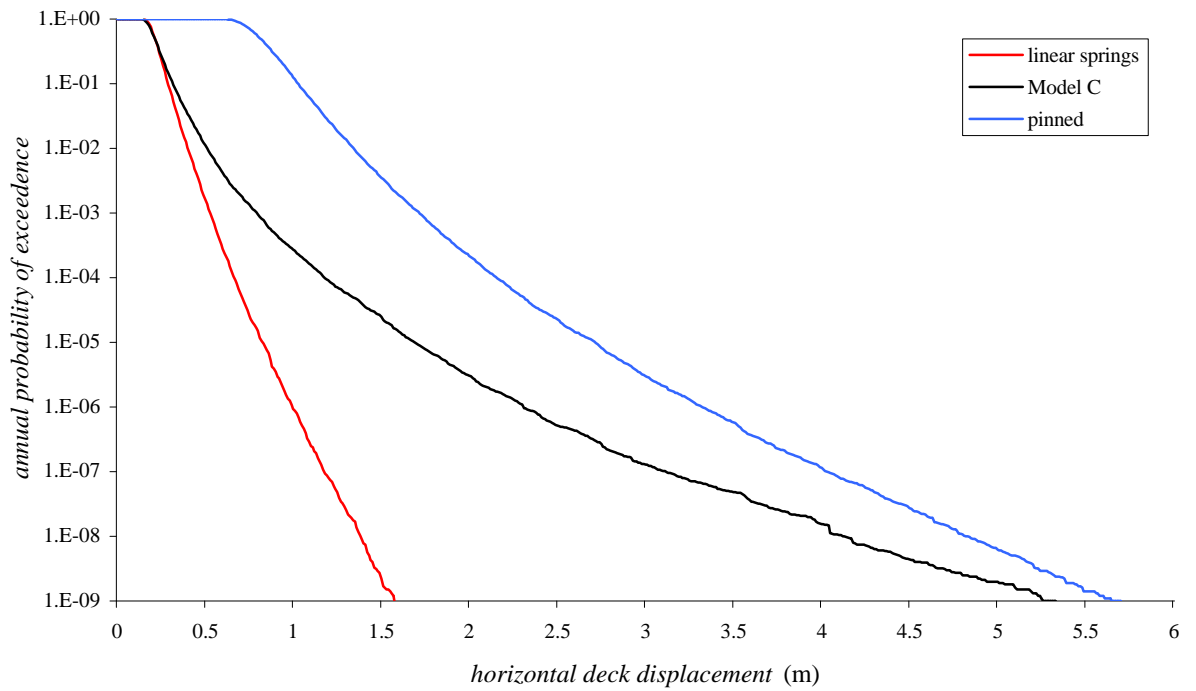


Figure 6.25 - Annual probabilities of exceedence of deck displacements under various foundation assumptions including wind and current

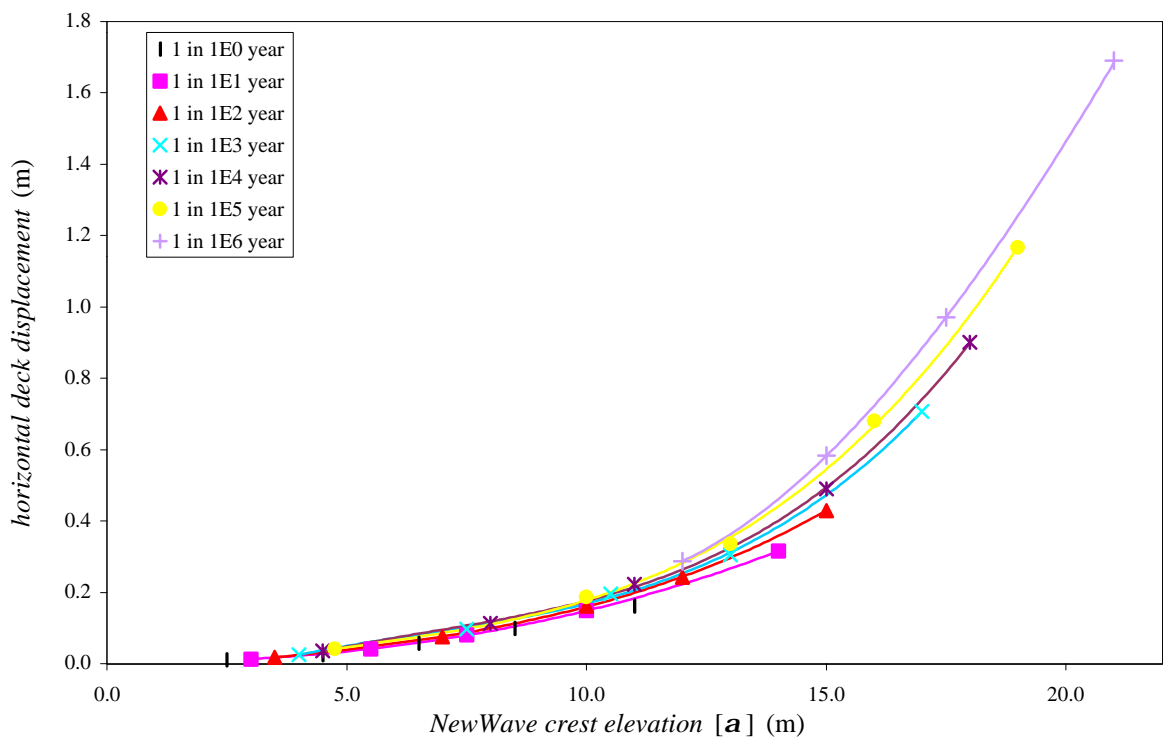


Figure 6.26 - Horizontal deck displacements for all NewWave elevations

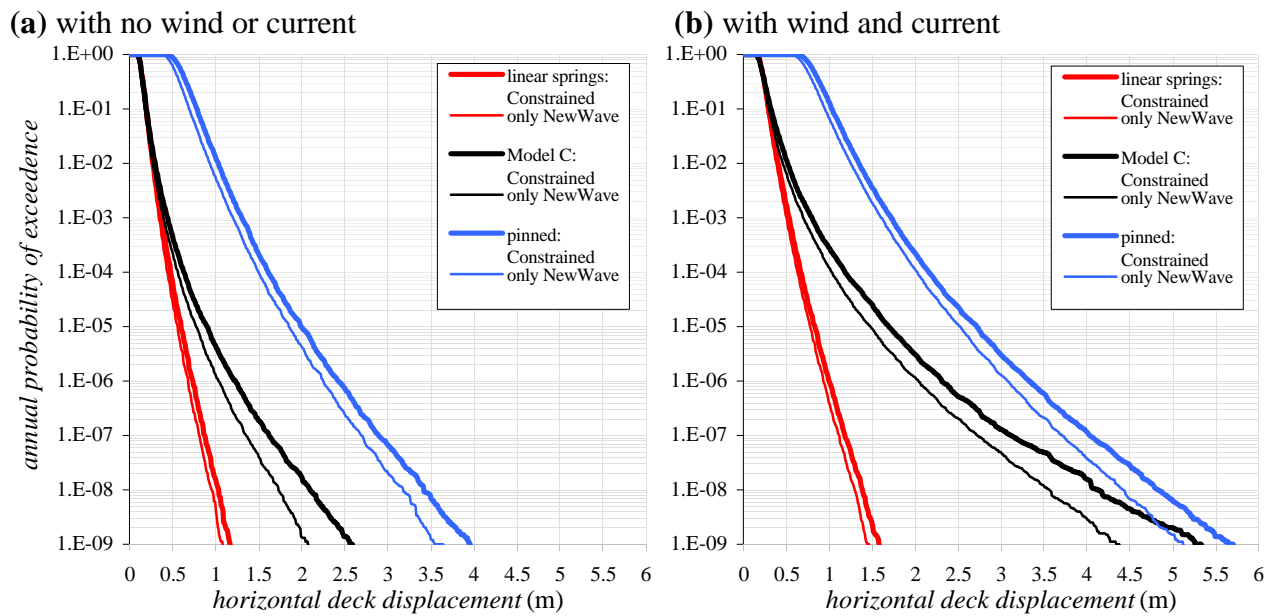


Figure 6.27 - Comparisons of probability of exceedence values with and without the random background

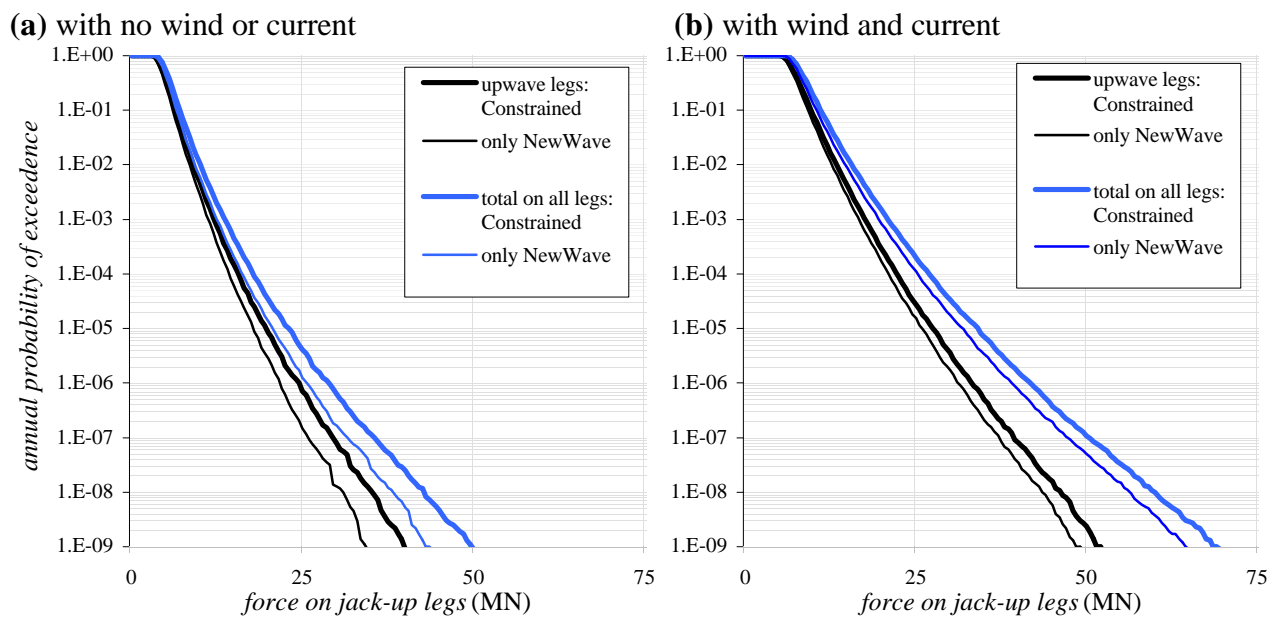


Figure 6.28 - Comparisons of the force on the jack-up

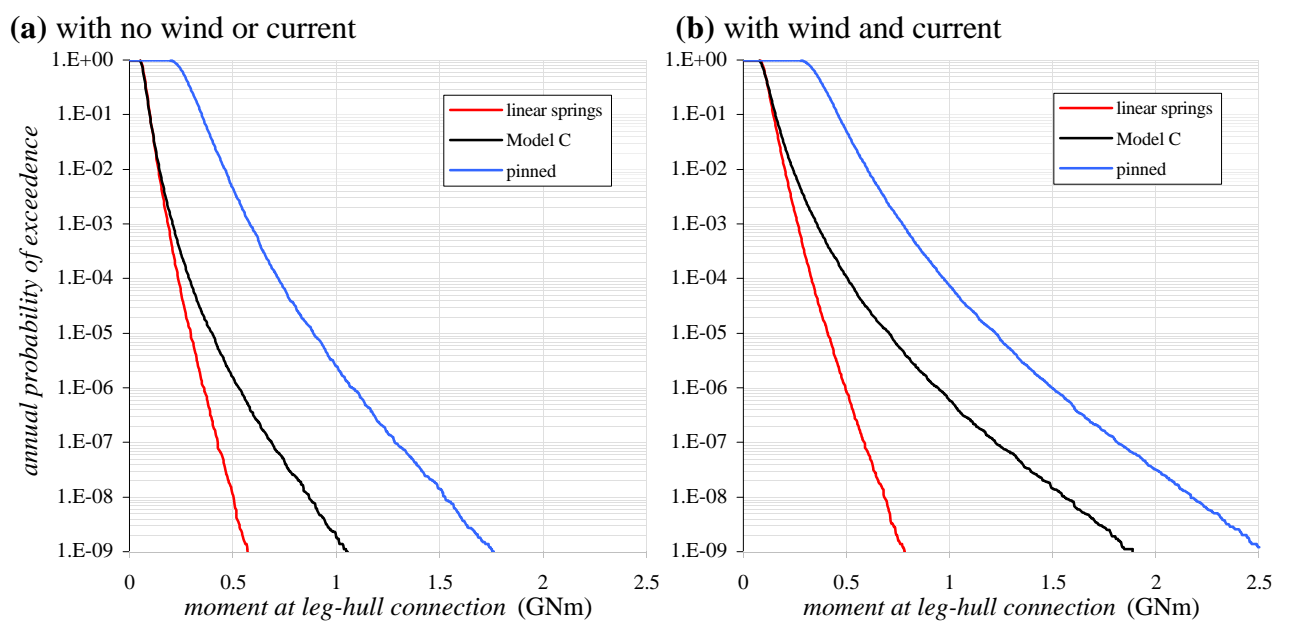


Figure 6.29 - Long-term probability of exceedence levels for the moment at the leg-hull interface

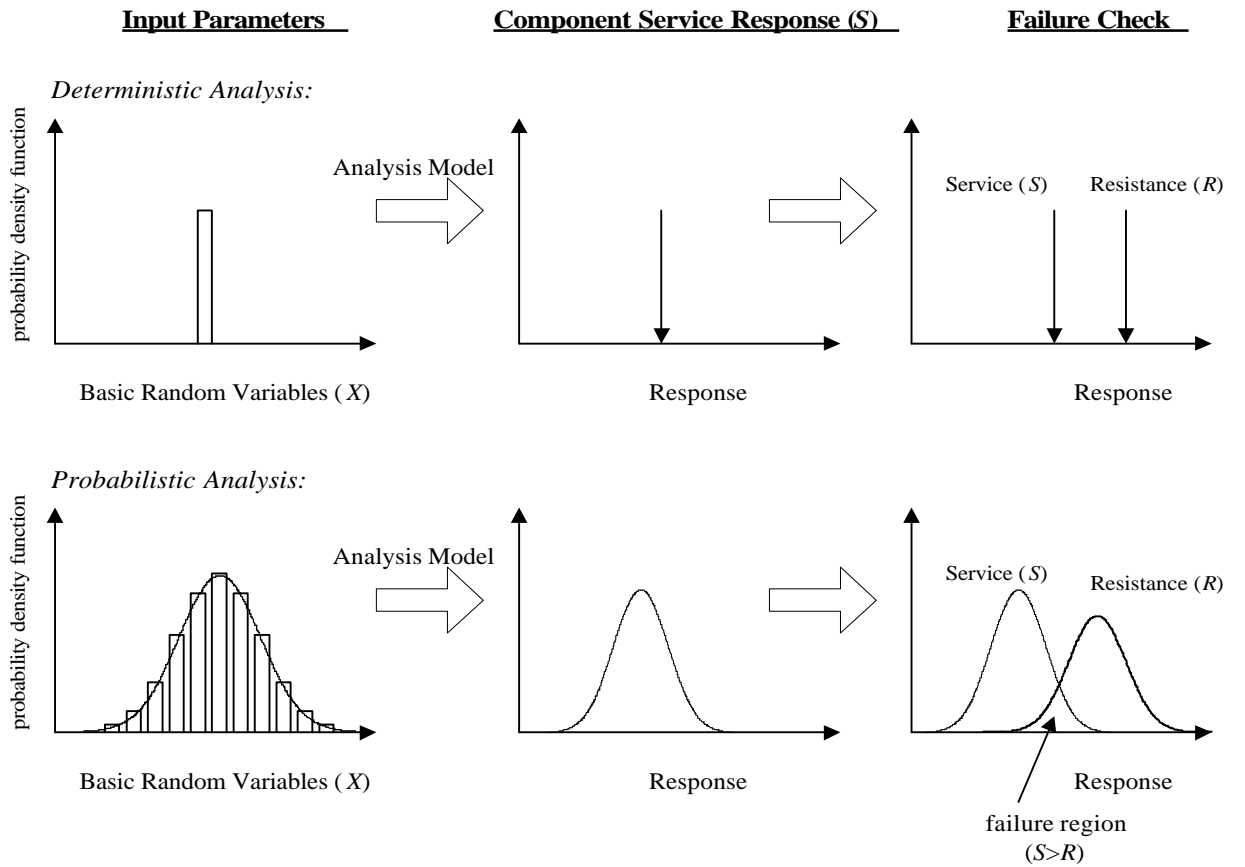


Figure 7.1 - Illustration of deterministic and probabilistic methods

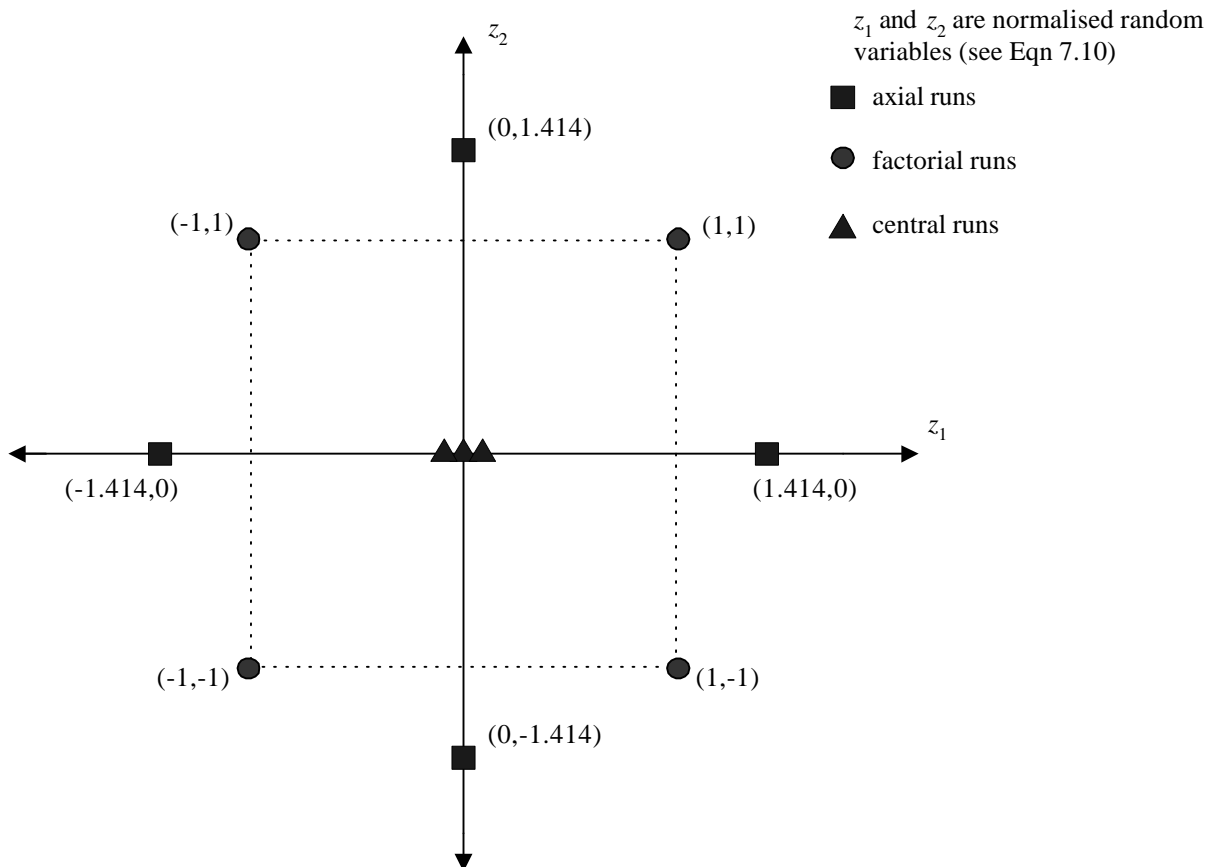


Figure 7.2 - Central composite design method for $k = 2$

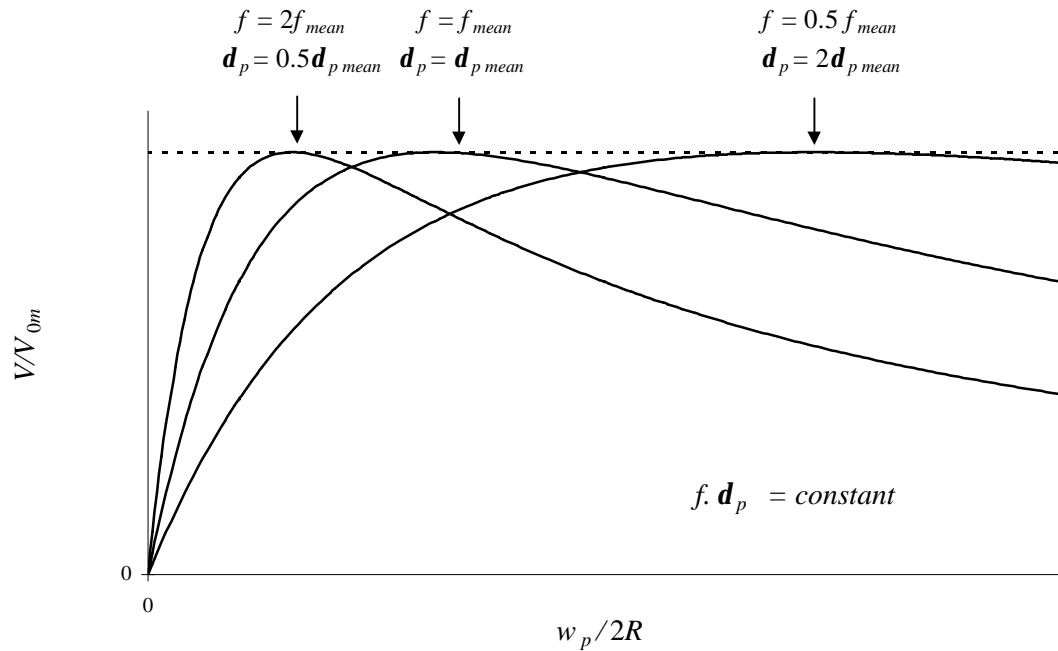


Figure 7.3 - Definition of $f - d_p$ (based on hardening law of Eqn 3.10)

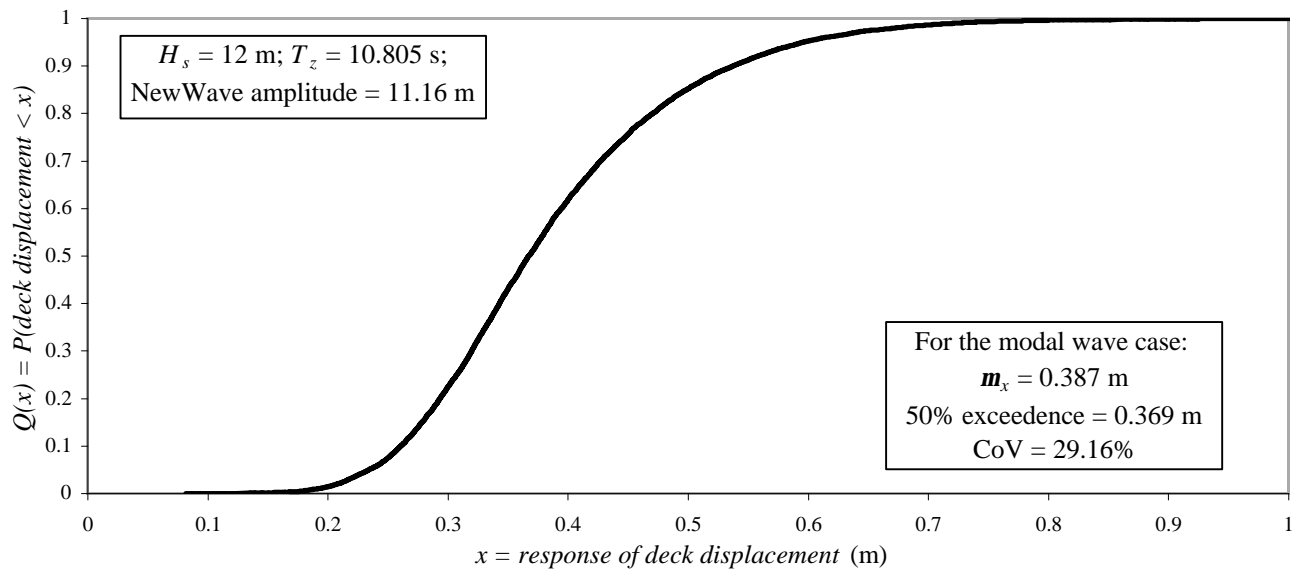


Figure 7.4 - Extreme deck displacement distribution for the modal most probable highest wave amplitude in the 100 year sea state

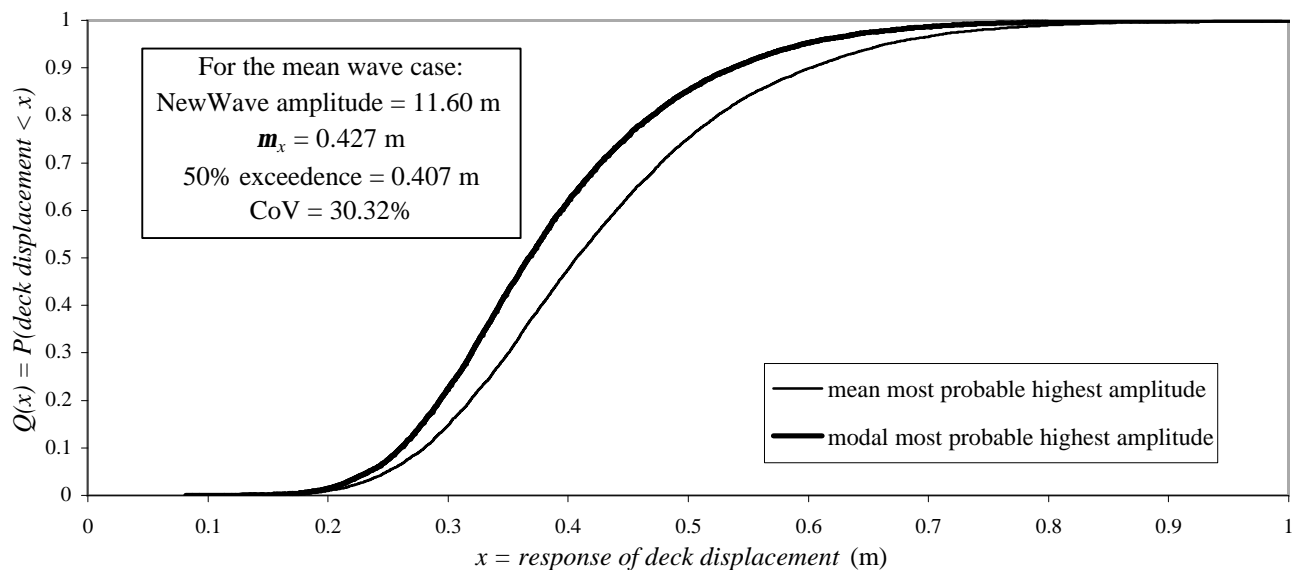


Figure 7.5 - Extreme deck displacement distributions for the mean and modal most probable highest wave amplitudes

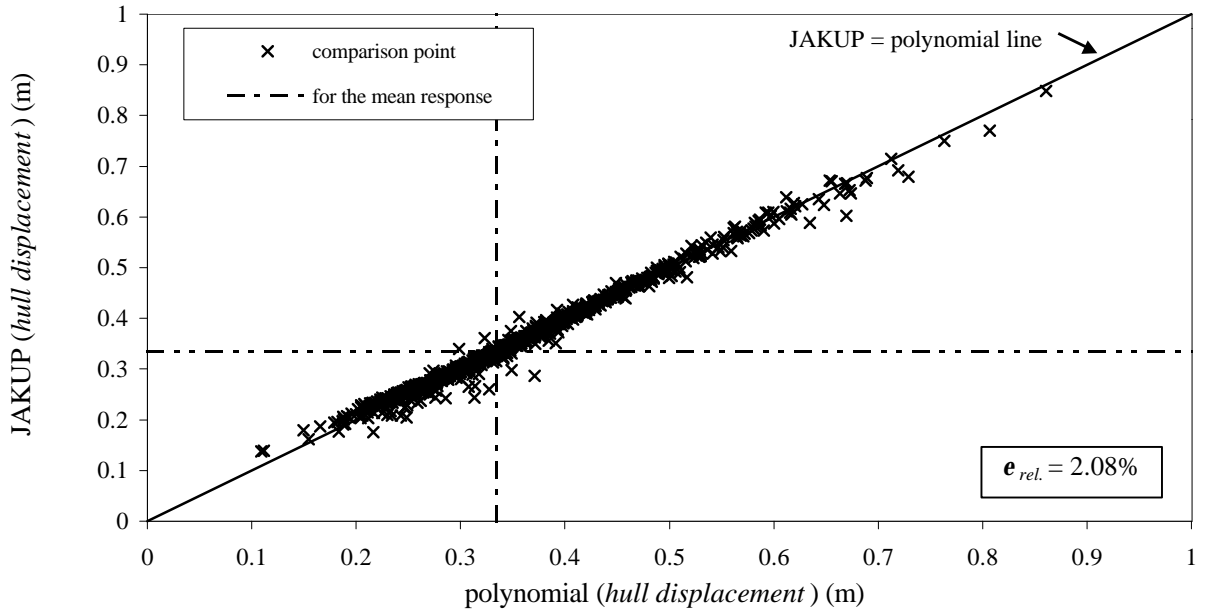


Figure 7.6 - Comparison of deck displacements predicted by the RS and evaluated by JAKUP for 1000 sets of basic random variables (X)

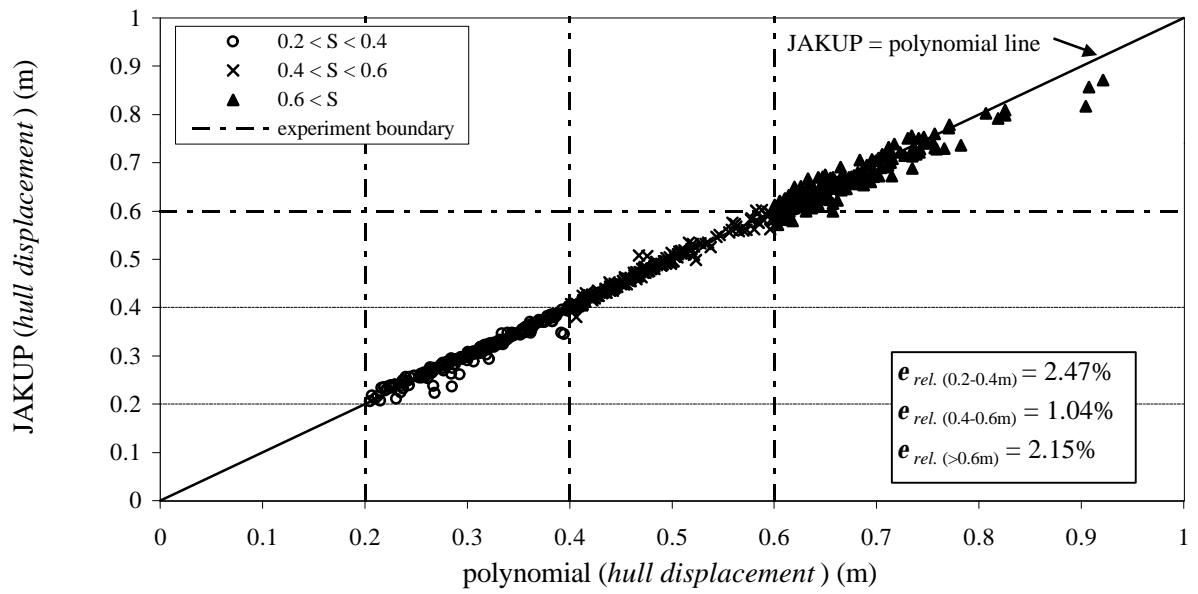


Figure 7.7 - Comparison of response evaluated by the RS and JAKUP for 200 sets of X at three levels of deck displacement

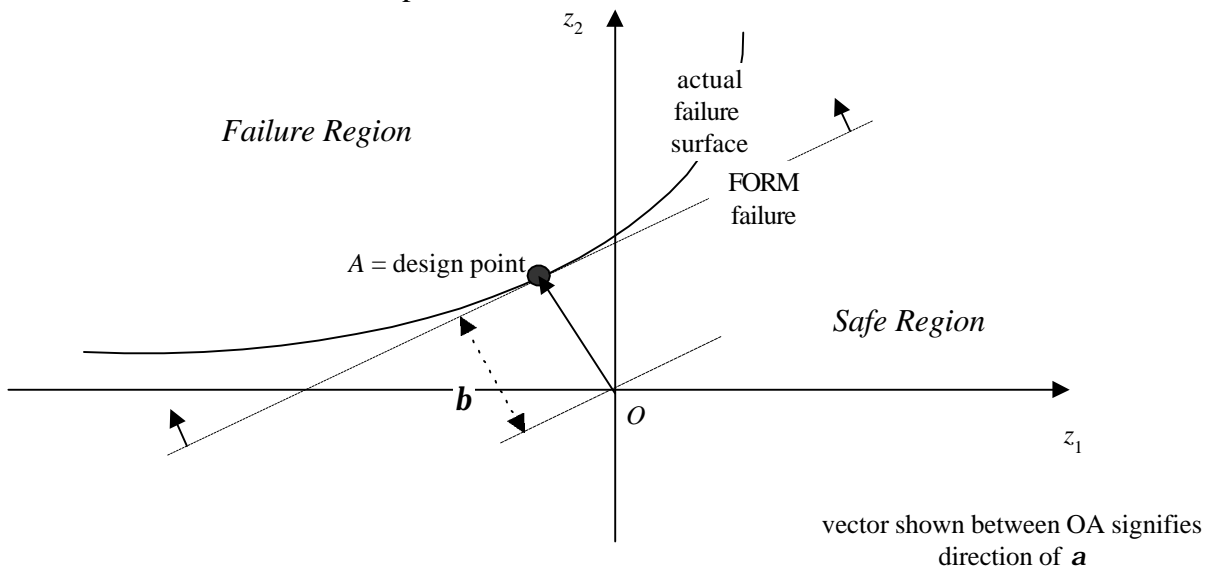


Figure 7.8 - Definitions used in FORM for the two-dimensional case (after Thoft-Christensen and Baker, 1982)

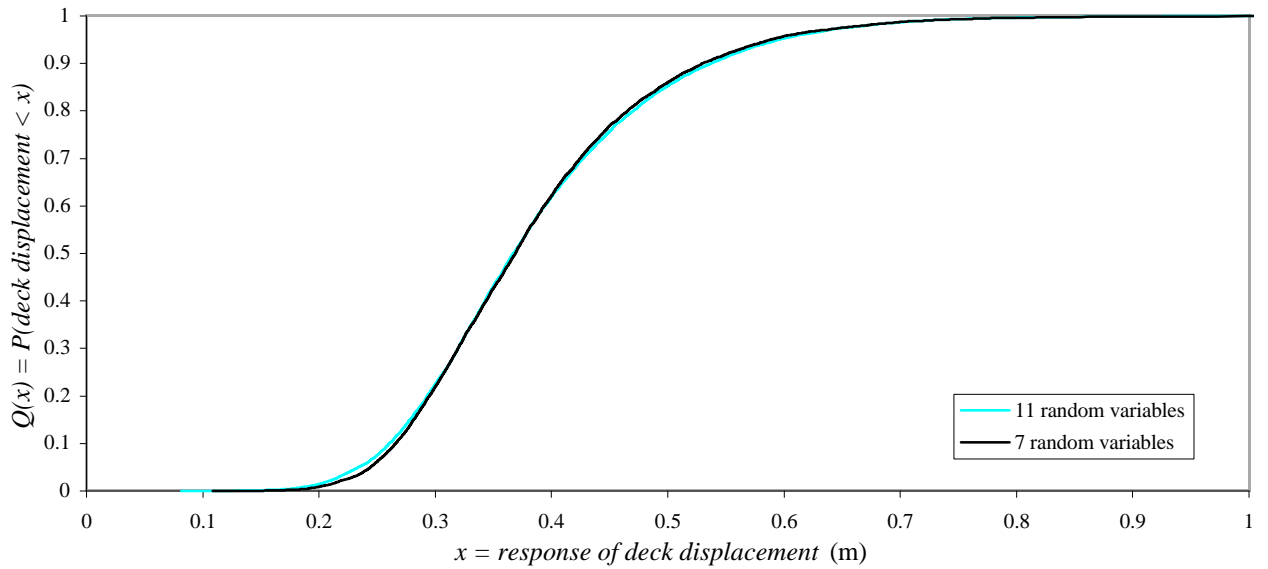


Figure 7.9 - Short-term extreme deck displacement distributions for the modal most probable highest wave amplitude in the 100-year sea-state for sets of 11 and 7 random variables

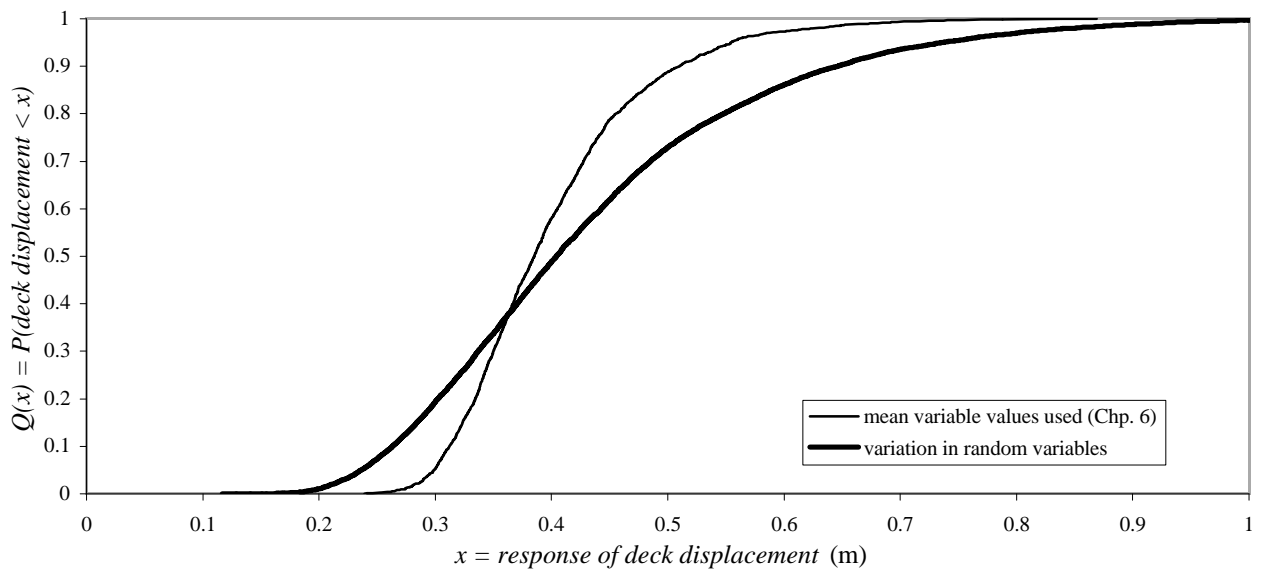


Figure 7.10 - Extreme deck displacement distributions for the 100-year sea-state with and without variation in the basic variables

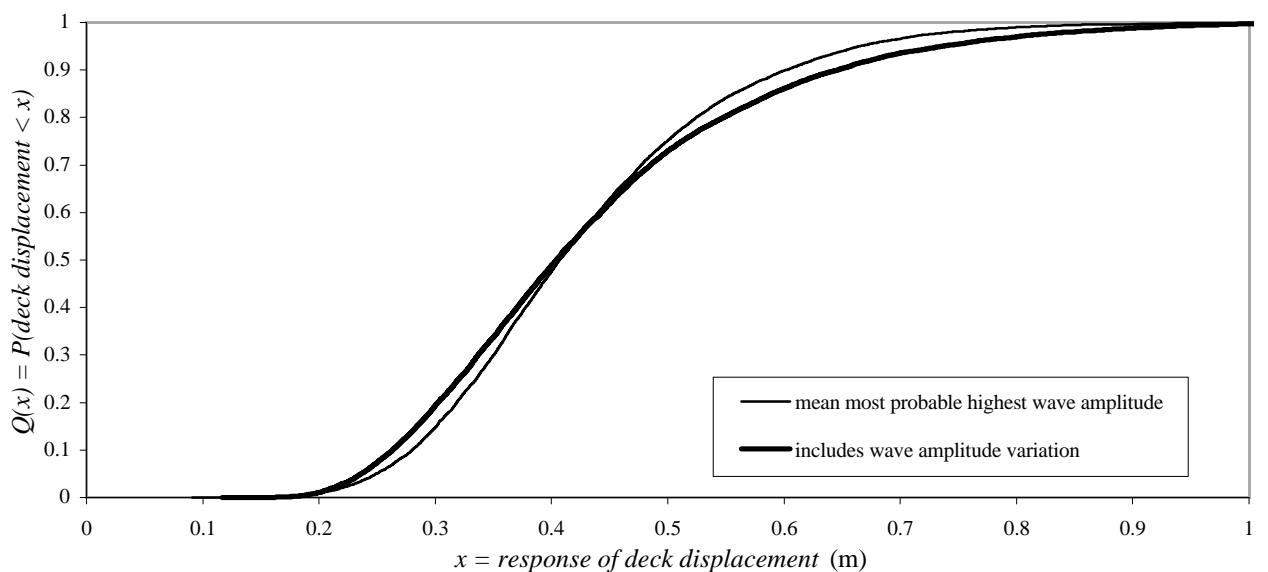


Figure 7.11 - Significance of the inclusion of short-term extreme wave amplitude variation in the extreme deck displacement distributions

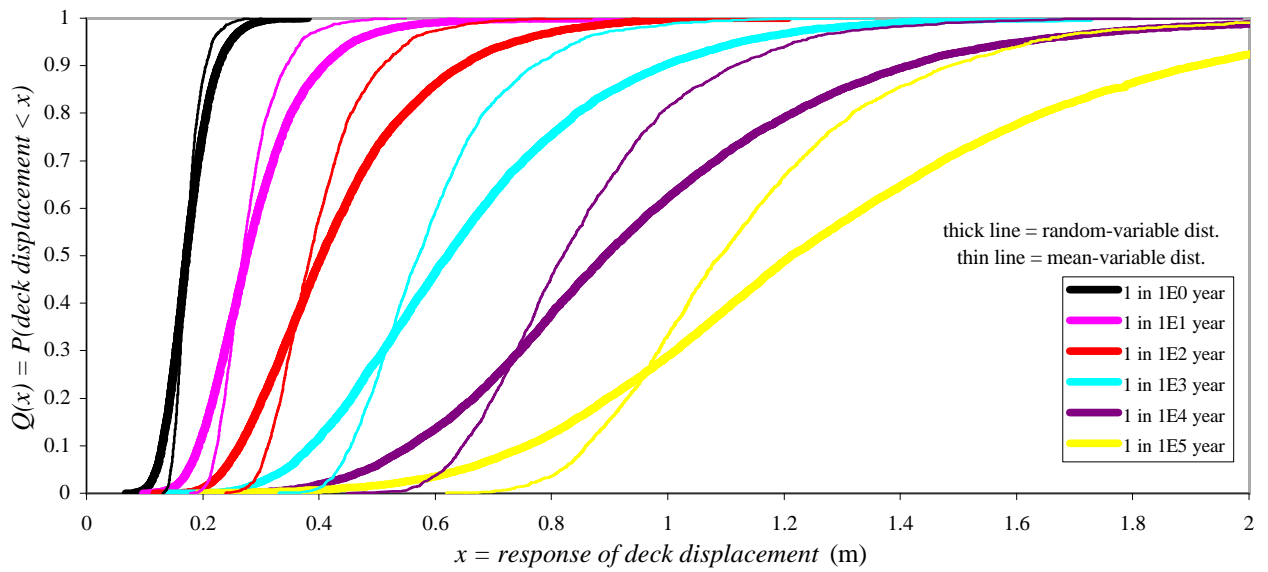
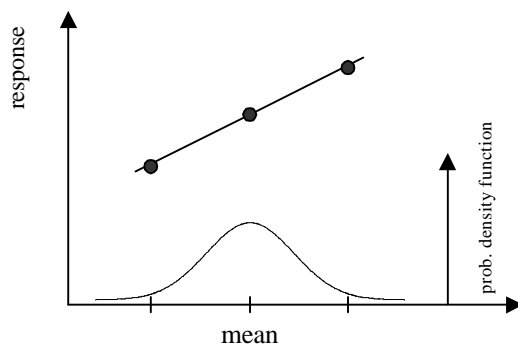
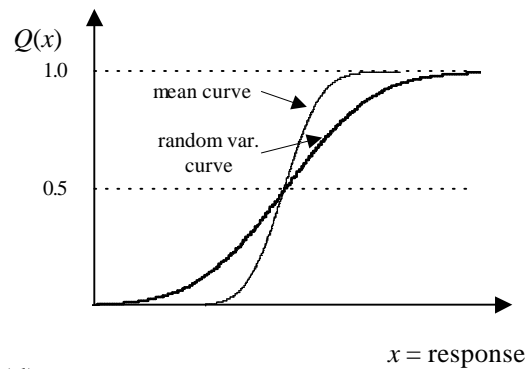


Figure 7.12 - Distributions for six short-term sea-states with and without variation in the basic variables

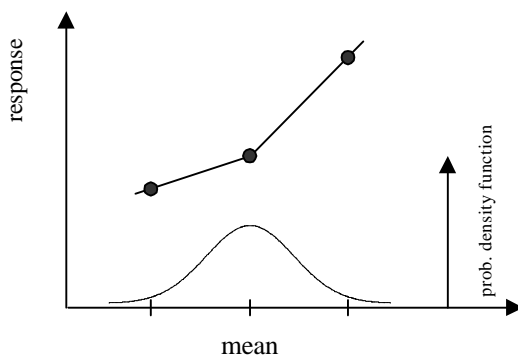
(a) Linear response



(b)



(c) Non-linear response



(d)

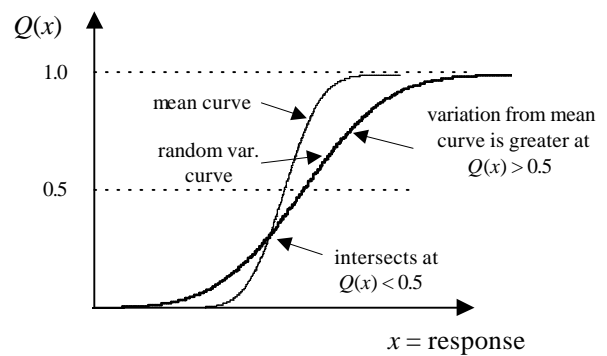


Figure 7.13 - Comparison of linear and non-linear response to short-term statistics

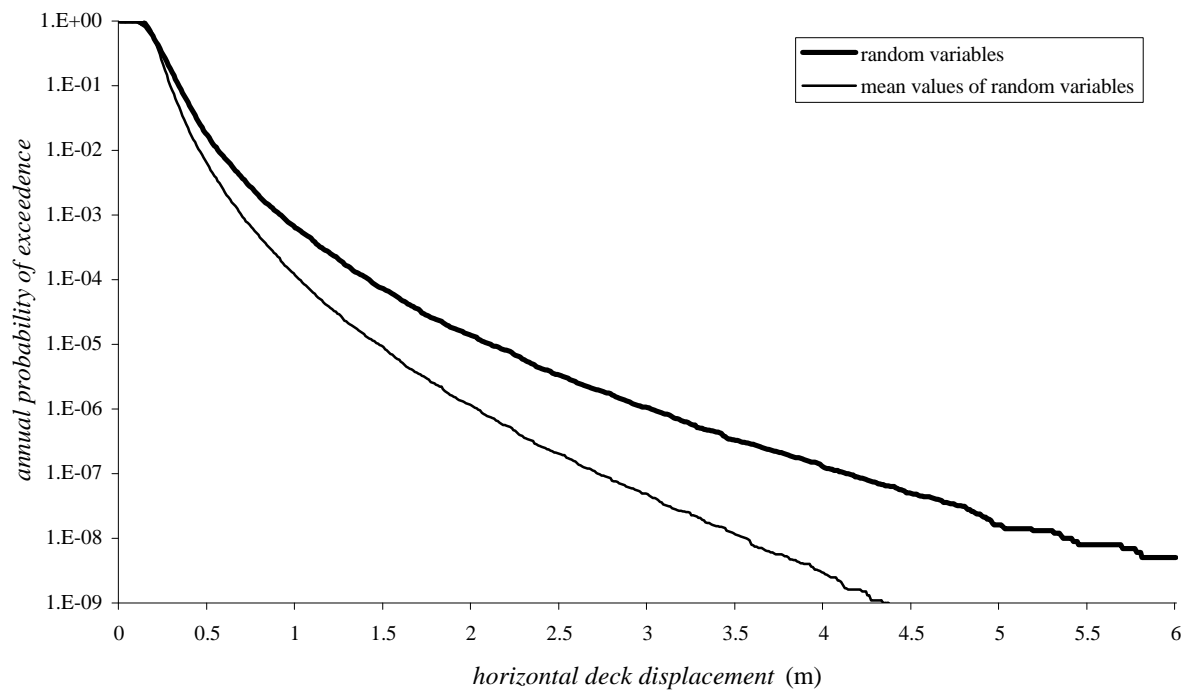


Figure 7.14 - Comparison of annual probabilities of exceedence of deck displacements for variable input parameters and their mean values (including wind and current)